

Propagation and Performance Measurements Over the Berlin-Bocksberg Digital Troposcatter Communications Link

John J. Lemmon
Timothy J. Riley



U.S. DEPARTMENT OF COMMERCE
C. William Verity, Secretary

Alfred C. Sikes, Assistant Secretary
for Communications and Information

March 1988

CONTENTS

	Page
LIST OF FIGURES	iv
LIST OF TABLES	iv
ABSTRACT	1
1. INTRODUCTION	1
2. BACKGROUND	2
3. MULTIPATH MEASUREMENT TECHNIQUE AND EQUIPMENT	3
4. TEST CONFIGURATIONS AND DATA ACQUISITION SYSTEM	8
5. DATA PROCESSING	16
5.1 PN Probe Data	17
5.2 RSL Data	20
5.3 Spectral Data	21
5.4 Digital Performance Data	21
5.5 Meteorological Data	23
6. DISCUSSION OF RESULTS	24
6.1 Summary of Propagation and Performance Data	24
6.2 Comparison of Measured and Theoretical Values of Delay Spread	38
7. CONCLUSIONS	41
8. ACKNOWLEDGMENTS	42
9. REFERENCES	43
APPENDIX A: Average Power Impulse Functions	45
APPENDIX B: Cumulative Distributions of Pulse Width	59
APPENDIX C: Cumulative Distributions of Pulse Width Rate-of-Change	73
APPENDIX D: Cumulative Distributions of RSL	81
APPENDIX E: Cumulative Distributions of 1-Second BER	113
APPENDIX F: Meteorological Data	133

LIST OF FIGURES

	Page
Figure 1. Average BER vs. $2\sigma/r$.	4
Figure 2. Path profile.	5
Figure 3. Probe block diagram.	7
Figure 4. Test configuration--Bocksberg site.	11
Figure 5. Test configuration--Berlin site.	12
Figure 6. Signal spectra: Averages of 100 spectra of the PN channel probe signal. Left: (a) horizontal polarization and (b) vertical polarization during a period of poor propagation conditions. Right: (a) horizontal polarization and (b) vertical polarization during a period of good propagation conditions.	22
Figure 7. Values of 2σ and BER, February 14-28, 1986.	25
Figure 8. Pulse width, receiver 1 and BER, February 14-28, 1986.	26
Figure 9. Pulse width, receiver 4 and BER, February 14-28, 1986.	27
Figure 10. Pulse width rate of change and BER, February 14-28, 1986.	28
Figure 11. Received signal level (medians), receivers 1 through 4 and BER, February 24-28, 1986.	29
Figure 12. Received signal level, receiver 1 and BER, February 14-28, 1986.	30
Figure 13. Received signal level, receiver 4 and BER, February 14-28, 1986.	31
Figure 14. Values of 2σ and BER, February 24-28, 1986.	32
Figure 15. Pulse width rate of change and BER, February 24-28, 1986.	33
Figure 16. Pulse width rate of change, Mode 2 and BER, February 24-28, 1986.	34
Figure 17. Geometry for path-length calculation.	40

LIST OF TABLES

	Page
Table 1. Characteristics of the Pseudonoise (PN) Probe	9
Table 2. Test Configurations	10
Table 3. Recorded Analog Signals and Sample Rates	15
Table 4. Time Blocks and Number of 5-Second Records Processed on Tape-by-Tape Basis	19

PROPAGATION AND PERFORMANCE MEASUREMENTS OVER THE BERLIN-BOCKSBURG DIGITAL TROPOSCATTER COMMUNICATIONS LINK

John J. Lemmon and Timothy J. Riley*

This report discusses propagation and performance measurements that were obtained over a digital troposcatter communication link between Bocksburg, West Germany, and West Berlin. The measurements were unusual because three general types of data were collected simultaneously over the link: propagation data, digital performance data, and meteorological data. The propagation data include received signal level (RSL) and multipath measurements made with a channel probe; the performance data consist of bit-error data obtained from a 1.544 Mbps T1 bank; and the meteorological data (in the form of radiosonde messages) have been used to generate profiles of the radio refractive index over the link.

The basic principles and instrumentation of the channel probe and the test configurations used to obtain these data are discussed. Then the results of analyses of these data are presented and discussed. These results include the measured impulse response of the channel, delay spread, RSL, bit-error ratios, and refractive index profiles. Potential relationships among these results are investigated in order to assess the impact of various troposcatter channel conditions on digital radio performance. In particular, the report discusses both the definition and methods of utilizing the all-important parameter of delay spread. These considerations range from the simple parameter of 2σ values to a more complete evaluation of the dynamic properties of delay-spread derived from the channel probe data.

Previous studies have addressed many facets of troposcatter propagation. This report attempts to bring all of these facets together, to present a more complete description of the troposcatter channel, and to enhance future digital upgrades of existing troposcatter links.

Key words: troposcatter; multipath; PN channel probe

1. INTRODUCTION

The U.S. Army recently completed equipment installation of a digital troposcatter communication system between Bocksburg, West Germany, and West Berlin. The radio system is composed of a modified Army AN/GRC-143 tactical troposcatter radio operating with the MD-918/GRC Digital Data Modem at a nominal bit rate of 10 Mbps. This is the first digital upgrade of an existing analog troposcatter link in the Defense Communications System (DCS) in Europe

*The authors are with the Institute for Telecommunication Sciences, National Telecommunications and Information Administration, U.S. Department of Commerce, Boulder, CO 80303.

and it was, therefore, important to evaluate both the propagation factors and the digital performance over this link. Moreover, the Defense Communications Agency (DCA) required a formal link acceptance test prior to the cutover of the link to operational traffic.

One of the most important parameters to be measured is the delay spread of the signal in the propagation path. The measurement of delay spread over the Berlin-Bocksberg link was specified as part of the test and acceptance program, which was conducted by GTE Government Systems Corporation, Communication System Division, Needham Heights, MA, under contract to the U.S. Army. The instrument required to make the delay spread measurement was a pseudonoise (PN) channel probe, designed and built by the Institute for Telecommunication Sciences (ITS), Boulder, CO. The purpose of this report is to outline the support that was furnished by ITS to GTE in performing the channel probe measurements during the test and acceptance program and to summarize the data that were obtained by ITS.

The primary objective was to obtain propagation data, including measurements of delay spread and received signal level, in conjunction with measurements of digital transmission performance. The simultaneous collection of propagation and performance data over the same transmission channel can provide new insights into performance criteria and adaptive techniques that will be valuable to the Army as well as the DCA in planning and implementing future digital upgrades of other troposcatter links. It is also expected that the data will be useful in enhancing analytical models of digital troposcatter systems.

2. BACKGROUND

A common propagation problem in both line-of-sight and transhorizon radio links is caused by multipath, resulting from reflections or refraction/scatter in the transmission medium. Multipath can be more detrimental in the digital transmission mode than in its analog counterpart. A significant number of performance measurements have been reported that demonstrate the catastrophic effect that multipath can have on digital transmission. Examples of specific measurements have been discussed by Dougherty and Hartman (1977), Anderson et al. (1978), Barnett (1978), and Hoffmeyer et al. (1986); a review of this field with extensive references has been given by Hubbard (1984). However,

there are techniques that use the multipath to provide a form of in-band diversity improvement; such is the case with the MD-918. The modem is designed to take advantage of the delay spread of the signal over a certain range.

Figure 1 (from Gadoury, 1983) shows plots of laboratory measurements of average bit-error-rates (BER) of the MD-918 versus delay spread for various values of E_b/N_0 . The delay spread is expressed as the ratio of the two-sided root-mean-square (rms) width of the power impulse response (2σ) to the data symbol time T . For 10 Mb/s quadrature phase shift-keyed (QPSK) modulation such as that used in the MD-918, the symbol time is twice the bit time (twice 100 ns). The curves in Figure 1 clearly show the improvement in modem performance as $2\sigma/T$ increases from zero. However, when $2\sigma/T$ is greater than about 0.7 (2σ greater than 140 ns) BER increases with increasing delay spread. It is, therefore, important to know what values of delay spread are encountered in practice.

The primary purpose of ITS in the test and acceptance program for the Berlin-Bocksberg digital tropo link was to furnish the equipment necessary for the delay-spread measurements. The PN channel probe, described in Section 3, was interfaced to the modified AN/GRC-143 radio at the 70 MHz IF point. Details of the interface arrangement are discussed in Section 4.

The test signal was propagated over the path in the 4.5 to 5 GHz band. The path length is approximately 210 km. The path profile for the link, shown in Figure 2, indicates that the dominant propagation mechanism is expected to be troposcatter, but that the link may be diffractive under subrefractive conditions. The data presented in this report were collected during the last 2 weeks of February 1986, during which time the signal was transmitted from Bocksberg, with Berlin as the receive site.

3. MULTIPATH MEASUREMENT TECHNIQUE AND EQUIPMENT

Delay spread has been measured previously over a few selected troposcatter links using a system commonly known as a RAKE communication system (Price and Green, 1958; Barrow et al., 1969; Sherwood and Suyemoto, 1977). The RAKE system measures the value of a correlation function at the output of a finite number of taps along a tapped-delay line. The test signal uses a pseudonoise (PN) code, which is cross-correlated in the receiver with a locally generated replica of the PN code.

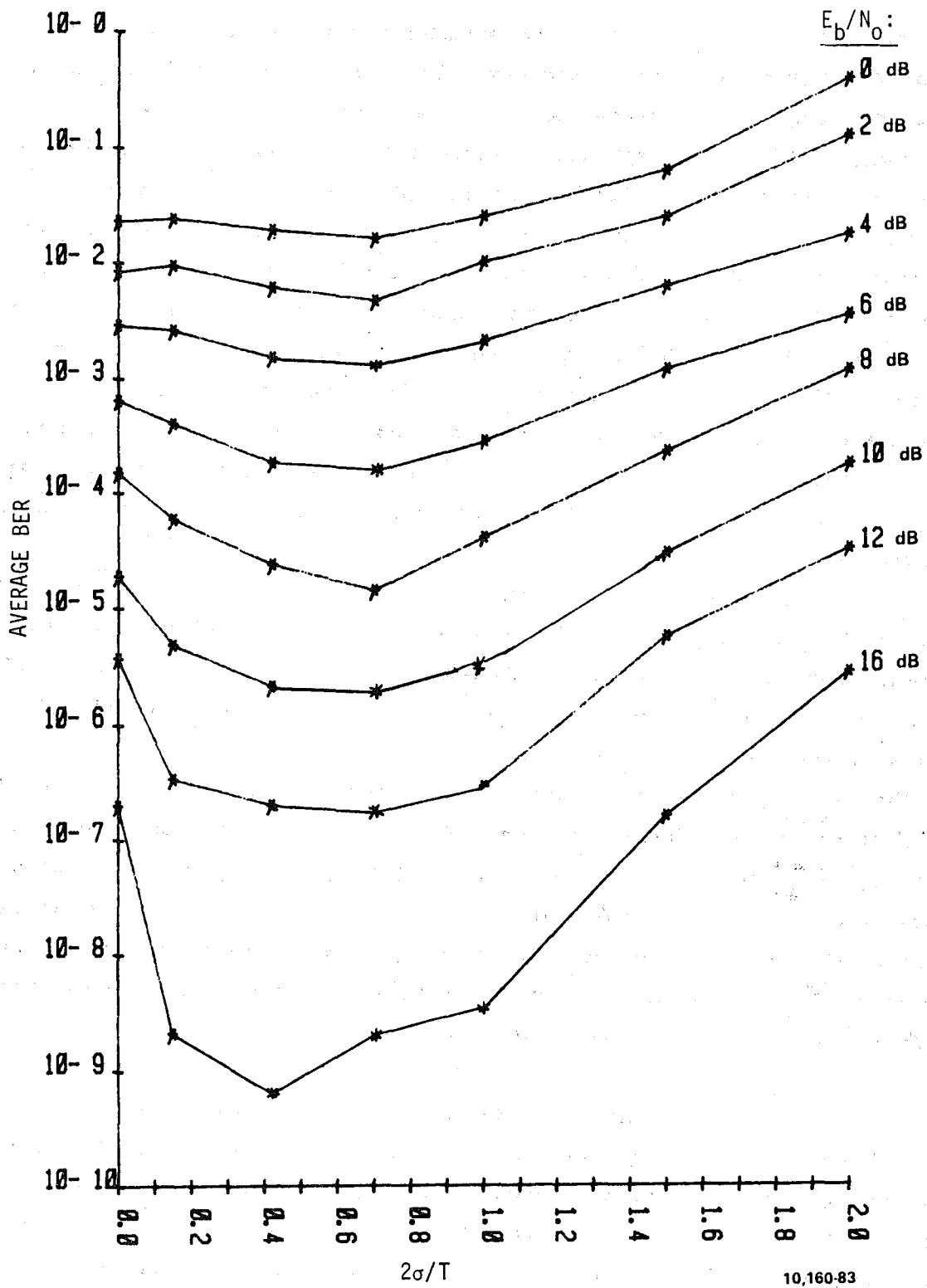


Figure 1. Average BER vs. $2\sigma/\tau$.

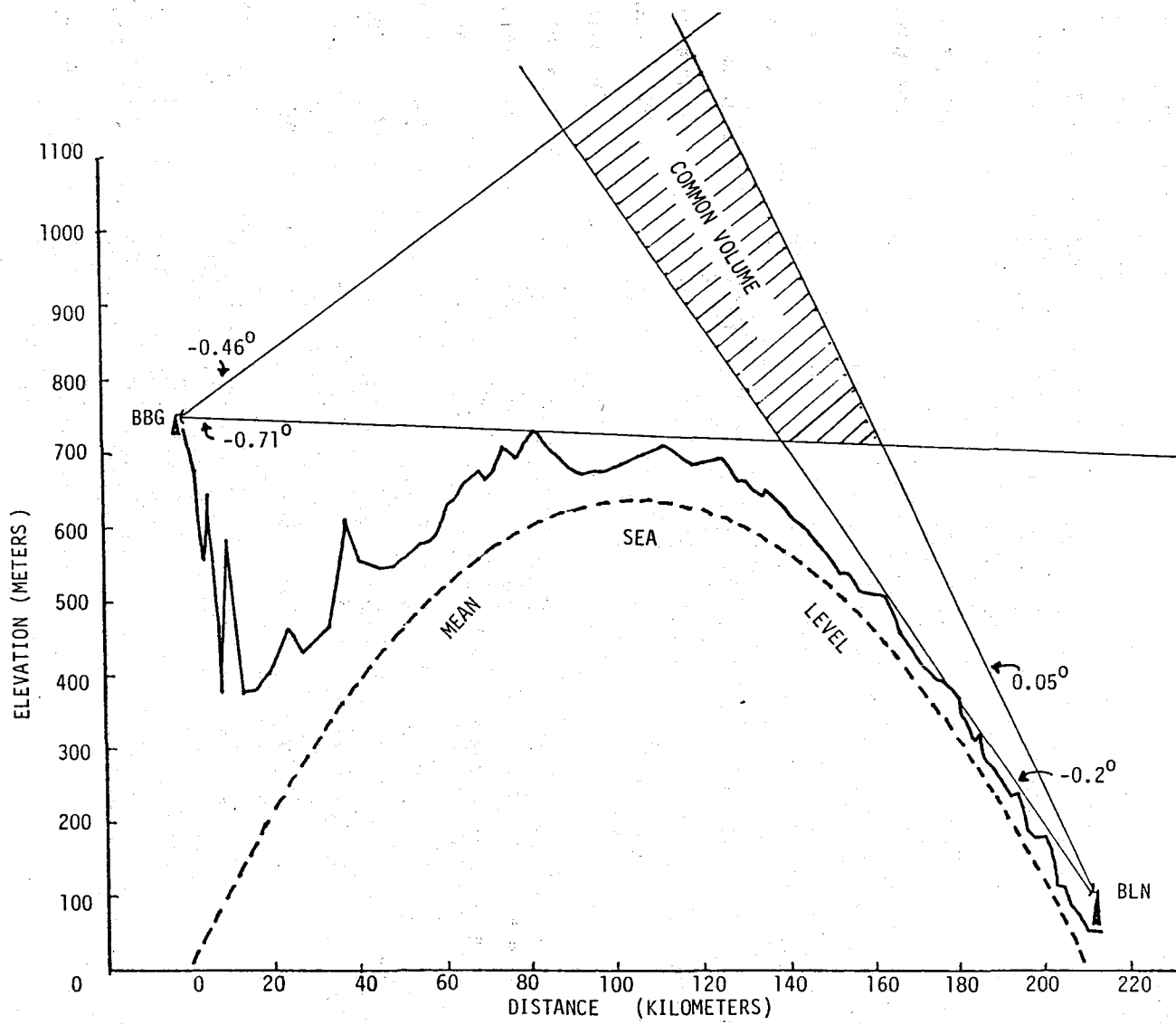


Figure 2. Path profile.

The instrumentation used in the ITS PN channel probe is similar to that of the RAKE system, with the exception of the correlation process. The ITS system uses a time-multiplex type correlation detector in the receiver as opposed to the tapped-delay line used in the RAKE system. Delay between the received code and the locally generated replicum is achieved by clocking the PN generator at a slightly slower rate in the receiver than in the transmitter. In this manner, delay is continuously varying, thereby enabling one to measure the correlation function (impulse response of the radio channel) as a function of time delay. The rate of delay change is variable, and the code length and clock rate can be selected over specified ranges to meet different transmission channel conditions. A detailed description of the theory and implementation of the ITS channel probe is given by Linfield et al. (1976). Delay spread measurements taken over troposcatter links in the past using the ITS probe have been discussed by Hubbard¹.

The correlation process in the probe receiver takes advantage of time-bandwidth tradeoff, which permits the data to be recorded at a relatively low rate (small bandwidth), but with high equivalent time resolution. For example, the bit time for a PN code clocked at 10 MHz is 0.1 μ s. For a 511 bit code at this clock rate, a code word is 51.1 μ s in length. If a correlation function were developed for each code word, the bandwidth requirement for the data acquisition system would be quite broad. However, this data rate is not necessary if the dynamic changes in the transmission channel are much slower. In the PN channel probe receiver the correlation process is slowed so that many code words are processed while one correlation function is developed. For example, the data rate for the tests described here was selected to be one correlation function per second. However, the range of time delays over which the correlation function is measured corresponds to the 51.1 μ s period of the PN code. Thus, 1 s of processing time in the receiver corresponds to 51.1 μ s in channel response time (a time-bandwidth factor of approximately 2×10^4).

A simplified block diagram of the probe is shown in Figure 3. For UHF band and troposcatter systems, an IF of 70 MHz and a PN clock rate of 10 MHz are used. These values were chosen to make the system compatible with existing

¹Hubbard, R.W. (1983), Delay-spread measurements over troposcatter links, NTIA Tech. Memo. 83-84, March (limited distribution).

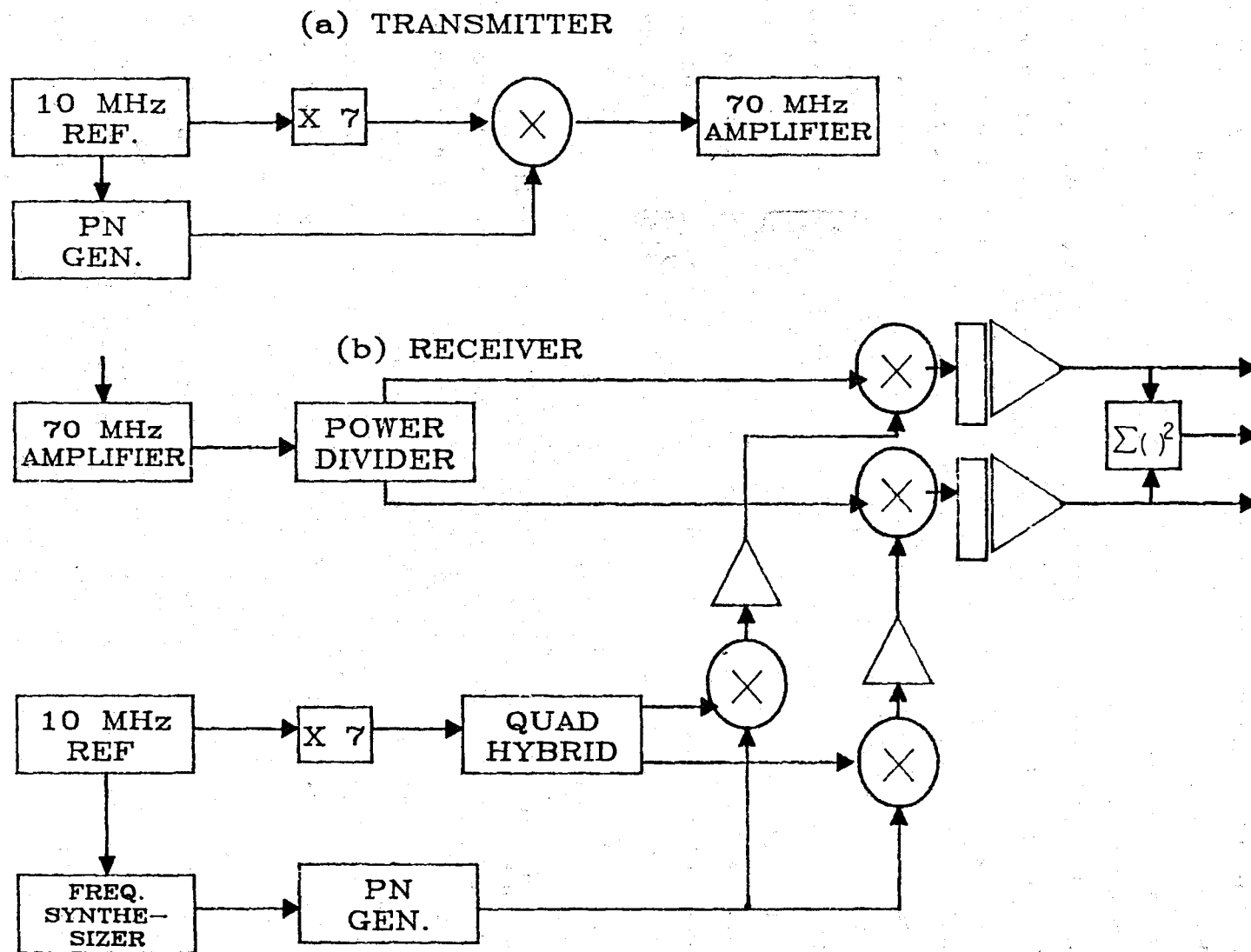


Figure 3. Probe block diagram.

communication systems that use a standard 70 MHz IF and to limit the PN test signal bandwidth to a value commensurate with the power amplifiers of those systems. In order to maintain frequency coherence between the tropo radio and the probe, the 10-MHz reference from the radio interface rack (LORAN C) was used as the probe reference signal in parallel with the tropo radio.

The receiver of the probe is configured for dual-channel operation, but only one channel is illustrated in Figure 3. The two independent channels allow data to be collected simultaneously from two diversity links, as was done during the tests discussed in this report. The probe receiver develops four signals from each channel. Two correlators are used to develop the in-phase and quadrature components of the equivalent low-pass impulse response of the transmission channel. Relative phases between multipath components can therefore be determined. The third signal is developed from the sum-of-the-squares processing of the in-phase and quadrature signals, which is the power impulse response of the channel. The fourth signal is the received signal level (RSL), measured as a power level in the IF amplifier stages. All of these signals were recorded on digital magnetic tape for this test program. Specific formats are discussed in Section 4. A list of the PN probe characteristics as it was configured for this program is given in Table 1.

4. TEST CONFIGURATIONS AND DATA ACQUISITION SYSTEM

The basic test configuration was established by the prime contractor for the project (GTE) to meet the requirements of the test and acceptance procedures. The GTE tests included the measurement of the received signal levels (RSL) and other parameters pertinent to the performance of the radio system. Digital performance was measured with an appropriate bit error detector using a predetermined digital test signal at the designated transmission rate.

The only part of the basic test configuration that was furnished by ITS was the PN channel probe system. The PN test signal requires the total baseband of the radio, and thus cannot be transmitted simultaneously with the data test signal. However, the troposcatter radio system uses quadruple diversity in a dual space/dual frequency configuration, so that probe data and digital performance data can be obtained simultaneously over the link if the radio is configured for dual diversity operation. In other words,

Table 1. Characteristics of the Pseudonoise (PN) Probe

(a) Transmitter

Reference Frequency	10 MHz
Center Frequency	70 MHz
Test Signal	PN Binary Code
PN Shift Register	n=9 states
PN Code Length	$(2^n - 1) = 511$ bits
PN Clock Rate	10 MHz
Modulation	Biphase
Power Amplifier Output	5 dBm (maximum) 0 dBm (nominal)

(b) Receiver

Type	Multiplex Correlation
Dynamic Range (RSL)	60 dB
Dynamic Range (Power Impulse)	30 dB
Number of Channels	2
Reference Frequency	10 MHz
Center Frequency	70 MHz
PN Clock Rates	10 MHz nominal; variable for the following data rates.
Impulse Data Frame Rates	1, 2, 5, 10, and 50 frames/s; Operator selectable.
Impulse Resolution	0.1 μ s
Maximum Delay Response	51.1 μ s
Data Signals (Each Channel)	Co-phase Impulse Quad-phase Impulse Power Impulse Log Power Impulse Received Signal Level (RSL)

one diversity pair can be used to receive the probe signal while the other diversity pair is receiving the digital performance test signal. This and the other configurations that were used in the test are listed in Table 2. The frequency diversity signals are transmitted with different polarizations (horizontal and vertical) and are identified by polarization rather than by frequency throughout this report.

The control for the various configurations was provided at the transmitter terminal through the use of coaxial switches to change the input test signals. Command signals for the coaxial switches were sent via the service channel from the receive site to the transmit site. The order and timing used for the configurations were determined by GTE. The test proceeded through the various configurations in a cyclic fashion, operating in a given configuration for a duration of 13 minutes before proceeding to the next configuration. At the transitions between configurations, the system was put into configuration 1 for a duration of approximately 2 minutes, during which time GTE processed and recorded data. Thus, the test cycled through all four configurations over a period of 1 hour. The complete test configurations are shown in block diagram form in Figures 4 and 5.

Table 2. Test Configurations

Configuration Number (Mode Number)	Active Receivers (Being Recorded)	Diversity Test Signals	
		Horizontal	Vertical
1	Receivers 1 and 4	MD 918 Data	MD 918 Data
2	Receivers 1 and 2	Probe Data	MD 918 Data
3	Receivers 3 and 4	MD 918 Data	Probe Data
4	Receivers 1 and 4	Probe Data	Probe Data

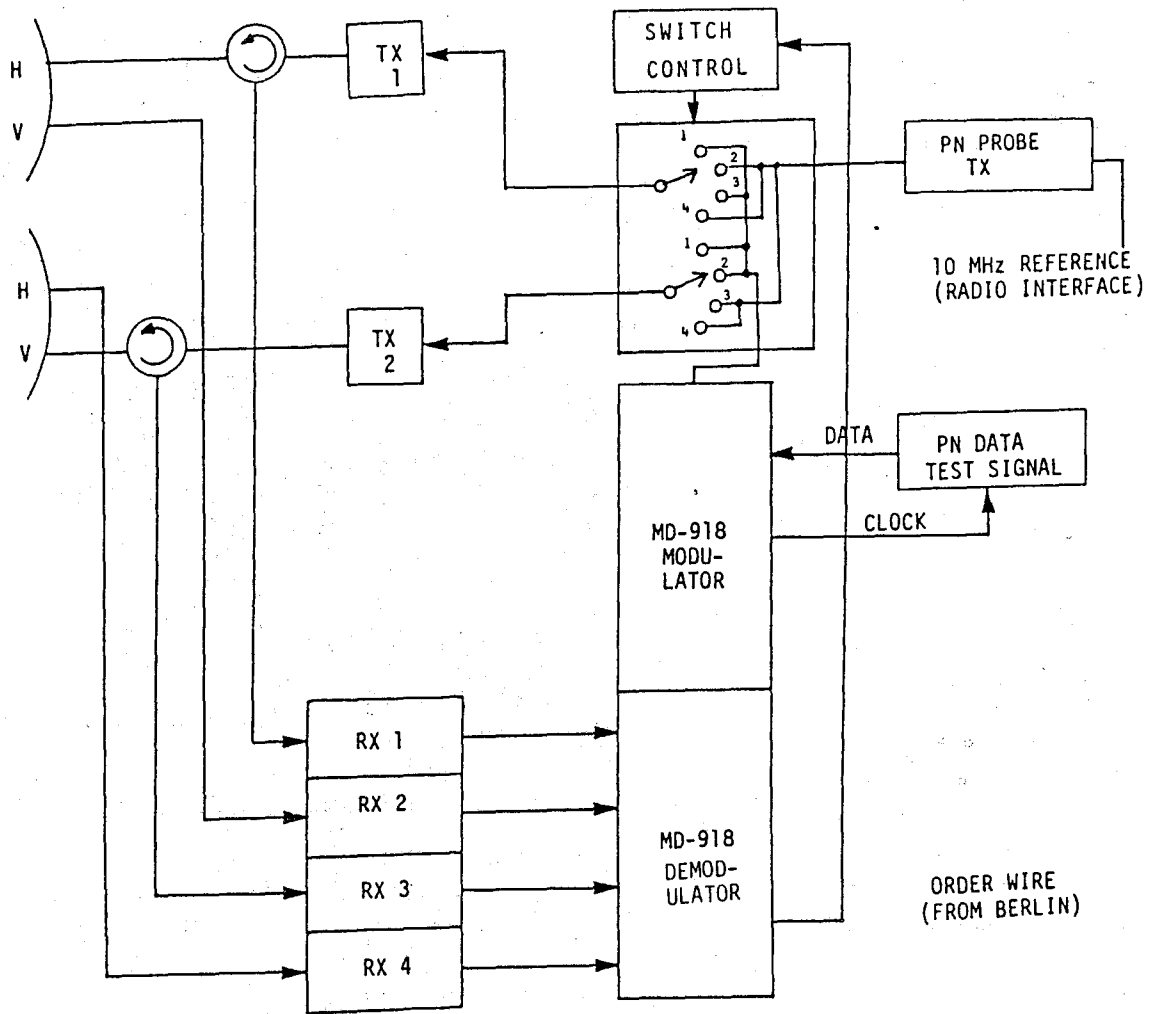


Figure 4. Test configuration--Bocksberg site.

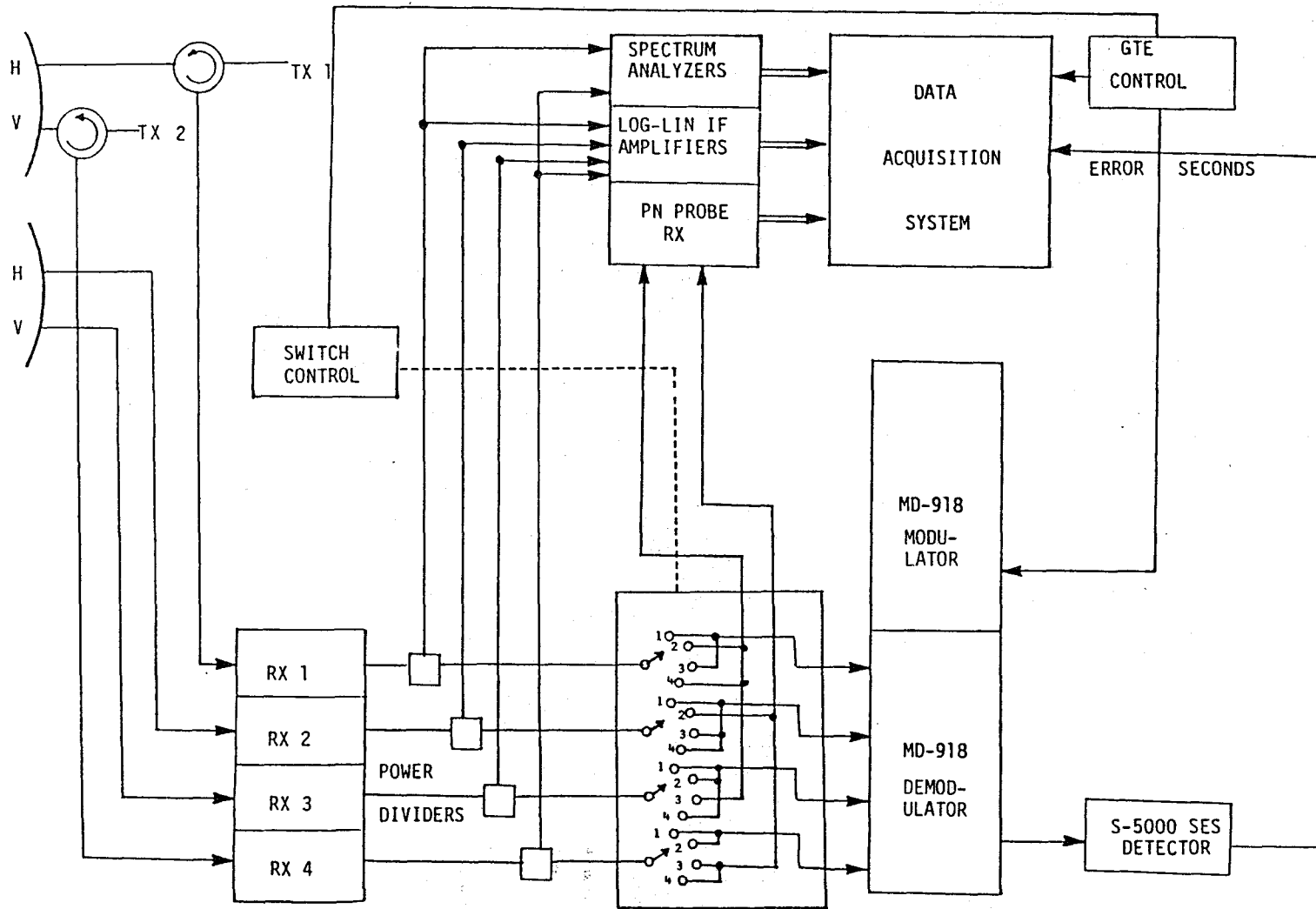


Figure 5. Test configuration--Berlin site.

In addition to the data accumulated by GTE, ITS enhanced the test program by acquiring data in an independent data system. The data acquisition system is based on an LSI-11/23 minicomputer system with digital magnetic tape as the storage medium. It also uses a dual floppy-disk drive for both program control and data storage. An operator's CRT/printer terminal is also an integral part of the system. Data are acquired in 1-second intervals (coincident with the errored-second performance monitoring instruments discussed below). The data are double-buffered at the input, compiled into a 5-second file, and recorded on the magnetic tape. One buffer is acquiring new data as the other buffer is being read to the tape.

Two different data recording protocols are available; data can be recorded onto magnetic tape only when digital errors are detected or data can be recorded continuously. However, in test configuration 4, only the PN probe signal was transmitted, so that the bit error detector used by GTE generated continuous errors by comparing the probe signal to the digital test signal. Thus, data were recorded continuously in test configuration 4 regardless of the data recording protocol.

The ITS acquired a total of 32 magnetic tapes of test data in parallel with the GTE system. Data were recorded continuously on 5 of the tapes and only when bit errors were detected for the remaining 27 tapes. An on-line storage (variable persistence) oscilloscope was used to monitor continuously the power impulse response from the probe receiver and a strip-chart recorder was used to monitor the RSL. A standard IRIG Code B time-code generator was used to record time and date information on all data tapes. The following signals were recorded:

1. in-phase and quadrature components of the impulse response and the power impulse response from each of the two channels of the PN probe receiver
2. RSL (received signal level) of each tropo receiver and the two channels of the PN probe receiver
3. spectrum of the received signal in each diversity polarization. These data include both the probe and digital test signal in accord with the applicable test configuration discussed above.
4. digital performance (error) data
5. test configuration number
6. time code

The latter two signals were used in the data processing procedures discussed in Section 5.

The RSL and spectral data were developed from the 70 MHz IF signals at the receivers, using power dividers and log-linear amplifiers. The latter isolated the ITS data system from that used by GTE, where a common IF signal is fed to each data system. Two commercial spectrum analyzers were used at the outputs of the log-linear amplifiers and the spectra for recording were taken from the vertical display outputs of these instruments. The two instruments were connected so that two spectral measurements were made each second, one on the horizontally polarized signal and one on the vertically polarized signal.

The ITS instrumentation also included a method for recording the configuration of the test system via two TTL signals that were provided by GTE. Each of the two signal levels could assume either a high or a low value, and each of the four possible combinations corresponded to a particular test configuration number.

Analog data inputs were sampled at different rates, commensurate with the Nyquist requirements for the various signals. For example, the impulse functions from the PN probe require the highest sampling rate for the necessary resolution. Therefore, these functions (total of six signals) were sampled at a rate of 4 kHz. The response was measured once per second in the first 20 ms only, as this part of the function includes time delays to beyond 1 μ s. Thus, each response was sampled 80 times. Four additional A/D channels were sampled at a 100-Hz rate. These were used to record the received signal spectra from the tropo receivers and the RSL of the two channels of the PN probe receiver. The remaining six A/D channels were sampled at a 10-Hz rate and were used to record the RSL of each of the four tropo receivers as well as the two TTL signals used to determine the test configuration number. Table 3 lists the recorded signals and sampling rates that were used in each of the 16 A/D channels.

The digital performance data were measured in the ITS system using a recording error analyzer (Tau Tron S-5000) operating in the external error mode. This instrument measures synchronous errored seconds (SES) and registers the number of bit errors in each errored second. The data source for the instrument was an error pulse train developed in the bit error detector (HP 3764A Digital Transmission Analyzer) used by GTE to measure the radio

performance. In this manner, the two sets of data (ITS and GTE) are completely coherent and complimentary. The arrangement also provided isolation between the two instruments so that there was no danger of one loading the other. Since the SES data were taken on a 1-second interval, they can readily be correlated with the impulse response functions taken over the same time interval. The HP 3764A monitored the error performance of one T1 bank in an AN/FCC-99 multiplexer. The other five T1 banks were loaded with another PN code stream that was looped back and forth over the link to simulate full load conditions. At no time during the tests was the error performance of the full mission bit stream monitored.

The ITS provided additional support to the test and acceptance program by obtaining available meteorological data from the U.S. Air Force in Berlin. These consisted of radiosonde data that can be used to develop refractive index profiles for the link. The radiosonde launch sites were at Lindenberg, East Germany; Hannover, West Germany; and Berlin. Computer programs developed at ITS were used on-site to compute and plot these profiles during the tests. The objective was to correlate test results with features of these profiles.

Table 3. Recorded Analog Signals and Sample Rates

A/D Channel	Signal	Sample Rate
0	Impulse response on probe channel A	4 kHz
1	Impulse response on probe channel B	4 kHz
2	Co-phase of impulse response on channel A	4 kHz
3	Quad-phase of impulse response on channel A	4 kHz
4	Co-phase of impulse response on channel B	4 kHz
5	Quad-phase of impulse response on channel B	4 kHz
6	Signal spectrum on tropo RX1	100 Hz
7	Signal spectrum on tropo RX4	100 Hz
8	RSL on probe channel A	100 Hz
9	RSL on probe channel B	100 Hz
10	RSL on tropo RX1	10 Hz
11	RSL on tropo RX2	10 Hz
12	RSL on tropo RX3	10 Hz
13	RSL on tropo RX4	10 Hz
14	Test configuration number	10 Hz
15	Test configuration number	10 Hz

5. DATA PROCESSING

The magnetic tape recordings and radiosonde data were returned to the ITS laboratories for processing and analysis. ITS has developed a set of computer programs to perform a variety of analyses on the data described above. The computer systems used for this purpose are the LSI-11/23, a TD-100 Time Series Analyzer, an FPS-100 Array Processor, and associated peripherals. The data analyses that can be performed include the following:

1. average impulse response
2. probability density functions (pdf) and cumulative distribution functions (cdf) of the impulse width
3. pdf and cdf of the time rate-of-change of the impulse width
4. computation of the two-sided rms width of the average power impulse response (2σ)
5. average signal spectrum
6. pdf and cdf of RSL
7. cdf of 1-second BER
8. profiles of refractive index

The individual impulse response functions that were used to compute the averages were first normalized so that each response had the same peak value. If the value of the average impulse power function at a time delay τ_i is denoted by $P(\tau_i)$, then σ is defined as

$$\sigma = \left[\frac{\sum_{i=1}^N P(\tau_i) (\tau_i - \bar{\tau})^2}{\sum_{i=1}^N P(\tau_i)} \right]^{1/2}$$

where N is the number of sample points (80) and $\bar{\tau}$ is the mean time delay:

$$\bar{\tau} = \frac{\sum_{i=1}^N P(\tau_i) \tau_i}{\sum_{i=1}^N P(\tau_i)}$$

The impulse width is defined as the width of an individual power impulse function at a threshold just above the noise floor of the PN probes, and the pulse width rate-of-change is computed as the difference between the pulse

width of an impulse function and the pulse width of the previous (1 second earlier) impulse.

It should be noted that during the test configuration setup for Phase II (transmit from Berlin and receive at Bocksberg), several changes to the equipment configuration were made. Both antennas at Bocksberg were realigned; a baseband interface problem between the MD-918 modem and the KG-81 encryption unit which caused intermittent burst errors was discovered and fixed, and one antenna feedhorn at Bocksberg was replaced. Any one or combinations of these changes could impact the absolute accuracy of the data analyses presented herein. Thus, no attempt has been made to compare the results of the data analyses to appropriate performance criteria, the responsibility for which resided with the prime contractor for the test and acceptance program. Rather, the primary objective of the data analyses has been to identify those periods during which the radio system performed relatively poorly, and to relate the performance to propagation conditions in the transmission channel.

5.1 PN Probe Data

The first step in computing average impulse functions and distributions of impulse width was to define the time blocks and test configurations over which each analysis was performed. Since the primary objective of the analyses was to relate system performance to propagation conditions, it was desirable to use time blocks that were small in comparison to the time scales over which propagation conditions and performance could vary significantly (several hours). On the other hand, time and cost constraints imposed a practical limit on the number of individual analyses that could be performed. As a compromise, the PN probe data analyses were performed on a tape-by-tape basis. Since the data were collected only for those 5-second blocks during which at least one digital error occurred, the time blocks corresponding to the various tapes are variable (approximately 3 to 17 hours), depending on the error performance of the radio system. In addition, there were periods of time during which no data were collected due to equipment failures and periodic RSL calibrations. However, most of the tapes span time blocks of approximately 6 hours.

As discussed above, four different test configurations were used during the test and acceptance program. However, only during test configuration 4 was data collected on a continuous basis, due to the error-recording protocol. For

this reason, emphasis was placed on this latter test configuration for the analyses of impulse response data, in order to obtain results that are not biased by the error performance of the radio system. In test configuration 4, channels A and B of the probe were interfaced to tropo receiver 1 (horizontal polarization) and tropo receiver 4 (vertical polarization), respectively, thereby enabling the impulse response to be analyzed in both polarizations.

The results of the PN probe data analyses on a tape-by-tape basis have been collected in Appendixes A through C. Analyses were performed for test configuration 4 on all of the tapes; in addition, analyses were also performed for test configurations 2 and 3 on the last 10 tapes (February 23-28). The time blocks corresponding to the tapes and the number of 5-second data blocks that were processed on each tape are listed in Table 4. Throughout this report all times are given in terms of Universal Time (UT); in Germany, local time is 1 hour ahead of UT.

Appendix A contains the average power impulse functions. No scale appears on the vertical axes because the PN receiver does not have a local signal source, and thus the impulse response magnitude could not be calibrated; however, the impulse functions are plotted on a linear scale and relative power levels within a given impulse function can be determined accordingly. The legend in each plot gives the start and end times for the analysis and the value of 2σ . The test configuration number ("mode number") is also shown in each legend.

The impulse functions corresponding to vertical polarization typically have a steep leading edge, followed by a tail with a relatively small amount of distortion corresponding to signal energy arriving at relatively large delay times. On the other hand, the impulse functions corresponding to horizontal polarization show a pronounced shoulder on the trailing edge and occasionally a distinct secondary peak, suggesting a mixed mode of propagation. Exceptions to this pattern can be seen in some of the impulse functions (for example, those corresponding to the time block on February 23, in which distinct shoulders appear on the leading and trailing edges for both horizontal and vertical polarization). These features of the impulse functions are discussed further in Section 6.

Appendix B contains cumulative probability distributions of the base width of the power impulse function. The data analysis software can also develop

Table 4. Time Blocks and Number of 5-Second Records Processed on a Tape-by-Tape Basis.

<u>Test Block</u>	<u>Test Configuration</u>	<u>No. Of 5-Second Records</u>	<u>Test Block</u>	<u>Test Configuration</u>	<u>No. Of 5-Second Records</u>
2/14, 15:56-	1	555	2/23, 09:50-	1	272
2/14, 20:01	2	676	2/23, 23:33	2	629
	3	461		3	434
	4	509		4	865
2/15, 11:40-	4	850	2/23, 23:41-	1	222
2/15, 16:18			2/24, 10:26	2	320
				3	121
2/15, 16:29-	4	576		4	1,528
2/15, 23:51					
2/16, 10:54-	4	791	2/24, 11:51-	1	752
2/16, 15:57			2/24, 18:47	2	508
				3	467
2/16, 16:10-	4	1,011		4	420
2/16, 22:49			2/24, 22:47-	1	128
			2/25, 16:09	2	475
2/16, 23:09-	4	1,732		3	276
2/17, 11:03				4	1,328
2/17, 13:21-	4	1,020	2/25, 16:18-	1	589
2/17, 20:18			2/25, 21:03	2	541
				3	410
2/18, 06:54-	4	510		4	680
2/18, 10:42					
2/18, 10:46-	4	678	2/25, 22:10-	1	132
2/18, 16:38			2/26, 11:01	2	137
				3	111
2/18, 17:07-	4	328		4	1,869
2/18, 20:37					
2/19, 08:10-	4	792	2/26, 11:36	1	196
2/19, 13:46			2/26, 18:33	2	671
				3	592
2/19, 14:42-	4	719		4	795
2/19, 19:45			2/26, 21:22-	1	216
			2/27, 09:27	2	37
2/20, 01:30-	4	317		3	200
2/20, 04:42				4	1,780
2/20, 15:25-	4	850	2/27, 09:35	1	92
2/20, 21:05			2/27, 18:43	2	73
				3	36
2/21, 15:27-	4	510		4	1,358
2/22, 01:20					
2/22, 11:01-	4	940	2/27, 21:04-	1	100
2/22, 23:03			2/28, 08:38	2	30
				3	37
				4	1,495

probability density functions of pulse width; however, these are not shown since they convey the same information as the cumulative distributions and the latter enable one to determine the median values more readily.

Appendix C contains cumulative probability distributions of the pulse width rate-of-change. Each individual rate-of-change was computed as the difference between the pulse width of an impulse function and the pulse width of the previous (1 second earlier) impulse. As with the pulse width data, probability density functions can be developed, but the cumulative distributions have proven to be more useful.

After the above analyses were completed, it seemed appropriate to examine the values of 2σ and pulse width rate-of-change over smaller time blocks for the period February 24-28. Therefore, these analyses were also performed for time blocks of approximately 1 to 4 hours over this period. In addition, certain analyses were performed over selected time blocks as deemed appropriate. The results of these analyses and further discussion of the probe data are presented in Section 6.

5.2 RSL Data

For the reasons given at the beginning of Section 5.1, the RSL data, like the probe data, were analyzed on a tape-by-tape basis. Although the RSL was monitored in both channels of the probe as well as in the four tropo receivers, only the latter have been systematically analyzed, since they, rather than the probe RSLs, are relevant to the performance of the radio system.

Both channels of the probe were calibrated in 5 dBm increments from -30 dBm to -110 dBm (noise) at the beginning of the test program by injecting known IF signal levels into the probe receiver. GTE personnel conducted RSL calibrations of the tropo receivers on a daily basis, which indicated that no significant drift of the calibrations or deviation from linearity occurred over the 2-week period during which ITS collected data. The tropo receivers were calibrated at power levels of -60 dBm, -80 dBm, and noise (approximately -100 dBm); calibration data were collected by ITS at the beginning of the test.

Appendix D contains cumulative probability distributions of RSL for the four tropo receivers on a tape-by-tape basis for test configuration 4 for all of the tapes. In addition, RSL distributions are presented for test

configurations 1, 2, and 3 for the last 10 tapes. The results are discussed in Section 6.

5.3 Spectral Data

Signal spectra from tropo receivers 1 and 4 were collected once per second using two commercial spectrum analyzers. Although the data processing software enables time averaged spectra to be computed, we have not developed software that would enable quantitative computations of spectral distortion, due to the fact that the characterization of spectral distortion is not straightforward and lies outside the scope of the present project. For this reason, the spectral data have not been systematically analyzed. However, it is interesting to observe the qualitative effects of propagation on the signal spectra. Figure 6 shows averages of 100 spectra of the PN channel probe signal with horizontal and vertical polarization during periods that are identified in Section 6 as periods of relatively good and relatively poor radio performance. No axes are shown in the figure; however, for a 10 Mbps QPSK signal the null-to-null width of the central spectral lobe is 20 MHz. Note that the sharp sidelobe structure that is present during favorable propagation conditions is almost entirely absent during conditions of poor performance.

5.4 Digital Performance Data

The digital performance data were processed by computing cumulative probability distributions of 1-second bit error rates (BER) for test configurations 1, 2, and 3. As explained above, no performance data were provided during test configuration 4 because the PN probe signal was transmitted over both diversity pairs. In calculating BER distributions, it is important that error-free seconds as well as errored seconds be taken into account. Since data were recorded only for those 5-second time blocks during which at least one bit error occurred, all seconds for which no data were recorded must be treated as error-free. For this reason, the BER distributions could only be computed over time blocks during which the radio system was continuously running, since periods of time during which the system was down (due to equipment failures and/or RSL calibrations) would otherwise be treated as error-free. As it turned out, the system was running continuously during

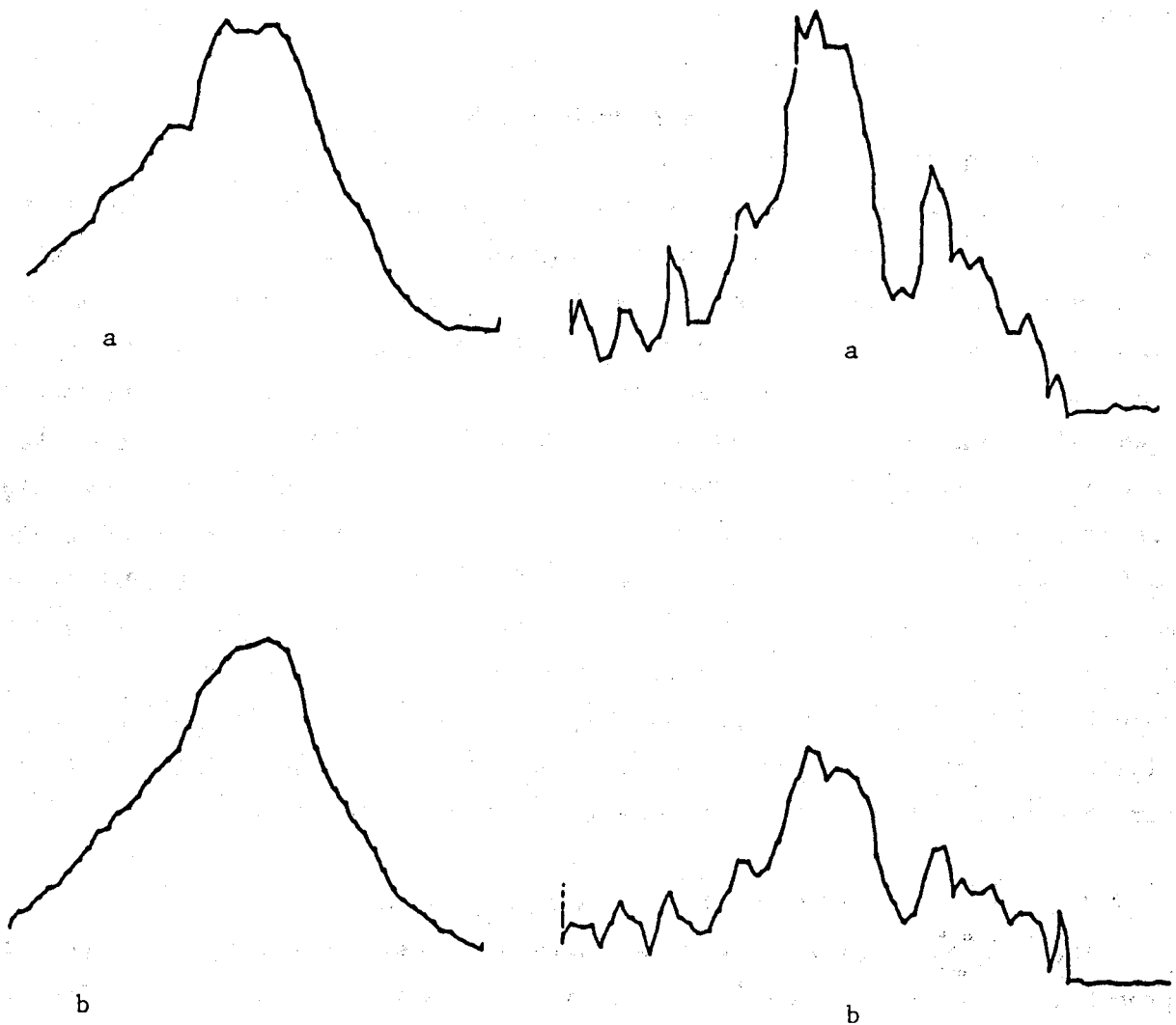


Figure 6. Signal spectra: Averages of 100 spectra of the PN channel probe signal. Left: (a) horizontal polarization and (b) vertical polarization during a period of poor propagation conditions. Right: (a) horizontal polarization and (b) vertical polarization during a period of good propagation conditions.

the time blocks spanned by some of the tapes. However, other tapes had to be split into as many as three time blocks.

Appendix E contains the cumulative probability distributions of 1-second BERs for test configurations 1, 2, and 3 over time blocks during which the system was continuously running. Each plot includes the start and end times for the analysis and the test configuration number (referred to as the mode number). Since transitions from one test configuration to another sometimes occurred during error-free periods when no data were recorded, the 1-second intervals within each such time period could not be unambiguously associated with a particular test configuration. These time periods were therefore excluded from the analyses, and the number of such seconds divided by the total number of seconds over which an analysis was performed is indicated in each plot as the "nebulosity," expressed as a percentage. The nebulosity can therefore be viewed as an uncertainty in the calculated BER distribution, and is typically a few percent.

The upper and lower limits of BER in the plots were determined by the bit rate of the T1 bank (1.544 Mbps) whose performance was monitored. Since one bit error is the smallest number of bit errors that can occur in any time interval, the smallest 1-second BER that could be measured was $1/(1.544 \times 10^6)$, or 6.48×10^{-7} . On the other hand, the Tau Tron instruments saturate at 10^5 bit errors. Therefore, the largest 1-second BER that could be measured was $10^5/(1.544 \times 10^6)$, or 6.48×10^{-2} .

5.5 Meteorological Data

The meteorological data consist of radiosonde messages that include values of atmospheric temperature, pressure, and dew point departure at various heights. These data can be used to compute the atmospheric refractive index using the Smith-Weintraub relation (Smith and Weintraub, 1953), which expresses the refractive index in terms of temperature, pressure, and water vapor content. The radiosonde data were used to develop profiles of temperature, relative humidity, and index of refraction. The results have been compiled in Appendix F.

Each plot is labeled by time and date and by the radiosonde launch site (Hannover, Lindenberg, or Berlin). Also, the elevations of the two ends of the link (Berlin and Bocksberg) are shown on the plots. In addition to the

profiles of temperature, relative humidity, and refractivity (measured in N-units), each plot shows two other profiles labeled as "normal" and "ducting." These latter two profiles illustrate the refractivity gradients that correspond to a normal atmosphere (-40 N-units/km) and to ducting conditions (-157 N-units/km).

6. DISCUSSION OF RESULTS

In this section the results of the data analyses are summarized and discussed. Emphasis has been placed on the relationships between propagation parameters and radio performance. Then the measured values of delay spread are compared with theoretical values derived by applying ray theory to the Berlin-Bocksberg path profile. This analysis indicates that the measured values of delay spread are often larger than theoretical expectations and provides additional insight into the effects of propagation on radio performance.

6.1 Summary of Propagation and Performance Data

For ease of presentation, the results of the data analyses in Appendixes A through E have been summarized in graphical form. Figures 7-16 each contain two sets of line plots; the upper and lower plots in each figure correspond to propagation and performance data, respectively. The performance (BER) data is discussed below; here we wish to focus attention on the propagation data.

Figure 7 shows a line plot of 2σ versus time on a tape-by-tape basis for test configuration 4. The values of 2σ were obtained from the plots in Appendix A; the number of samples used to compute each value is five times the number of 5-second records listed in Table 4. The value for each tape is plotted at the time that corresponds to the center of the time block for that tape.

The 2σ values for receiver 4 (vertical polarization) vary from approximately 90 ns to 140 ns, with the exception of the value on February 23 (170 ns), which corresponds to the unusual impulse functions that were mentioned in Section 5.1. For receiver 1 (horizontal polarization), the 2σ values are somewhat larger, varying from approximately 140 ns to 180 ns.

When interpreting delay spread measurements, it should be recognized that the measured impulse response is actually the convolution of the impulse response of the transmission channel with the impulse response of the PN probe

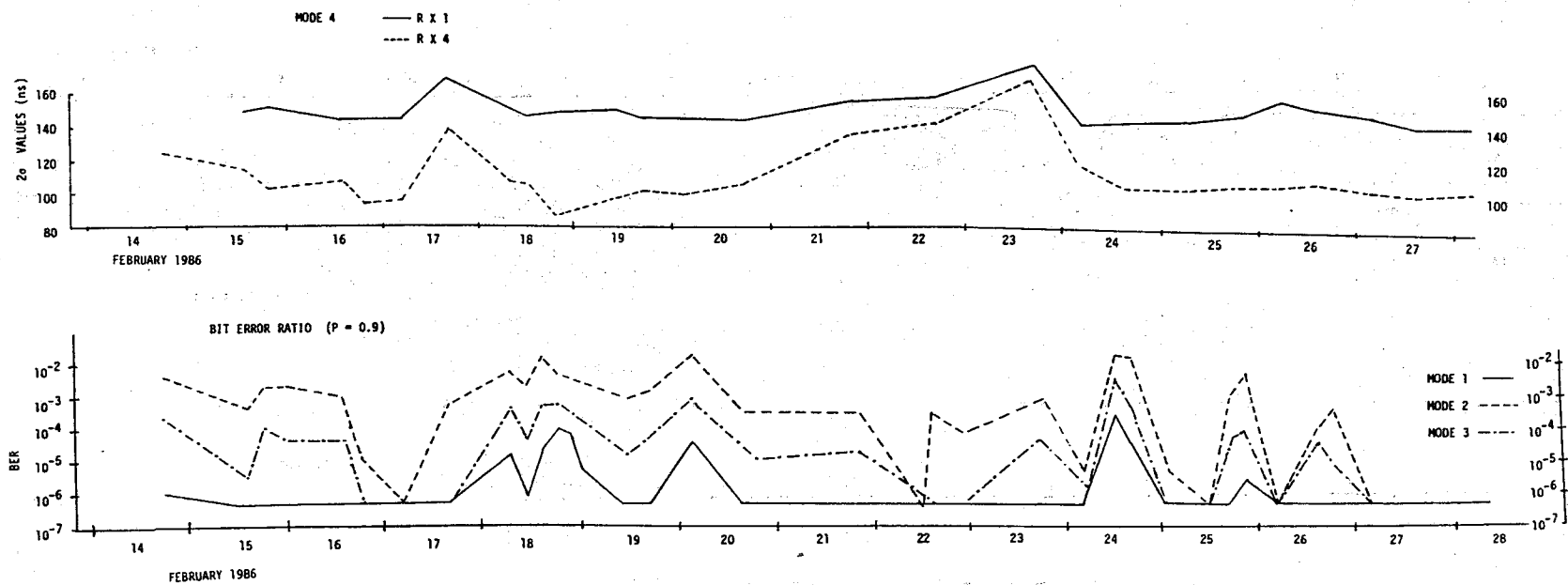


Figure 7. Values of 2σ and BER, February 14-28, 1986.

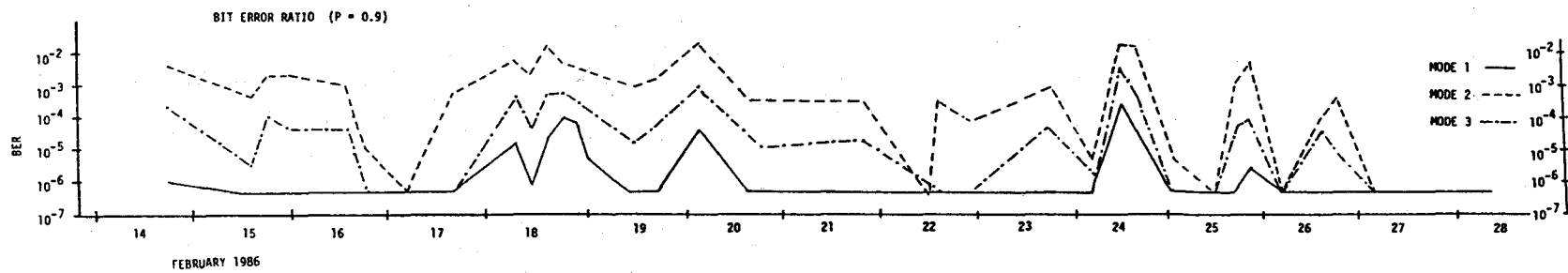
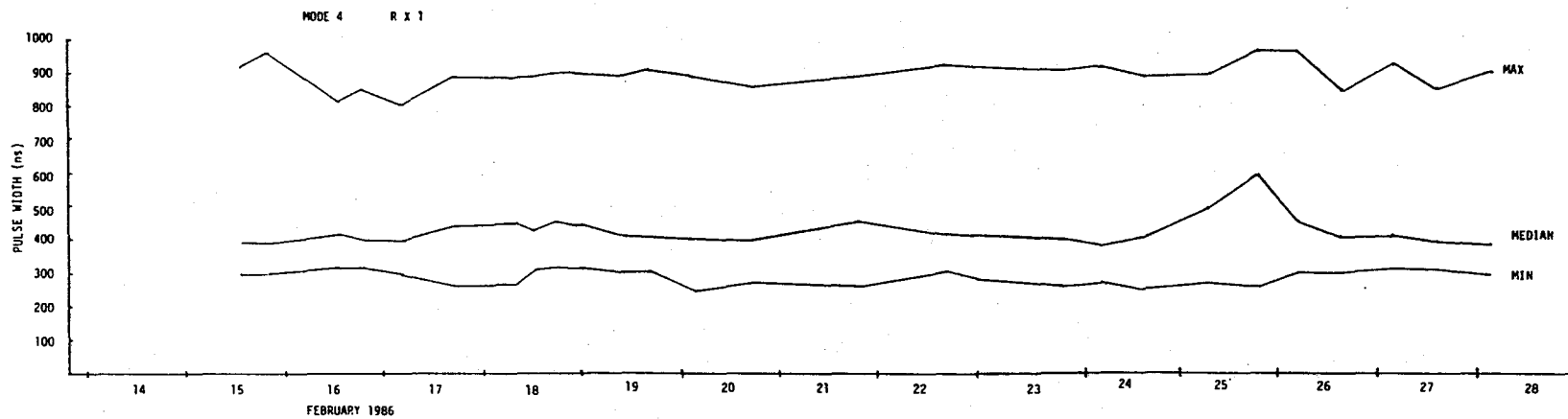


Figure 8. Pulse width, receiver 1 and BER, February 14-28, 1986.

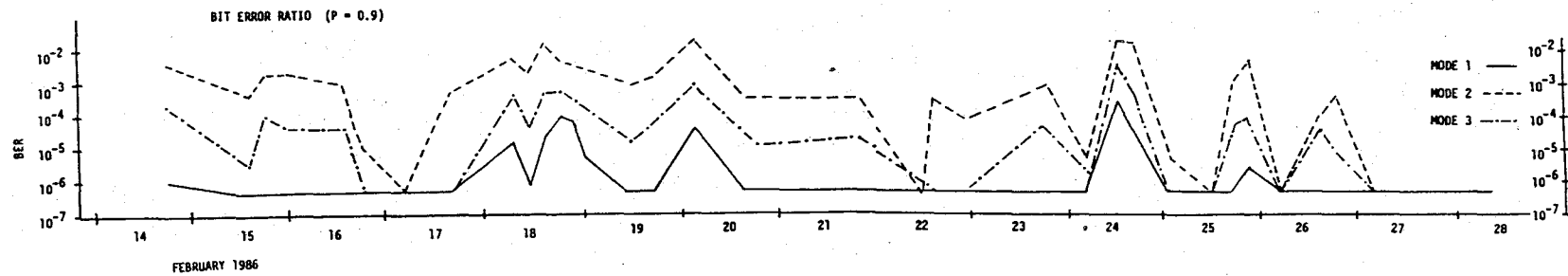
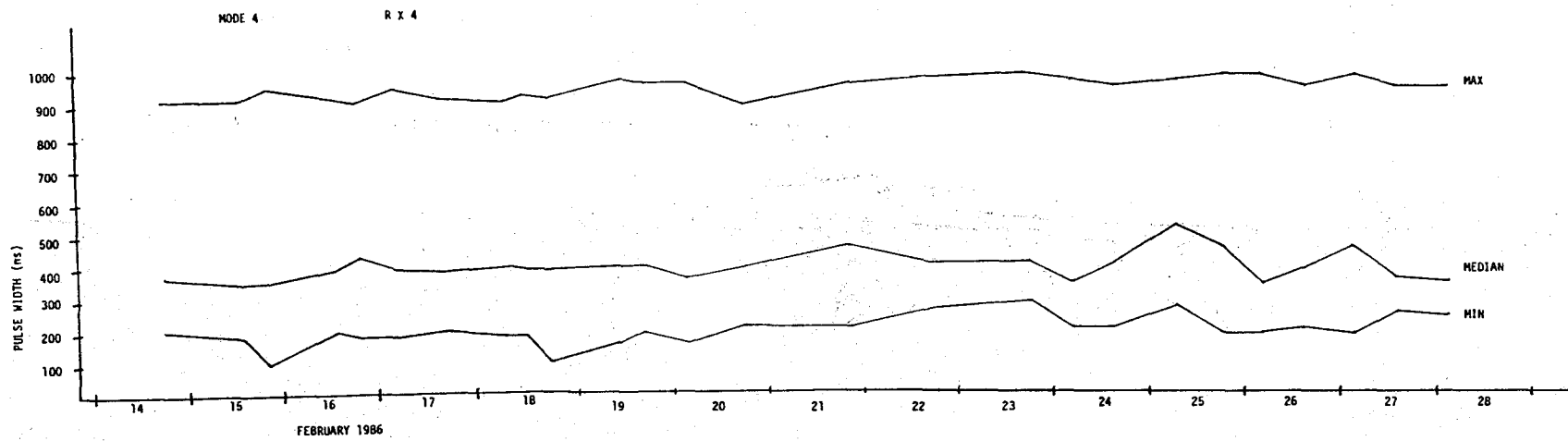


Figure 9. Pulse width, receiver 4 and BER, February 14-28, 1986.

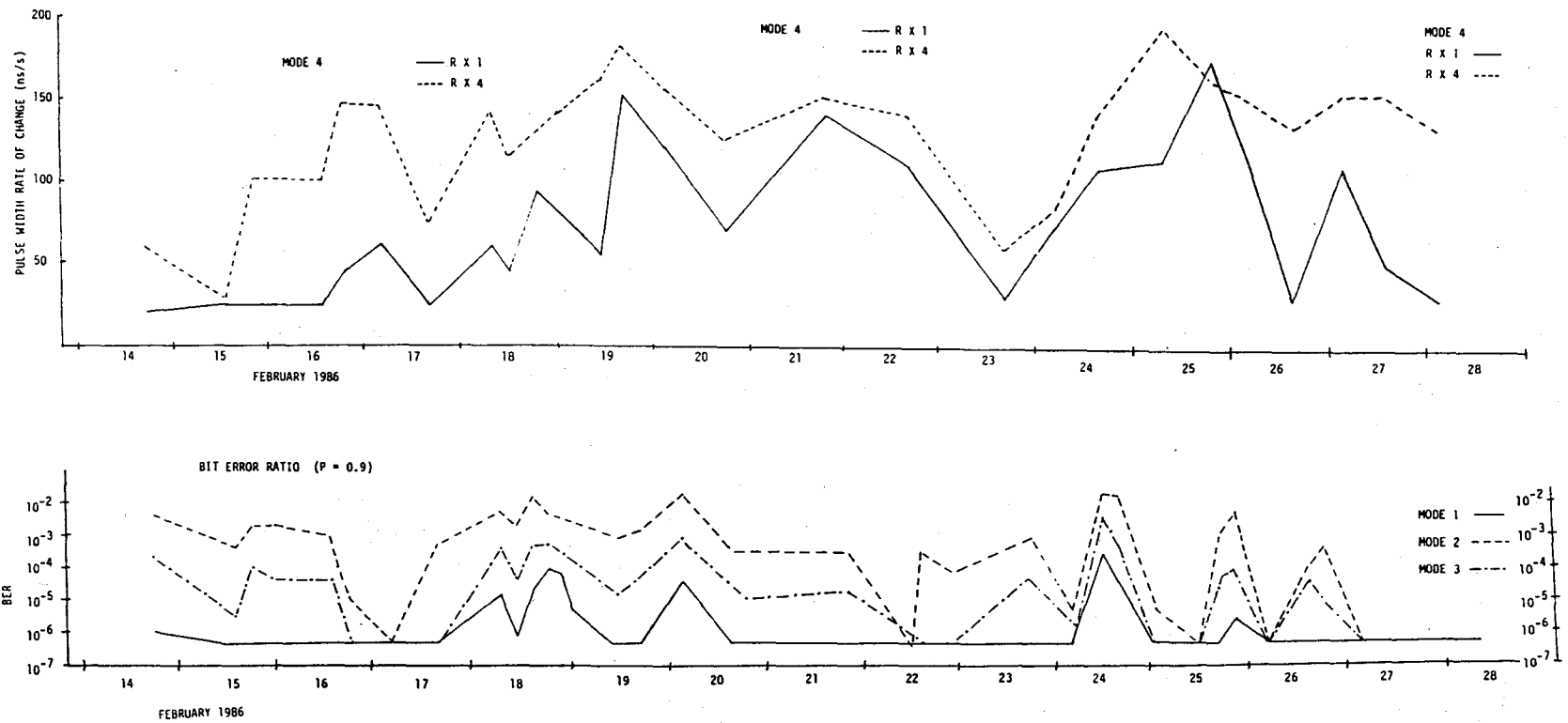


Figure 10. Pulse width rate of change and BER, February 14-28, 1986.

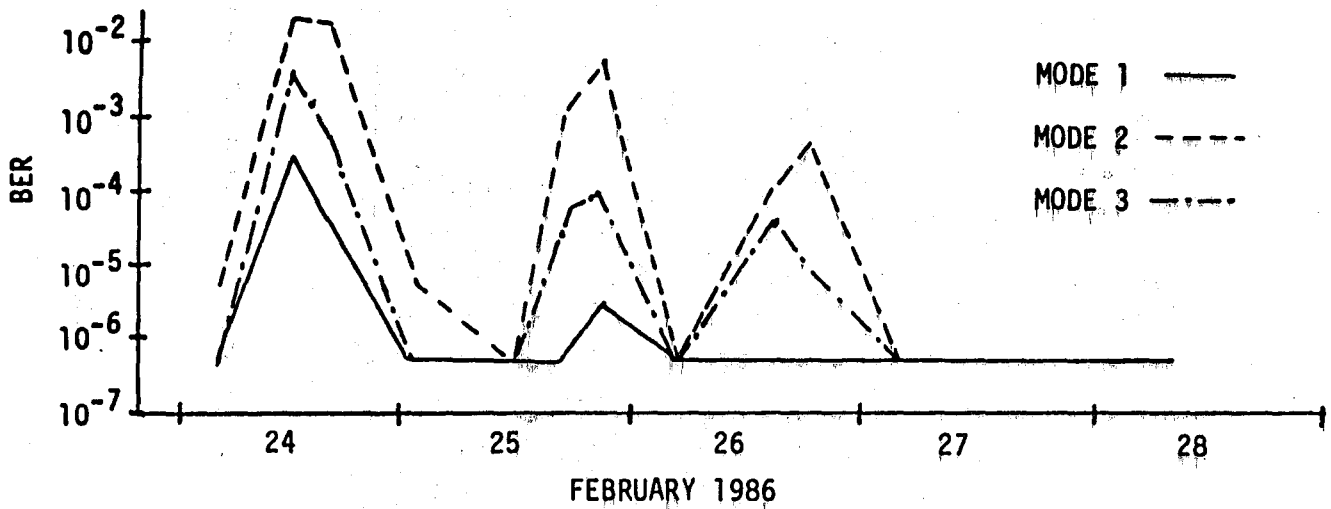
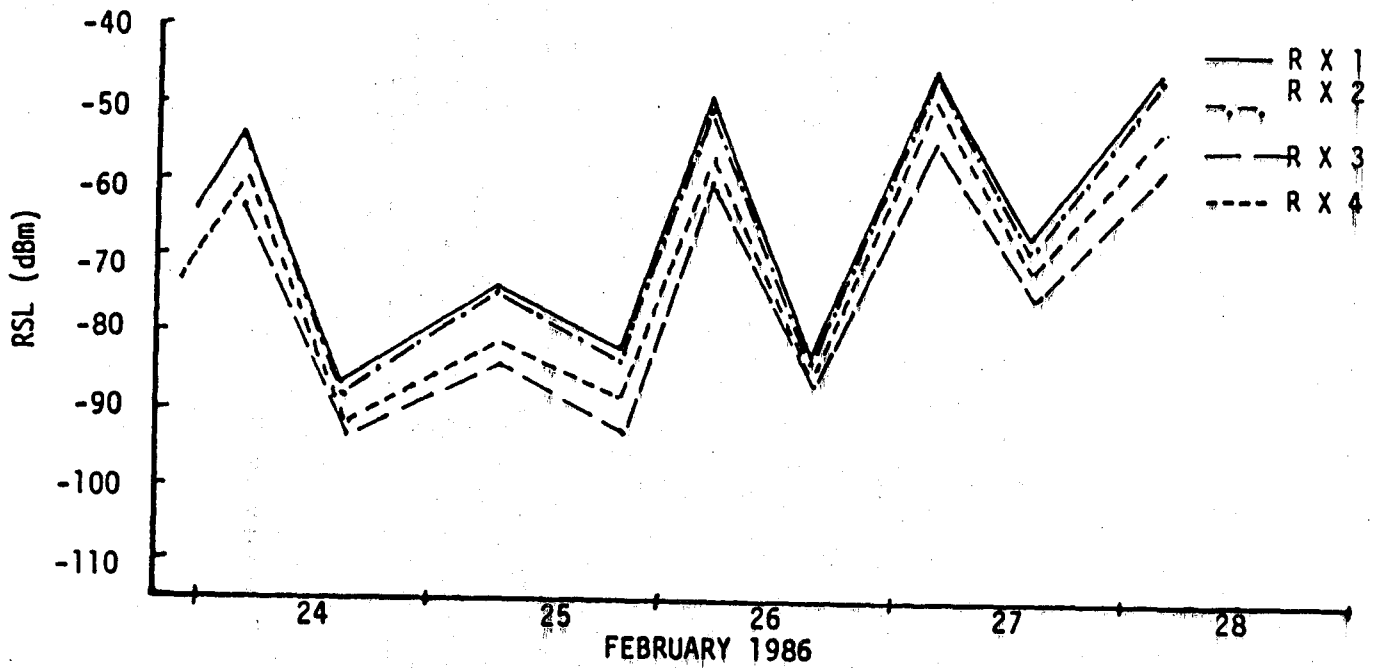


Figure 11. Received signal level (medians), receivers 1 through 4 and BER, February 24-28, 1986.

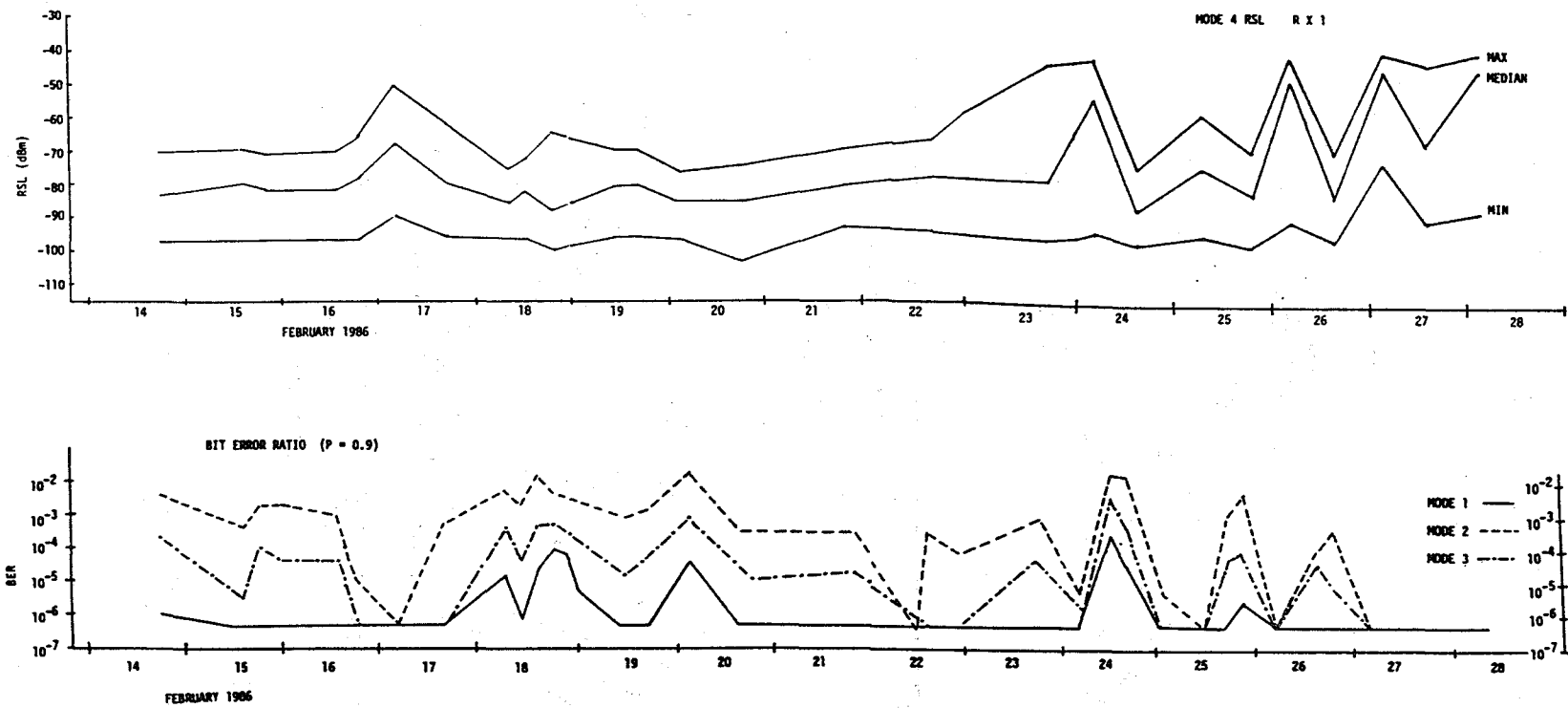


Figure 12. Received signal level, receiver 1 and BER, February 14-28, 1986.

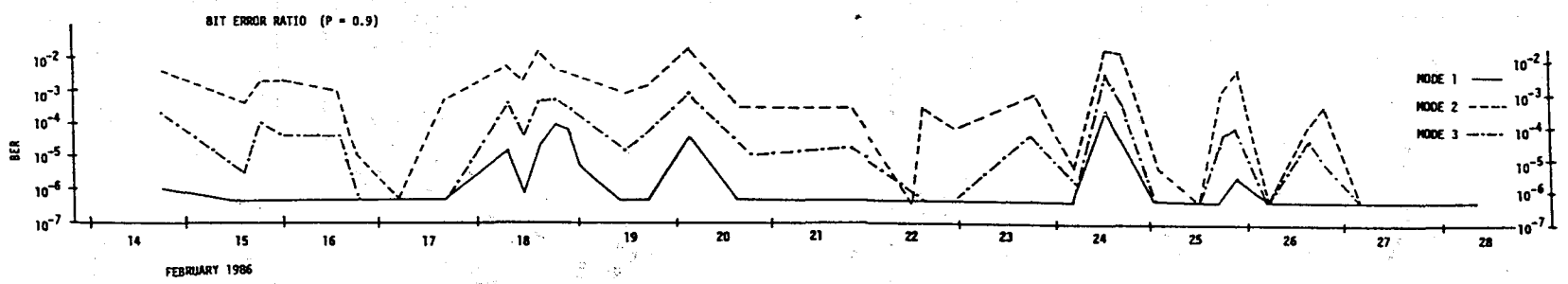
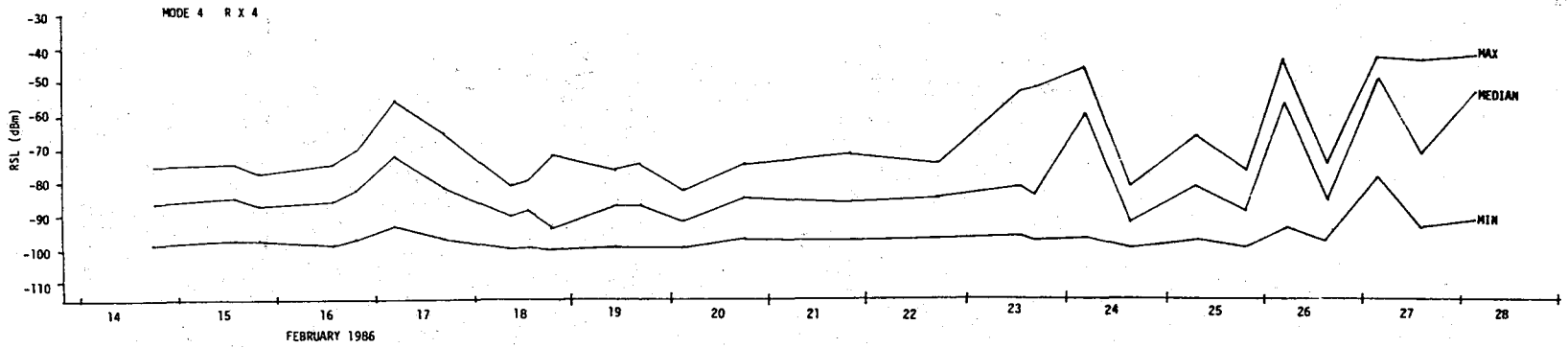


Figure 13. Received signal level, receiver 4 and BER, February 14-28, 1986.

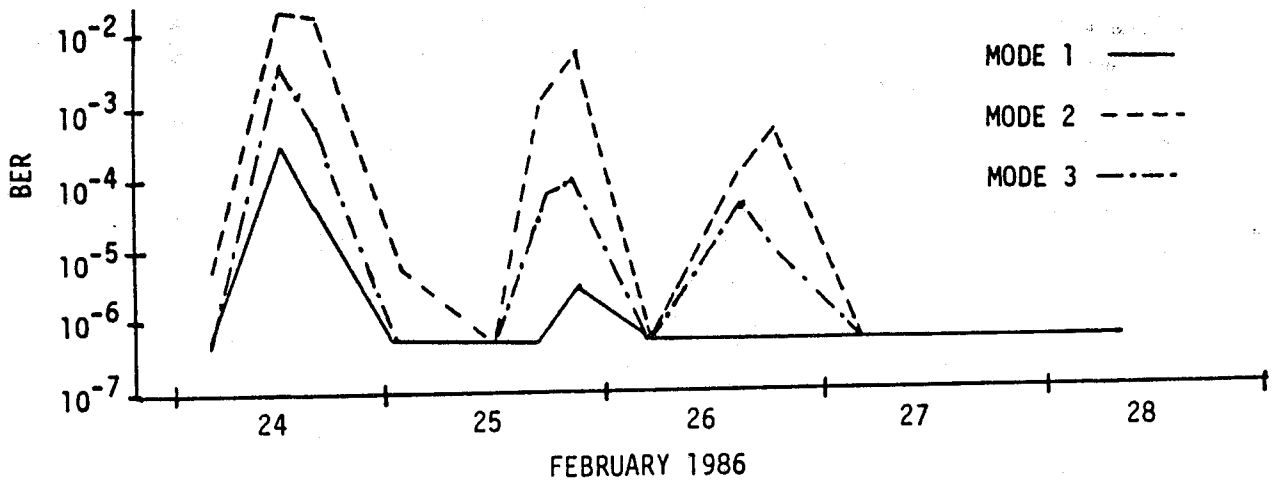
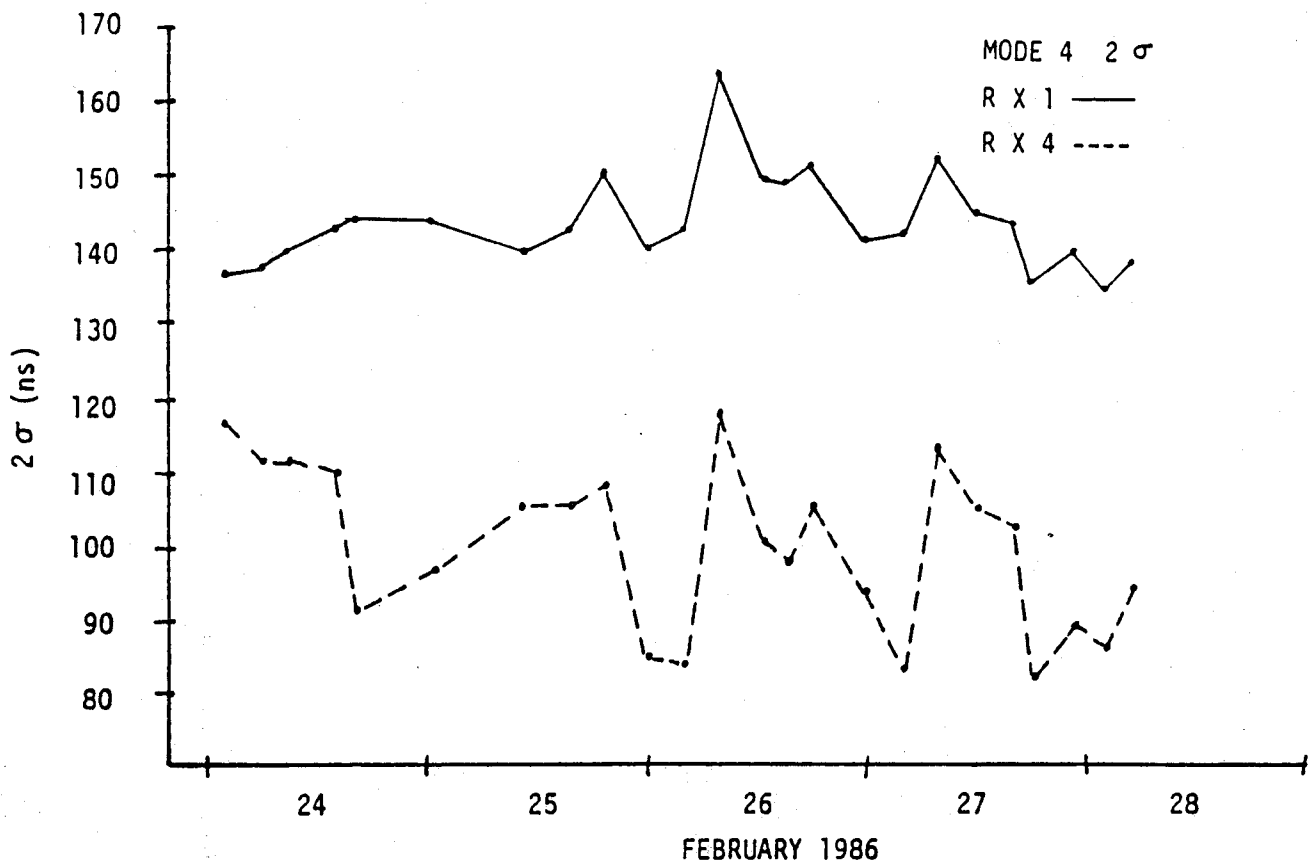


Figure 14. Values of 2σ and BER, February 24-28, 1986.

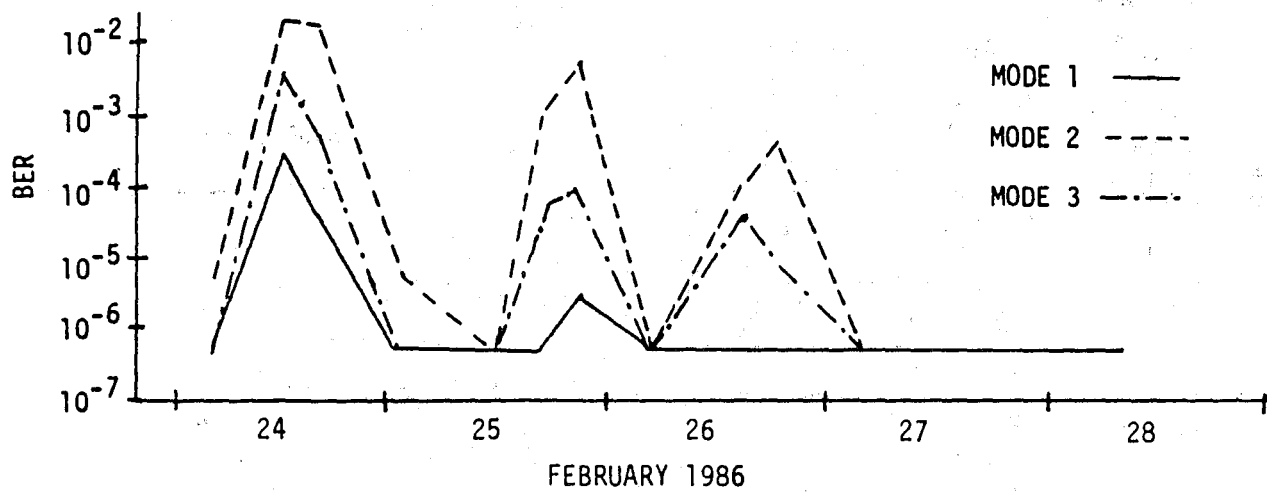
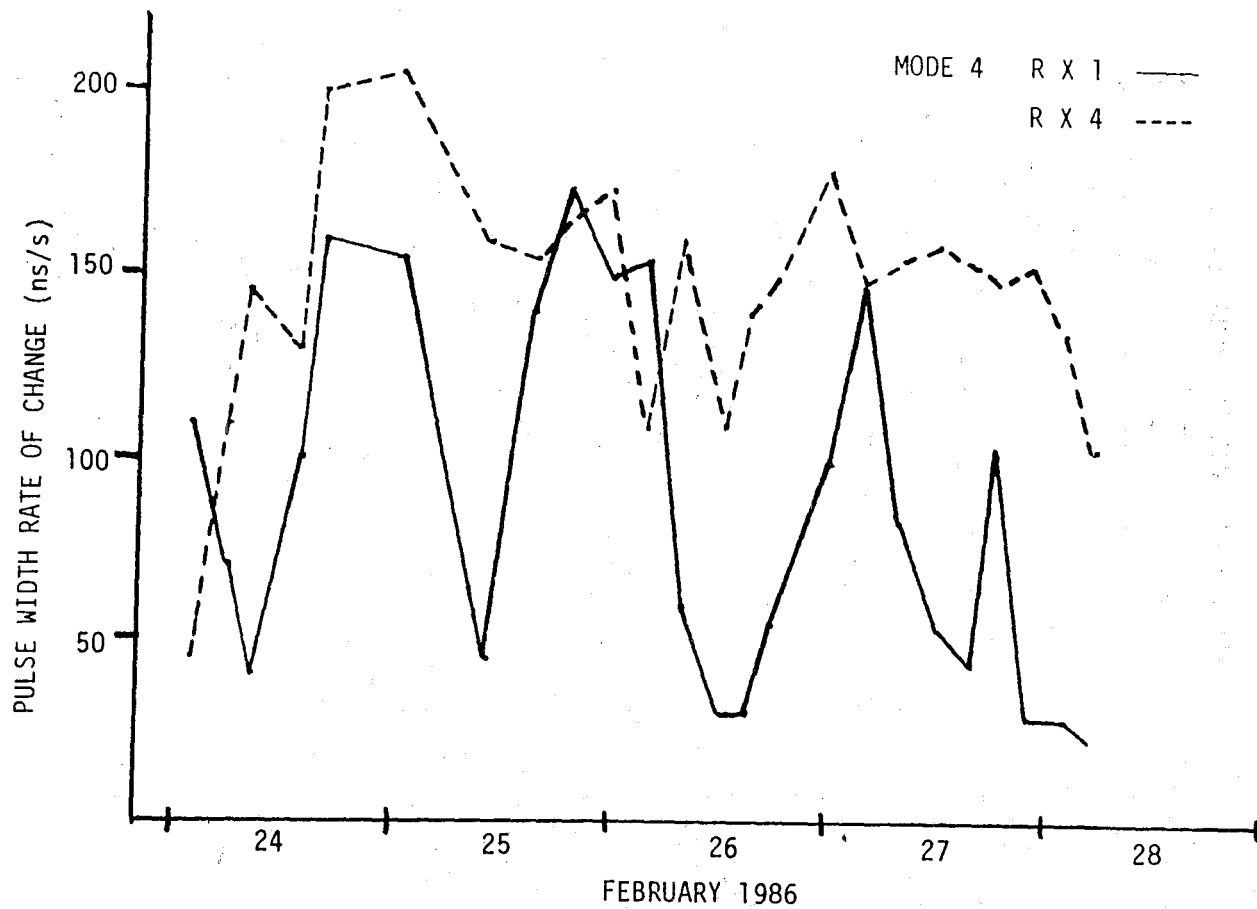


Figure 15. Pulse width rate of change and BER, February 24-28, 1986.

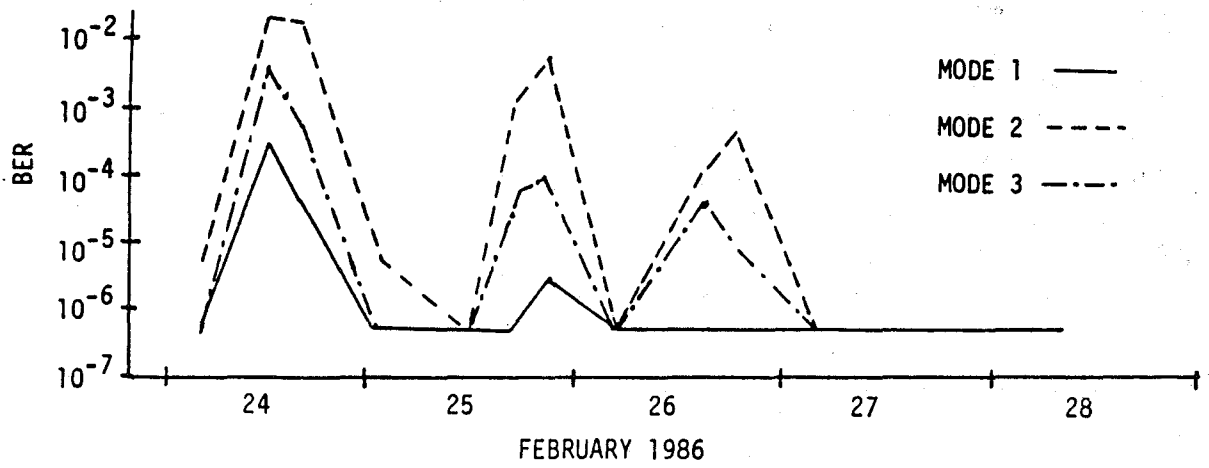
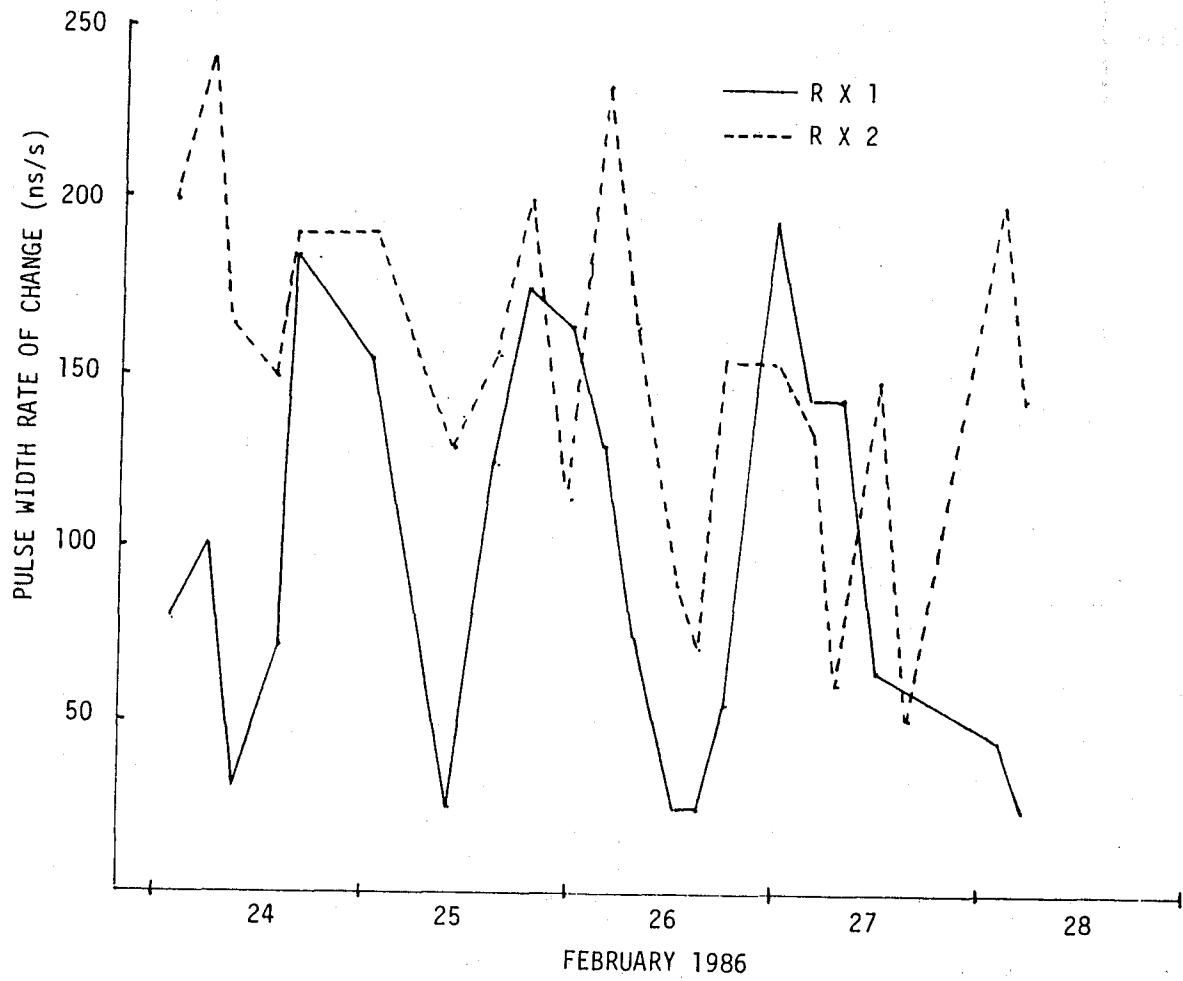


Figure 16. Pulse width rate of change, Mode 2 and BER, February 24-28, 1986.

used to make the measurement. The probe response is the autocorrelation function of the PN code, which is a triangular pulse whose base width is equal to two PN bit times (200 ns for a 10 Mbps clock rate). The power impulse response of the probe is, therefore, the square of the PN autocorrelation function. It is straightforward to calculate 2σ (twice the standard deviation) for such a pulse: the result is 63.2 ns. Thus, a nondispersive channel would have a measured 2σ equal to 63.2 ns.

If one attributes the multipath dispersion of the transmission channel to the difference between the measured 2σ and the value of 2σ that would be measured for a nondispersive channel (63.2 ns), the results presented herein imply multipath dispersions that vary from less than 30 ns to greater than 100 ns. Expressed in terms of the symbol time T (200 ns), $2\sigma/T$ varies from approximately 0.15 to 0.5. From this point of view, the curves in Figure 1 that show BER versus $2\sigma/T$ for the MD-918 imply that the median values of multipath dispersion encountered on the Berlin-Bocksborg link are well within the dynamic range of adaptive equalizers in the modem.

Figures 8 and 9 contain line plots of the pulse widths for receivers 1 and 4, respectively, for test configuration 4. Each figure shows three plots of pulse width, which correspond to the minimum, median, and maximum values of pulse width, obtained from the distributions in Appendix B. Although the maximum pulse widths are greater (by approximately 50 ns) for receiver 4 (vertical polarization), the median and minimum pulse widths are greater (by approximately 50 ns) for receiver 1 (horizontal polarization).

Line plots of the median pulse width rates-of-change for receivers 1 and 4 (test configuration 4) are shown in Figure 10. The median values were obtained from the cumulative distributions in Appendix C and require some explanation. The distributions have odd symmetry about zero rate-of-change, and, therefore, the median values are also zero. In order to parameterize the pulse width dynamics, the values corresponding to a cumulative probability of 0.75 are plotted in the figures. Due to the symmetry of the distributions, these values are actually the medians of the absolute value of the pulse width rate-of-change.

The median rates-of-change vary from approximately 20 ns/s to 200 ns/s and are greater for receiver 4. In view of the fact that median pulse widths are

typically on the order of 400 ns, these results indicate that the troposcatter channel is dynamic over time scales on the order of or less than 1 second.

Figure 11 shows plots of the median RSLs (obtained from the distributions in Appendix D) for receivers 1-4 (test configuration 4) for the period February 24-28. The trends are similar in all four plots. However, receiver 1 had the highest RSLs. Receiver 2 was down from 1 by approximately 1 dB, receiver 3 was down from 1 by approximately 9 dB, and receiver 4 was down from 1 by approximately 5 dB. Thus, the horizontally polarized diversity pair (receivers 1 and 2) had, on the average, approximately 7 dB greater RSL than did the vertically polarized diversity pair.

Figures 12 and 13 show RSL plots for receivers 1 and 4, respectively, for the period February 14-28 (test configuration 4). Each figure has three RSL plots, corresponding to the minimum, median, and maximum values of RSL obtained from the cumulative distributions in Appendix D. Although RSL has not been converted to path loss, the median RSLs vary from approximately -45 dBm to -90 dBm, corresponding to a 45 dB variation in path loss.

The BER data for all three diversity combinations are summarized in the lower portions of Figures 7-16. The values that are plotted correspond to a probability of 0.9 in the distributions in Appendix E. A probability of 0.9 was chosen rather than 0.5 (corresponding to the median value) because the median value was often less than the measurement resolution (6.48×10^{-7}).

As expected, the quadruple diversity had lower BERs than either of the dual diversity configurations. However, the vertically polarized diversity pair consistently had higher BERs than the horizontally polarized diversity pair. Thus, the horizontal diversity pair had higher RSLs, larger delay spreads, and lower BERs than the vertical diversity. Since a higher RSL is expected to improve performance, whereas a larger delay spread is expected to degrade performance, it appears that the differences in RSL (between the two diversities) influenced performance more strongly than differences in delay spread.

Furthermore, comparing the BER data with the delay spread results in Figures 7-9 and the RSL data in Figures 11-13 indicates that within a given channel, variations in RSL correlate with performance more closely than variations in delay spread. For example, the periods of good performance on the mornings of February 17, 24, 25, and 26 are accompanied by corresponding

rises in RSL, whereas the 2σ and pulse width values are not particularly small at these times (with the exception of the 2σ values on the morning of February 17). Also, the exceptionally large delay spreads on February 23 do not correspond to particularly poor performance. However, it should be recognized that the adaptive equalization in the MD-918 is designed to compensate for multipath dispersion, which is consistent with the observation that delay spread and performance are not well correlated.

On the other hand, the gross variations in the pulse width rates-of-change in Figure 10 appear to track the variations in BER. The fact that the rates-of-change were generally greater for receiver 4 (higher BERs) than for receiver 1 (lower BERs) corroborates the view that greater rates-of-change are associated with higher BERs.

In order to investigate the variations in delay spread with finer time resolution, values of 2σ and pulse width rates-of-change were computed for the period February 24-28 using time blocks of 1 to 4 hours. The results are shown in Figures 14 and 15. Although the 2σ values do not appear to correlate well with performance, the gross variations in the pulse width rates-of-change appear to track the variations in BER over this period. This trend can also be seen in Figure 16, which shows the pulse width rates-of-change for the same time blocks as the previous two figures, but for test configuration 2 (receivers 1 and 2, both horizontal polarization). Note that the peaks in the rates-of-change are larger for test configuration 2 than for 4. This further supports the idea that greater rates-of-change correspond to higher BER, since in test configuration 2 delay spread data were collected only during those 5-second blocks that contained errored seconds, whereas data were collected continuously in test configuration 4.

The meteorological profiles in Appendix F have been examined for features that correlate with periods of good and poor performance; however, no obvious trends have been noted. The surface refractivity showed little variation during the period February 14-28, and was close to 310 N-units. This value is consistent with other refractivity measurements in continental, temperate climates during the winter season (Bean et al., 1966; CCIR, 1978).

The refractivity gradients were generally close to that of a standard atmosphere (-40 N-units/km), with a tendency to be slightly subrefractive (smaller gradients). Occasional discontinuities in the refractivity gradient

(indicating the presence of atmospheric layers) appear in the refractivity profiles, and are often accompanied by temperature inversions. However, these inversions and/or layers do not appear to correlate in any obvious way with periods of good or poor performance. Similarly, no unusual features are apparent in the profiles during periods of unusually large or small delay spread.

It should be recognized that the radiosonde data are rather sparse; in fact, adjacent data points in the profiles are often separated by several hundred meters. Thus, the presence of thin reflecting/refracting layers would not generally appear in the profiles. Moreover, seasonal variations in refractivity could not be observed over the two week period during which data were collected.

6.2 Comparison of Measured and Theoretical Values of Delay Spread

The values of delay spread reported herein are comparable to those found by previous measurements over other troposcatter paths. For example, Sherwood and Suyemoto (1977) reported values of 2σ which varied from 50 ns to 370 ns with a mean of 180 ns, and Hubbard (1983, op. cit.), who reported values of pulse width measured with the PN channel probe, found values ranging from less than 200 ns to greater than 1 μ s. However, Sherwood and Suyemoto pointed out that their measured values of 2σ were somewhat larger than those predicted by the Bello (1969) channel model when standard input assumptions were made.

The Bello model, and variations of it, use turbulent scattering theory to compute the differential scattering cross section in the common volume, thereby determining the amount of scattered energy received from each point in the common volume. Ray tracing is then used to compute the relative delay times from each point in the common volume and the power impulse function is developed by integrating the received power over the common volume for each value of delay time. The delay spread can therefore be estimated by calculating the spread in arrival times of rays propagating from the transmitter to the receiver via scattering in the common volume.

The location of the common volume for the Berlin-Bocksberg link is illustrated with the path profile in Figure 2. The upper two rays correspond to the half-power beamwidths of the antenna patterns and the lower two rays

correspond to the antenna boresites. The common volume is the region enclosed by these rays. The take-off angles of the rays were determined by positioning the boresites on the radio horizons. For 30-foot antennas operating in the 4.5-5.0 GHz band, the half-power beamwidths are approximately 0.5 degrees. The rays corresponding to the half-power beamwidths therefore have take-off angles 0.25 degrees above boresite. Using this construction, the positions of the extremities of the common volume can be obtained directly from the path profile in terms of elevation above sea level and lateral distance along the path.

The path lengths for the various rays were then calculated using the construction shown in Figure 17. The ray paths are assumed to be straight lines over an earth of effective radius R_e . For a standard atmosphere, $R_e = 8497$ km. The angle ϕ for a point in the common volume can be expressed in terms of its lateral distance d_c along the path as $\phi = d_c/R_e$. Applying the law of sines to the triangle in Figure 17 implies that the ray path length d_θ is given by

$$d_\theta = (R_e+h)\sin\phi / \cos(\theta-\phi),$$

where h is the antenna elevation and θ is the ray take-off angle measured downward from the horizontal.

It was found that the path length difference for rays propagating through the highest and lowest points in the common volume is only 1 m, implying a delay spread of only several ns. For the rays propagating through the two lateral extremes of the common volume (in the plane of the propagation path), the path length difference is 6 m, which translates into a delay spread of approximately 20 ns. Of course, this calculation does not take into account the lateral extent of the common volume transverse to the propagation path. However, it is easy to show that the delay spread due to lateral spreading of the beams is comparable to that due to spreading in the vertical dimension (≈ 1 ns). Thus, for pure troposcatter propagation one expects a measured value of 2σ which is approximately 20 ns greater than that measured for a nondispersive channel (63.2 ns), or approximately 85 ns.

This was occasionally observed for vertical polarization, in which case the power impulse function consisted of a symmetric peak with very little distortion in either the leading or trailing edges. The fact that much larger

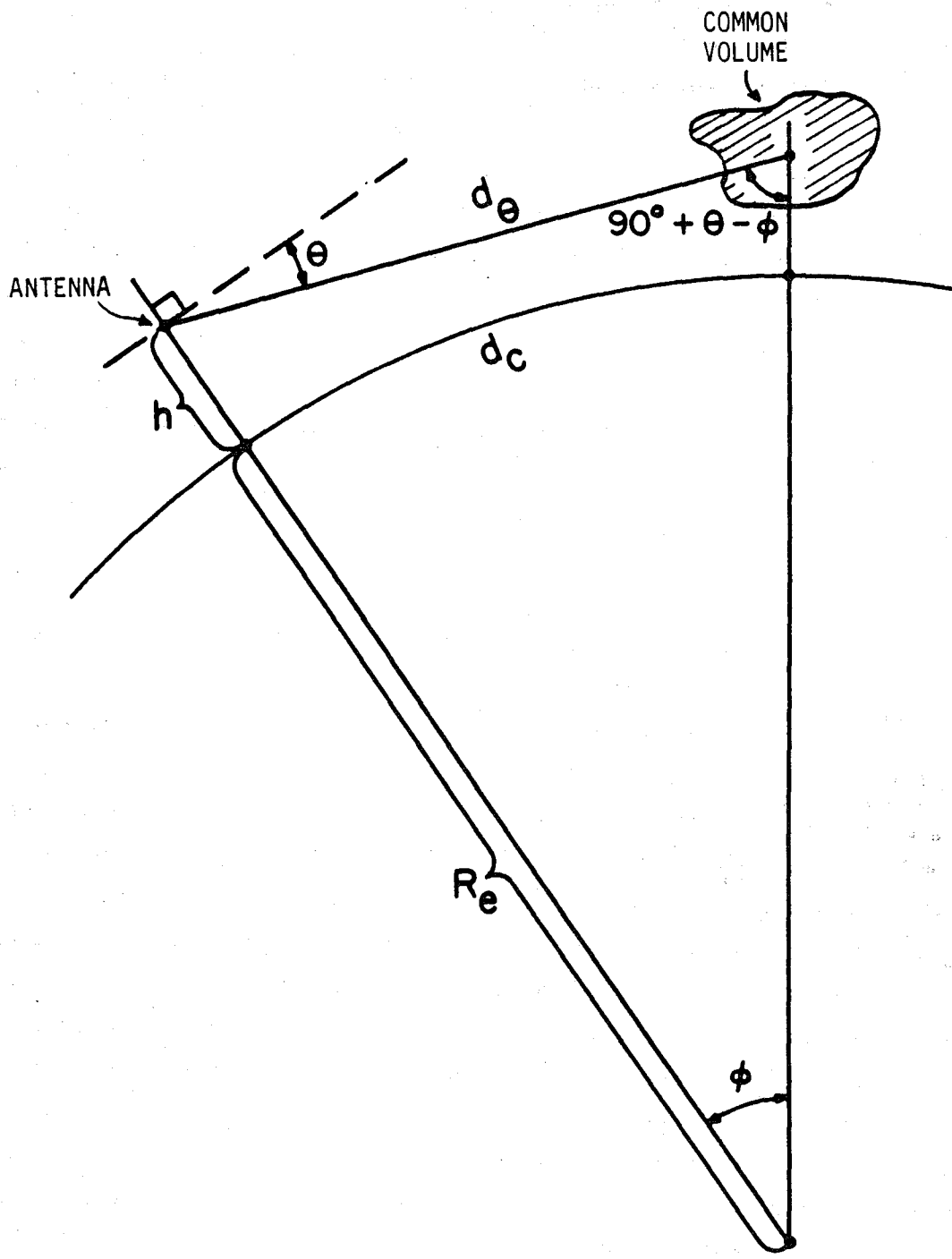


Figure 17. Geometry for path-length calculation.

values of 2σ were measured when shoulders appeared on the leading and/or trailing edges of the impulse functions suggests that these features were due to non-troposcatter modes of propagation. However, the ray tracing calculations discussed above imply that diffraction, foreground effects (if any are present), and/or reflections from atmospheric layers generate small (≈ 1 ns) contributions to delay spread, to be compared to discrepancies of tens of nanoseconds.

If the large delay spreads are not attributed to nontroposcatter modes of propagation, then a possible explanation is that fluctuations in the refractive index structure cause the ray paths to deviate from the straight lines shown in Figures 2 and 17, so that the common volume is substantially larger than that suggested by the naive ray tracing calculations discussed above. A second possibility is that fluctuations in channel conditions cause the time of arrival of signal energy to vary by tens of nanoseconds over the time interval during which the impulse response is measured. If this is the case, then the troposcatter channel is dynamic over time scales on the order of several milliseconds.

The question remains as to why the horizontally polarized diversity pair consistently had larger delay spreads and higher RSLs than the vertically polarized diversity pair. It was pointed out in Section 5 that several hardware problems with the radio system were discovered and fixed after the data discussed herein were obtained. Also, the horizontally and vertically polarized signals were transmitted from different antennas at Bocksberg.

7. CONCLUSIONS

The primary objective of this work, to obtain delay spread measurements in conjunction with digital performance data over the Berlin-Bocksberg tropo link, has been met. The PN channel probe proved to be quite valuable for this purpose; various propagation modes can readily be discerned from the impulse response data and dynamic changes in the transmission channel can be observed and analyzed.

The values of delay spread that were obtained over this link are comparable to those obtained from previous measurements over other troposcatter paths and are often larger than the value expected for pure troposcatter propagation. In particular, the values of the two-sided rms width of the power

impulse function, 2σ , varied from less than 90 ns to 180 ns, to be compared with a value of approximately 85 ns expected for pure troposcatter propagation. Ray tracing calculations suggest that the unexpectedly large values of delay spread are due to fluctuations in the refractive index structure over the link, although this could not be verified from the radiosonde data that were collected.

The variety of data that were collected result in a large number of possible analyses, not all of which were performed due to time and budget constraints. For example, scatter plots and correlation coefficients between propagation and performance data were not generated. However, the analyses that were performed illustrate the trends and gross relationships in the data. Variations in performance appeared to correlate well with variations in RSL, as expected. Delay spread did not correlate well with performance, which implies that the multipath dispersion encountered over the Berlin-Bocksberg link is within the dynamic range of the adaptive equalization of the MD-918.

It was also observed that channel dynamics is related to radio performance; in particular, periods of relatively poor performance were accompanied by large values (greater than 150 ns/s) of the pulse width rate-of-change. This indicates that the troposcatter channel is dynamic over time scales on the order of or less than 1 second and portends the need to take into account channel dynamics in the design of adaptive equalization techniques. Such an approach could greatly enhance the capability to combat the effects of multipath dispersion on digital transmission systems.

8. ACKNOWLEDGMENTS

The authors wish to acknowledge R.W. Hubbard for his many contributions and helpful suggestions throughout the course of this work. They also wish to acknowledge the contributions of L.E. Pratt in developing the hardware for the channel probe; E.M. Gray for her assistance in preparing the figures and appendixes; S. Bernal for manuscript preparation; GTE personnel for their cooperation during the test and acceptance program; and helpful discussions with W. Cybrowski, J.A. Hoffmeyer, G.A. Hufford, and S. Matsuura. This work was supported by the U.S. Army.

9. REFERENCES

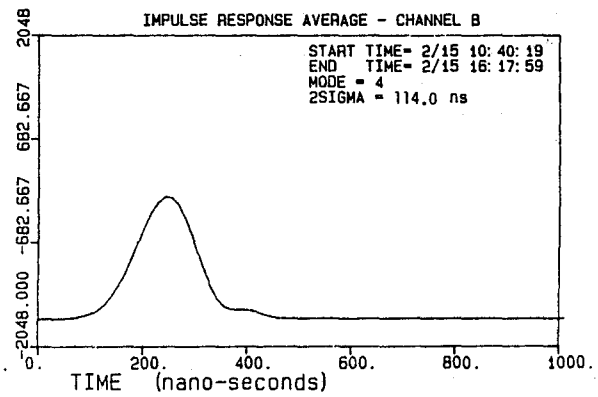
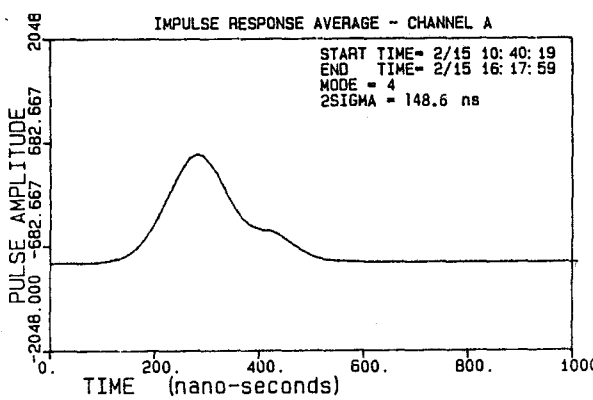
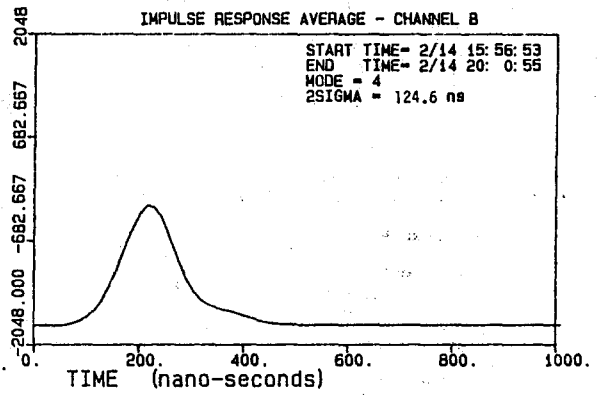
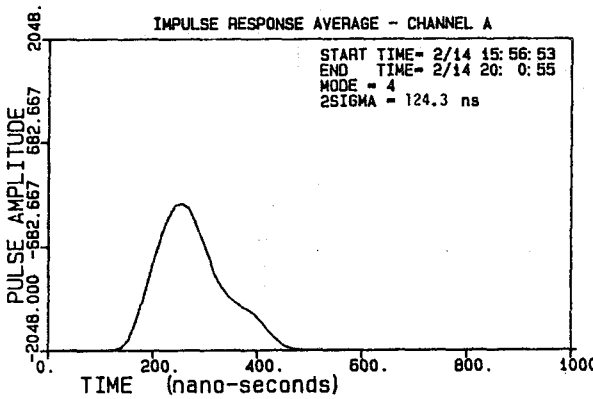
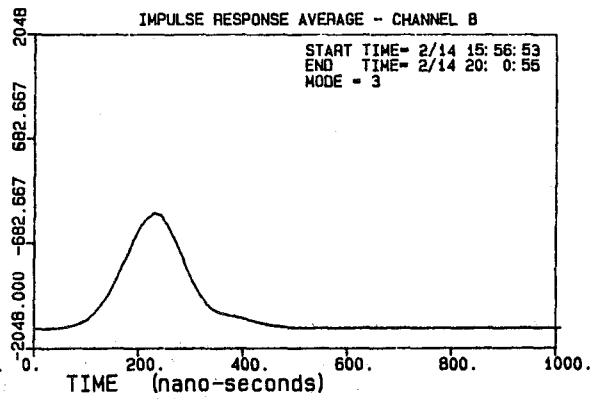
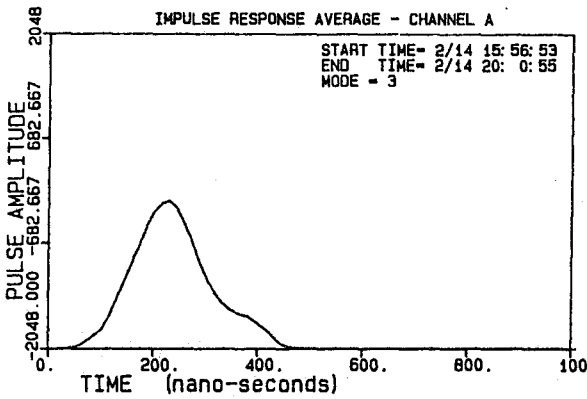
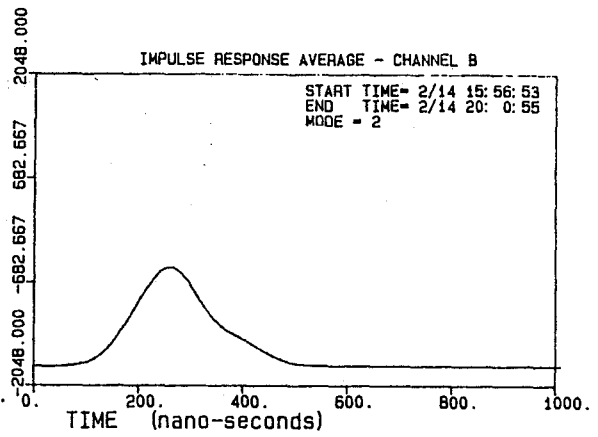
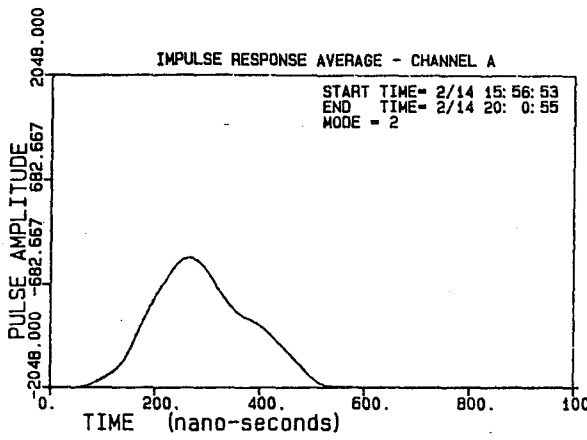
- Anderson, C.W., S. Barber, and R. Patel (1978), The effect of selective fading on digital radio, International Commun. Conf., Toronto, Canada, June.
- Barnett, W.I. (1978), Measured performance of a high capacity 6 GHz digital radio system, International Commun. Conf., Toronto, Canada, June.
- Barrow, B.B., F.G. Abraham, W.M. Cowan Jr., and R.M. Gallant (1969), Indirect atmospheric measurements utilizing RAKE troposcatter techniques, Proc. IEEE 57, April, pp. 537-551.
- Bean, B.R., B.A. Cahoon, C.A. Samson, and G.D. Thayer (1966), A World Atlas of Atmospheric Radio Refractivity, ESSA Monograph 1, (NTIS Order No. AD 648-805).
- Bello, P.A. (1969), A troposcatter channel model, IEEE Trans. Commun. Tech. COM-17, April, pp. 130-137.
- CCIR (1978), Radiometeorological data, Report 563-1, Vol. V, Propagation in Non-ionized Media, Recommendations and Reports of the CCIR, 1978, pp. 69-89.
- Dougherty, H.T., and W.J. Hartman (1977), Performance of a 400 Mbit/s system over a line-of-sight path, IEEE Trans. Commun. COM-25, No. 4, April, pp. 427-432.
- Gadoury, J.B. (1983), Error performance characterization study of a digital troposcatter modem (MD-918/GRC), Final Tech. Report DCA100-82-C-0031, July.
- Hoffmeyer, J.A., L.E. Pratt, and T.J. Riley (1986), Performance evaluation of LOS microwave radios using a channel simulator, IEEE 1986 Military Commun. Conf., Monterey, CA, No. 4.3.
- Hubbard, R.W. (1984), A review of atmospheric multipath measurements and digital system performance, NATO AGARD Conf. Proc. No. 363, Propagation Influences on Digital Transmission Systems: Problems and Solutions, Athens, Greece, No. 10, June.
- Linfield, R.F., R.W. Hubbard, and L.E. Pratt (1976), Transmission channel characterization by impulse response measurements, OT Report 76-96, August, (NTIS Order No. PB 258-577).
- Price, R., and P.E. Green, Jr. (1958), A communication technique for multipath channels, Proc. IRE 46, March, pp. 555-570.

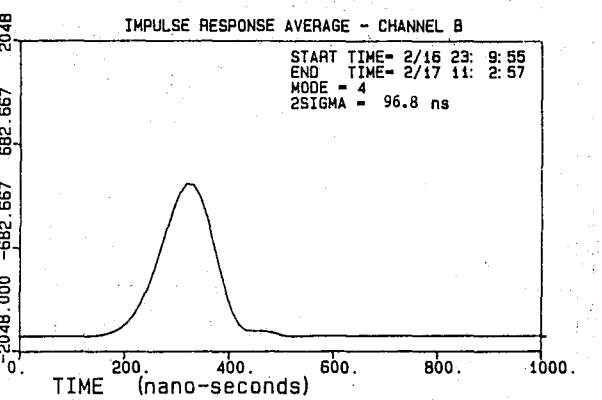
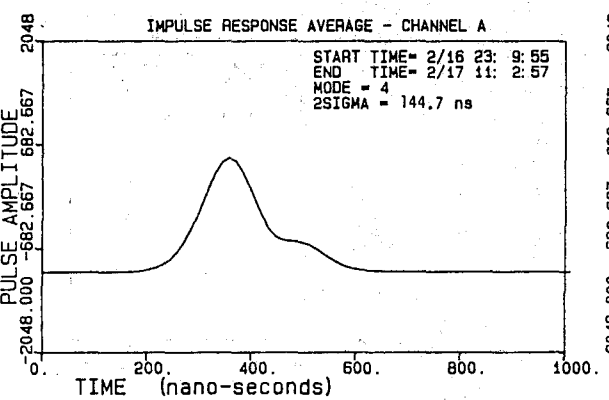
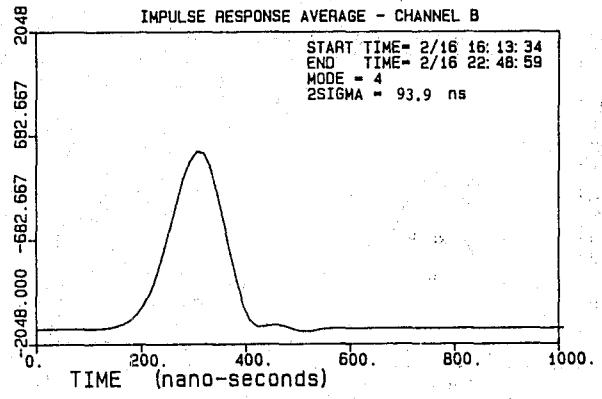
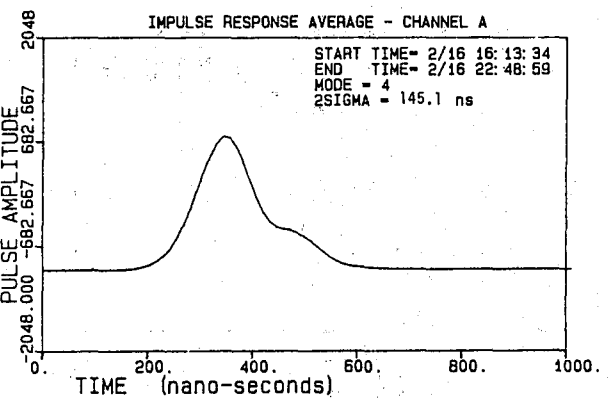
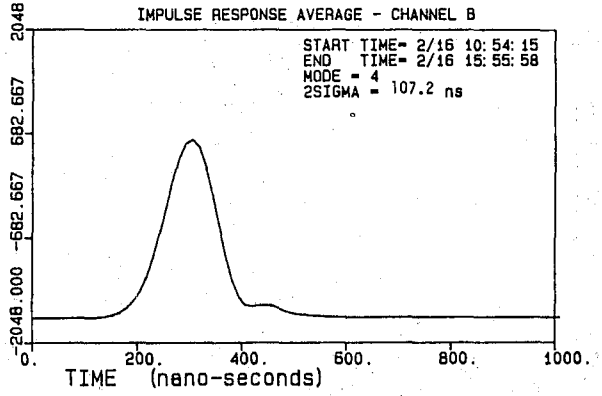
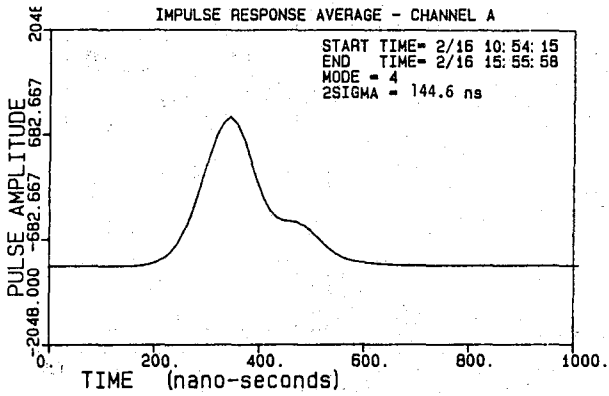
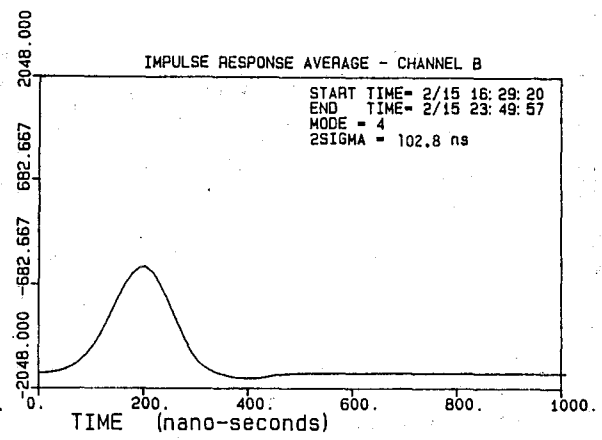
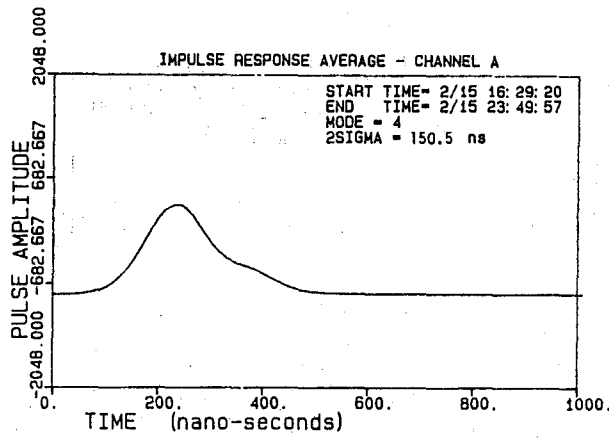
Sherwood, A., and L. Suyemoto (1977), Multipath measurements over troposcatter paths, USAF/ESD, Report No. ESD TR-77-252.

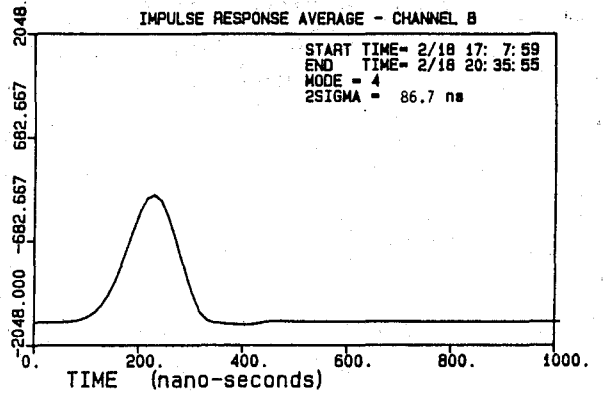
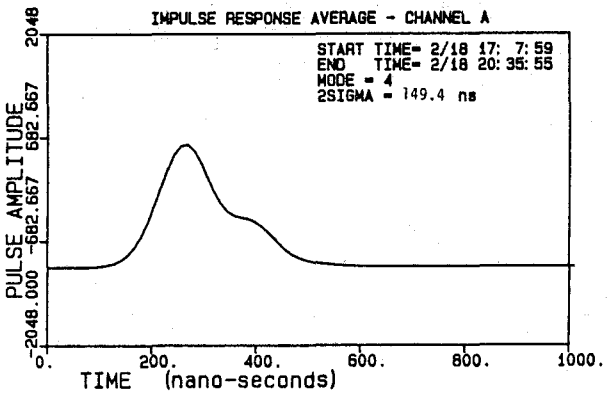
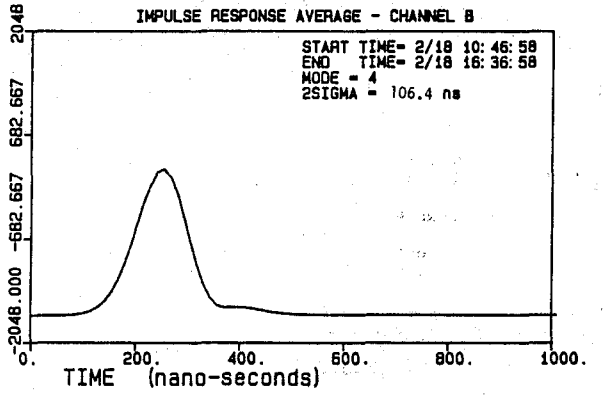
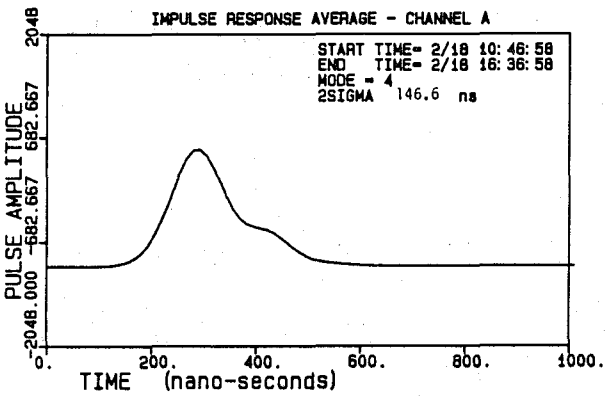
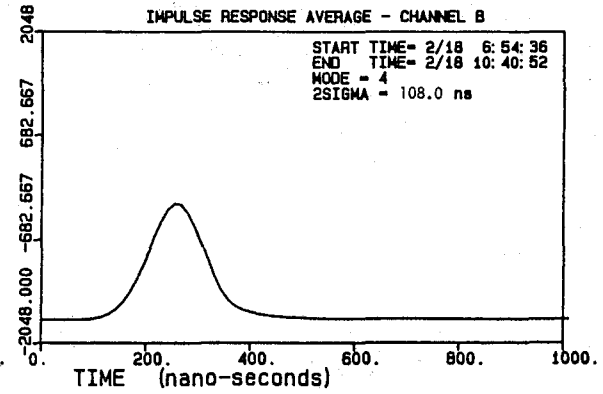
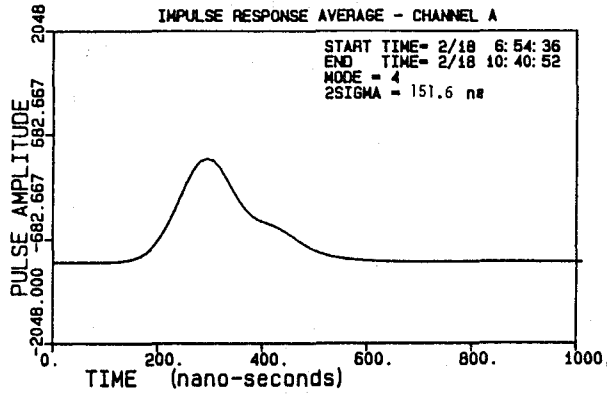
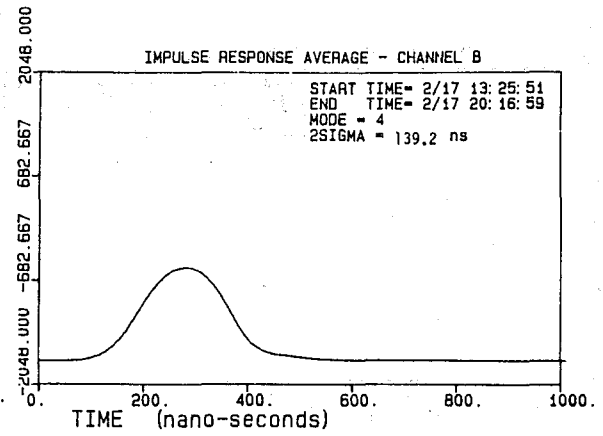
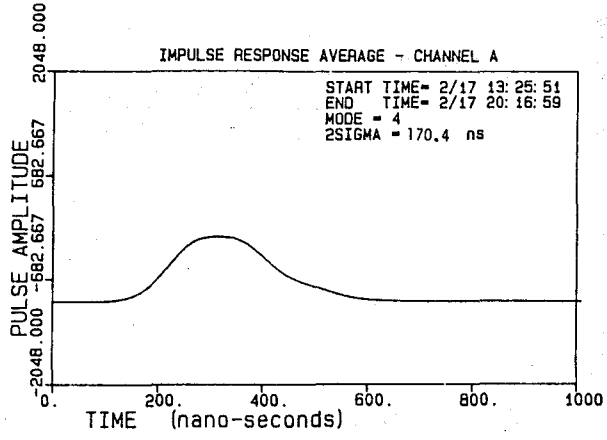
Smith, E.K., and S. Weintraub (1953), The constants in the equation for atmospheric refractive index at radio frequencies, Proc. IRE 41, August, pp. 1035-1037.

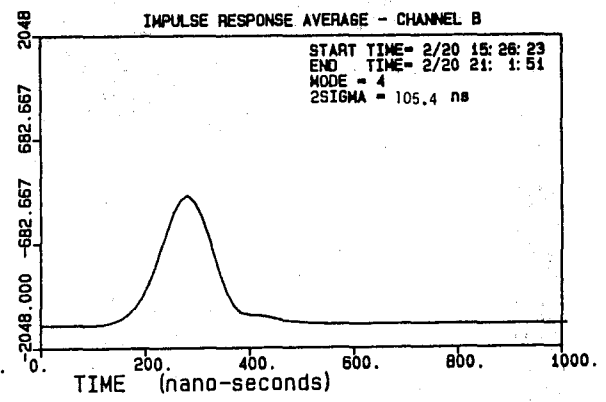
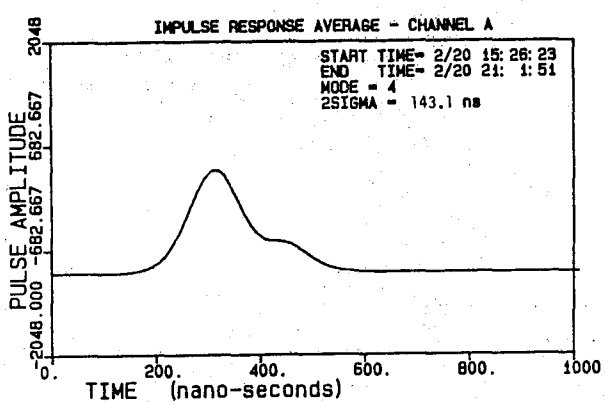
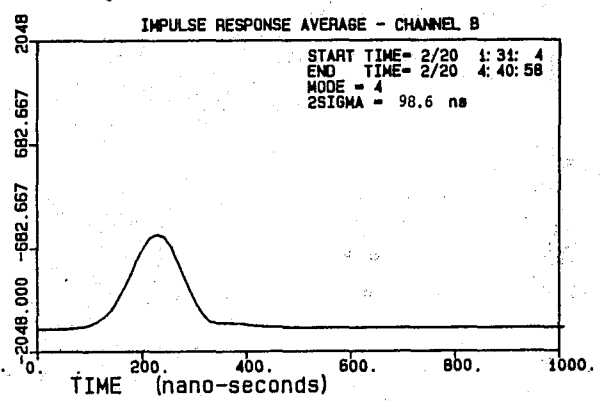
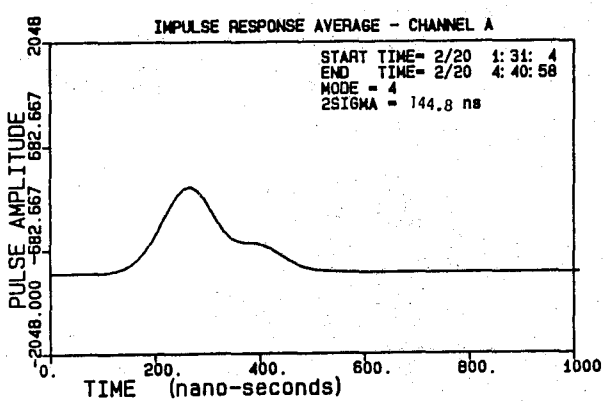
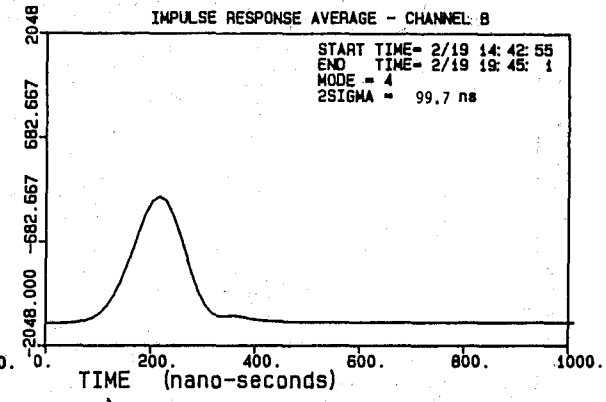
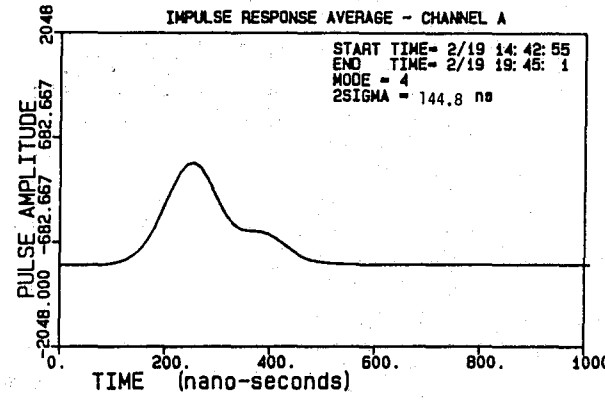
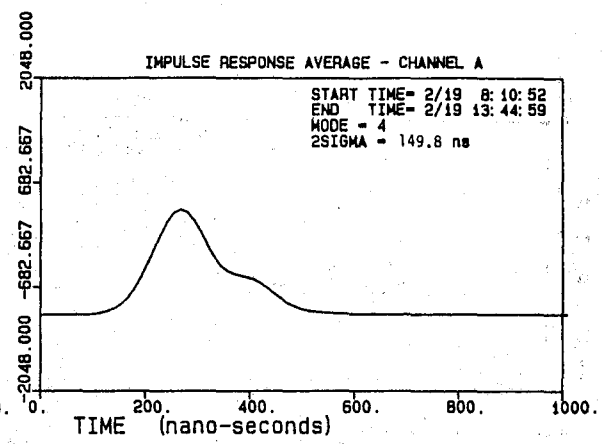
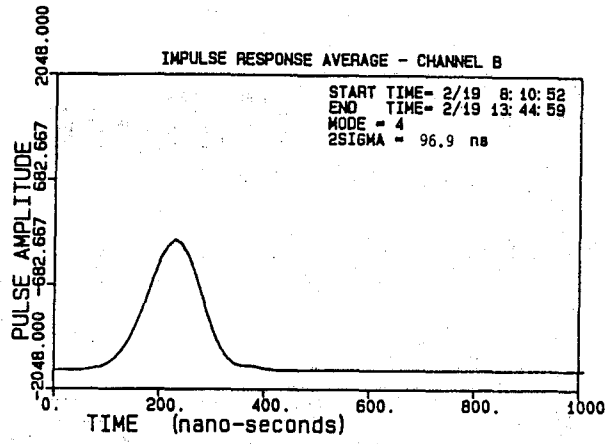
APPENDIX A

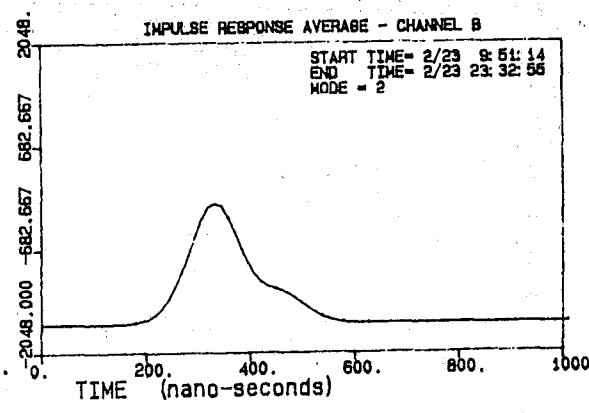
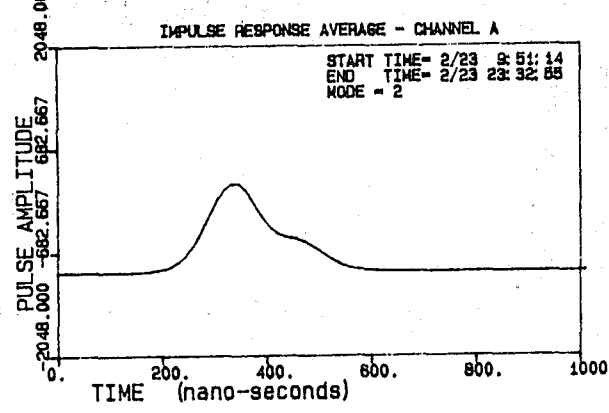
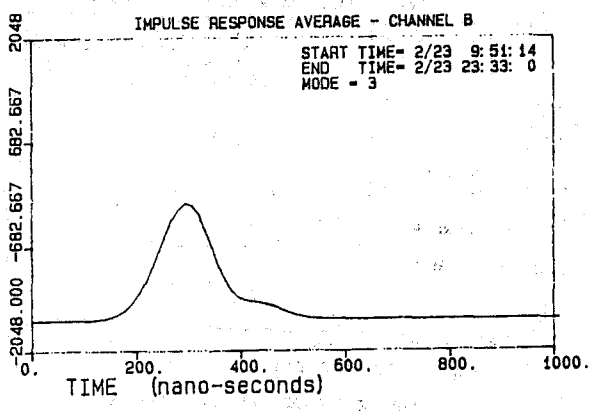
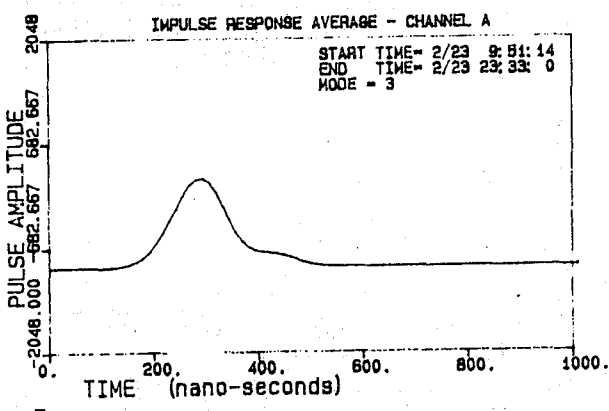
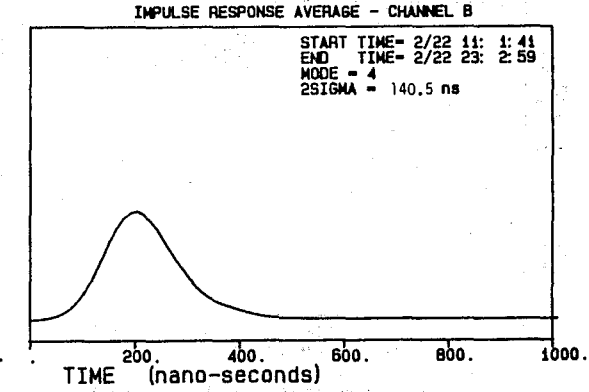
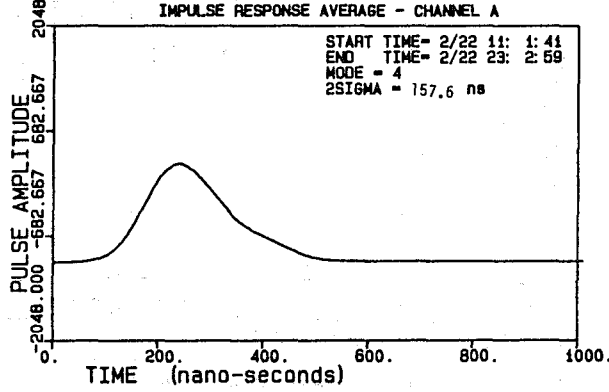
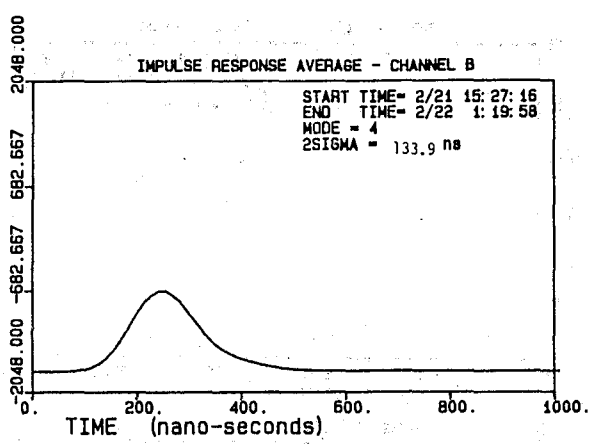
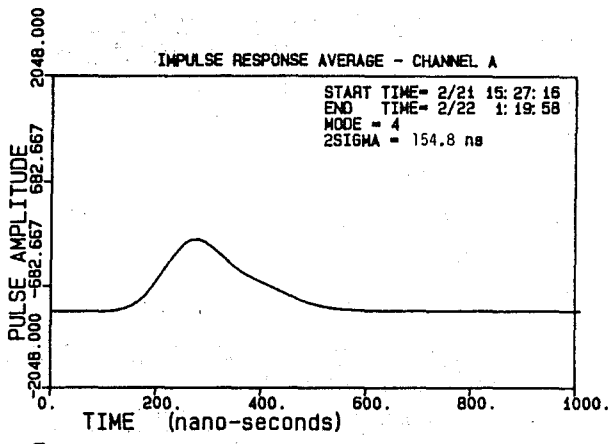
Average Power Impulse Functions

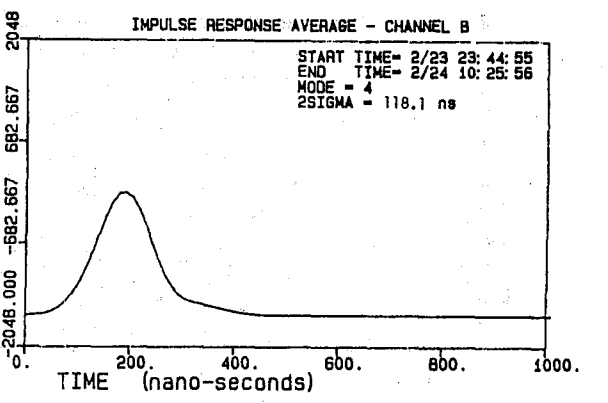
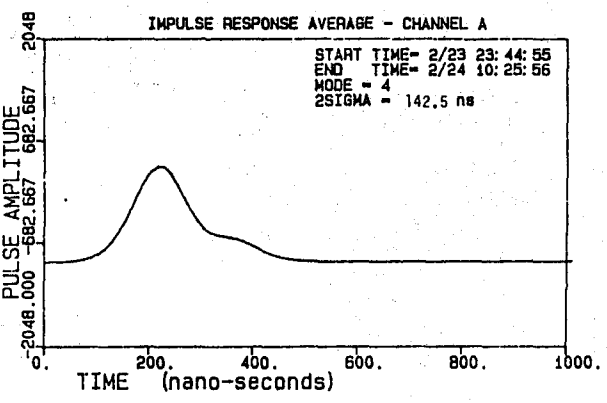
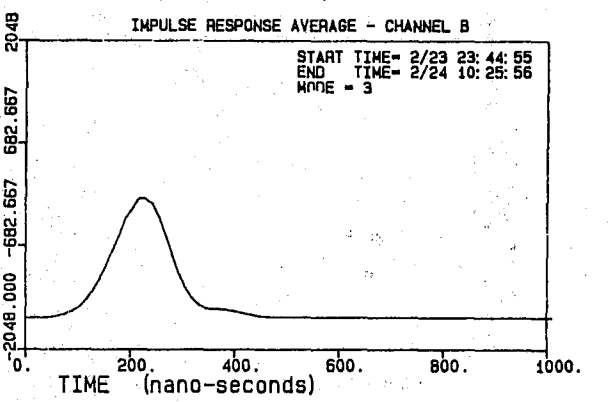
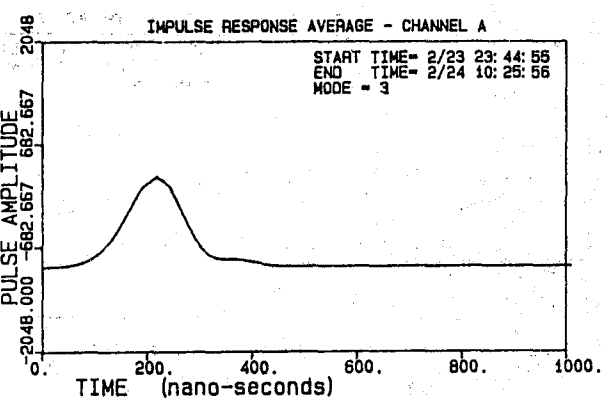
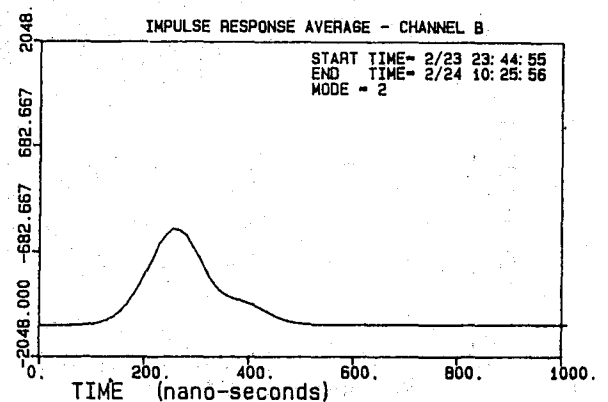
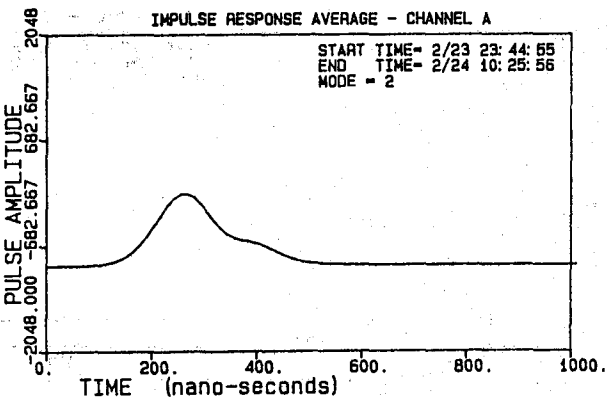
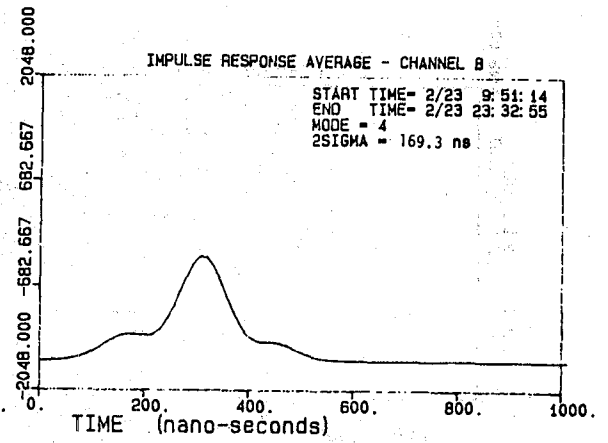
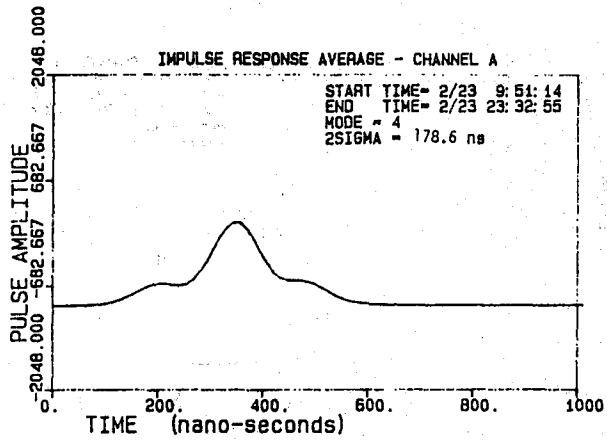


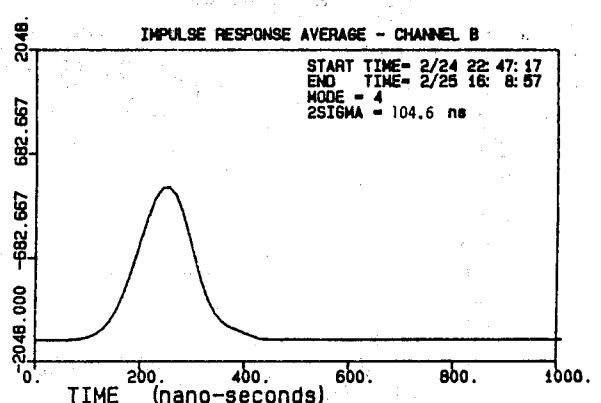
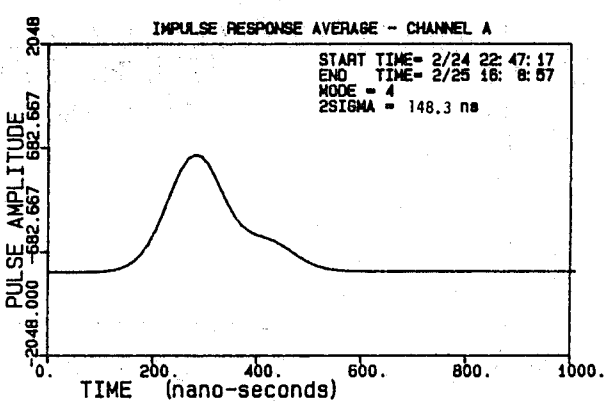
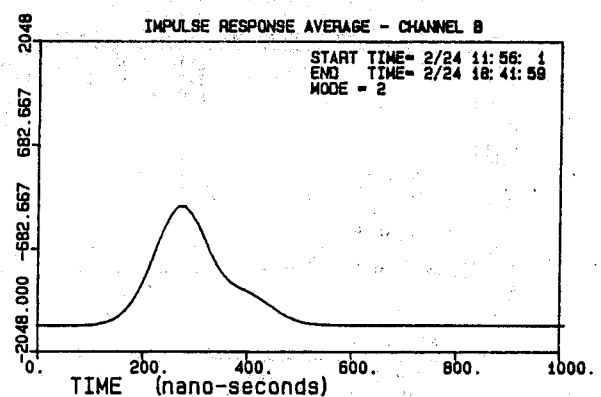
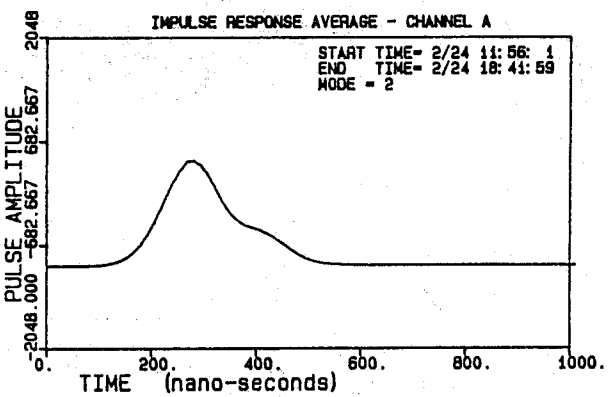
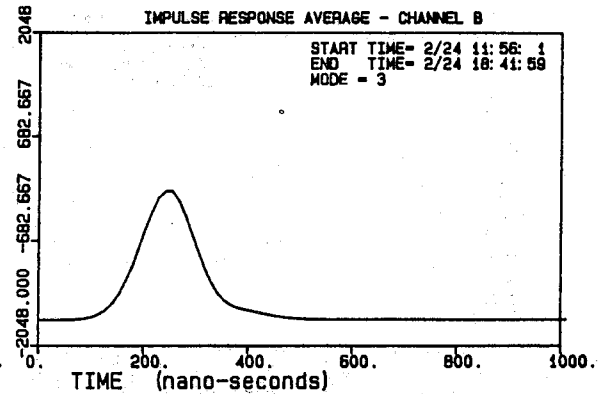
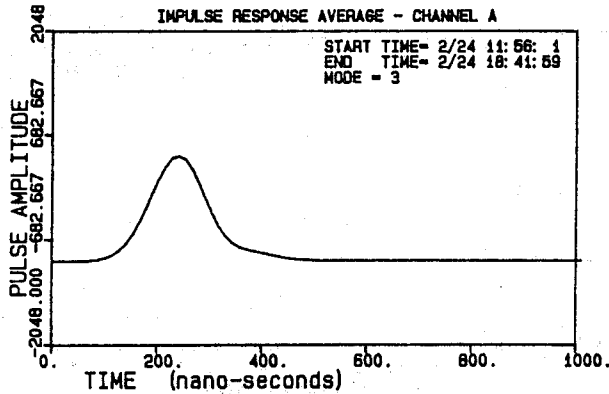
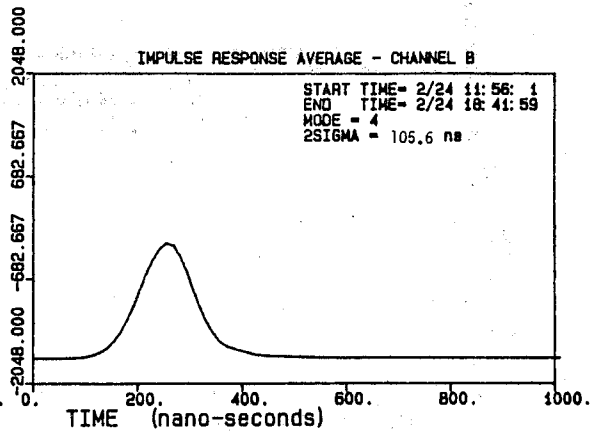
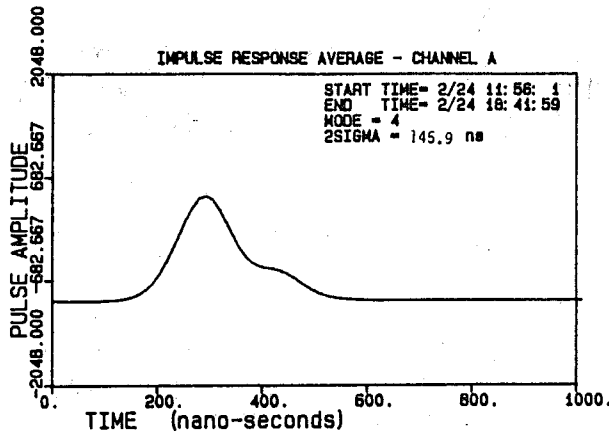


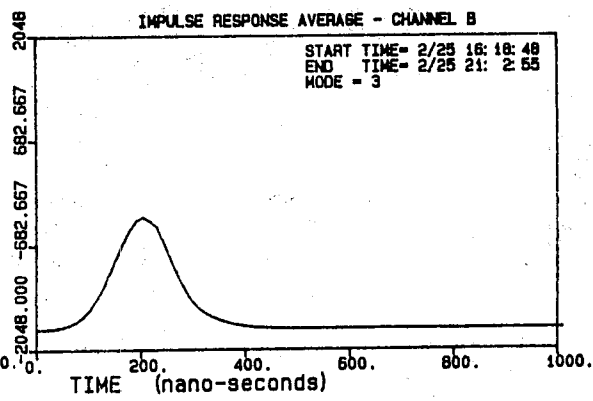
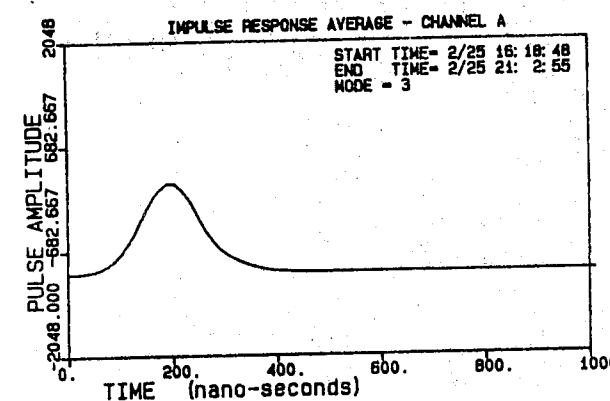
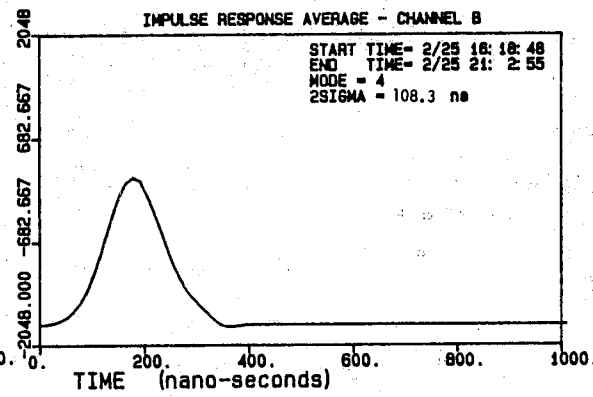
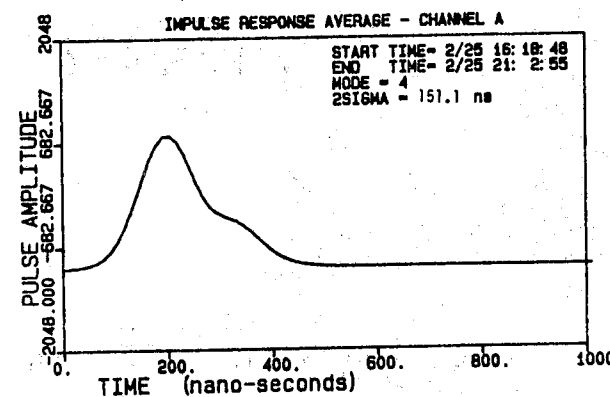
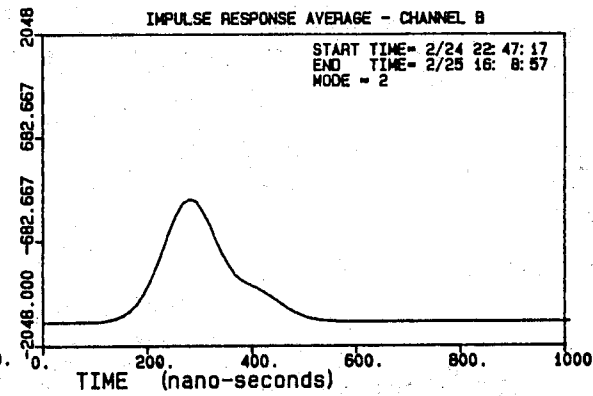
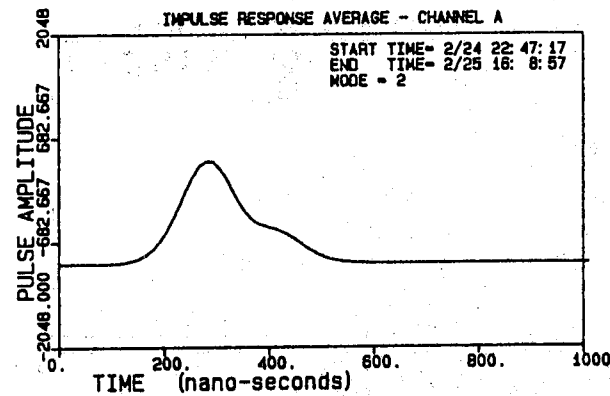
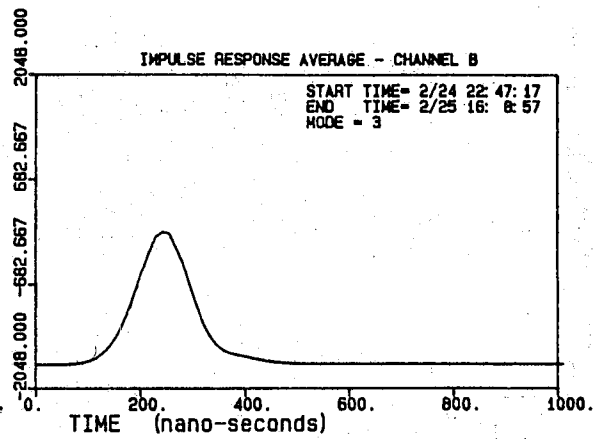
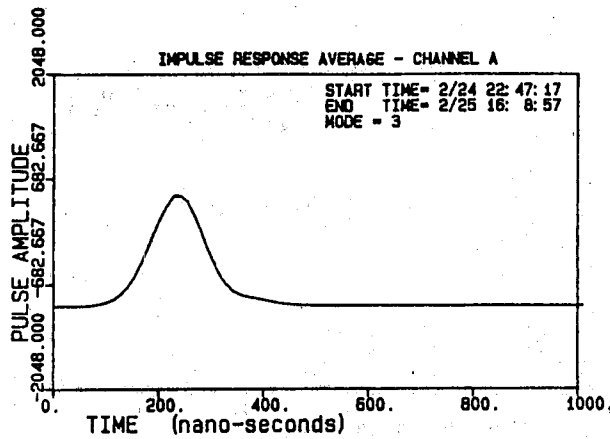


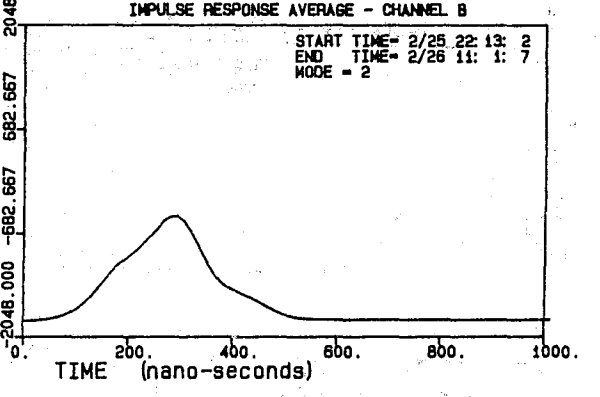
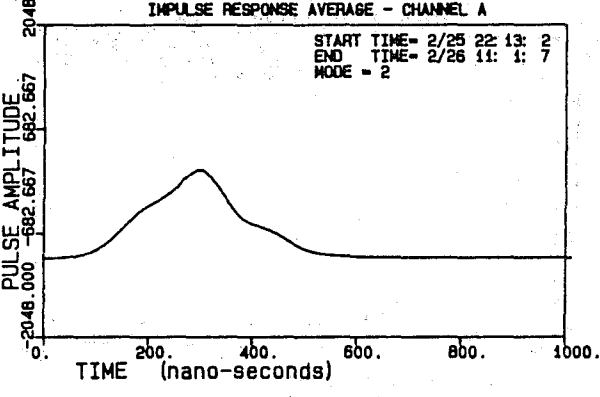
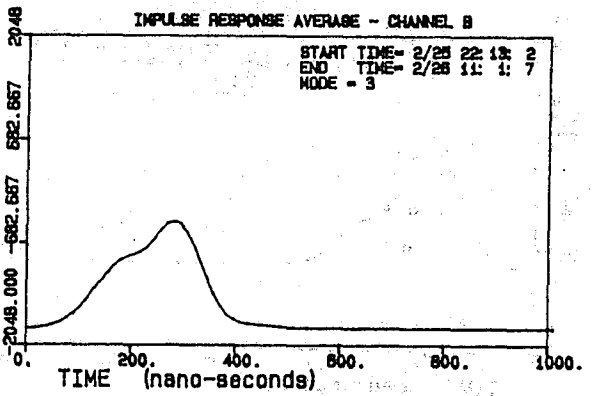
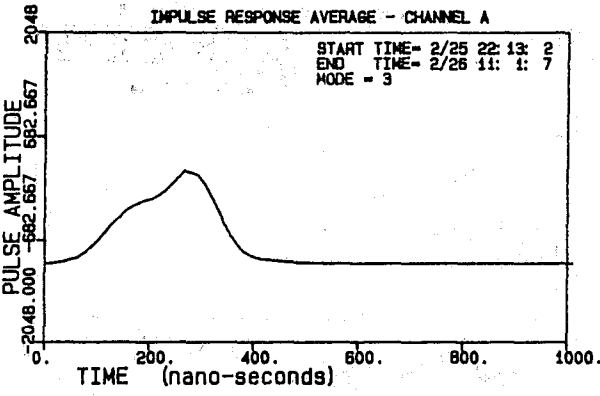
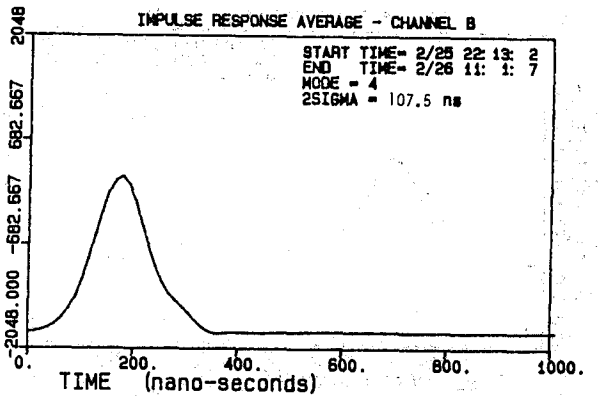
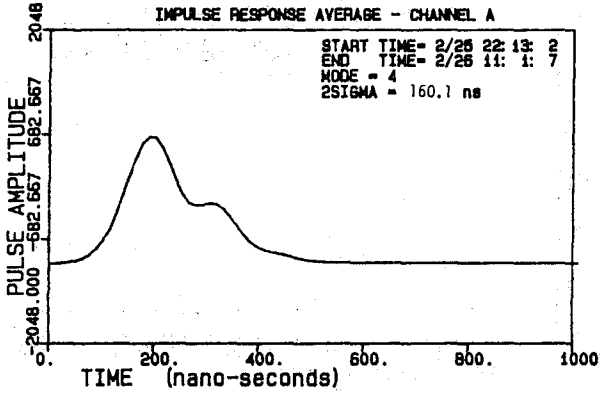
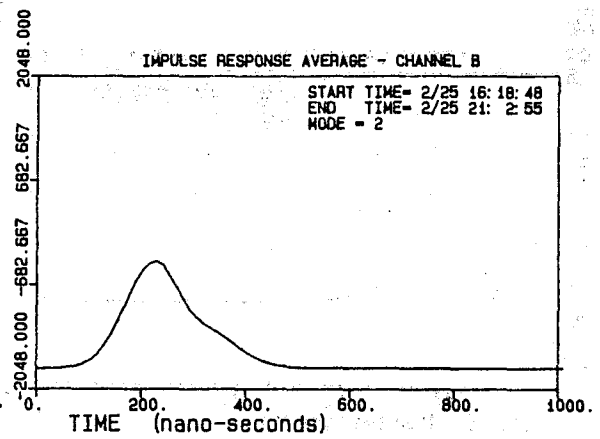
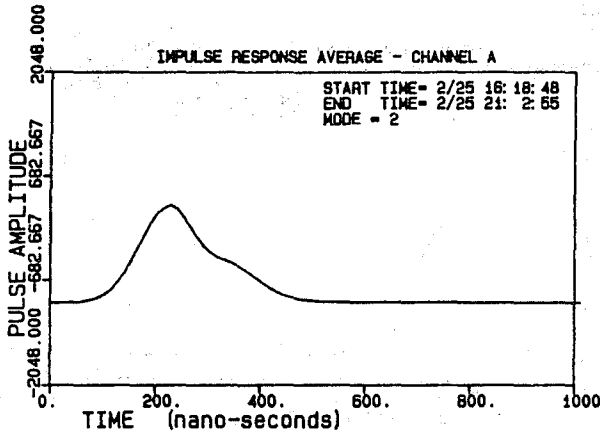


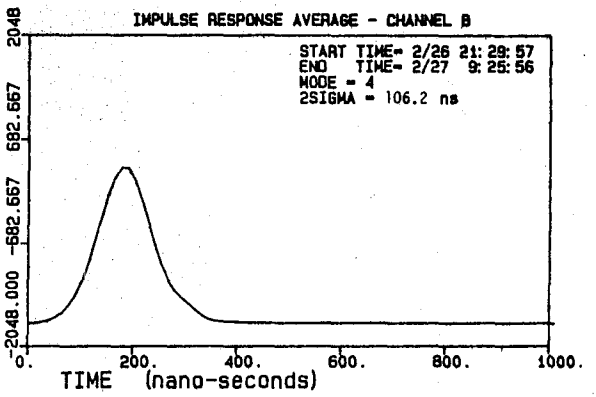
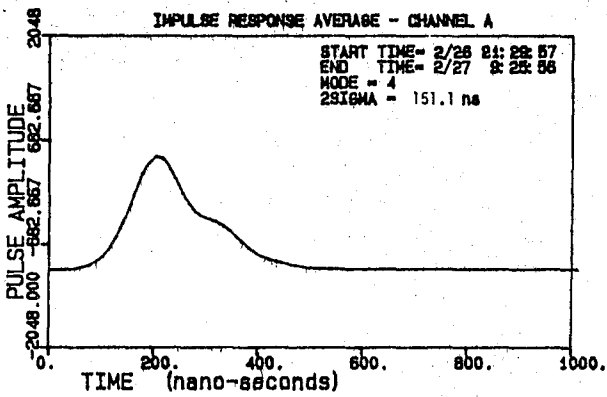
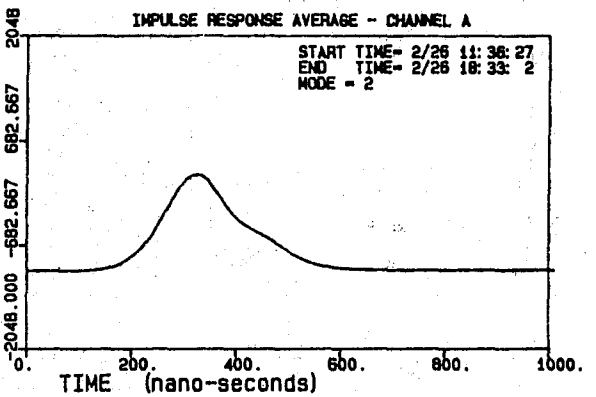
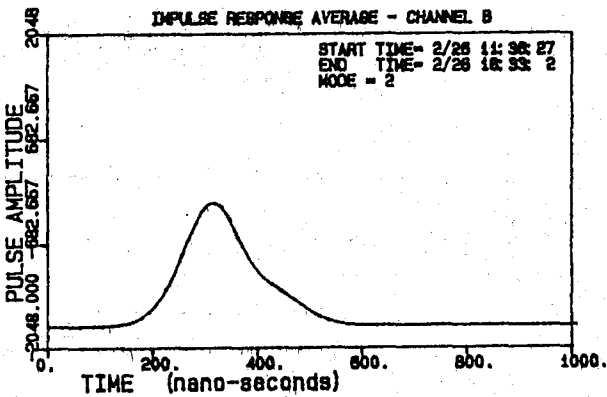
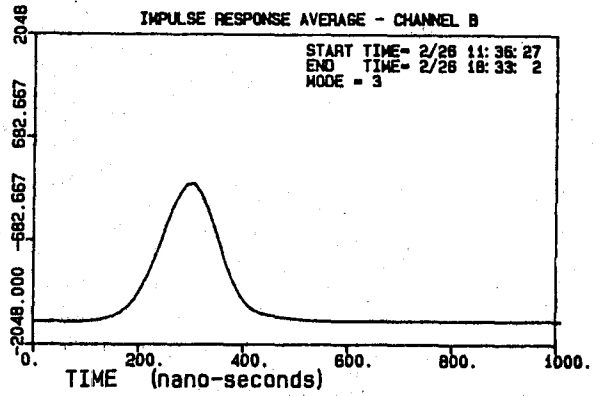
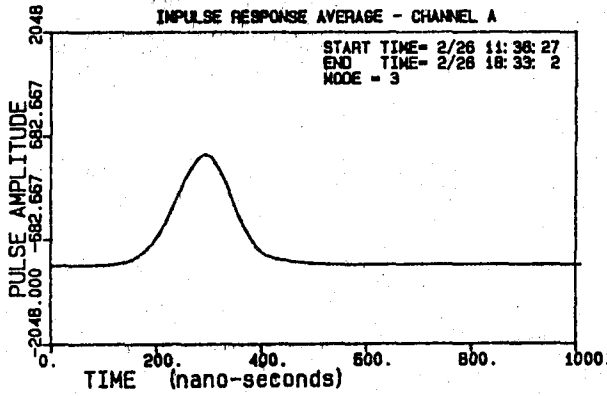
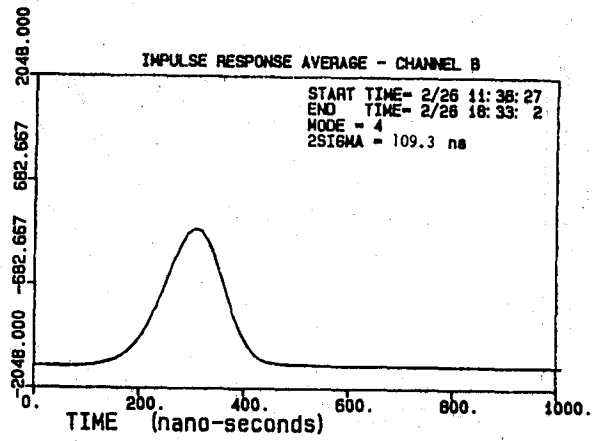
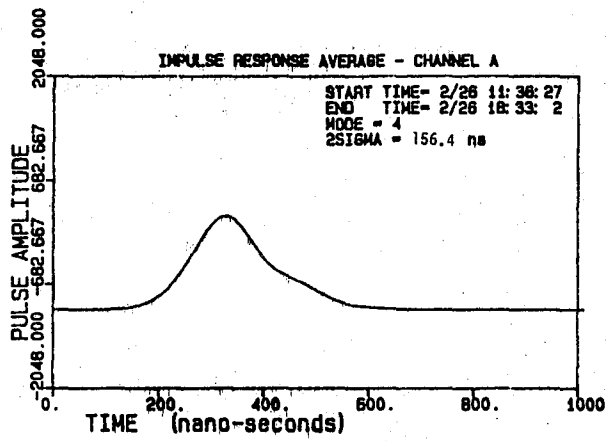


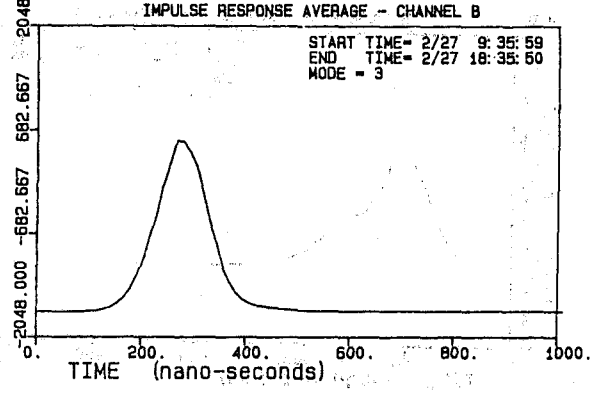
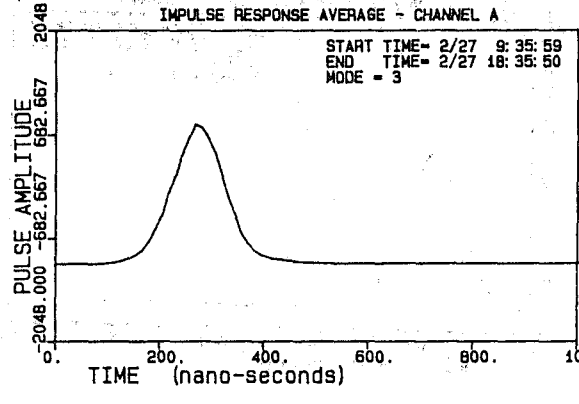
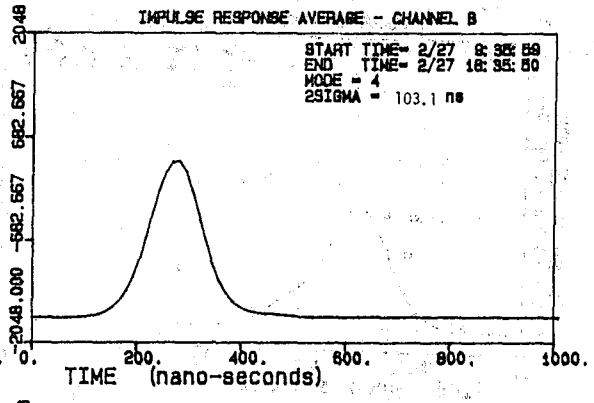
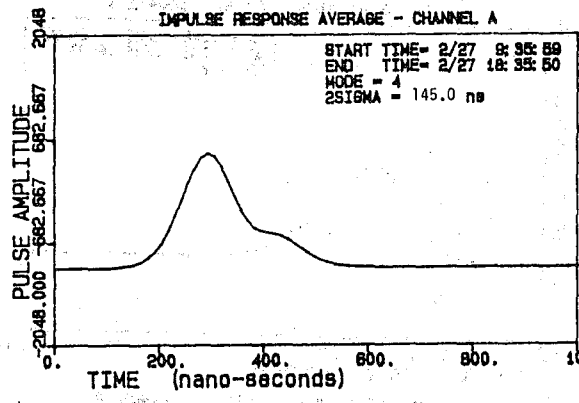
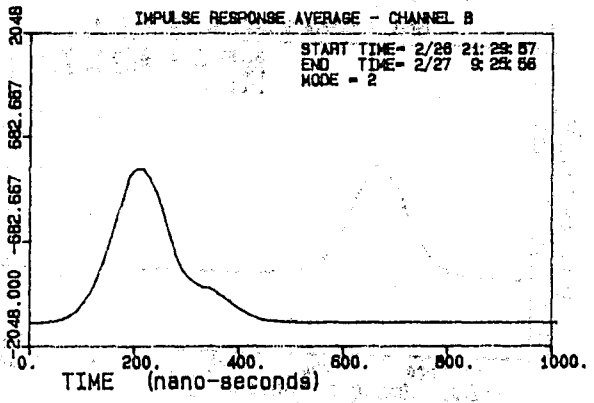
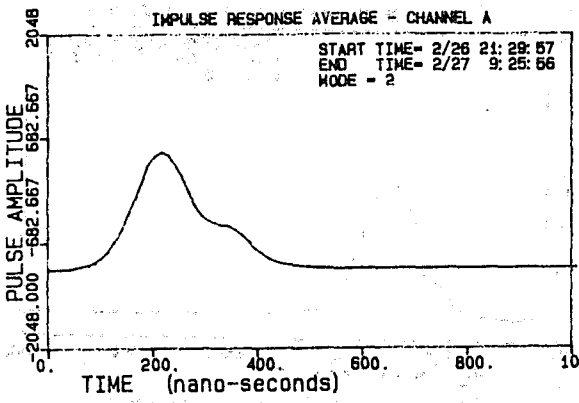
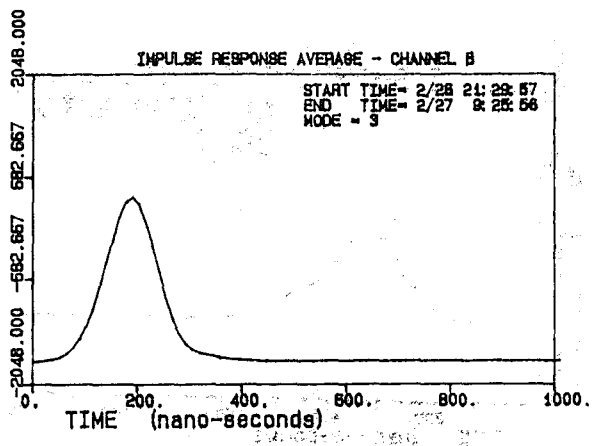
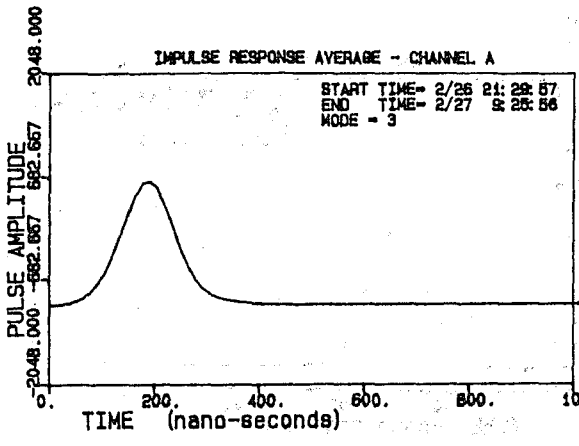


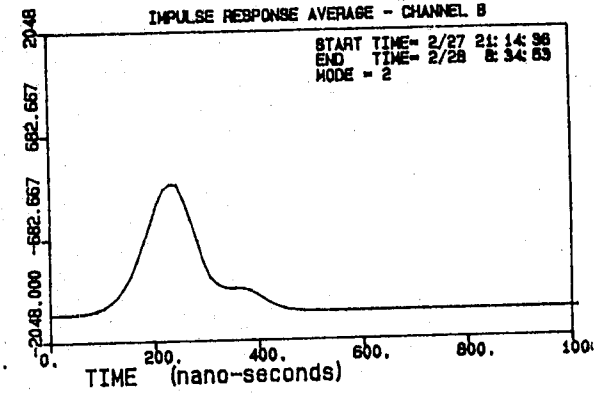
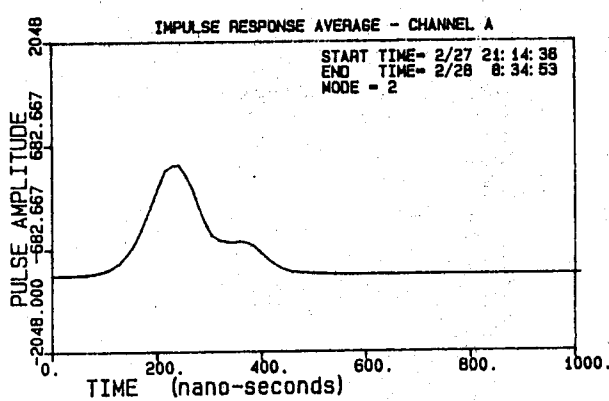
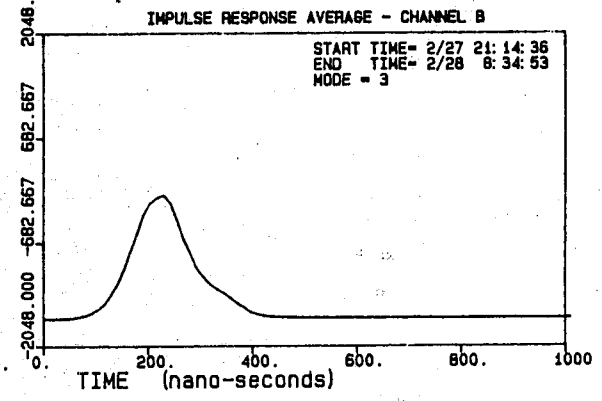
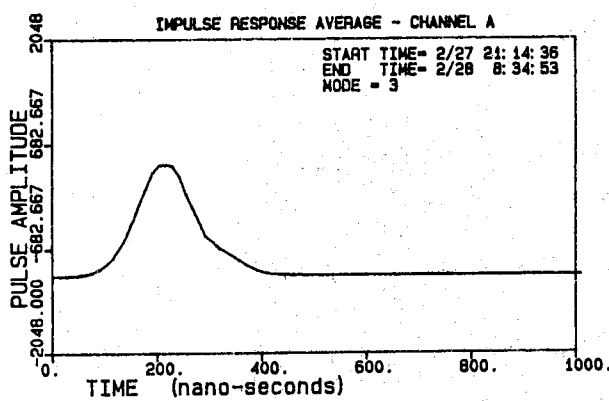
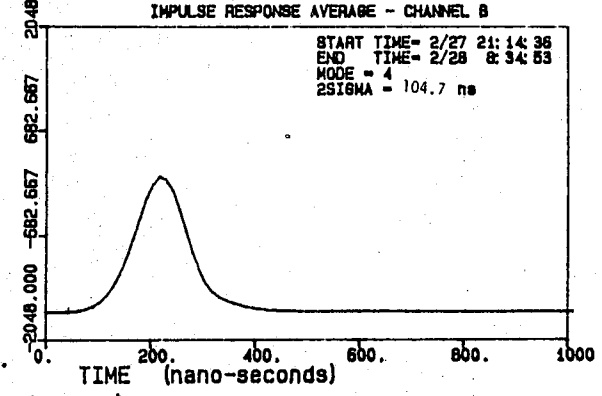
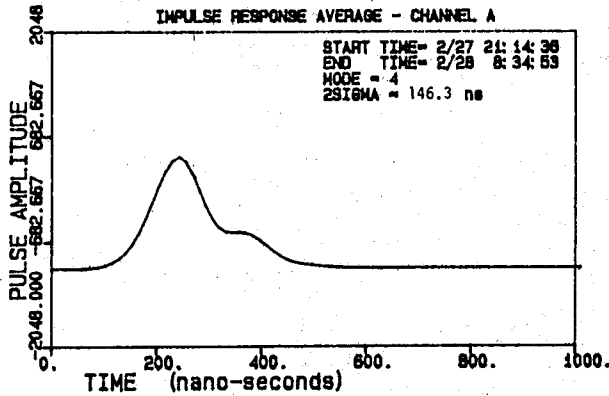
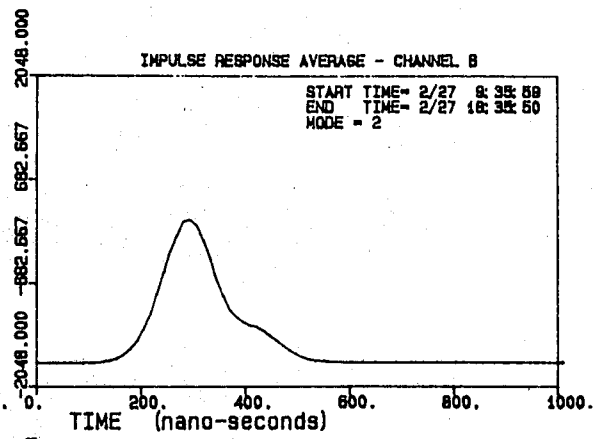
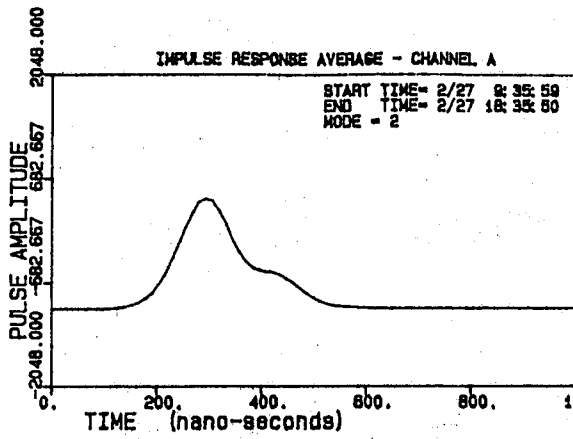












1. The first part of the document discusses the importance of maintaining accurate records of all transactions. This is essential for ensuring the integrity of the financial data and for providing a clear audit trail.

2. The second part of the document outlines the various methods used to collect and analyze data. These methods include direct observation, interviews, and the use of specialized software tools.

3. The third part of the document describes the results of the data collection and analysis. It shows that there is a significant correlation between the variables being studied, which supports the hypothesis.

4. The fourth part of the document discusses the implications of the findings. It suggests that the results could be used to inform policy decisions and to improve the efficiency of the system being studied.

5. The fifth part of the document concludes the study and provides a summary of the key findings. It also identifies some limitations of the study and suggests areas for future research.

6. The sixth part of the document provides a detailed description of the methodology used in the study. This includes information about the sample size, the data collection process, and the statistical methods used for analysis.

7. The seventh part of the document discusses the ethical considerations of the study. It emphasizes the importance of obtaining informed consent from all participants and of protecting their privacy.

8. The eighth part of the document provides a list of references to the literature cited in the study. This includes books, journal articles, and other sources of information.

9. The ninth part of the document provides a list of appendices. These include additional data, charts, and other materials that are relevant to the study but are too large to include in the main text.

10. The tenth part of the document provides a list of figures and tables. These are used to present the results of the data analysis in a clear and concise manner.

11. The eleventh part of the document discusses the limitations of the study. It notes that the sample size was relatively small and that the study was limited to a specific context.

12. The twelfth part of the document provides a list of references to the literature cited in the study. This includes books, journal articles, and other sources of information.

13. The thirteenth part of the document provides a list of appendices. These include additional data, charts, and other materials that are relevant to the study but are too large to include in the main text.

14. The fourteenth part of the document provides a list of figures and tables. These are used to present the results of the data analysis in a clear and concise manner.

15. The fifteenth part of the document discusses the ethical considerations of the study. It emphasizes the importance of obtaining informed consent from all participants and of protecting their privacy.

16. The sixteenth part of the document provides a list of references to the literature cited in the study. This includes books, journal articles, and other sources of information.

17. The seventeenth part of the document provides a list of appendices. These include additional data, charts, and other materials that are relevant to the study but are too large to include in the main text.

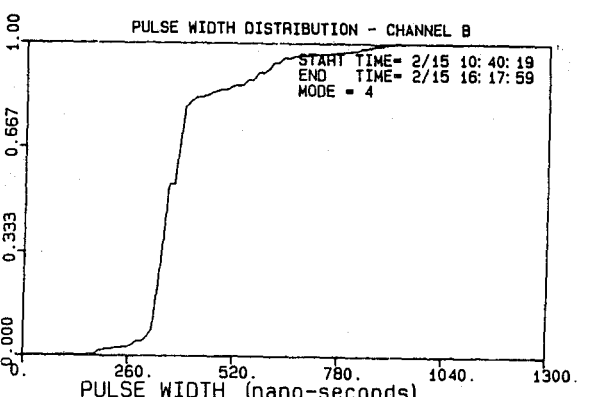
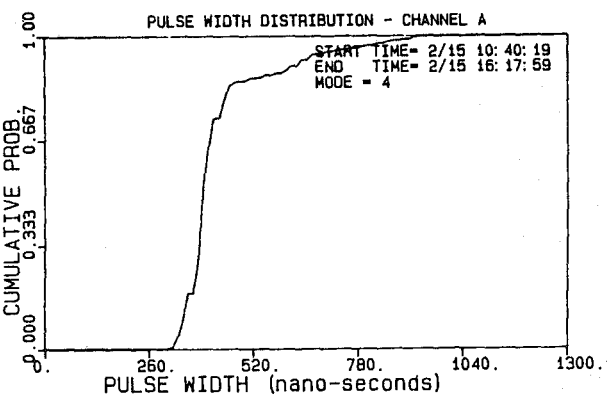
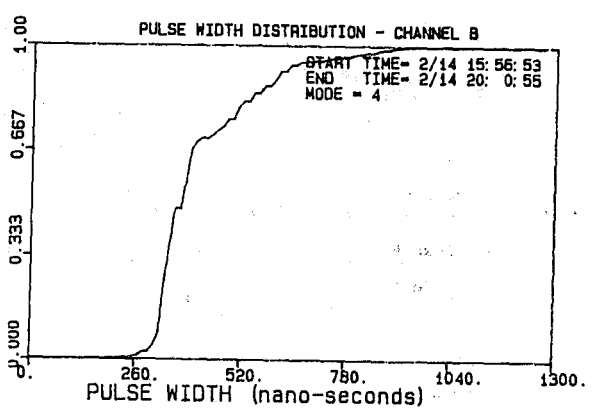
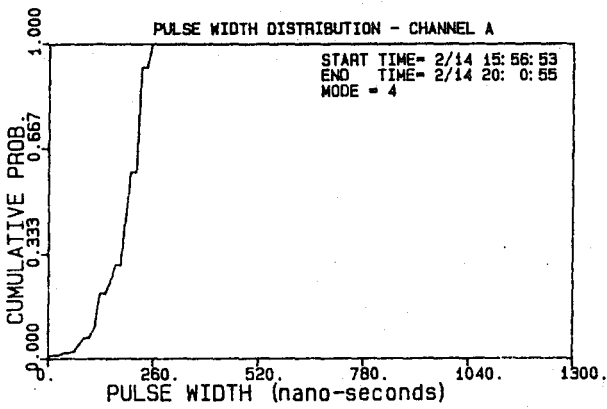
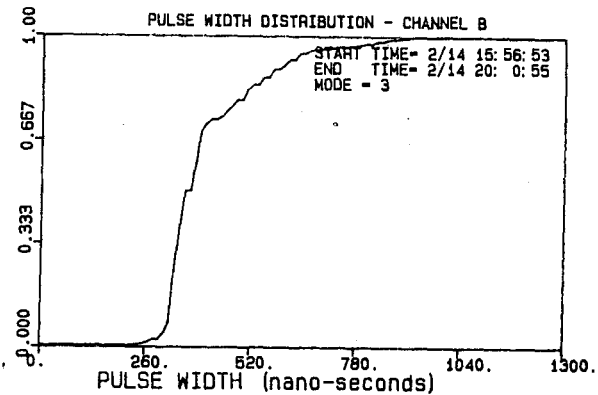
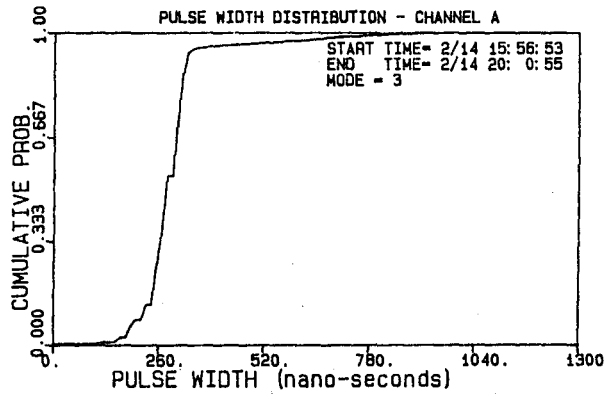
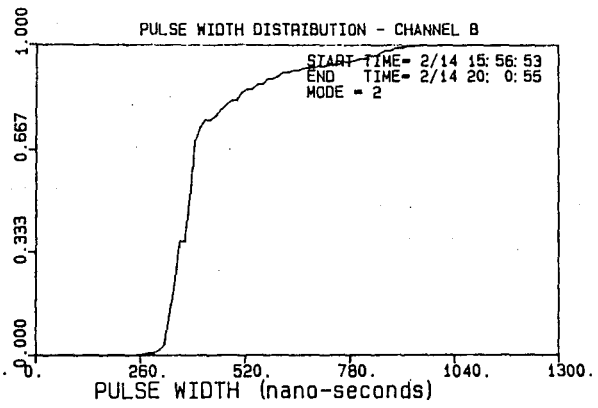
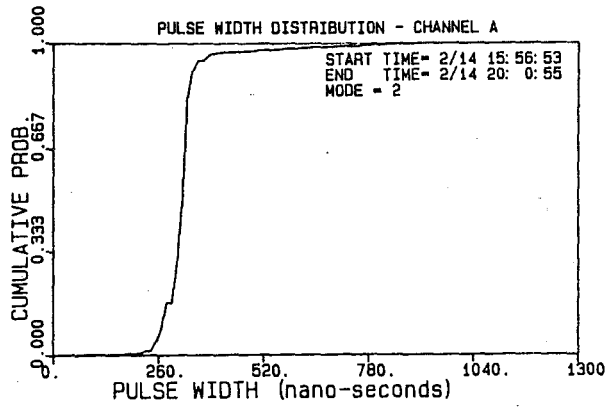
18. The eighteenth part of the document provides a list of figures and tables. These are used to present the results of the data analysis in a clear and concise manner.

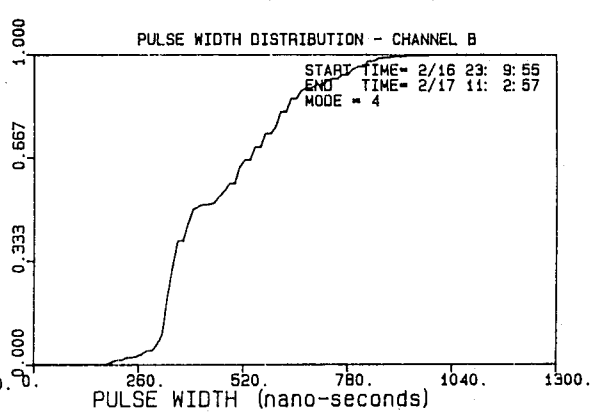
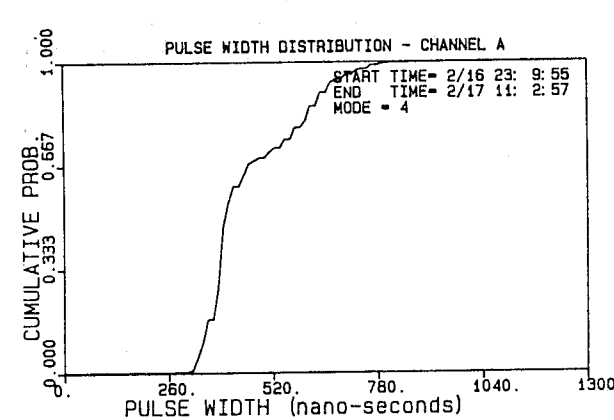
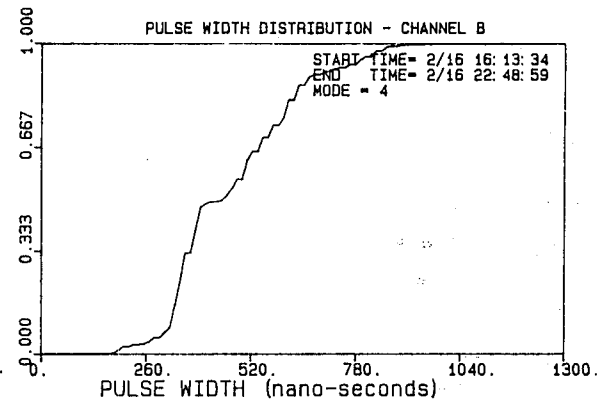
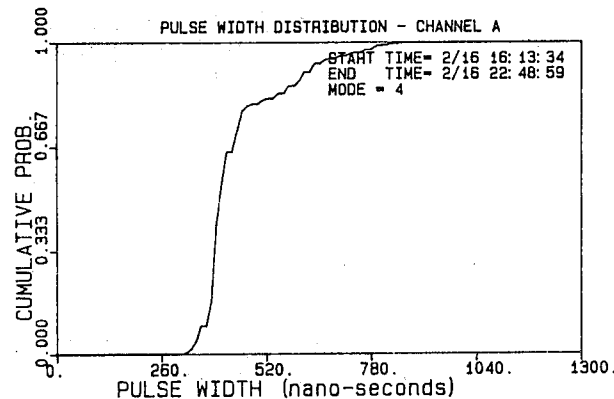
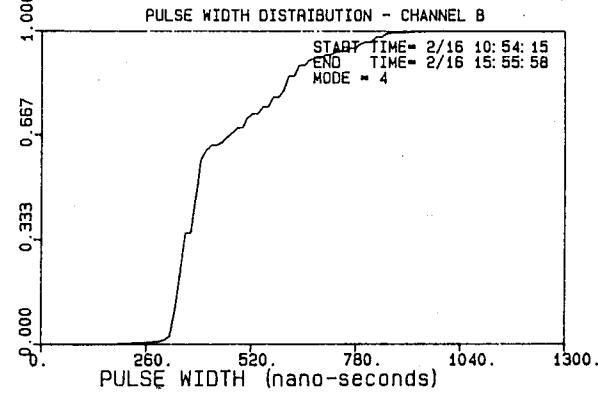
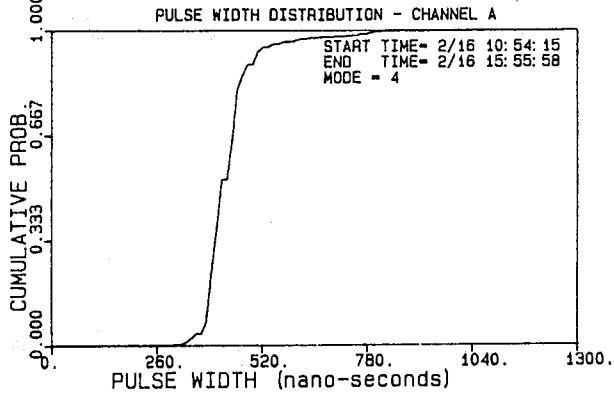
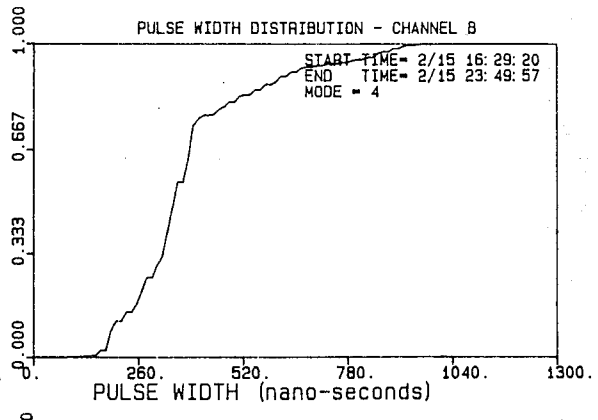
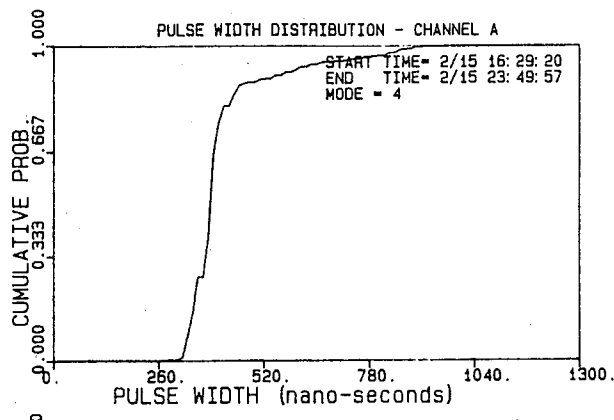
19. The nineteenth part of the document discusses the limitations of the study. It notes that the sample size was relatively small and that the study was limited to a specific context.

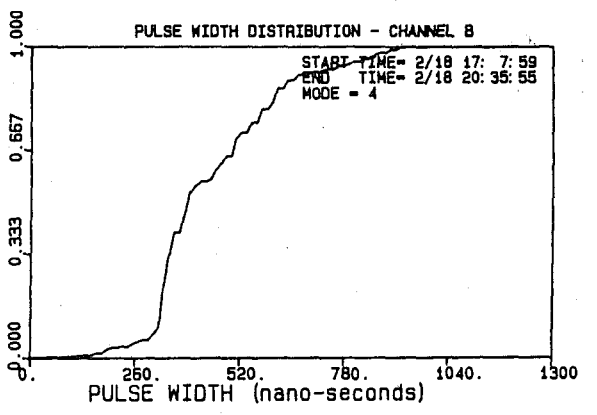
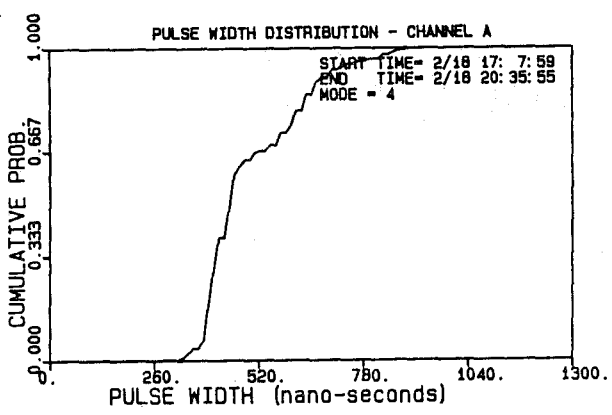
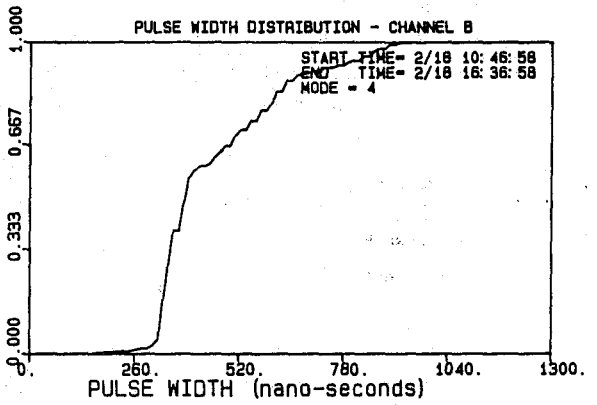
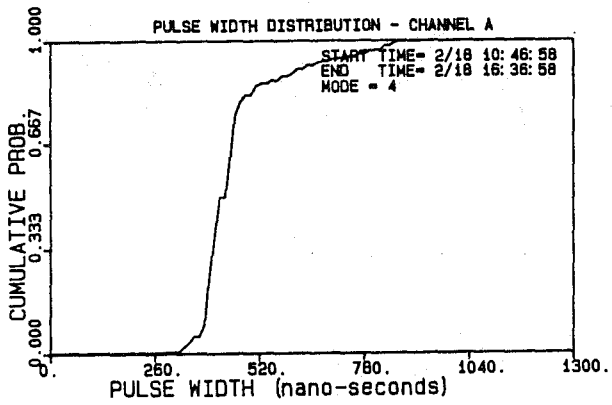
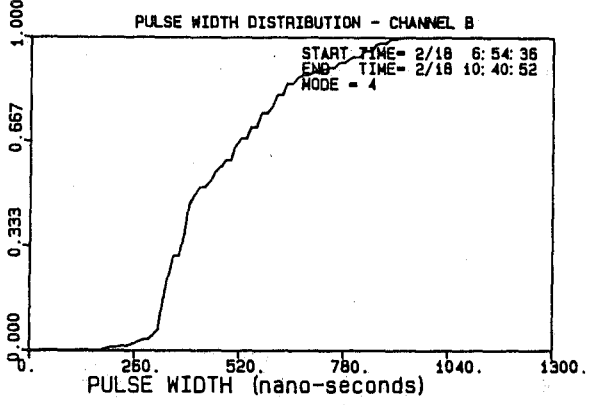
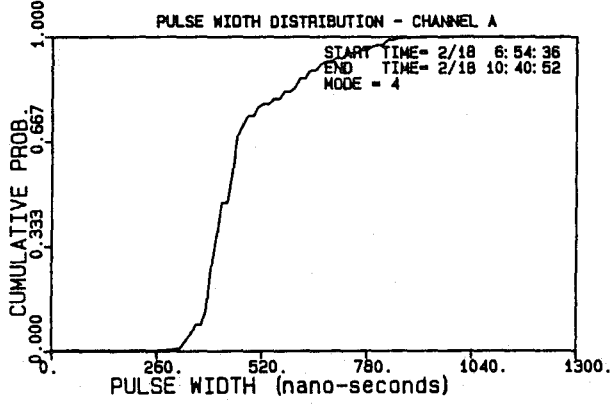
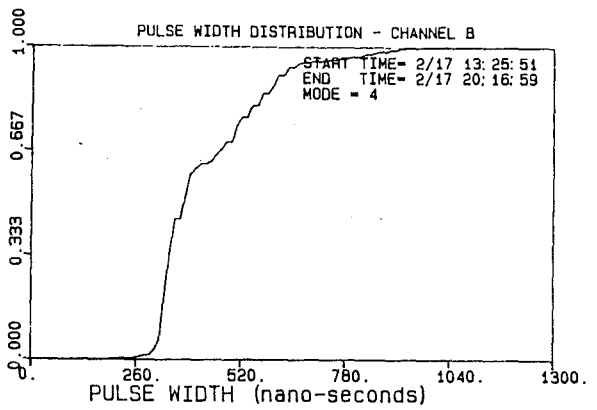
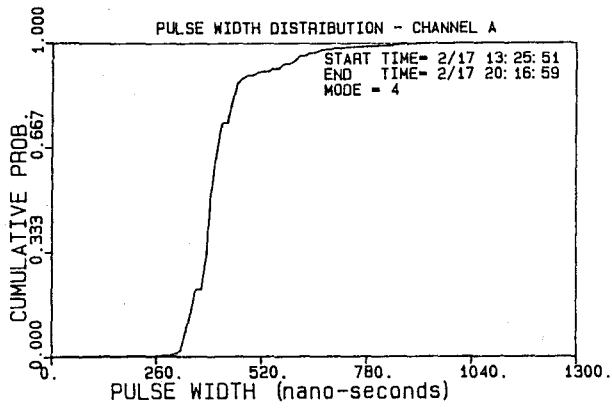
20. The twentieth part of the document provides a list of references to the literature cited in the study. This includes books, journal articles, and other sources of information.

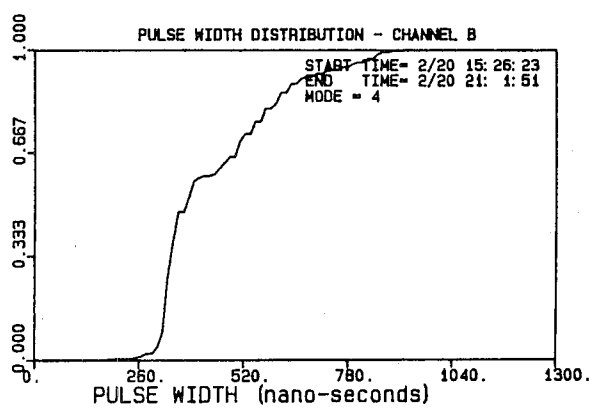
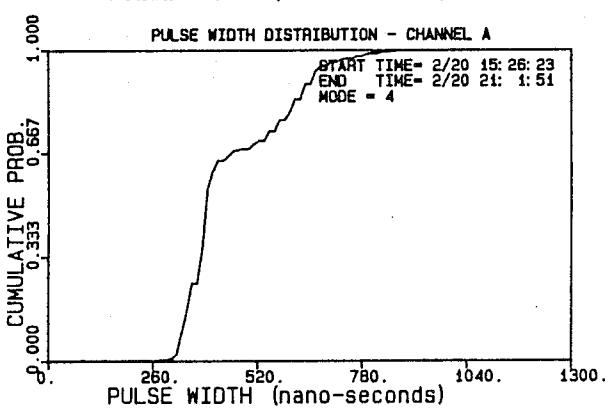
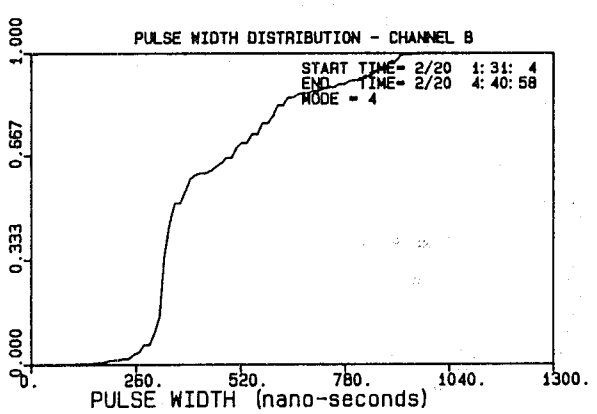
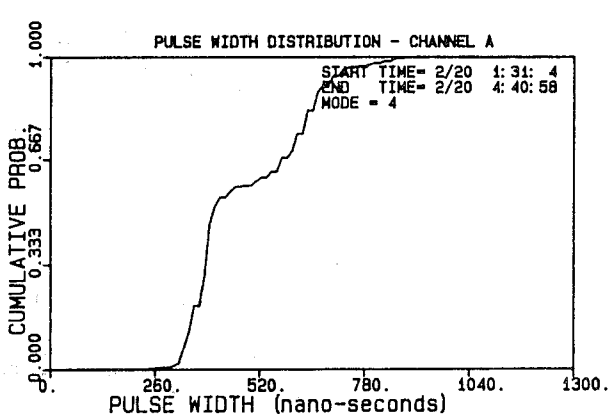
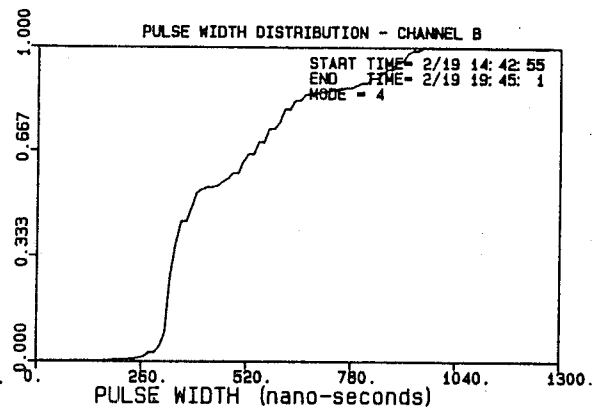
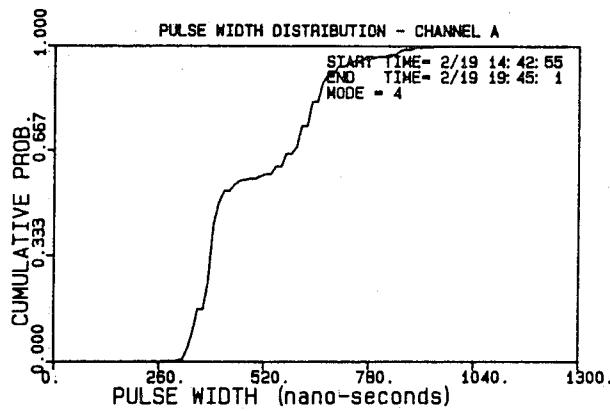
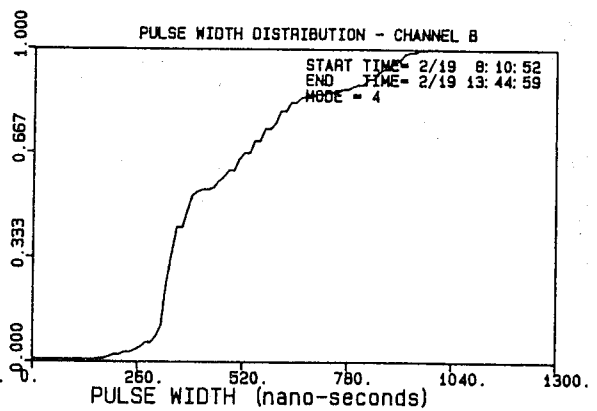
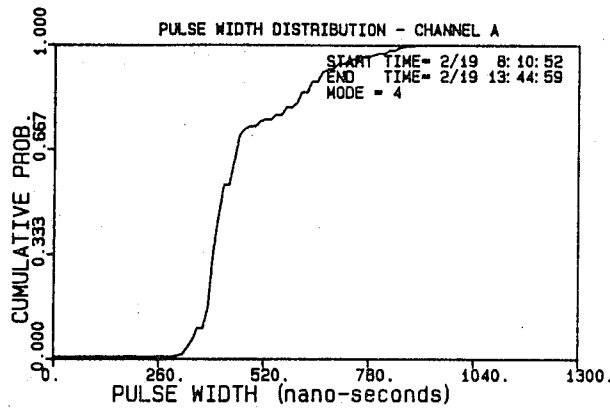
APPENDIX B

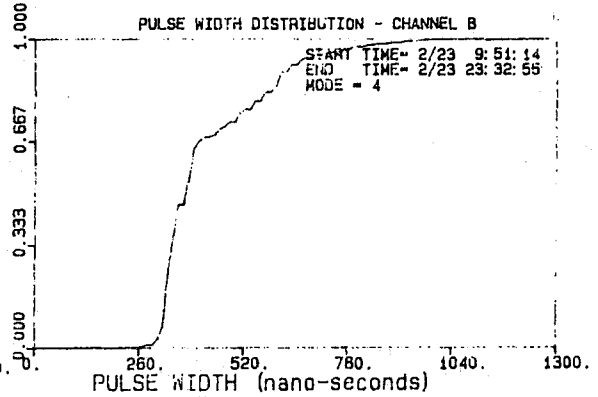
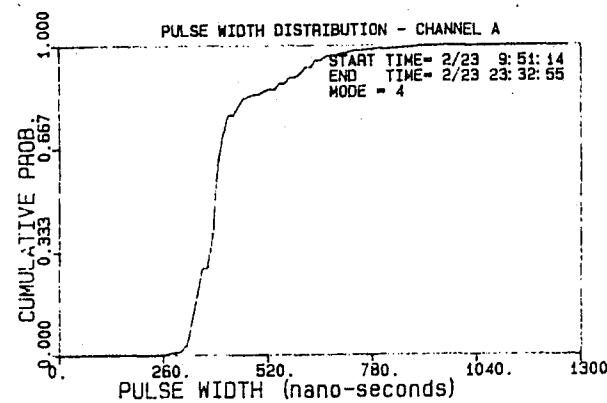
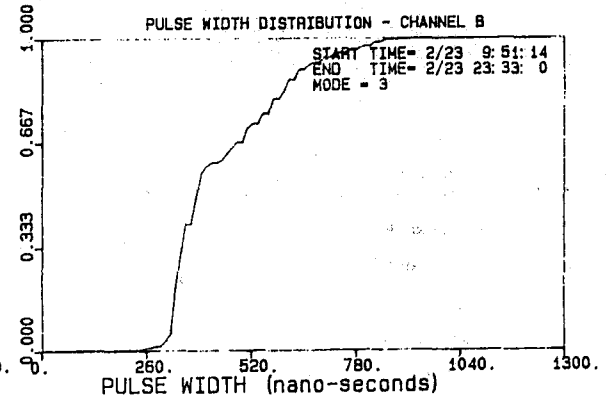
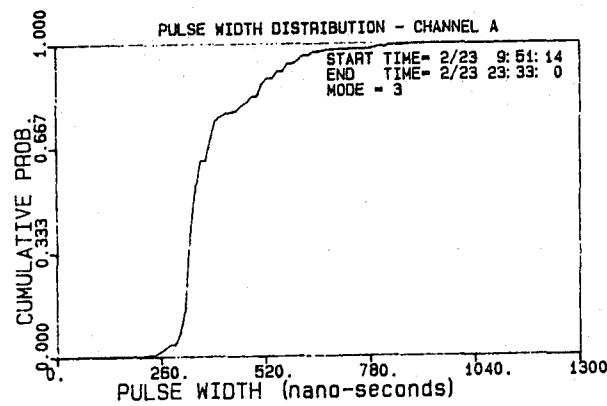
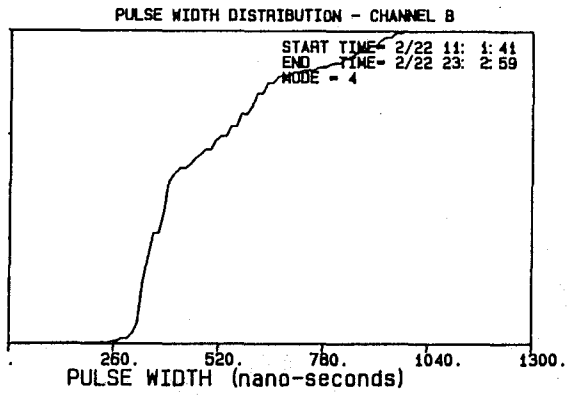
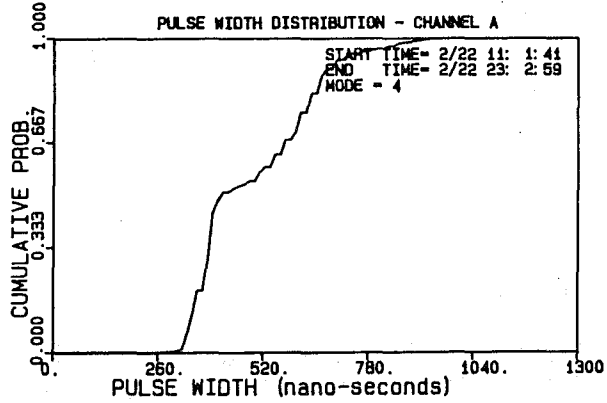
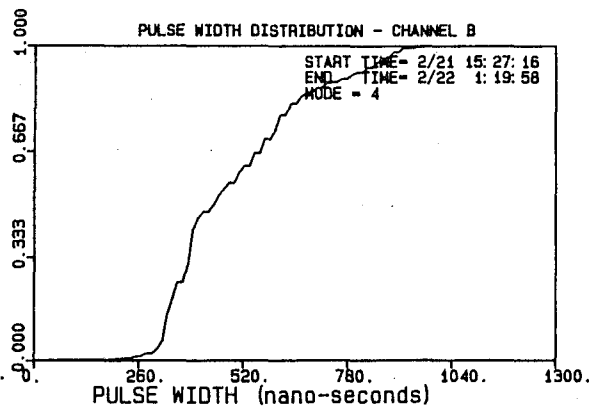
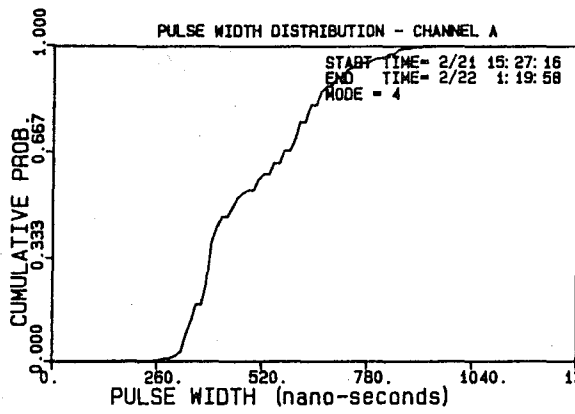
Cumulative Distributions of Pulse Width

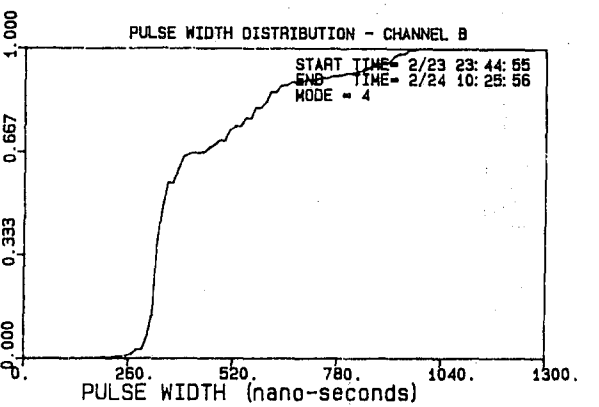
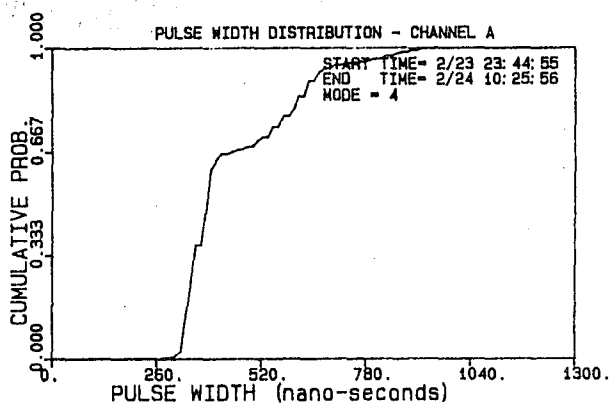
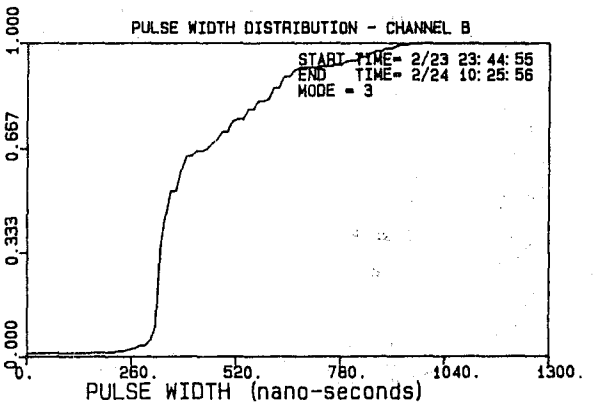
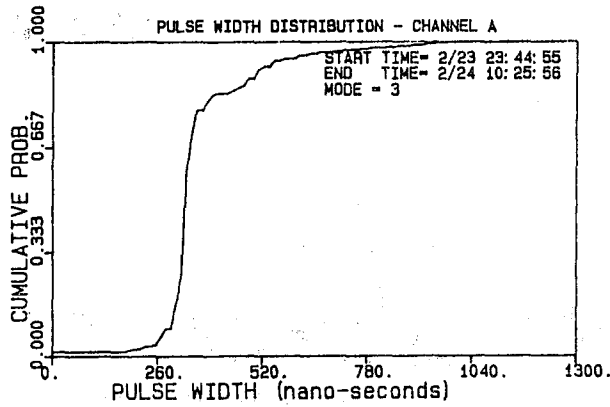
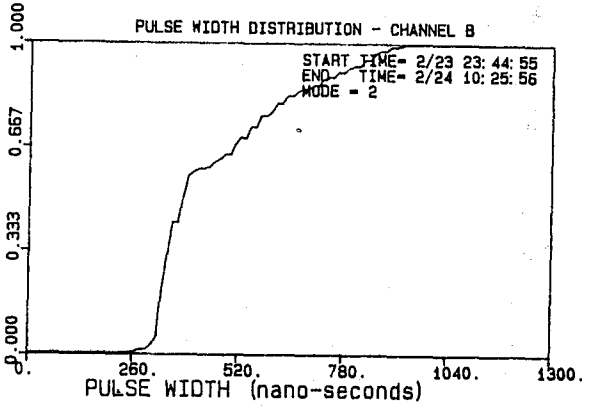
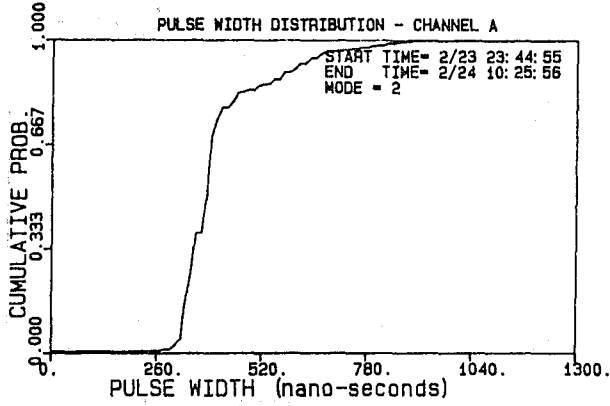
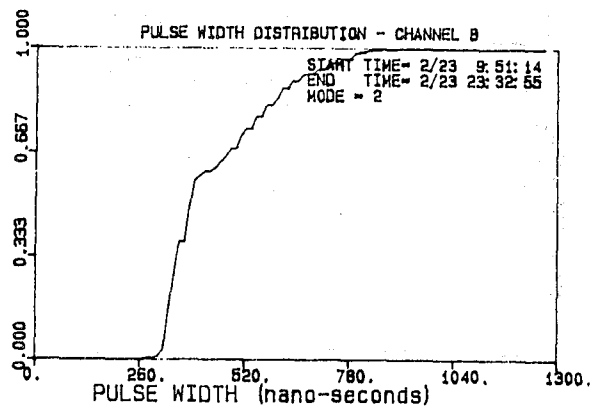
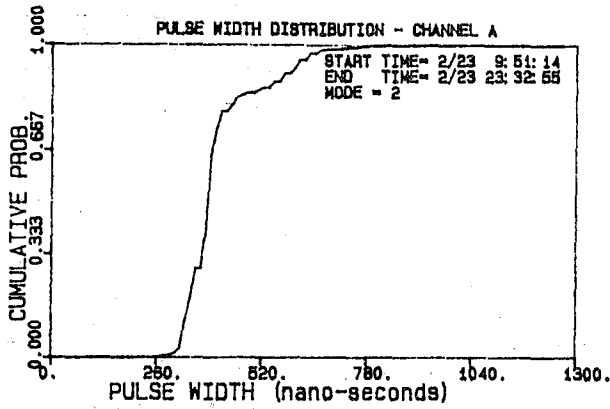


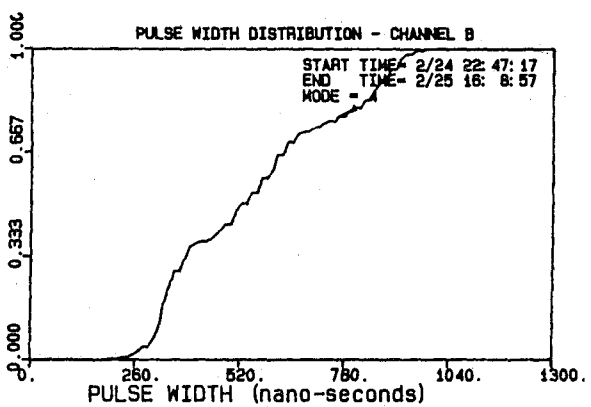
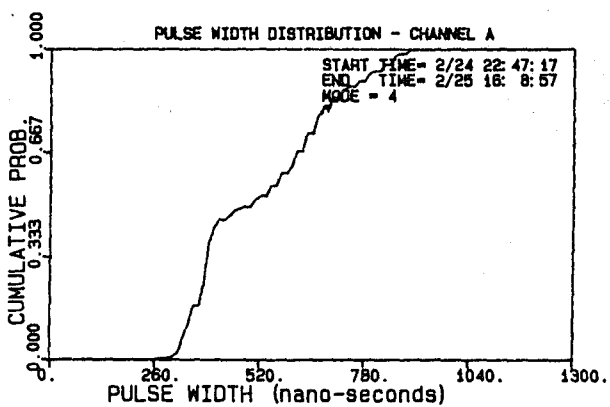
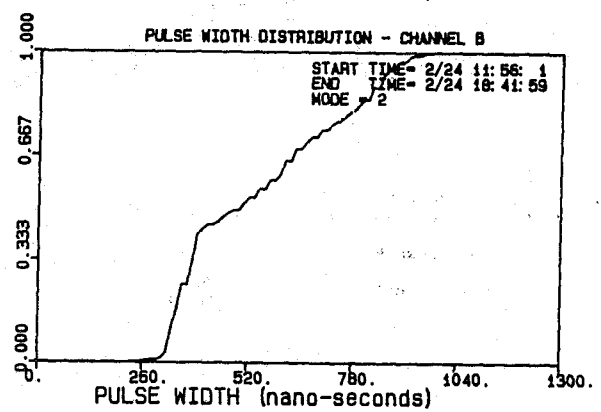
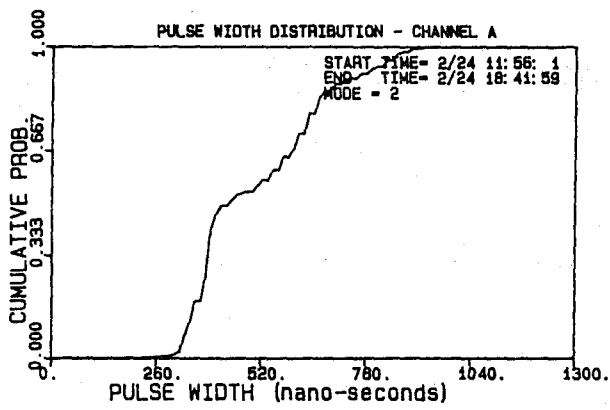
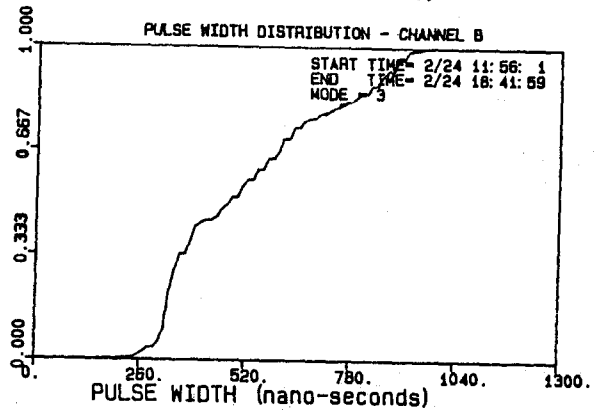
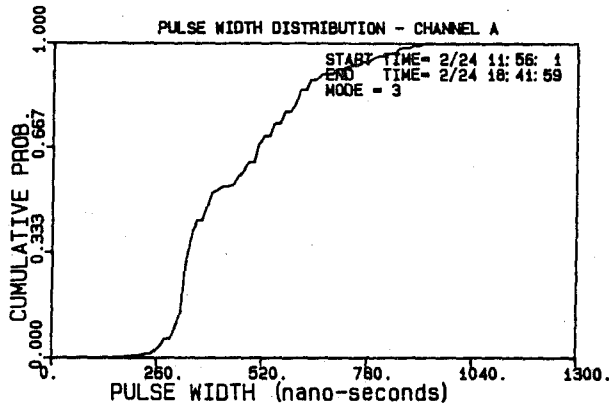
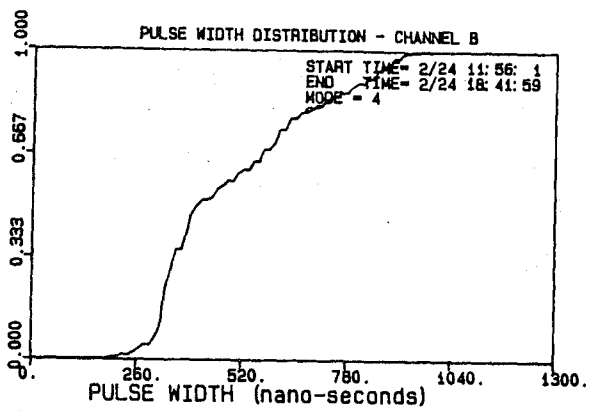
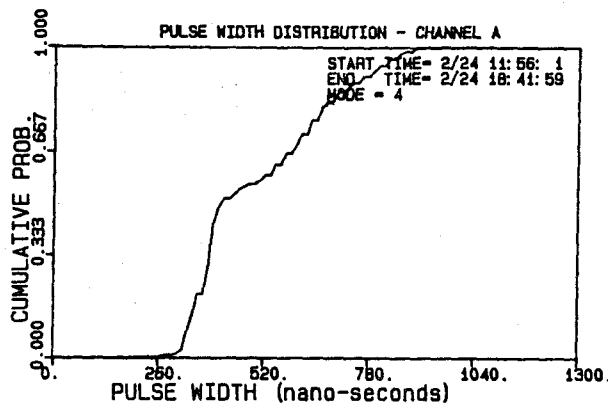


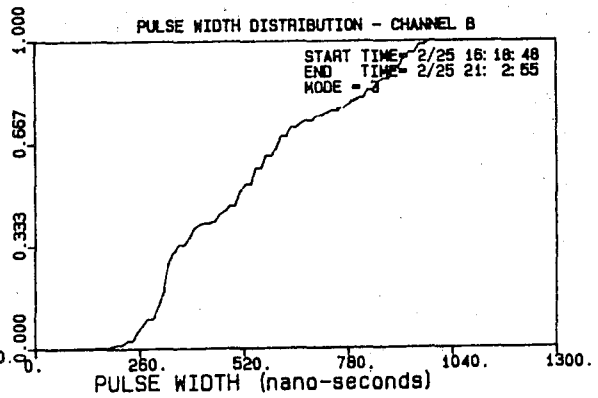
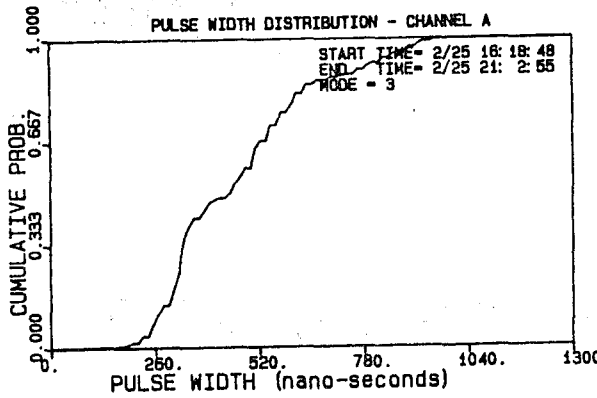
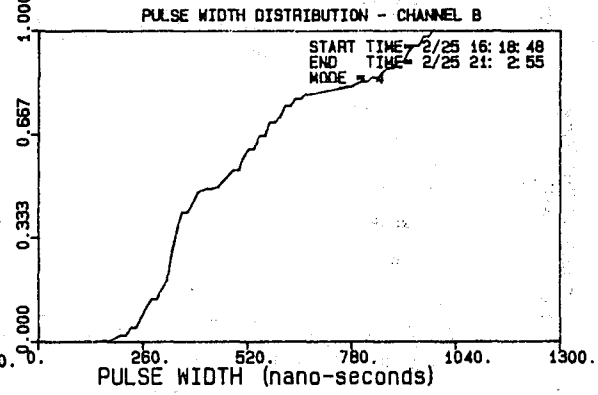
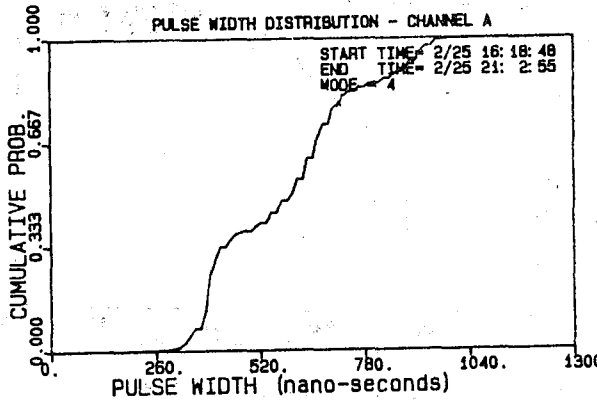
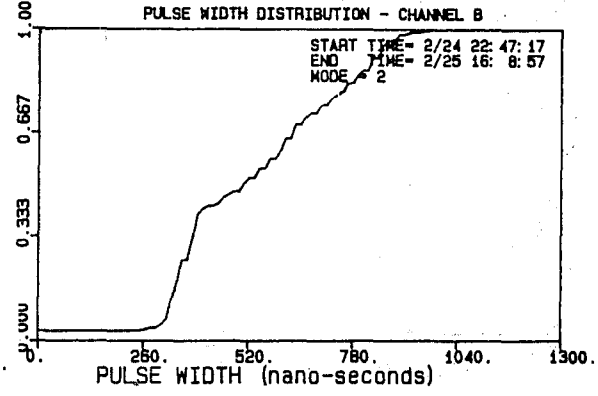
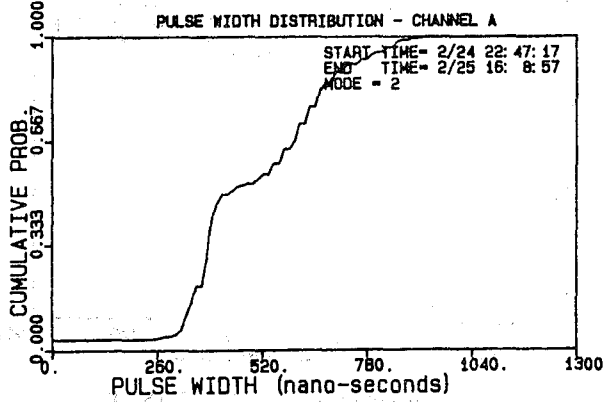
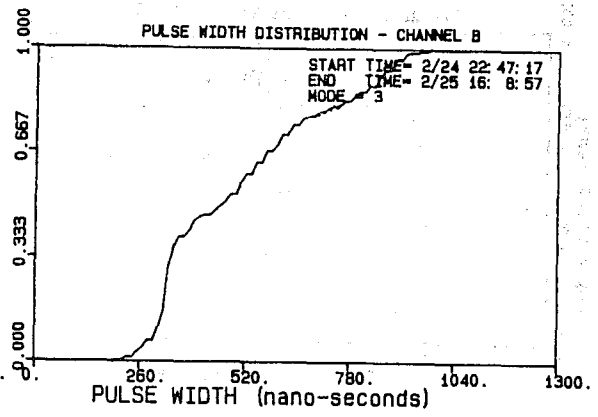
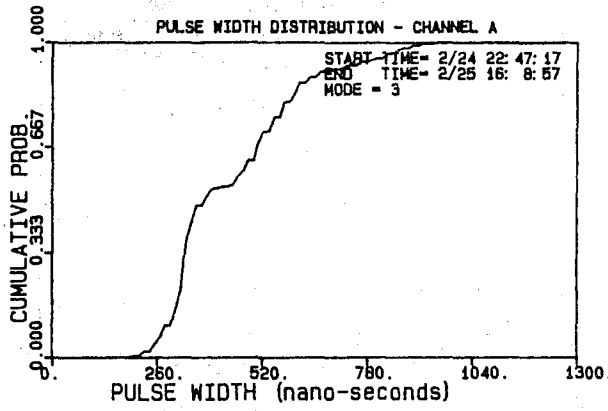


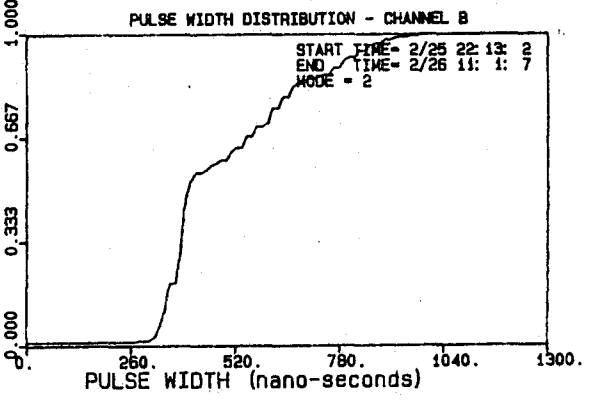
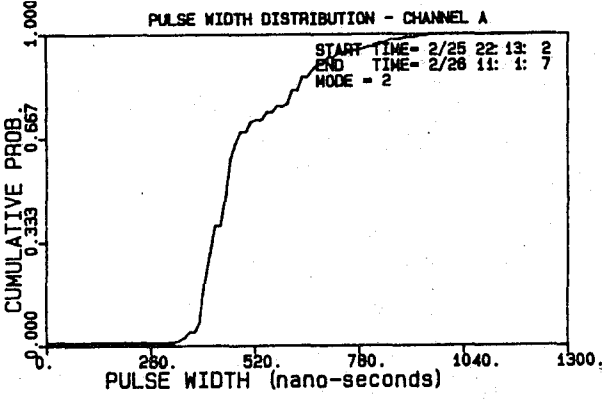
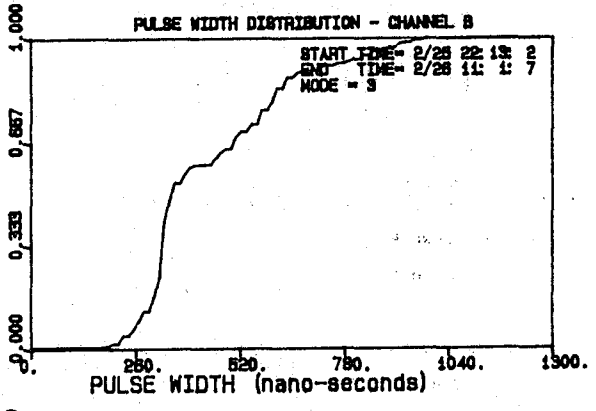
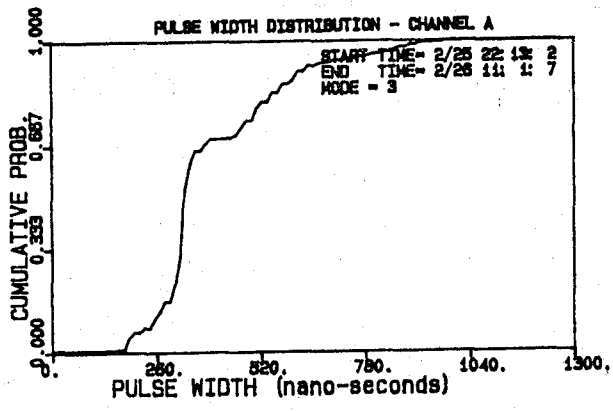
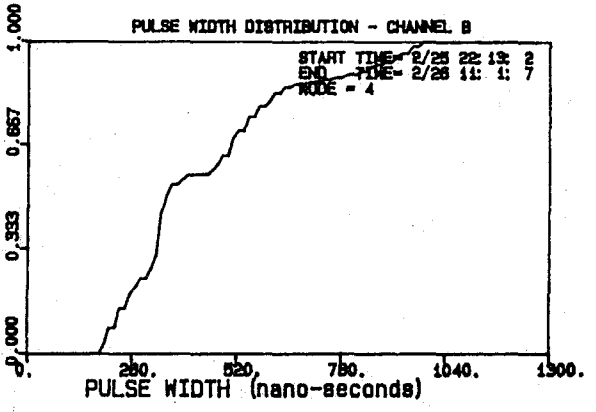
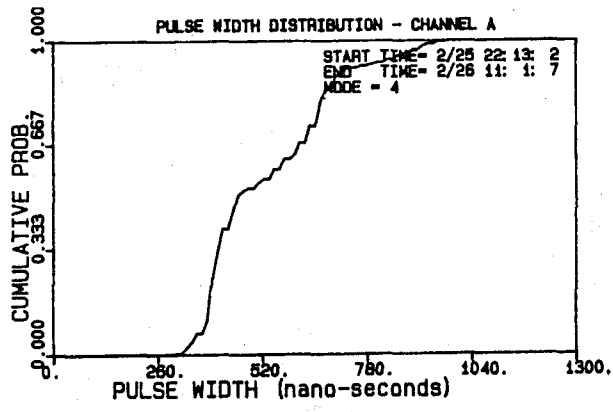
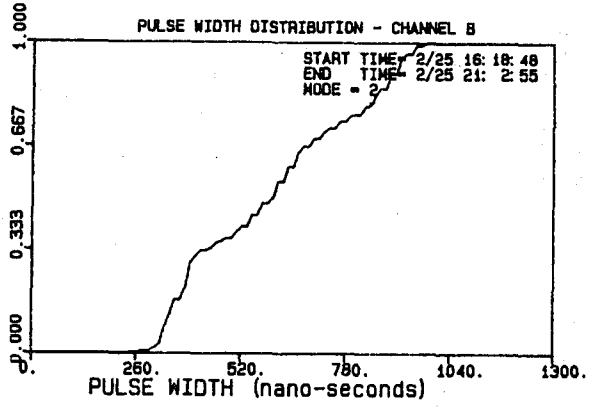
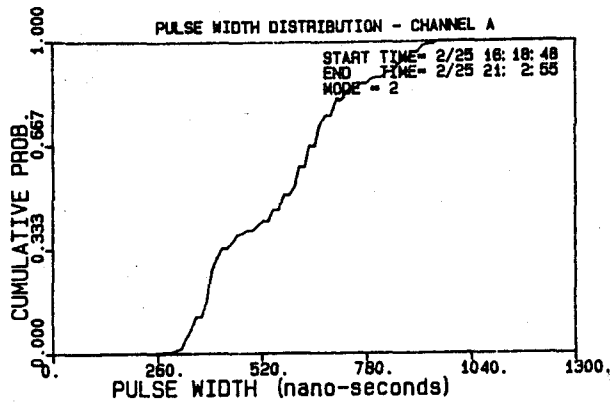


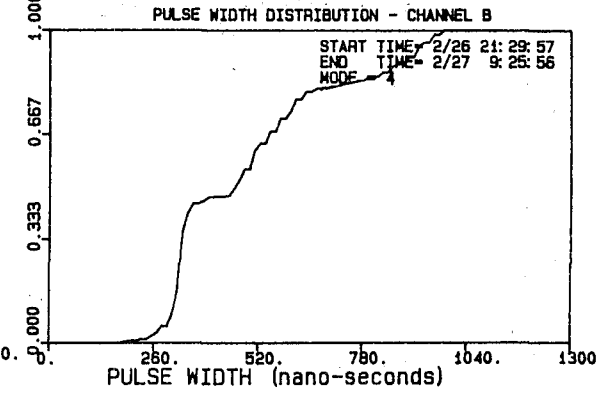
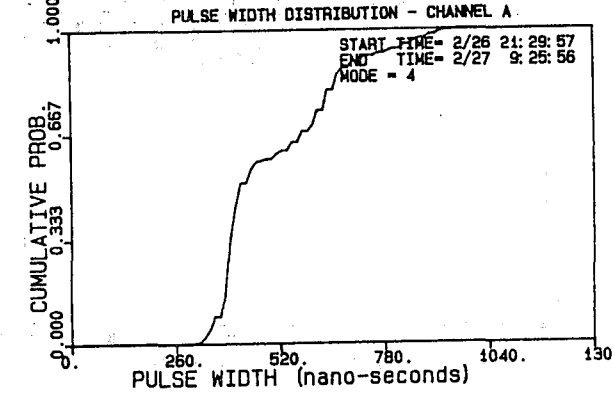
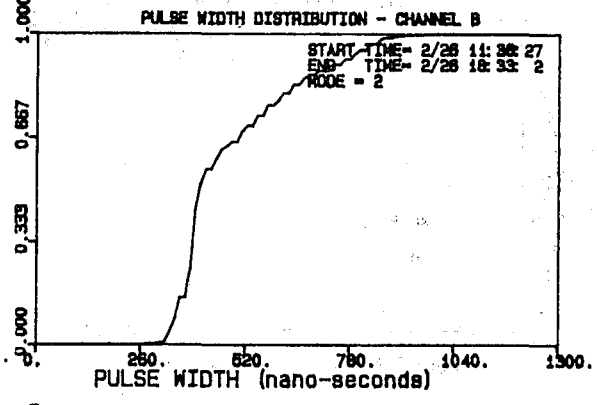
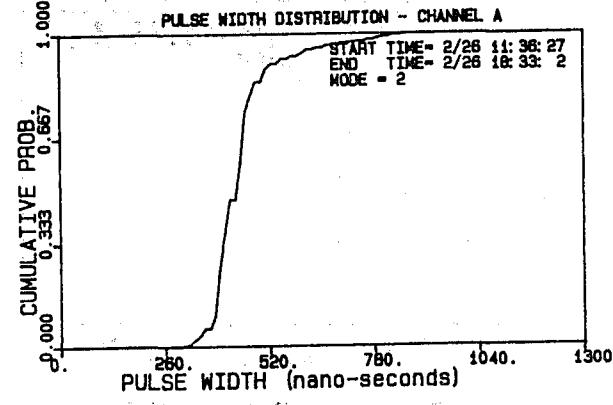
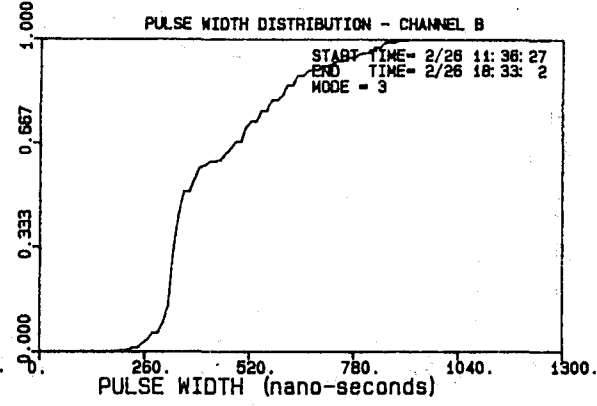
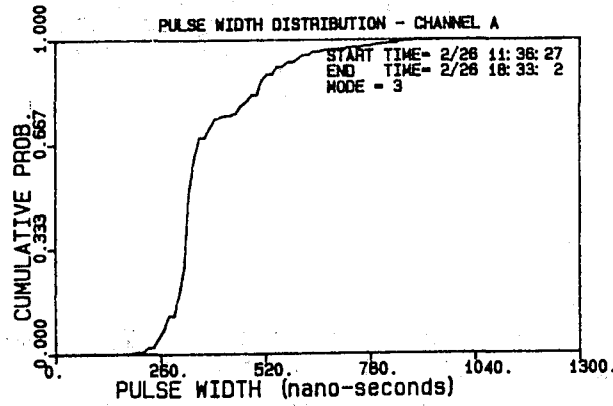
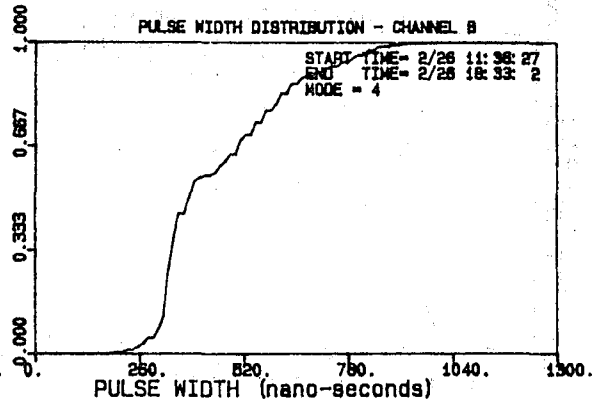
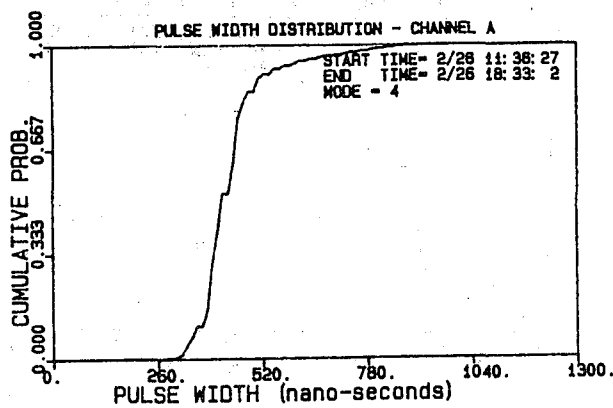


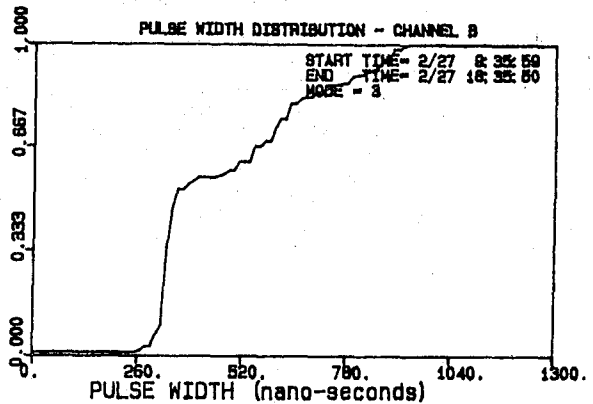
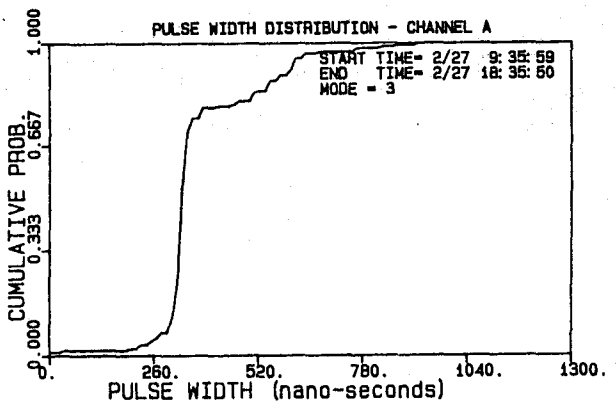
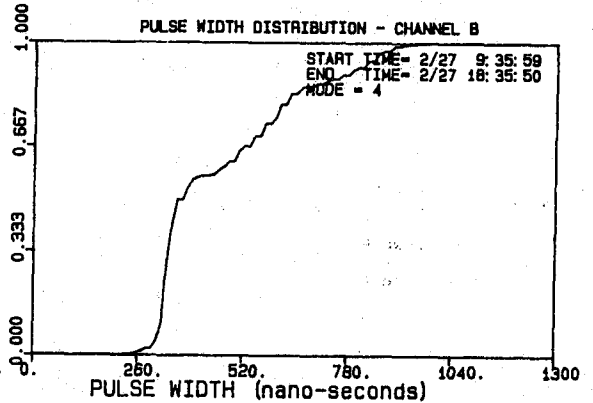
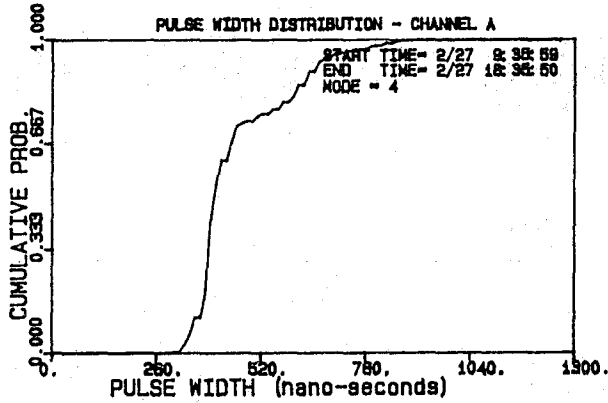
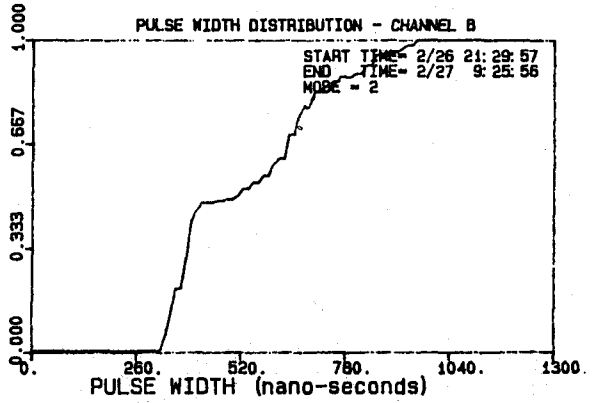
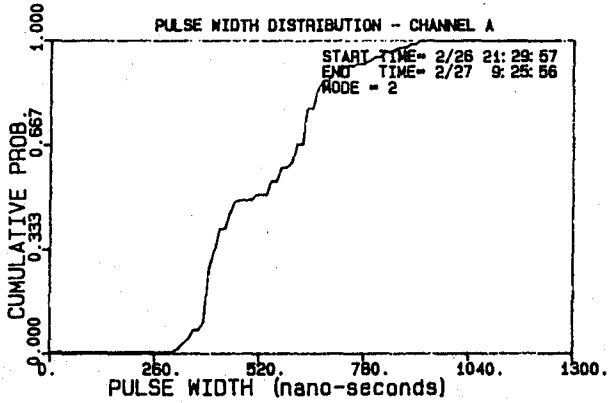
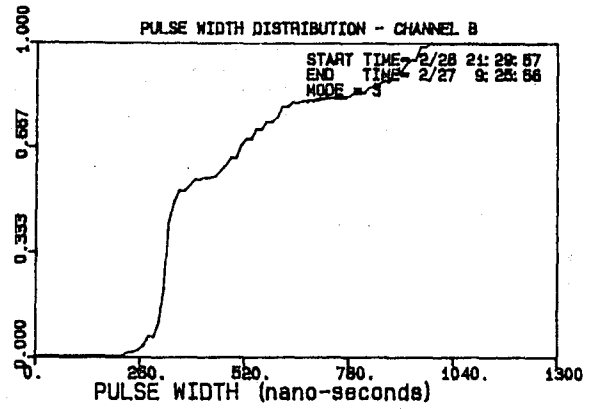
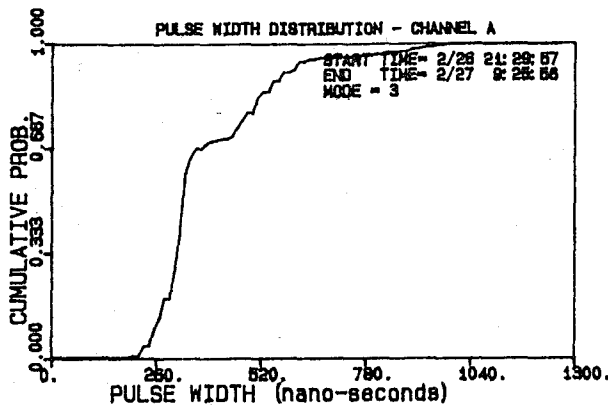


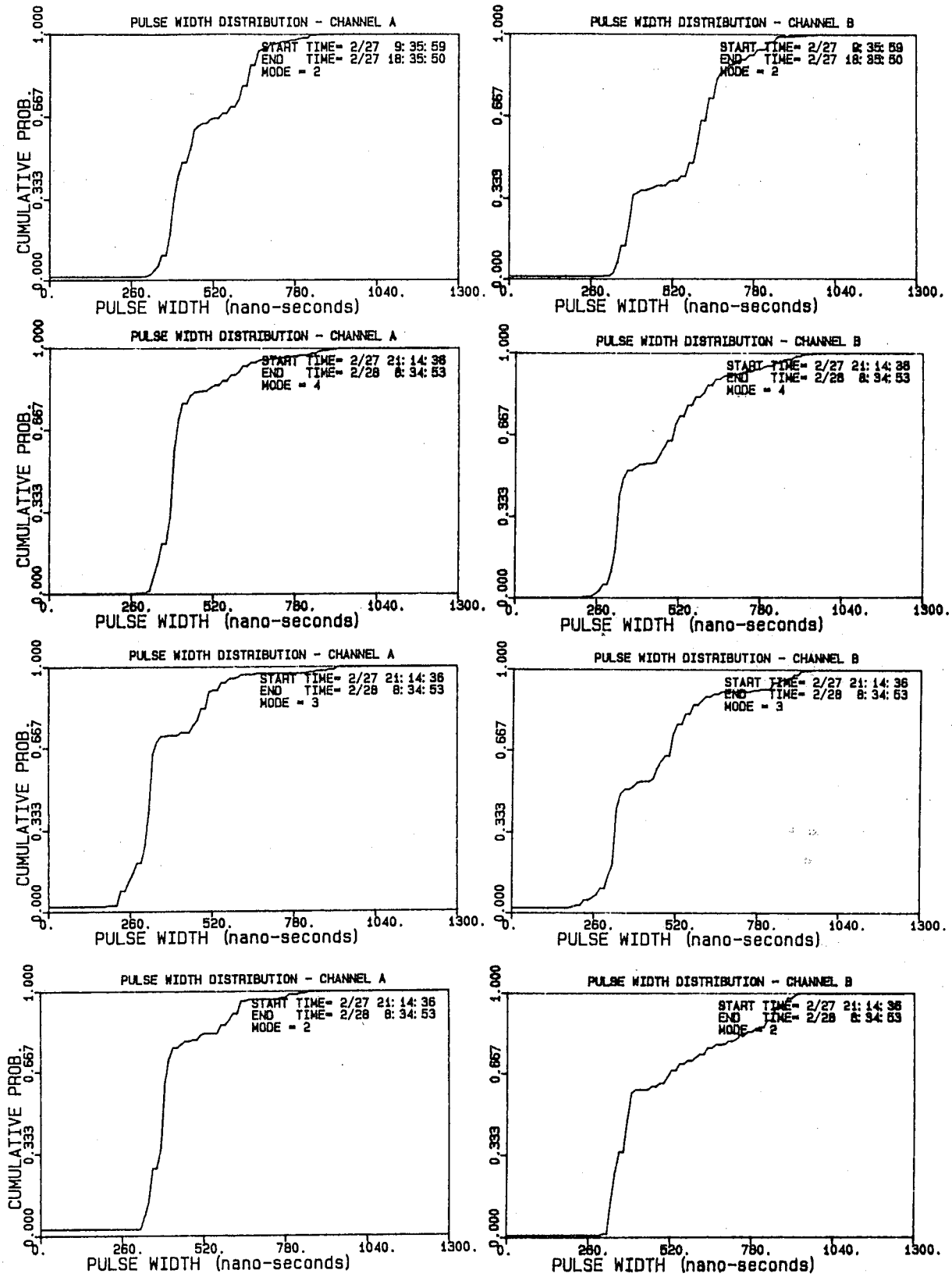








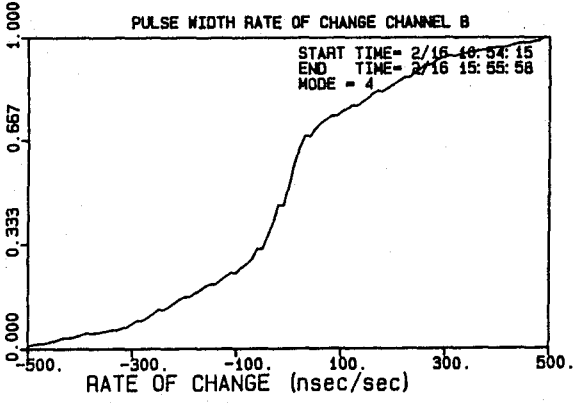
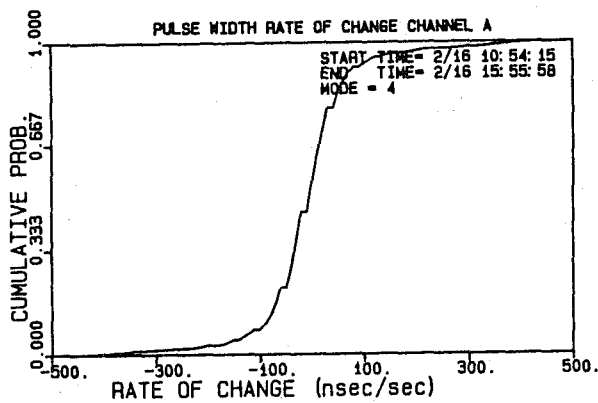
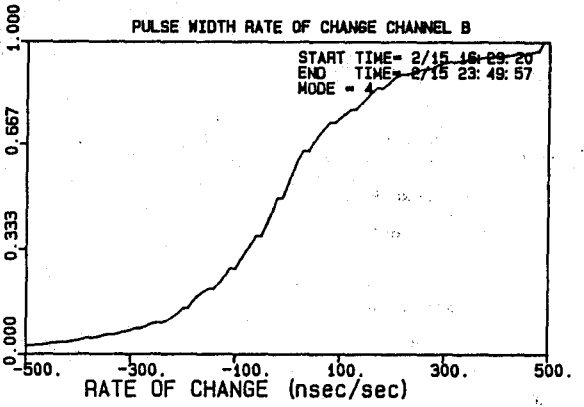
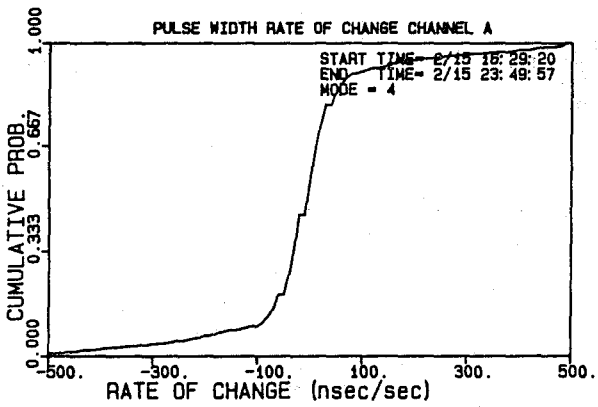
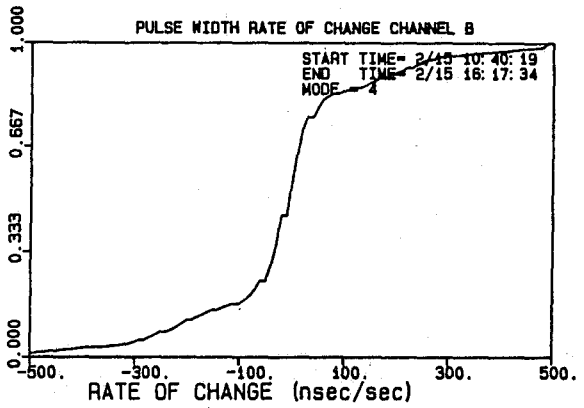
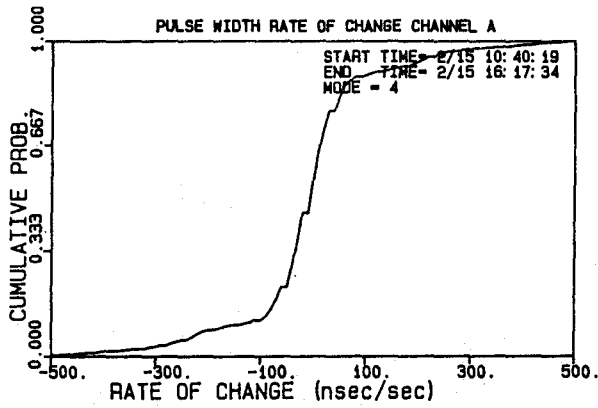
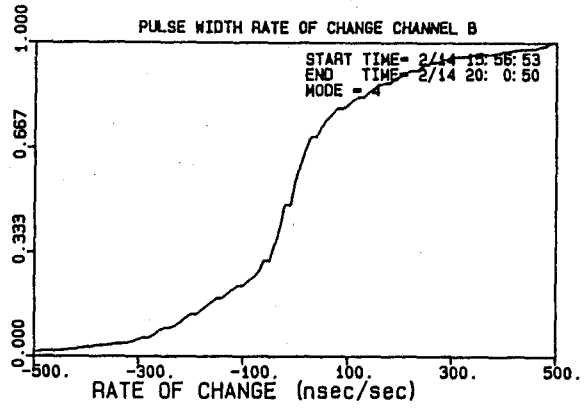
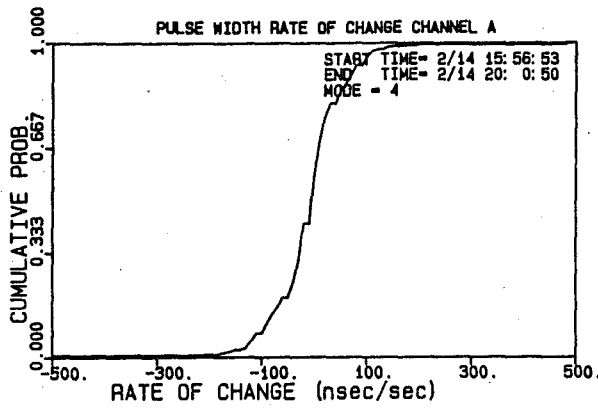


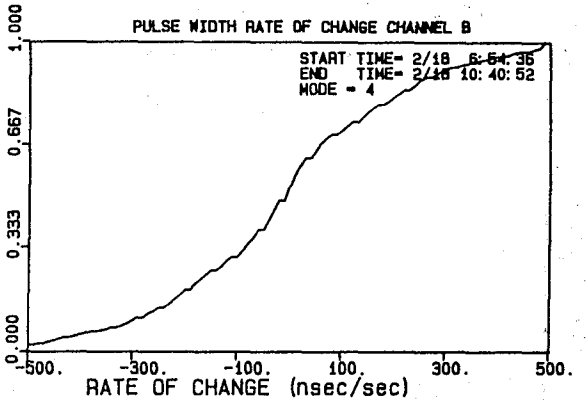
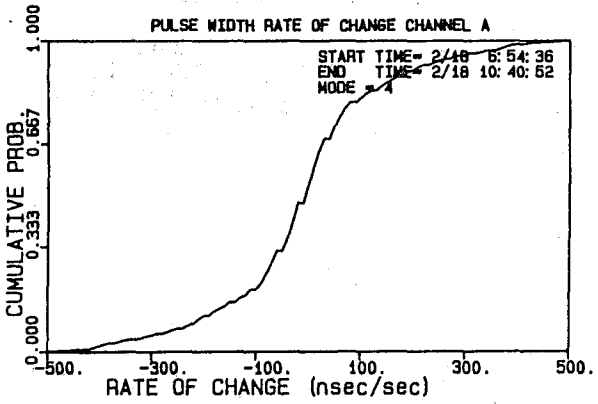
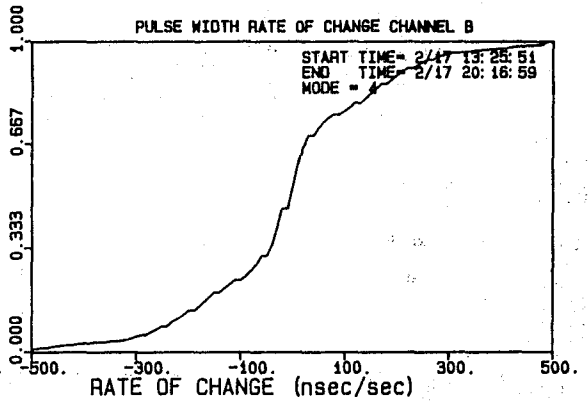
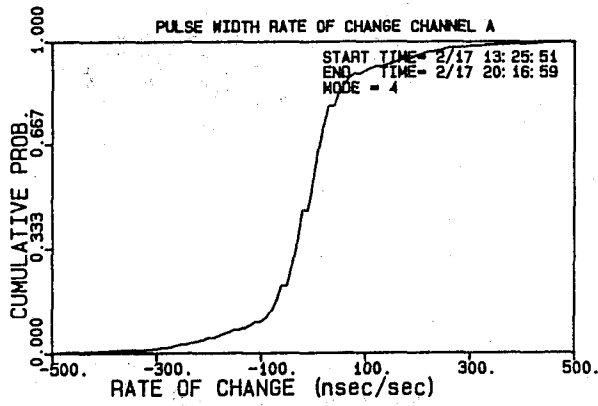
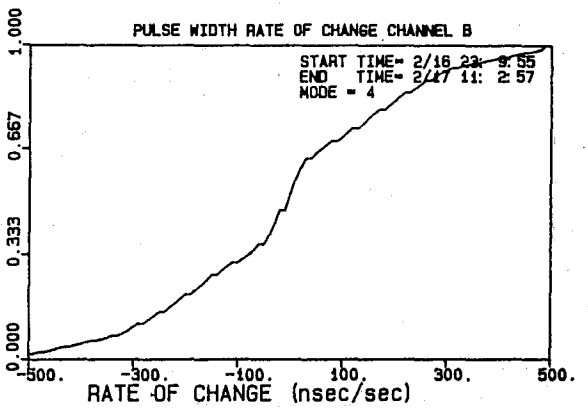
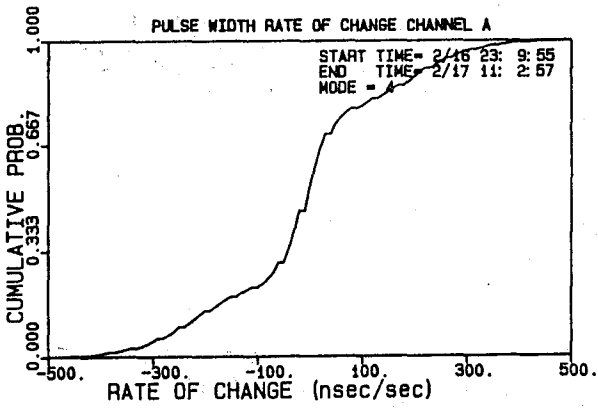
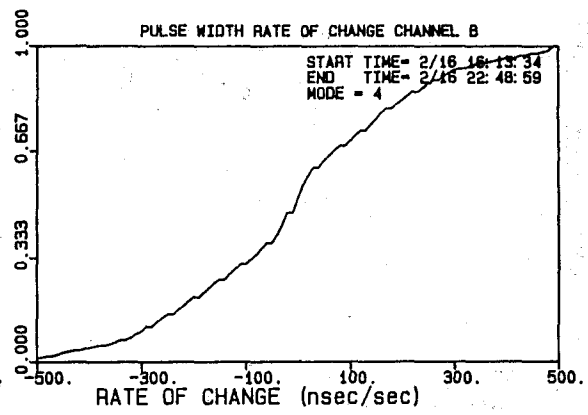
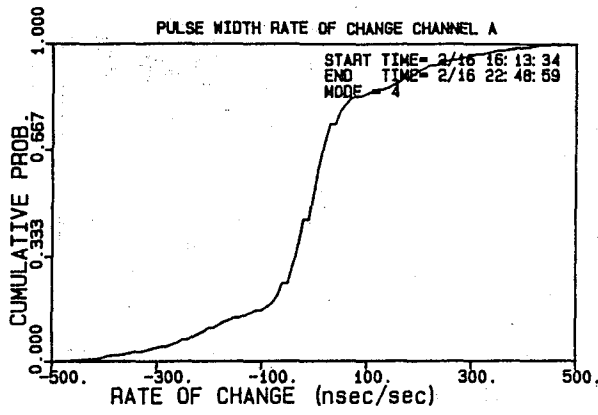


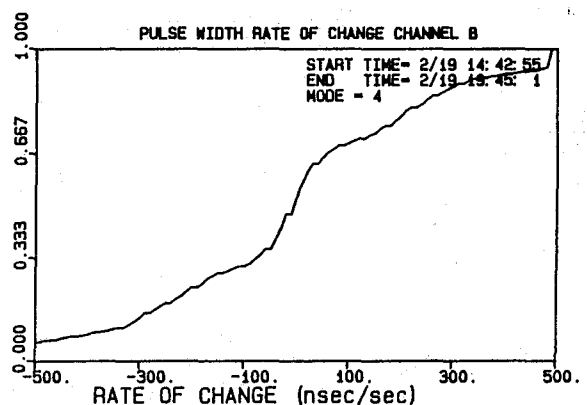
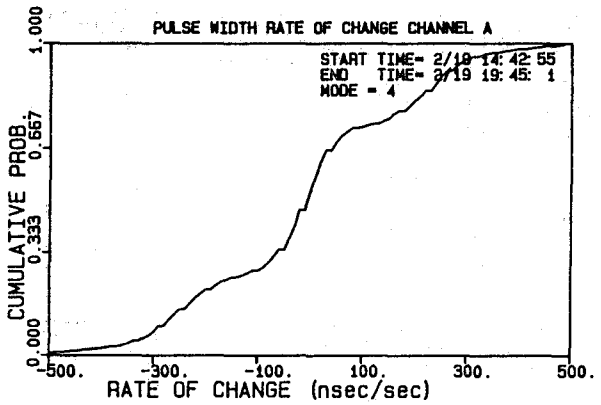
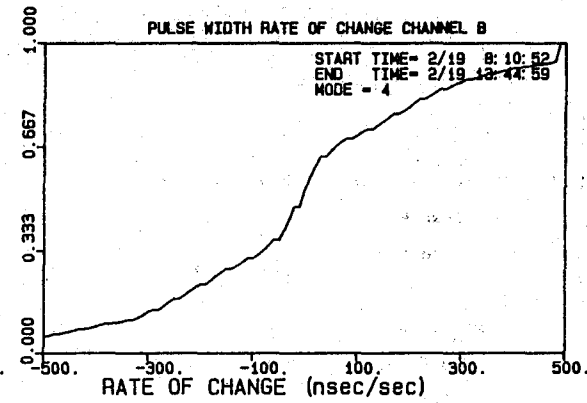
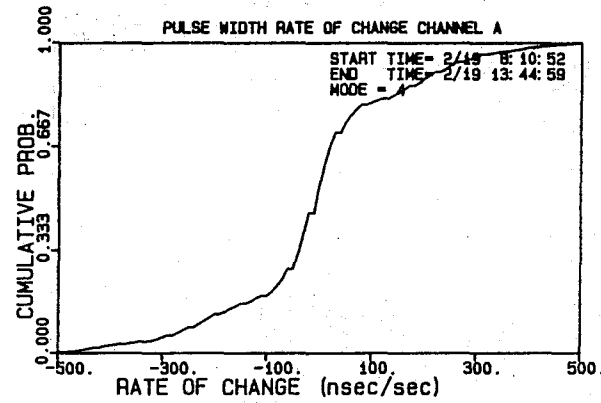
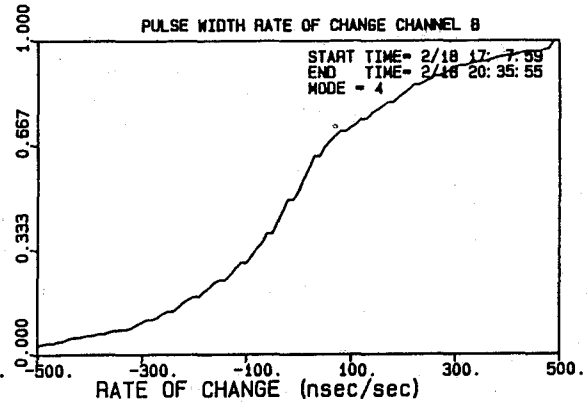
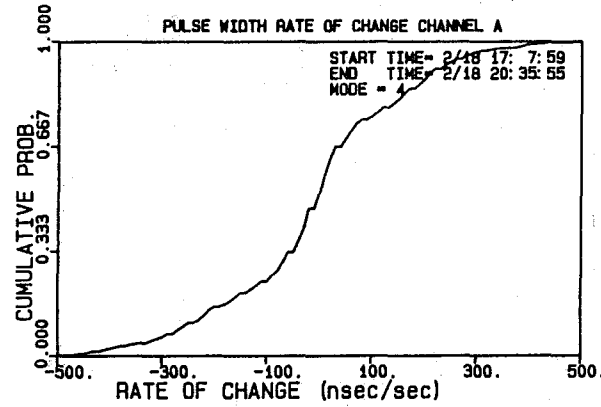
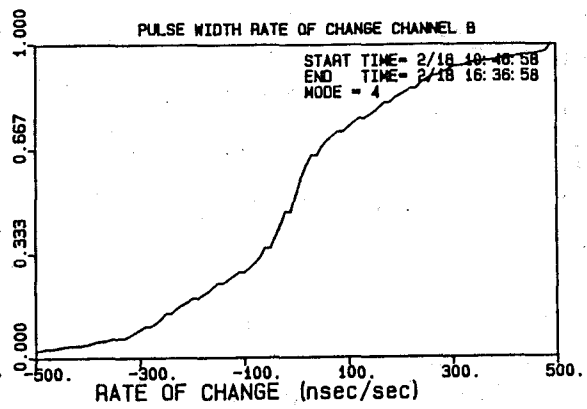
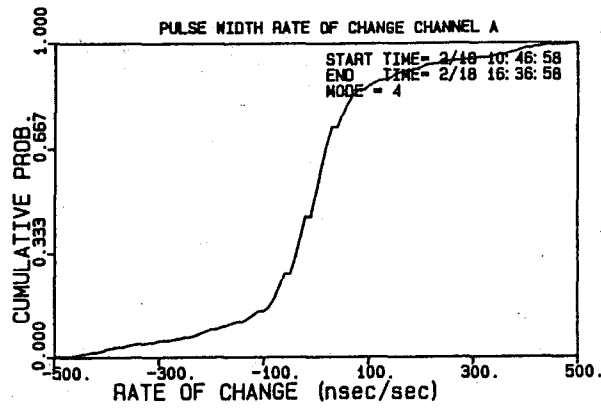


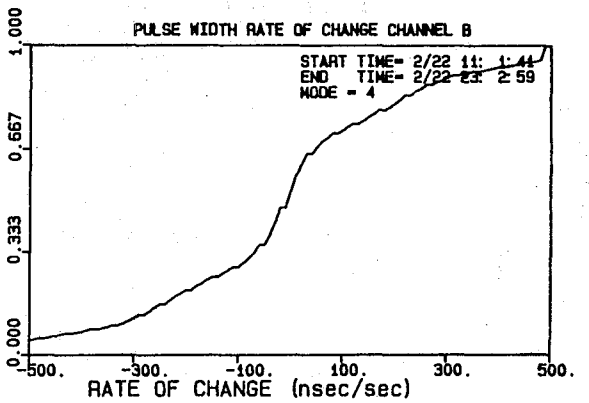
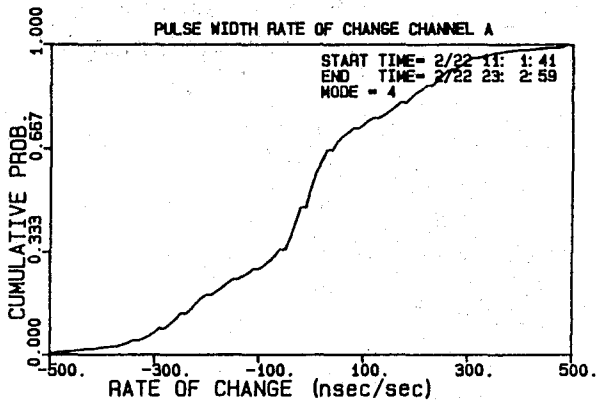
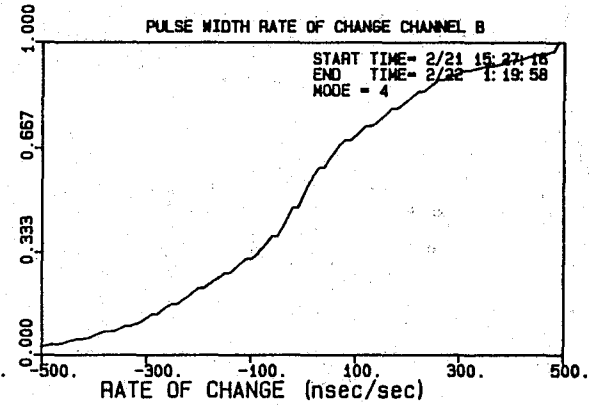
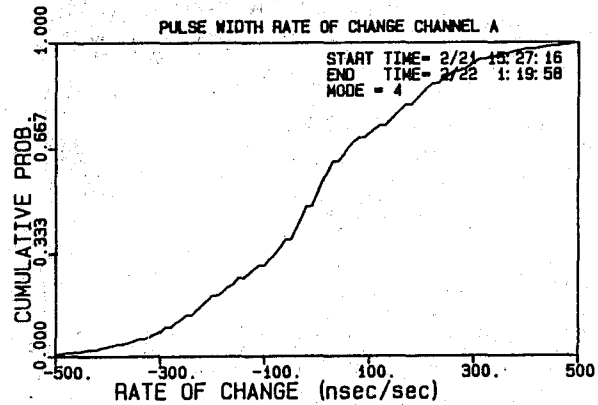
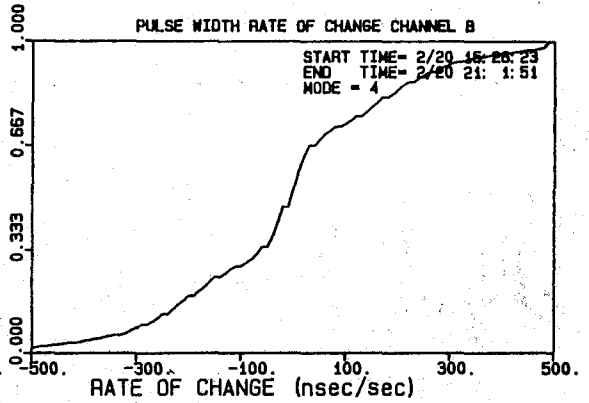
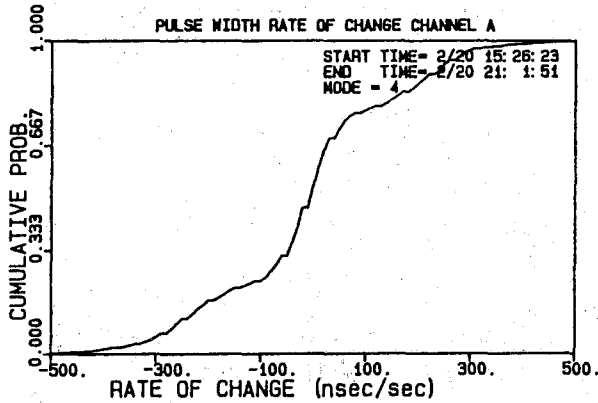
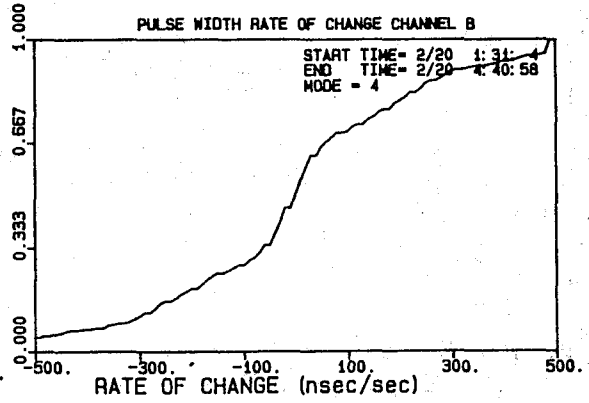
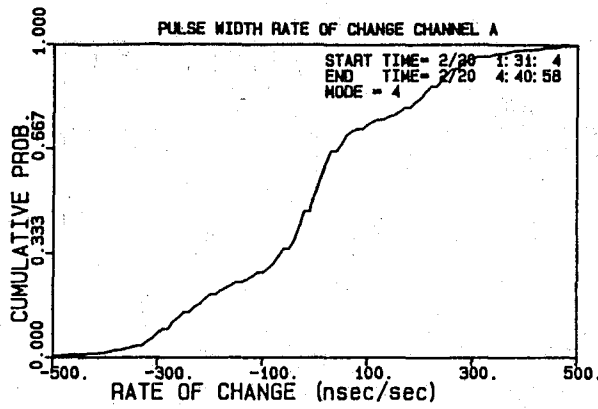
APPENDIX C

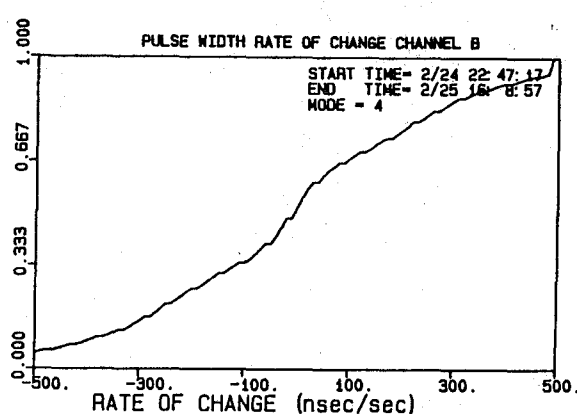
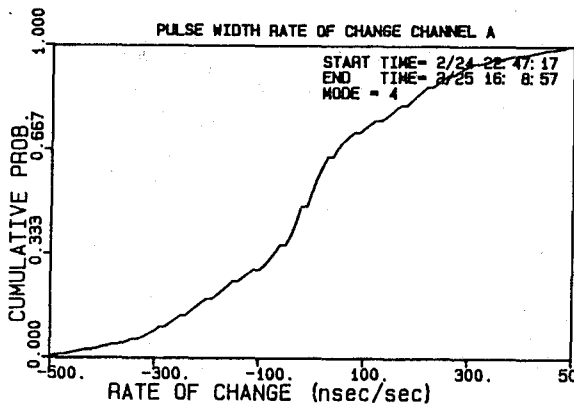
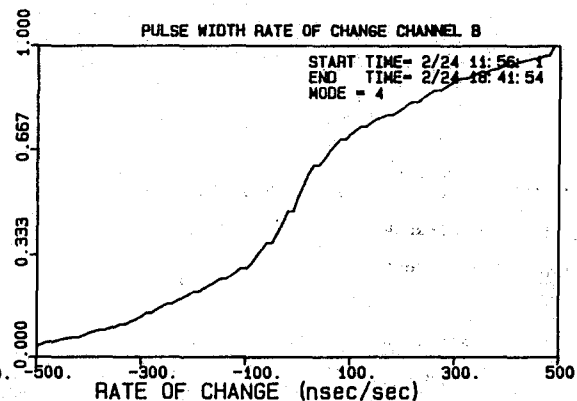
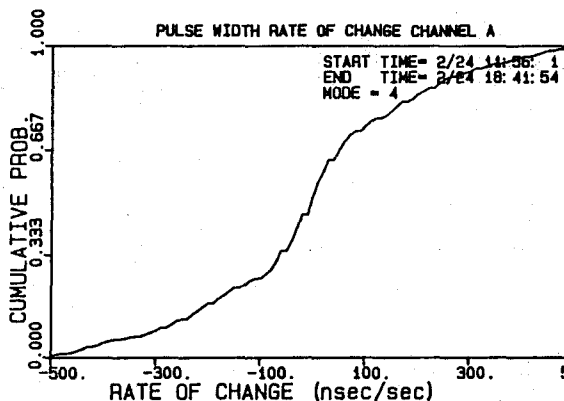
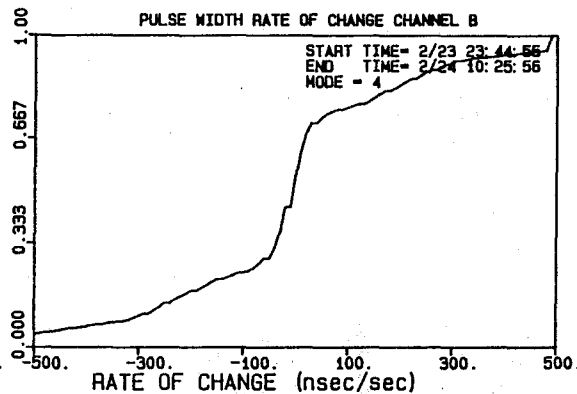
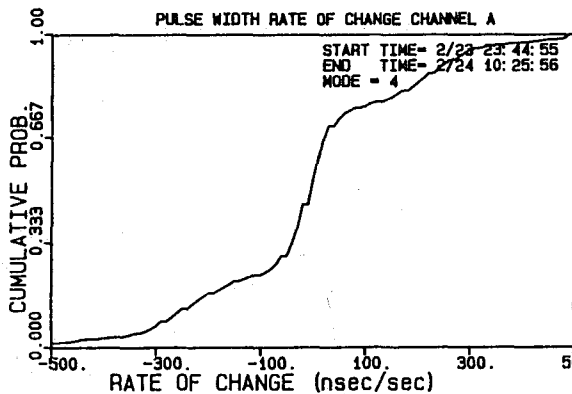
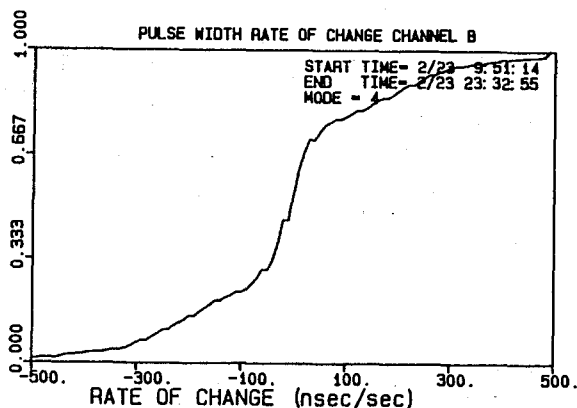
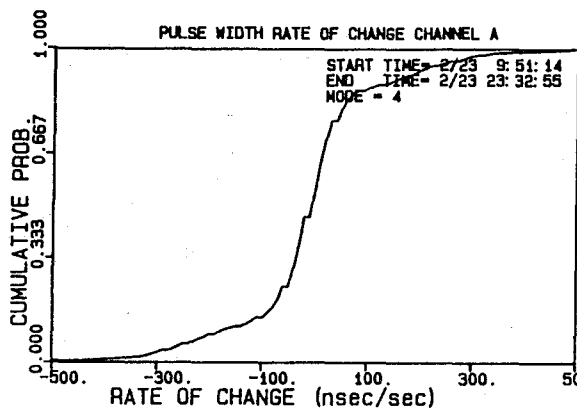
Cumulative Distributions of Pulse Width Rate-of-Change

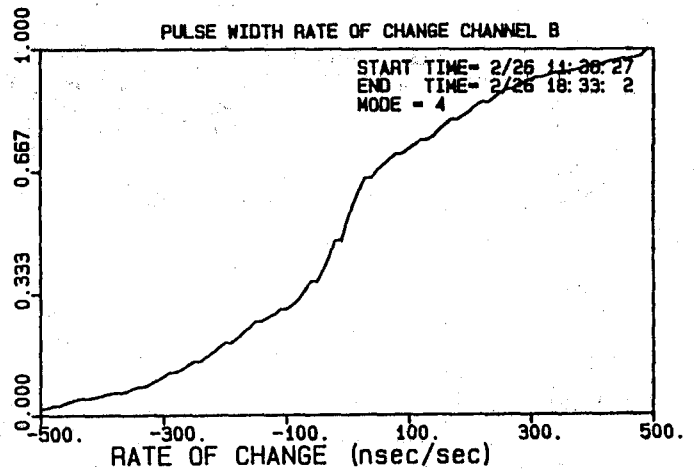
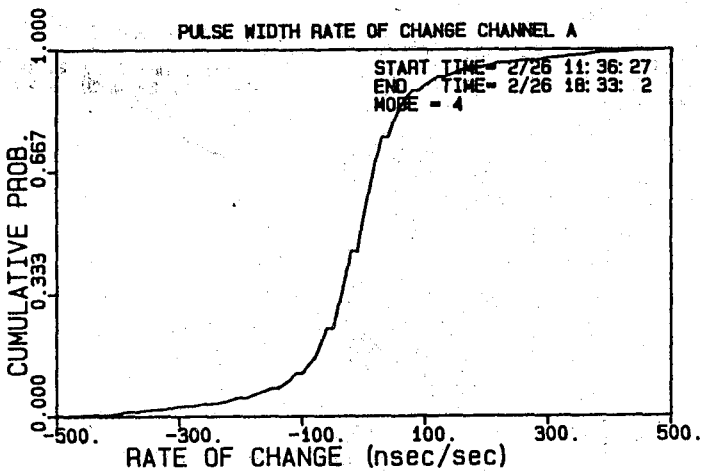
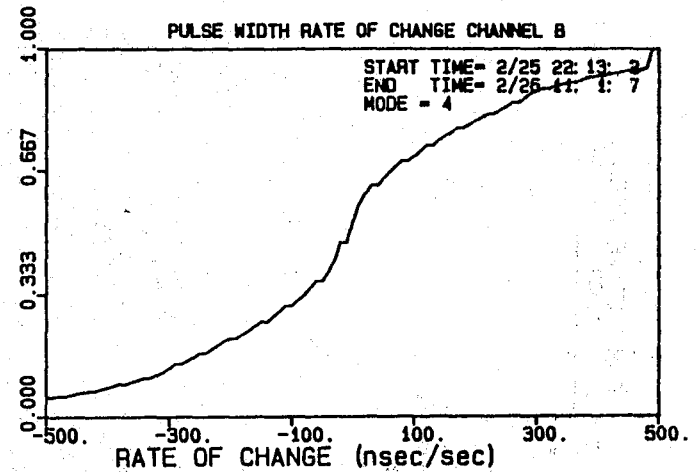
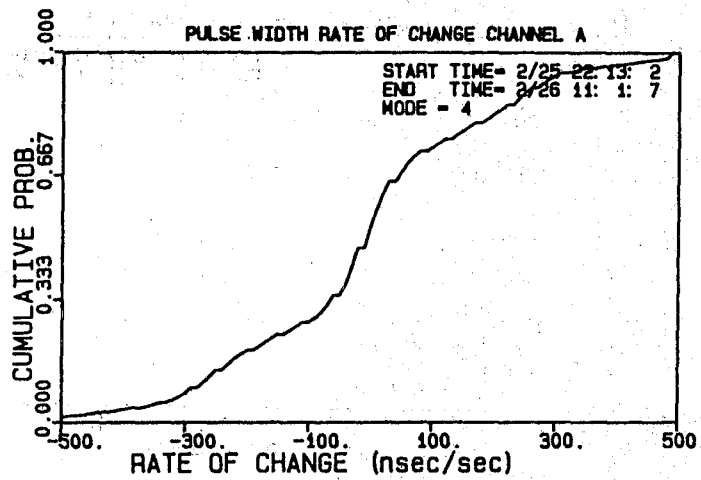
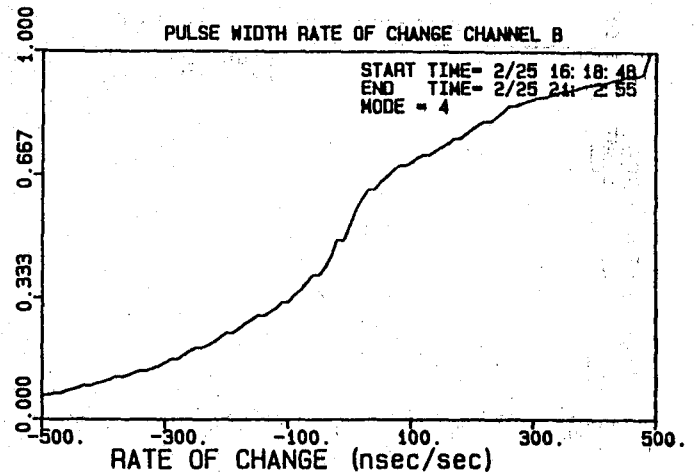
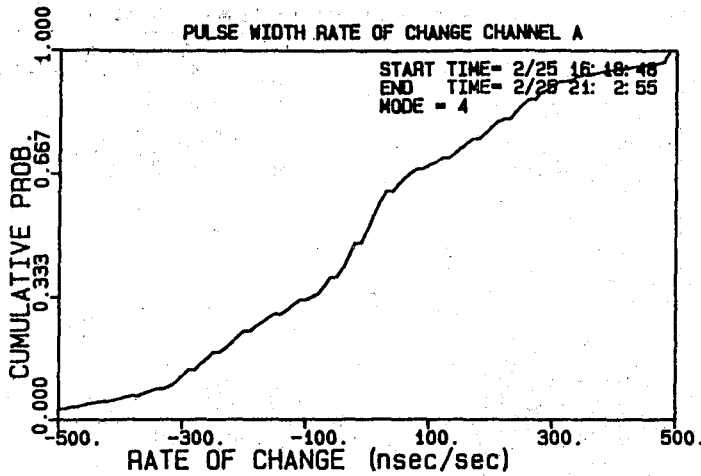


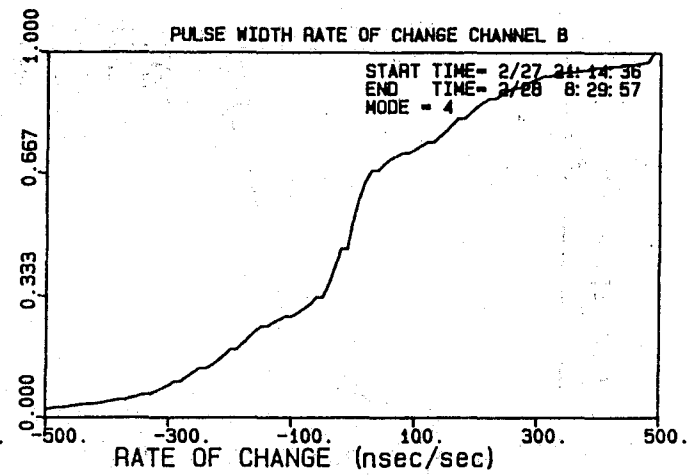
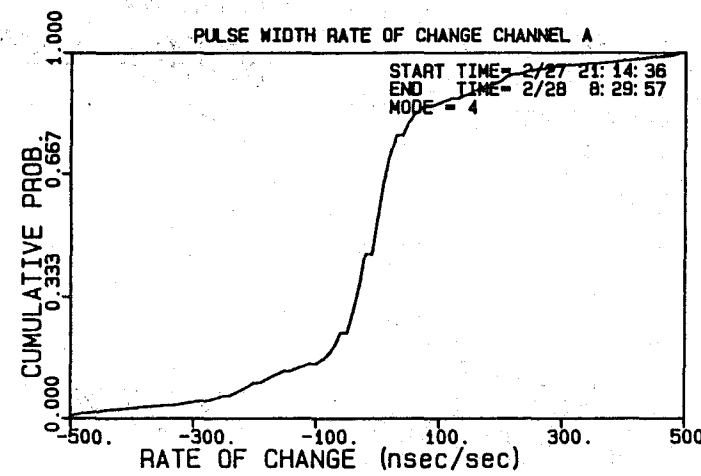
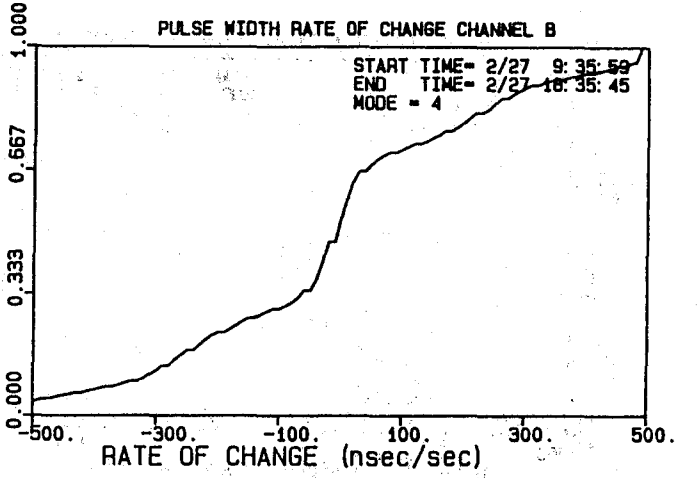
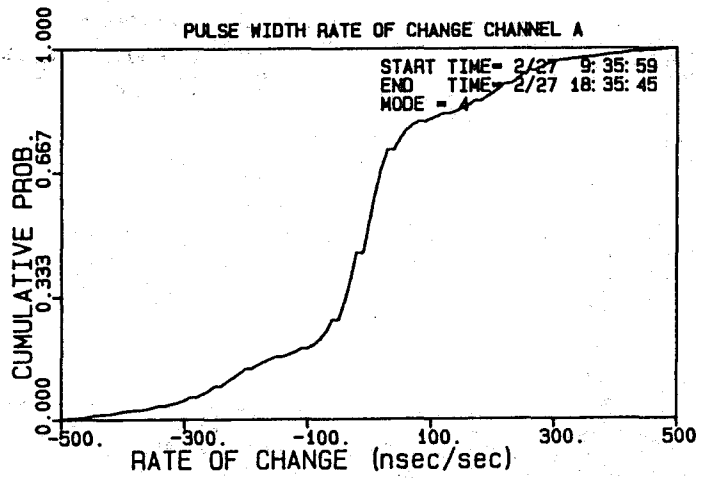
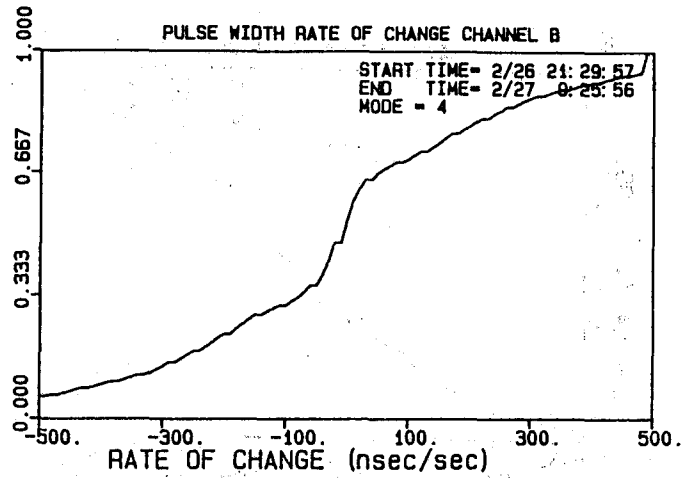
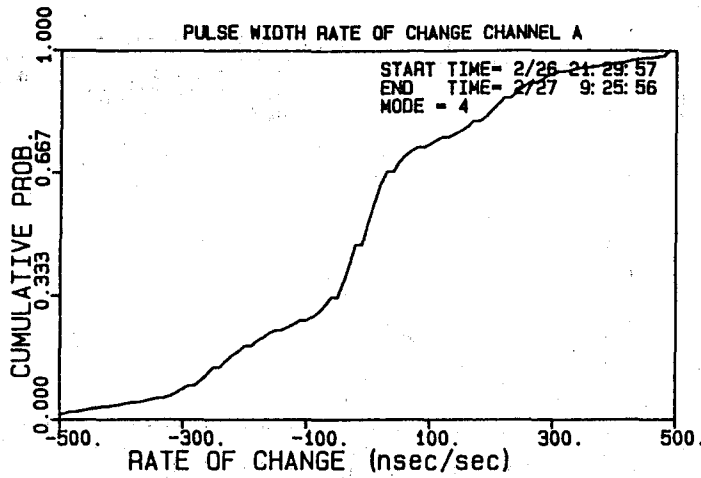






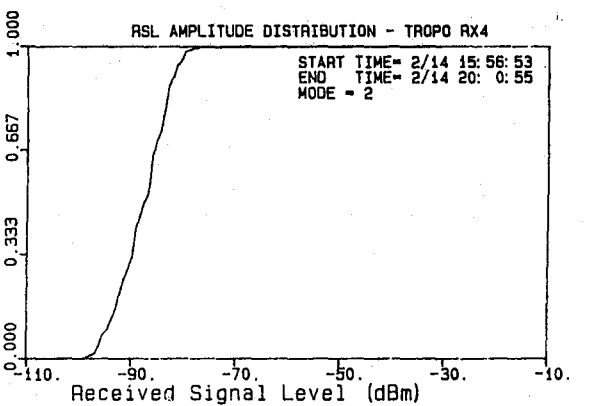
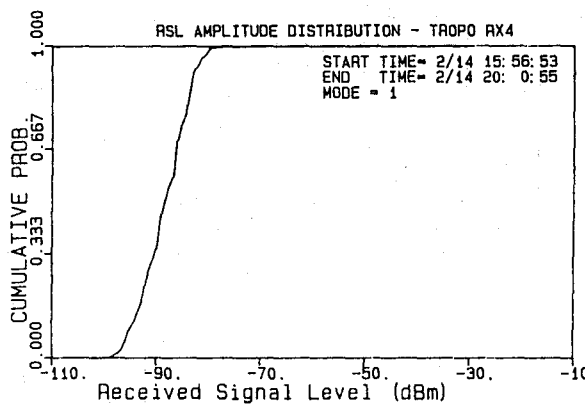
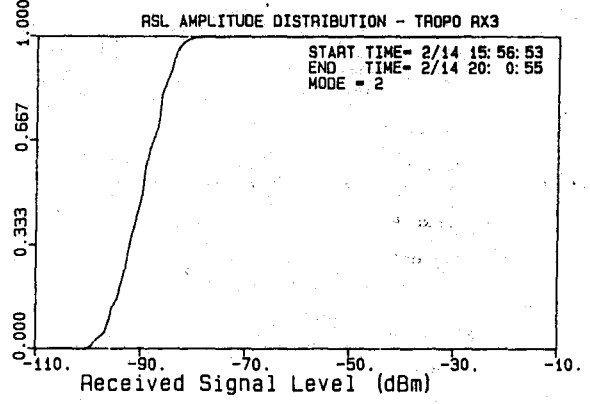
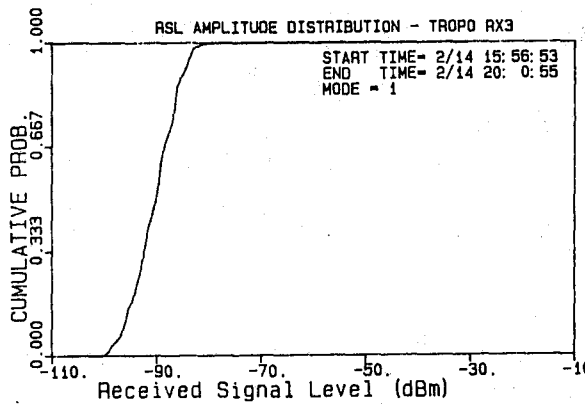
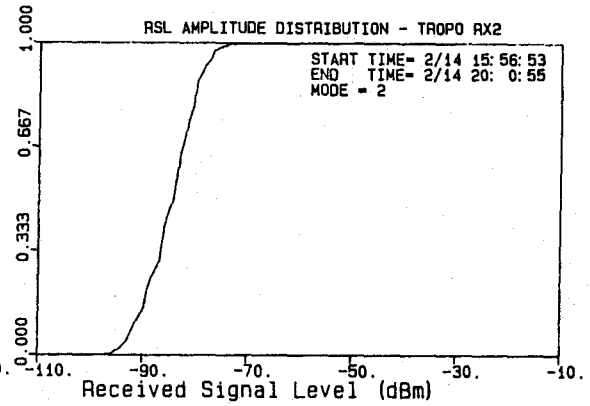
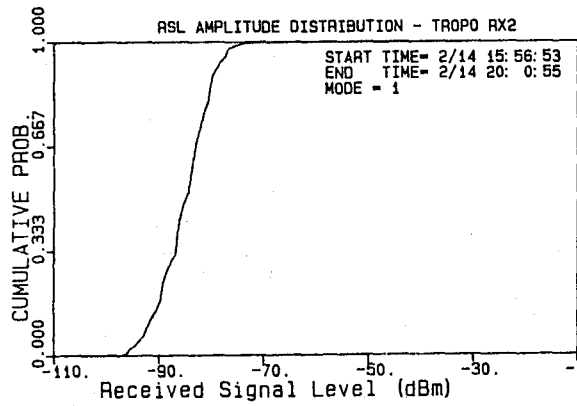
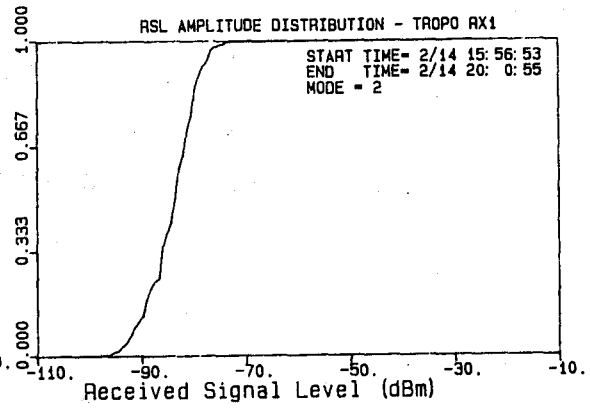
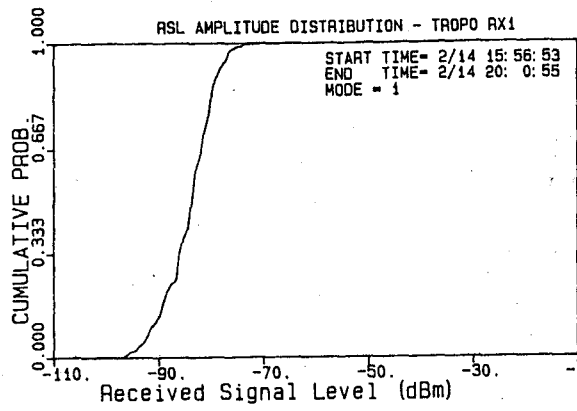


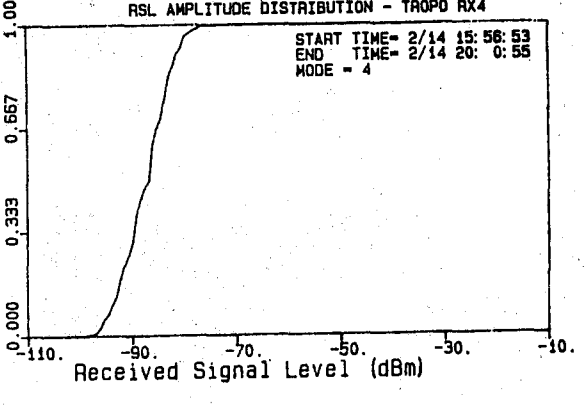
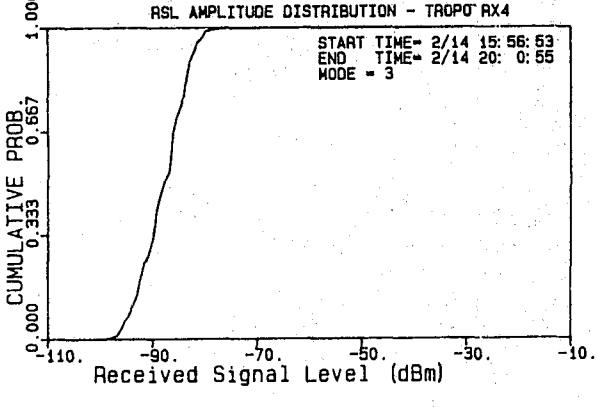
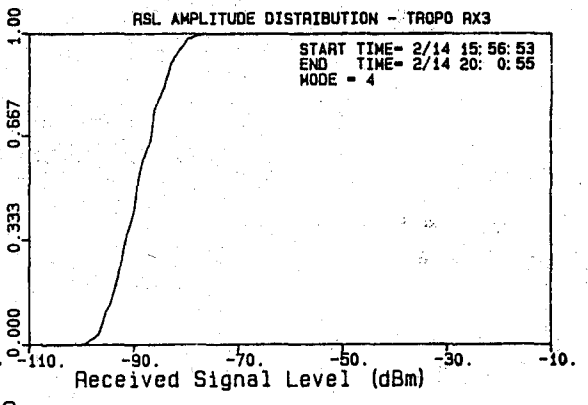
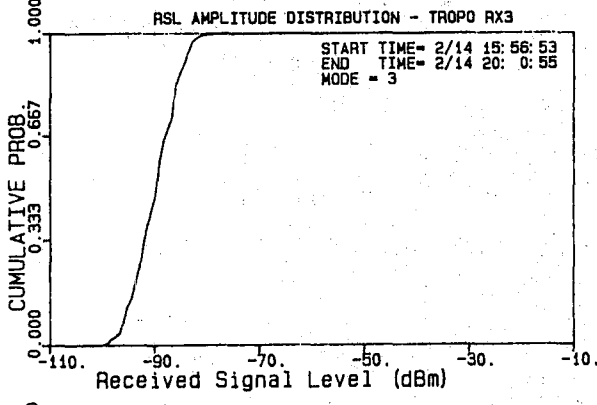
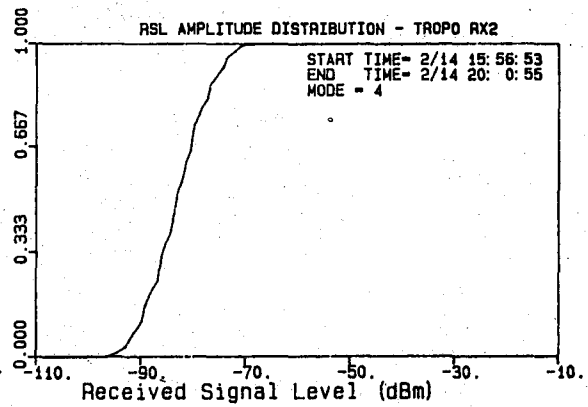
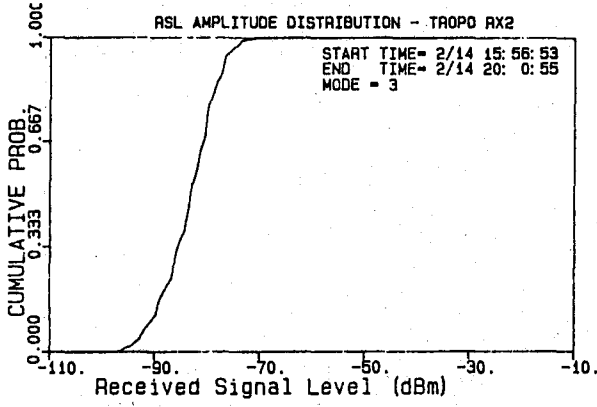
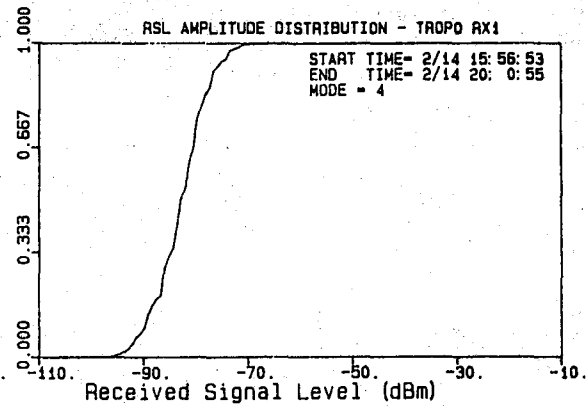
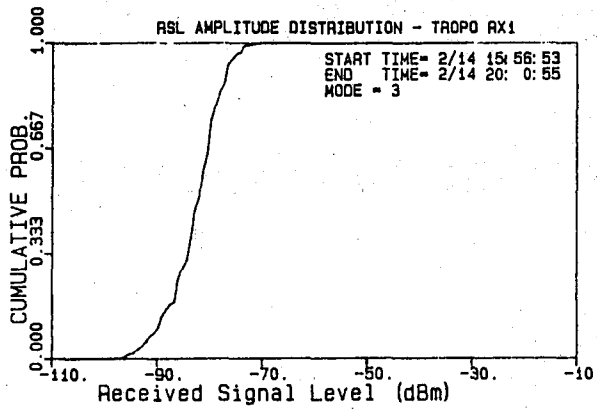


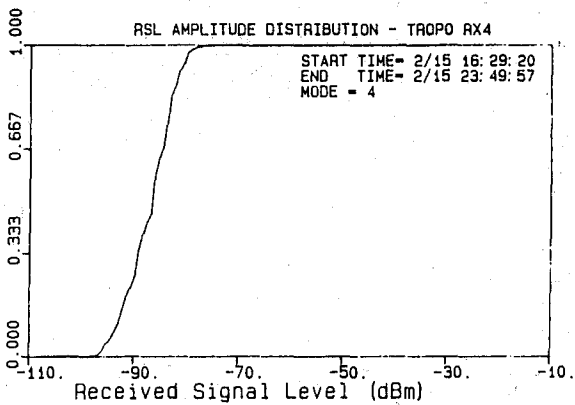
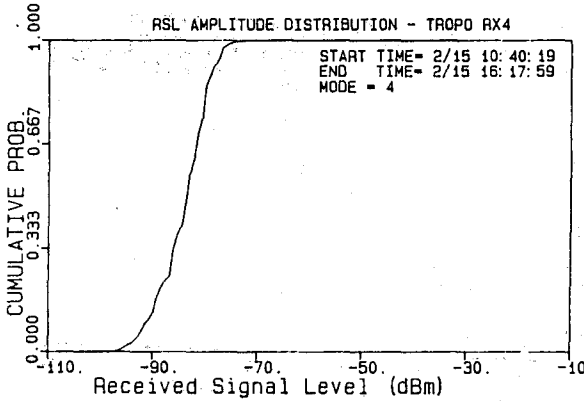
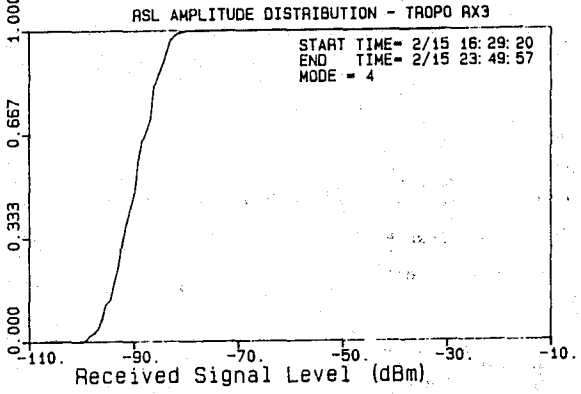
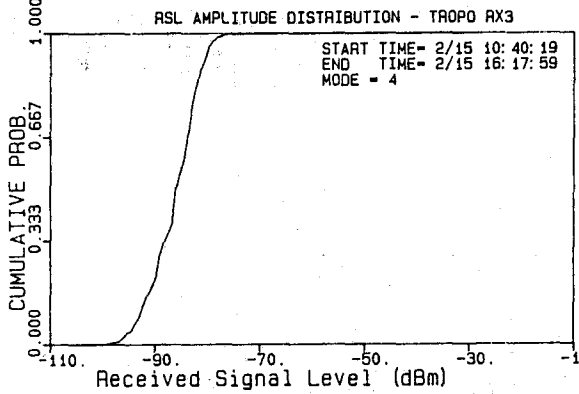
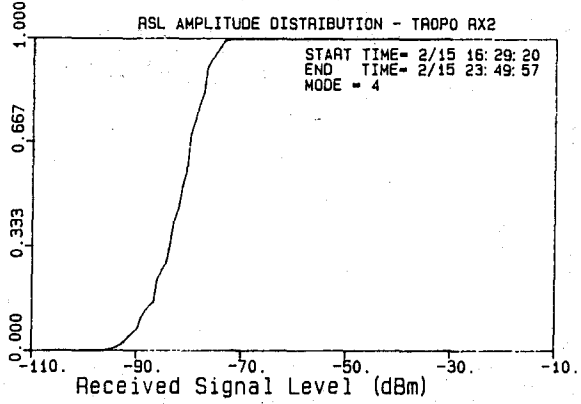
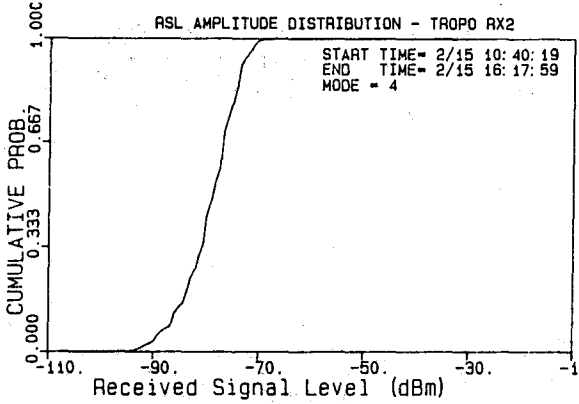
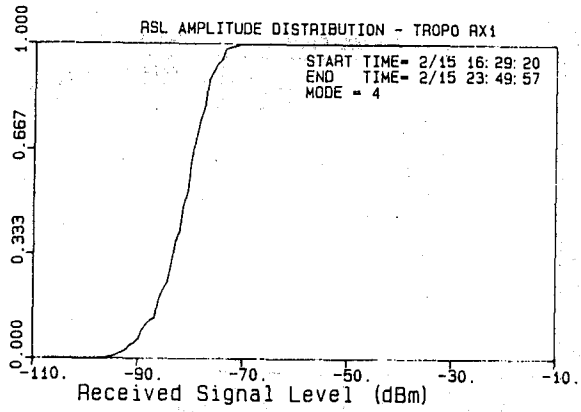
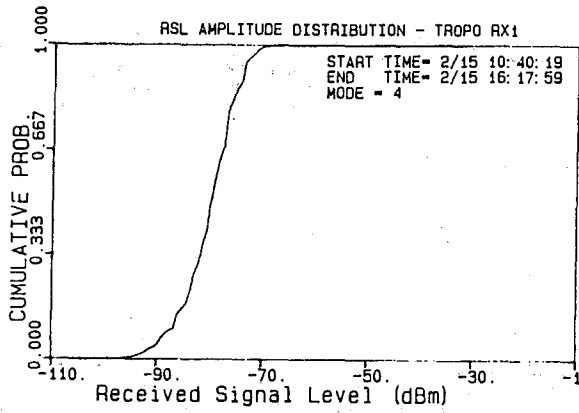


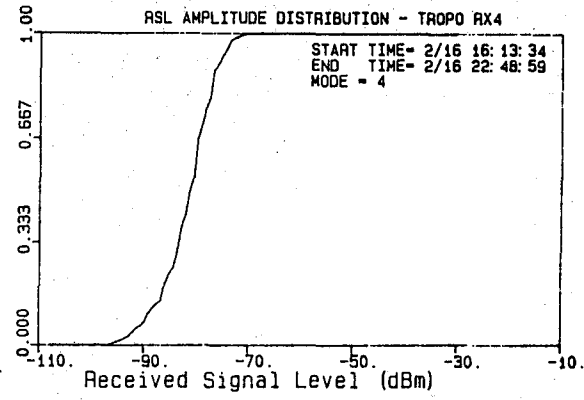
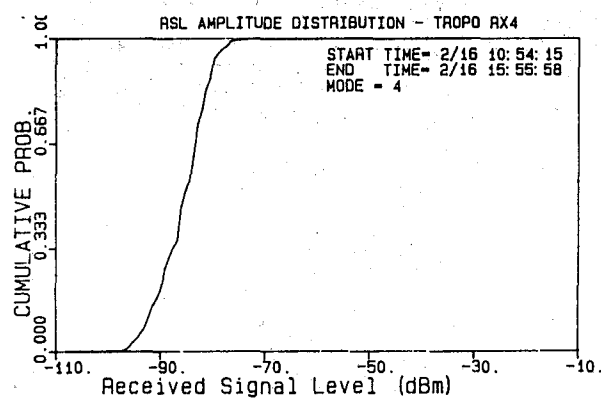
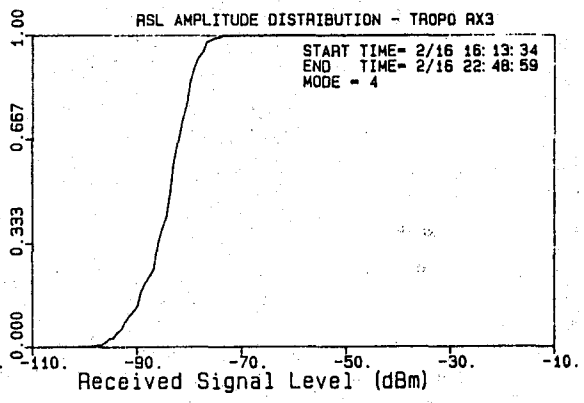
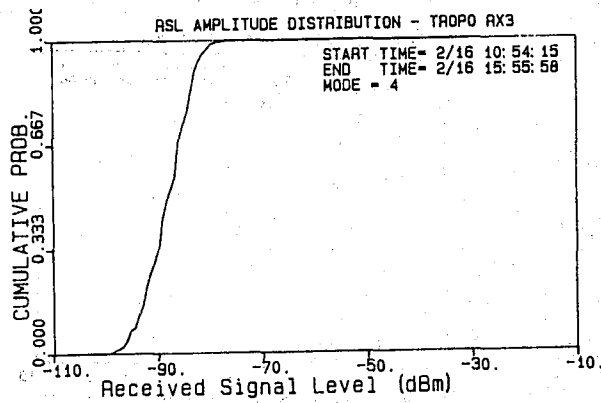
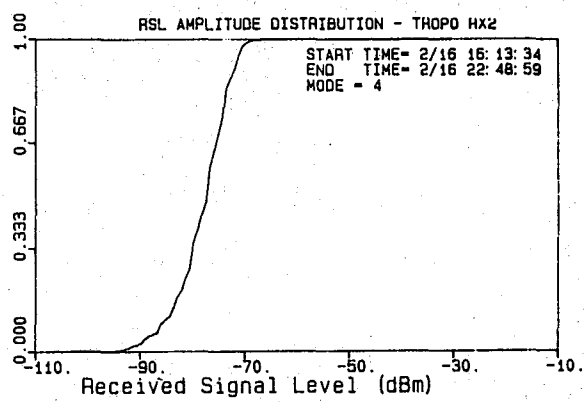
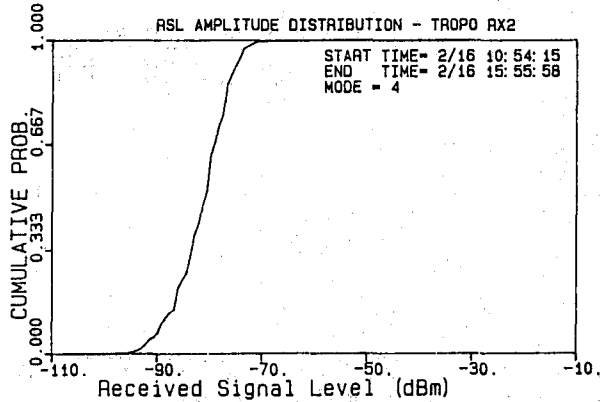
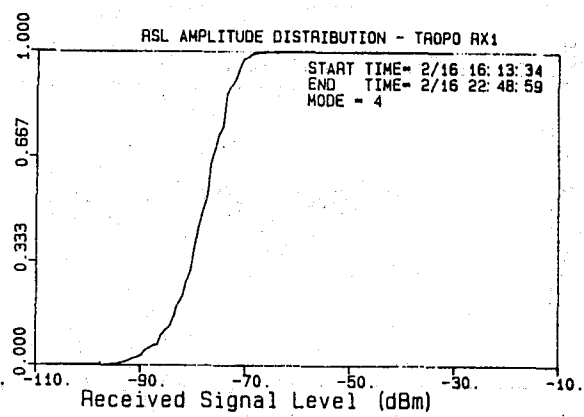
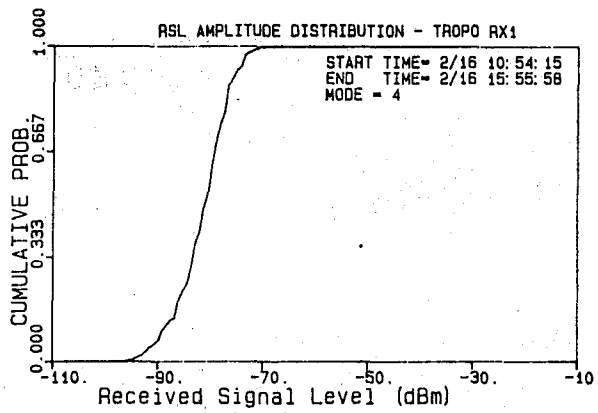
APPENDIX D

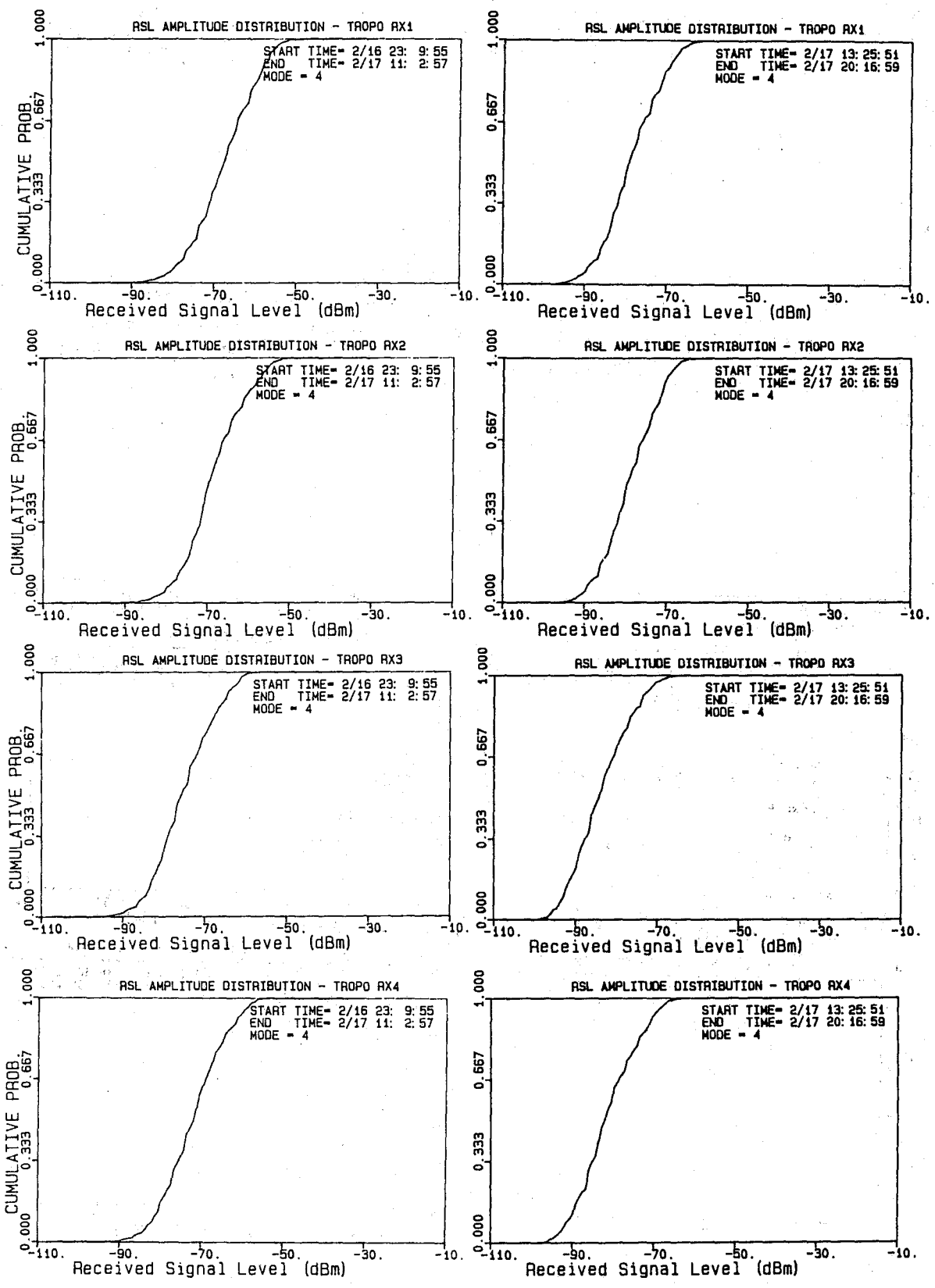
Cumulative Distributions of RSL

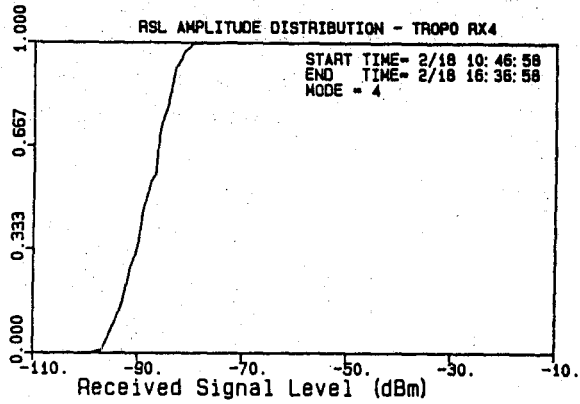
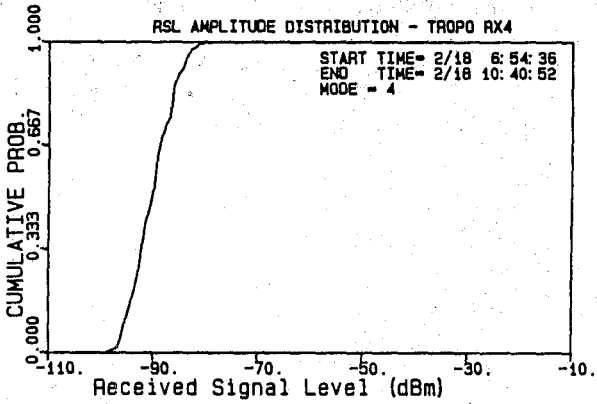
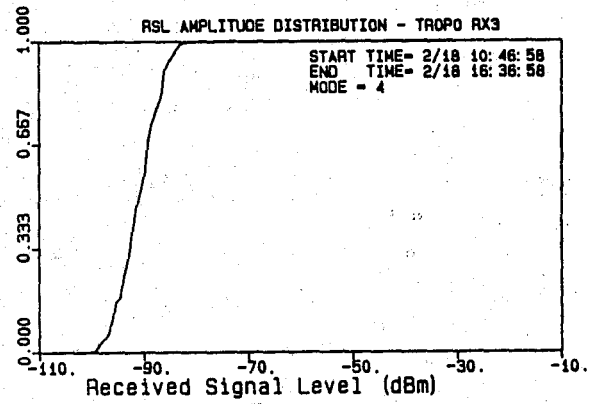
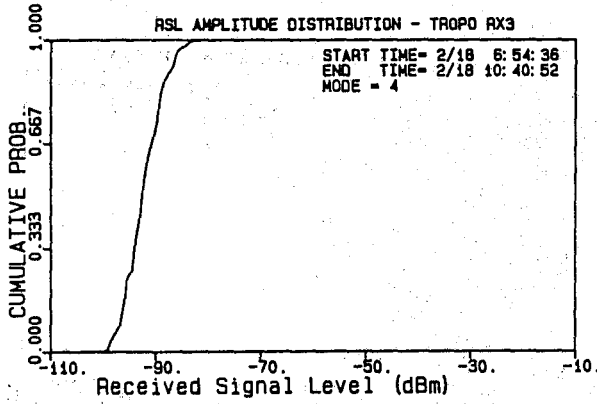
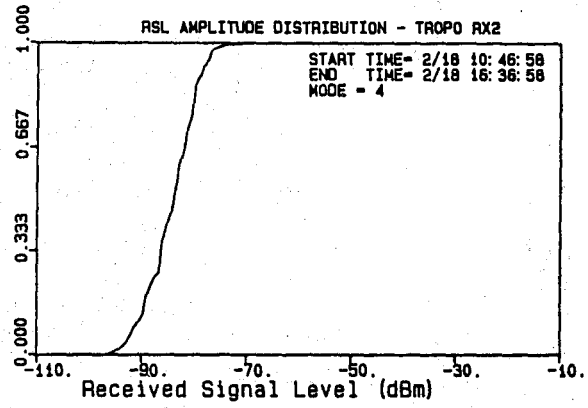
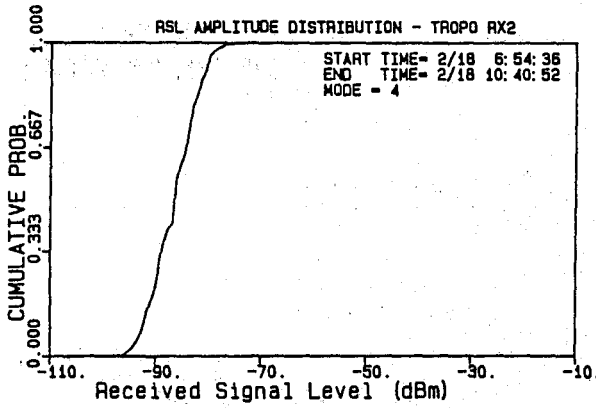
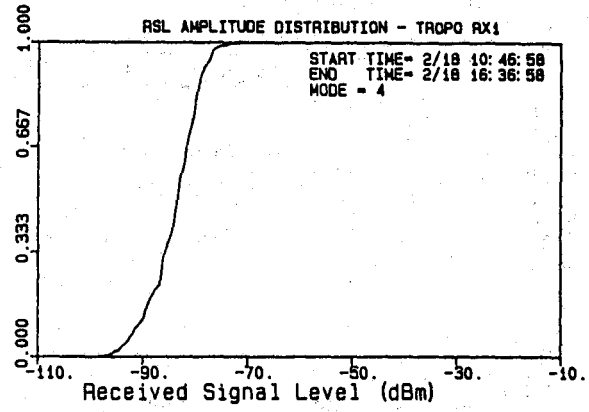
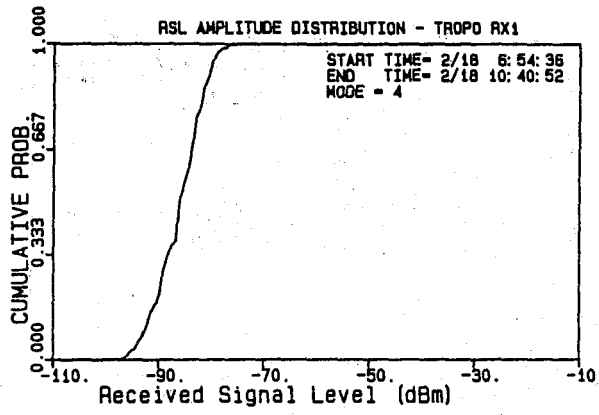


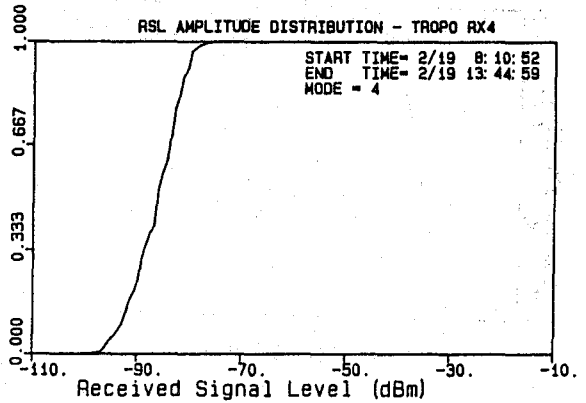
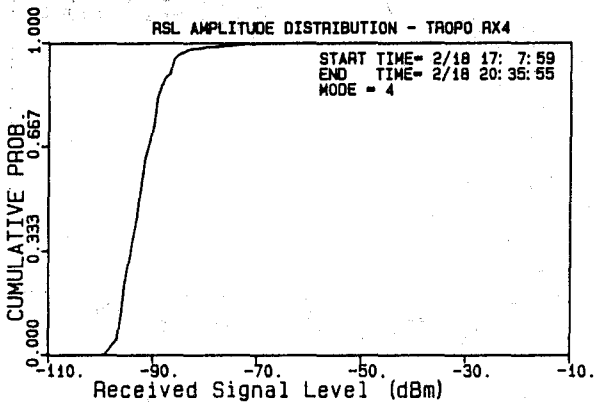
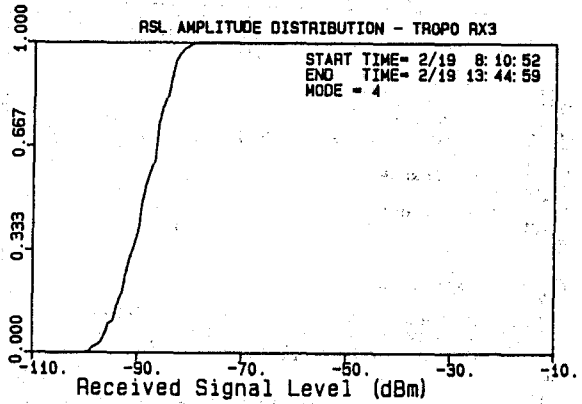
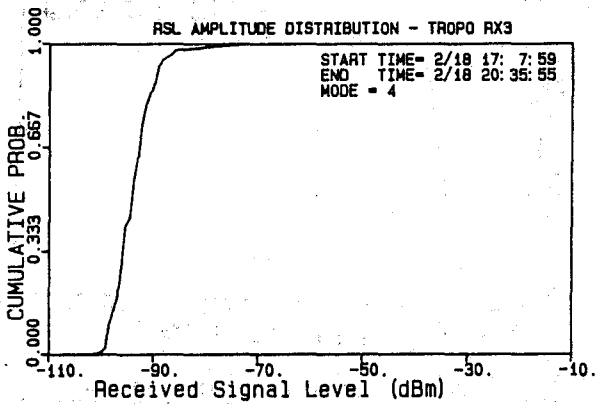
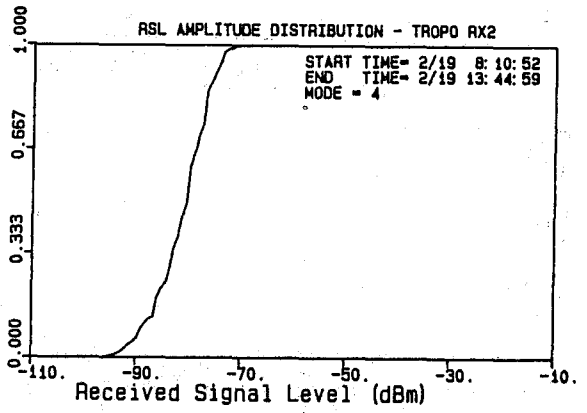
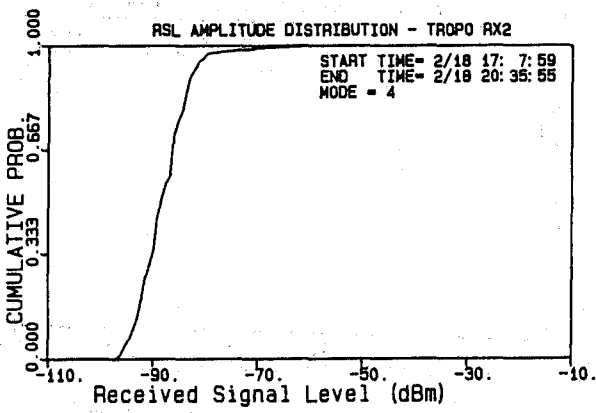
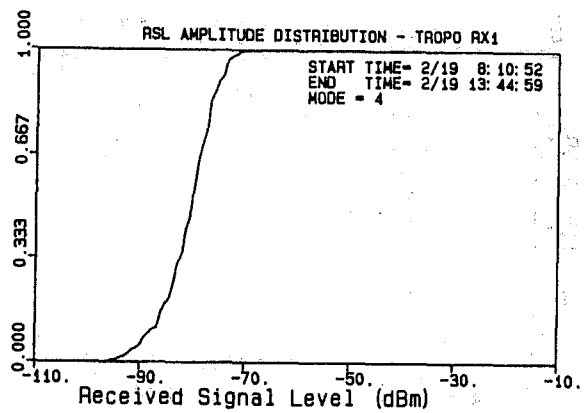
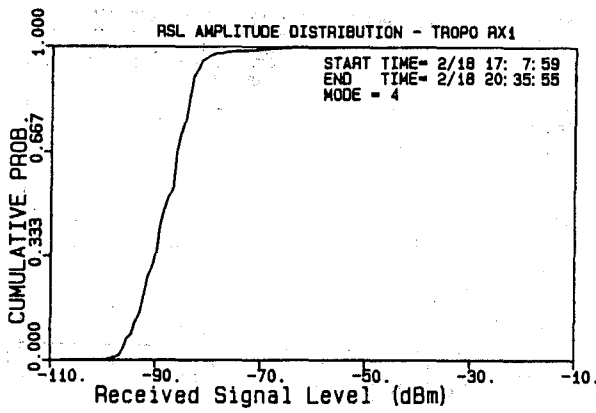


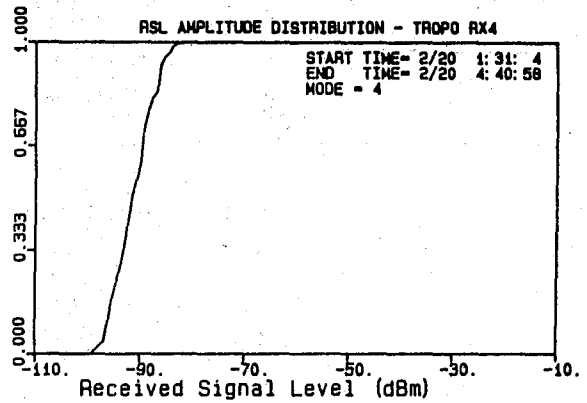
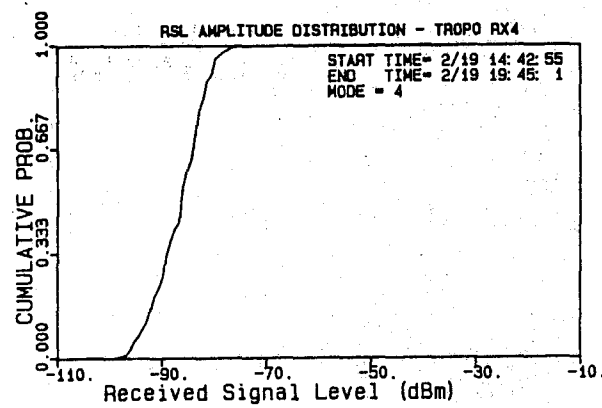
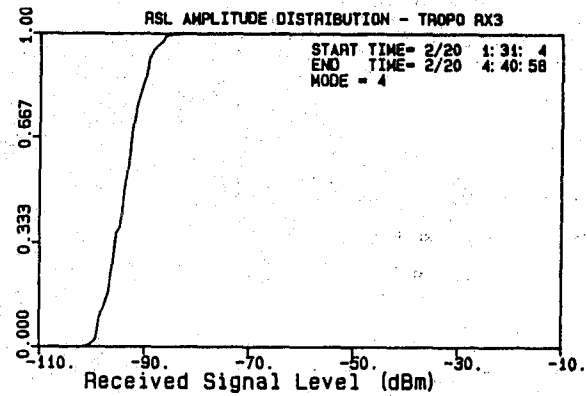
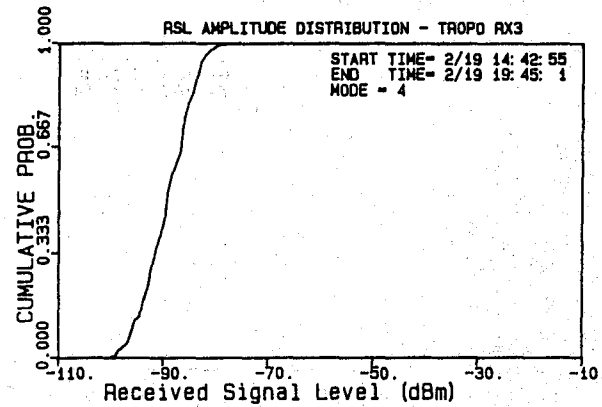
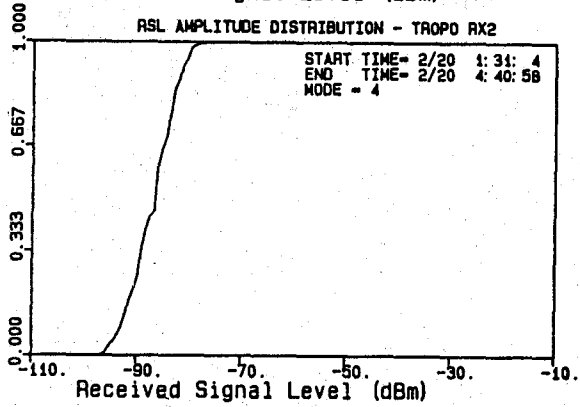
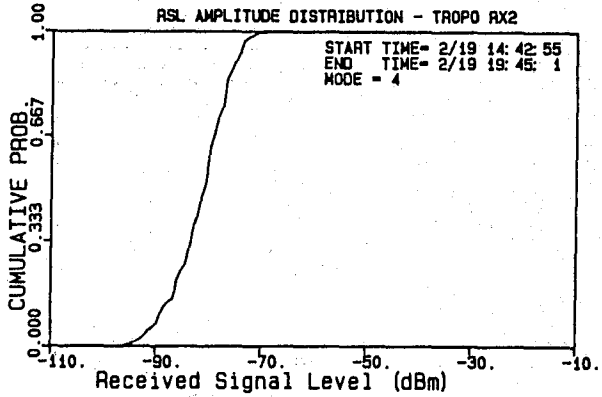
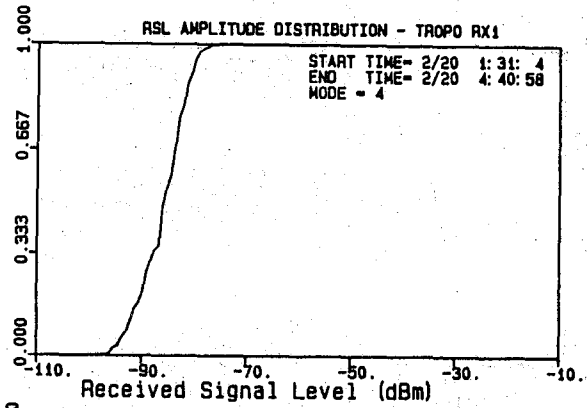
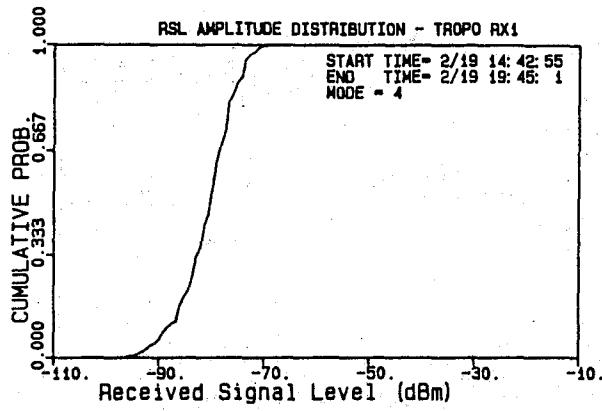


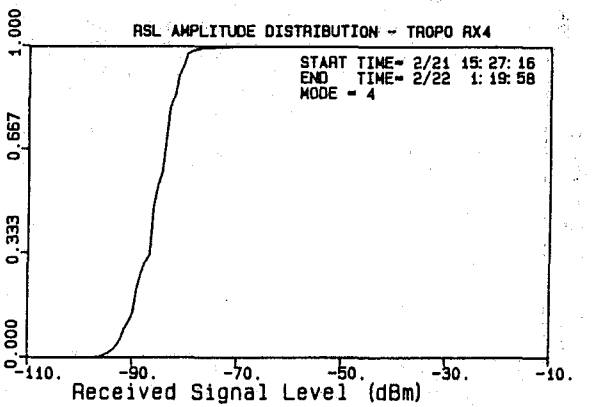
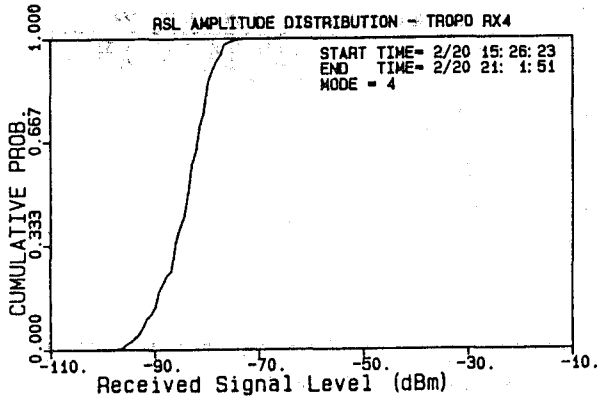
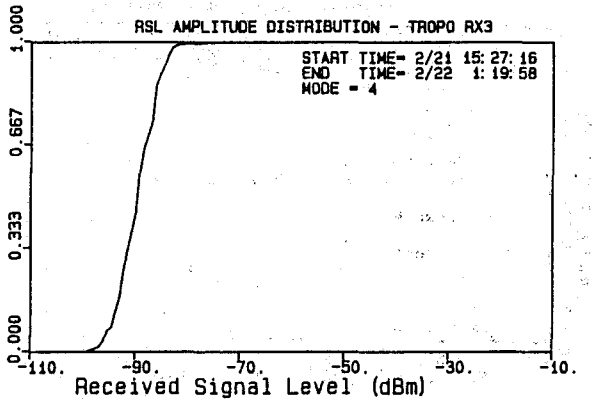
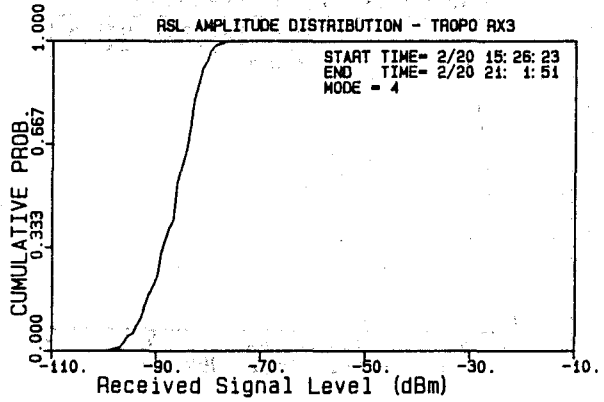
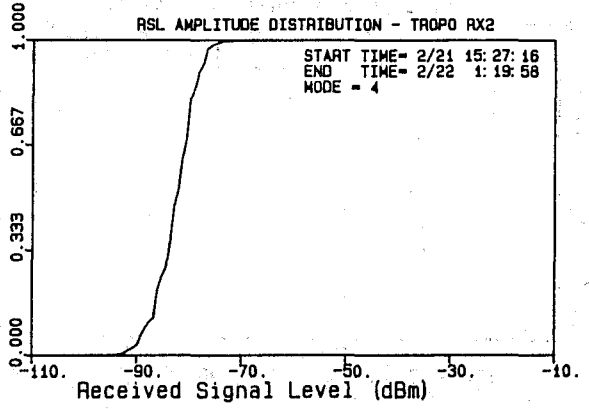
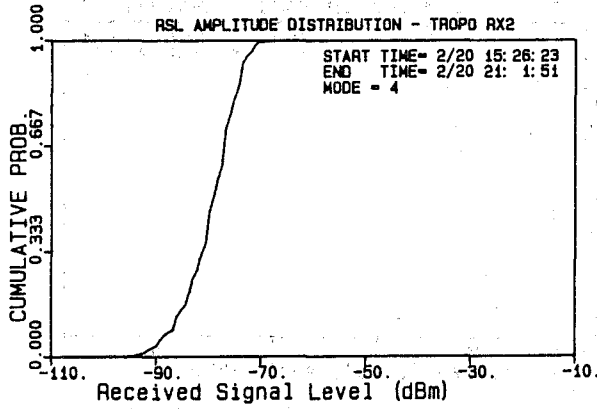
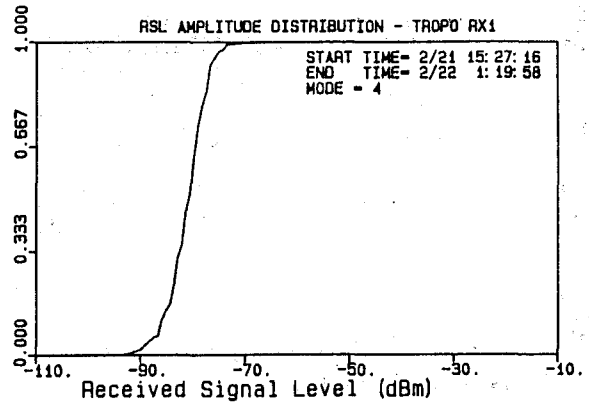
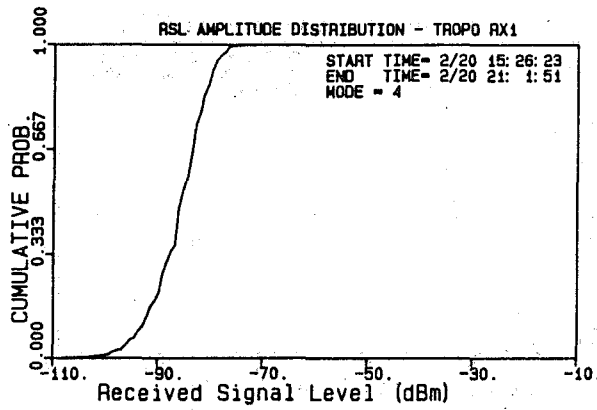


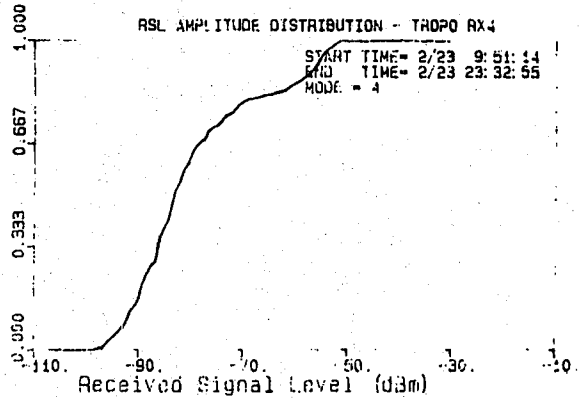
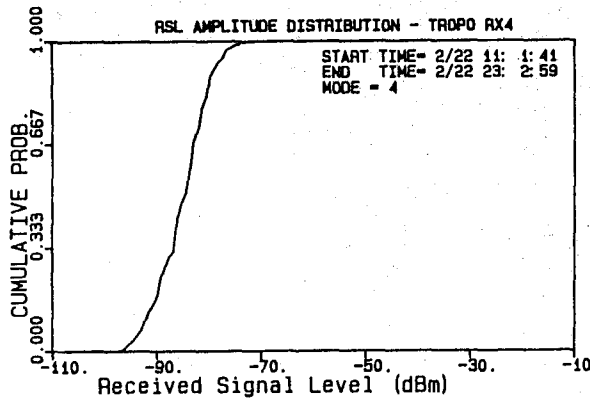
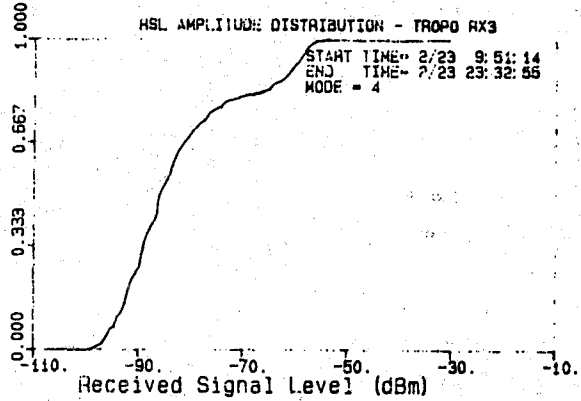
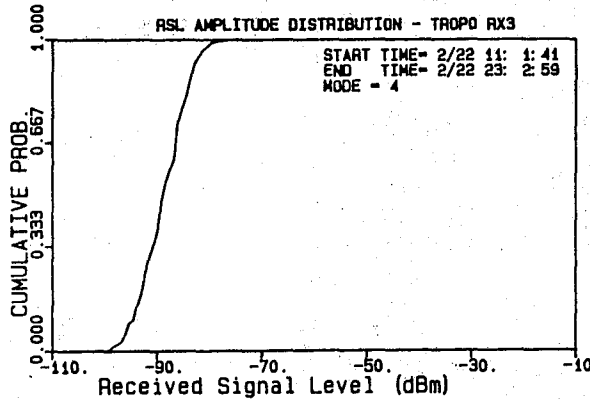
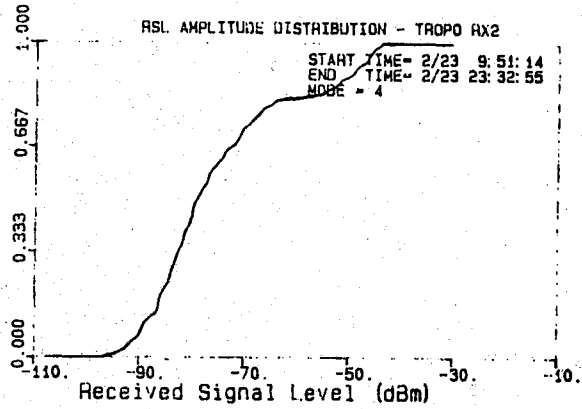
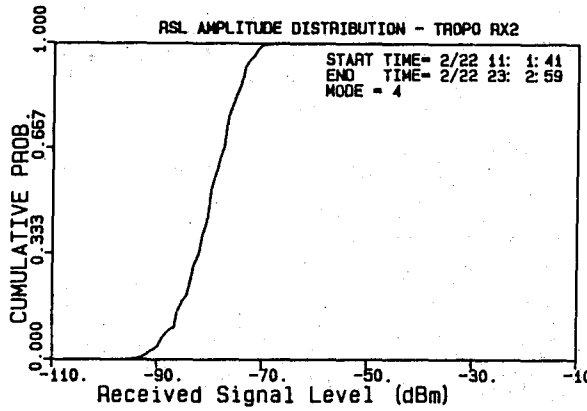
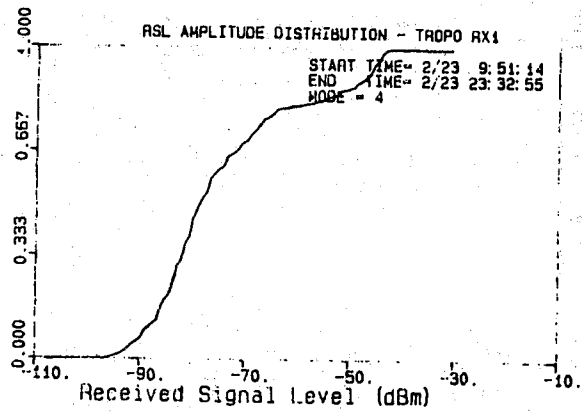
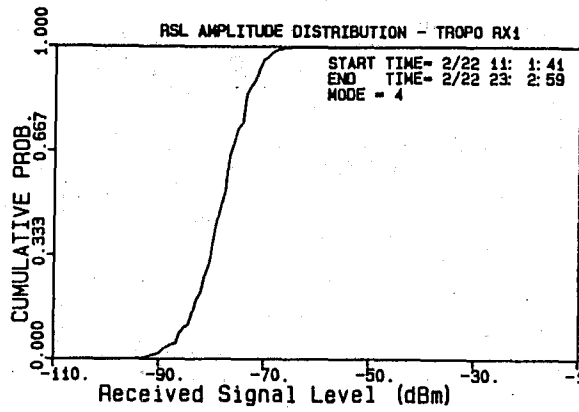


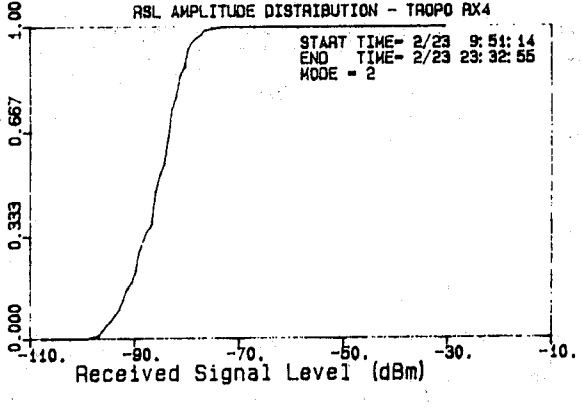
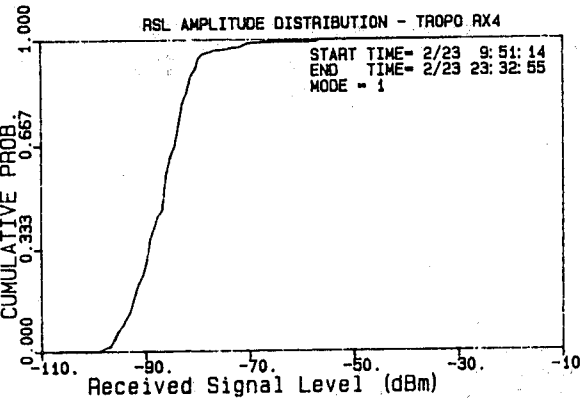
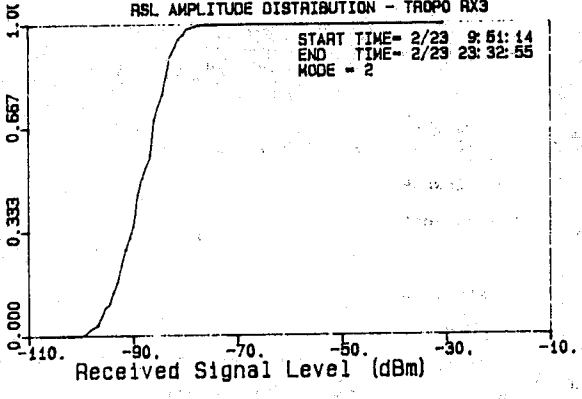
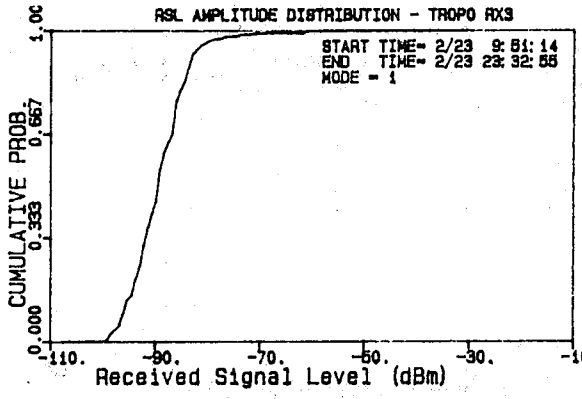
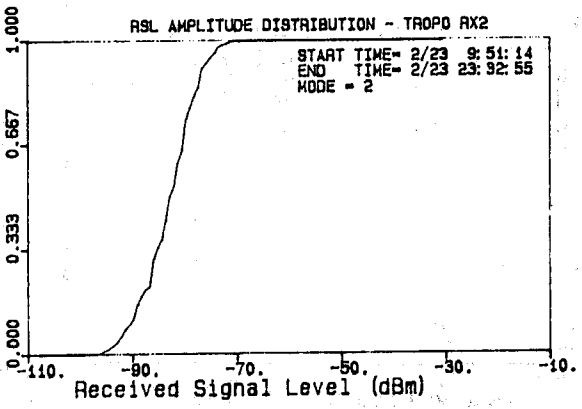
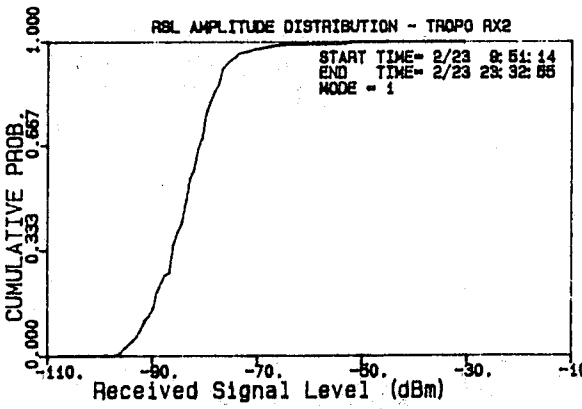
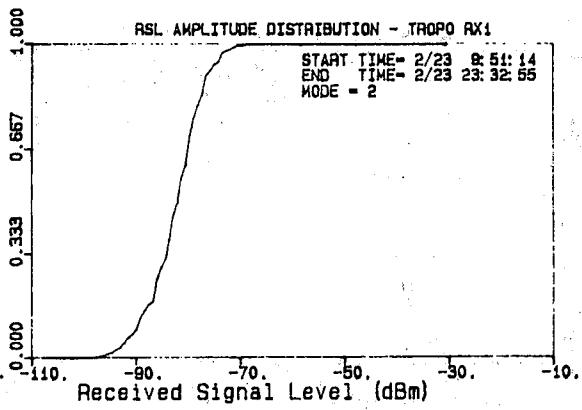
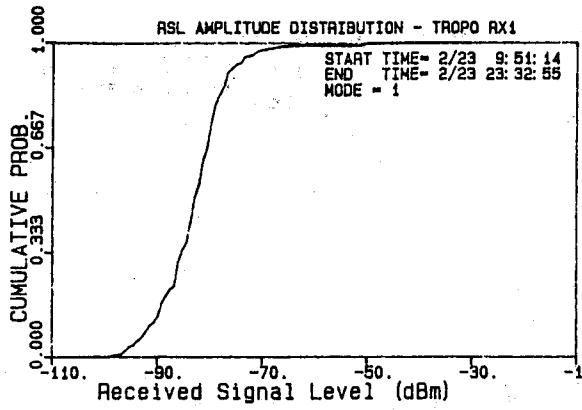


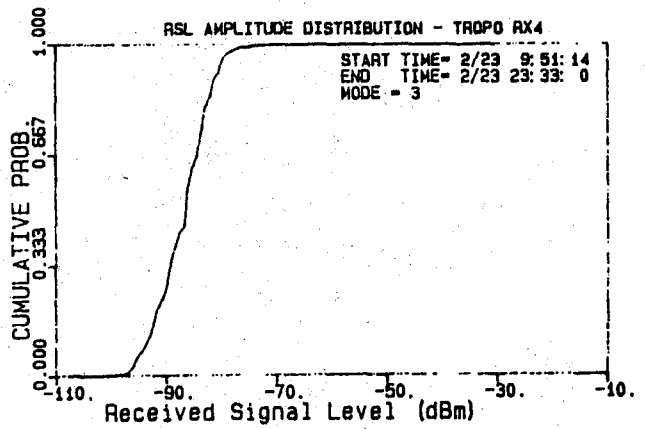
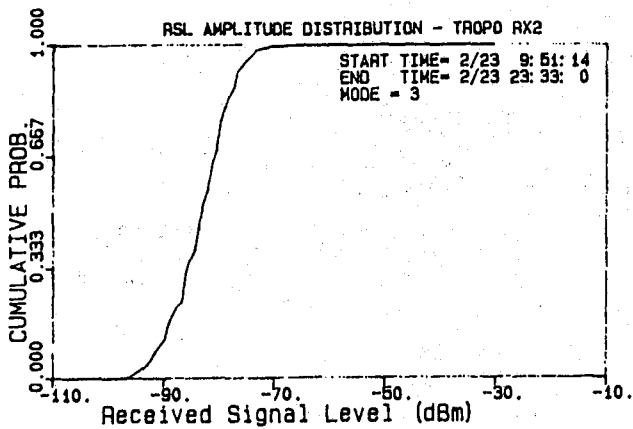
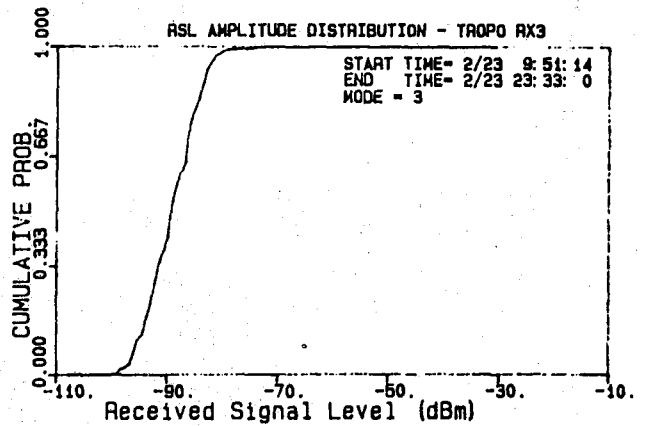
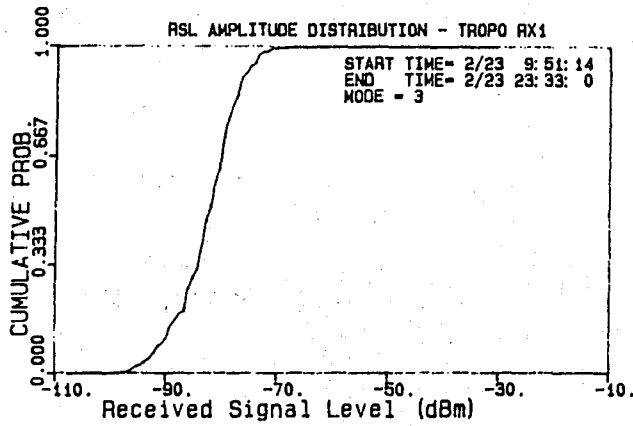


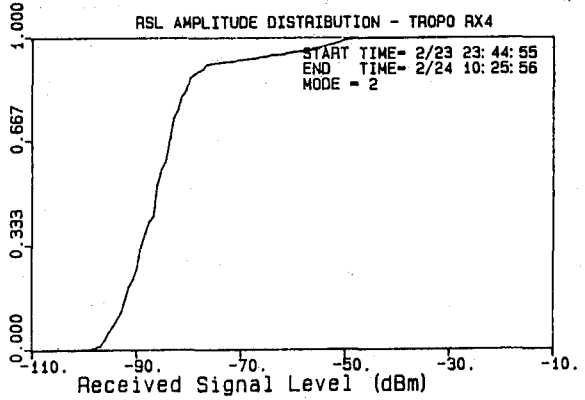
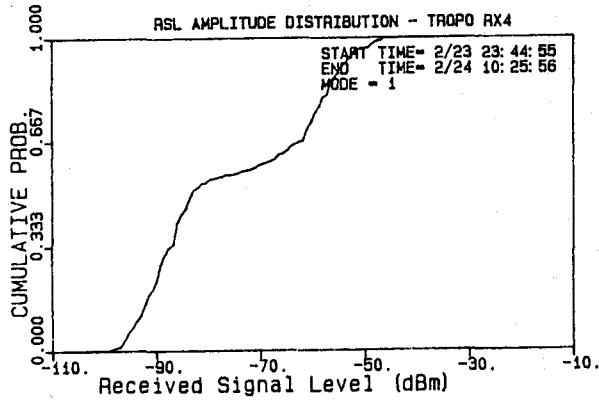
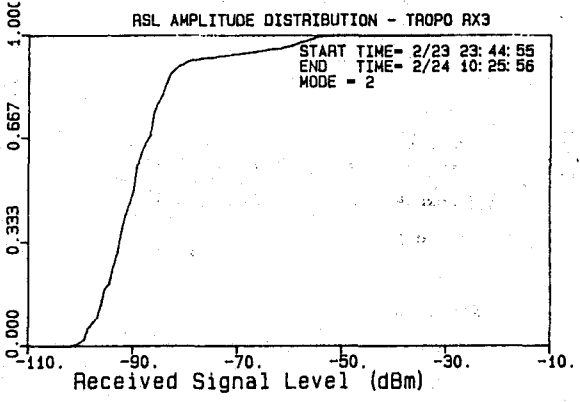
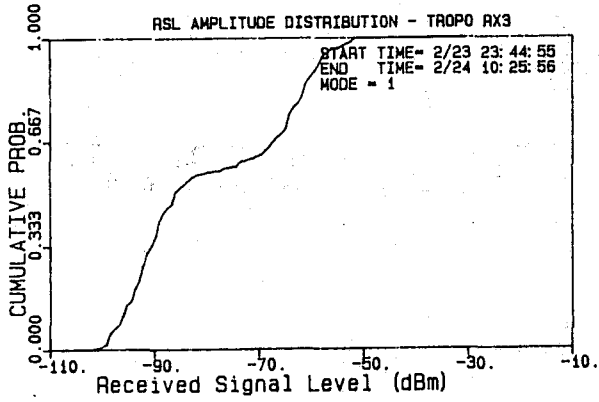
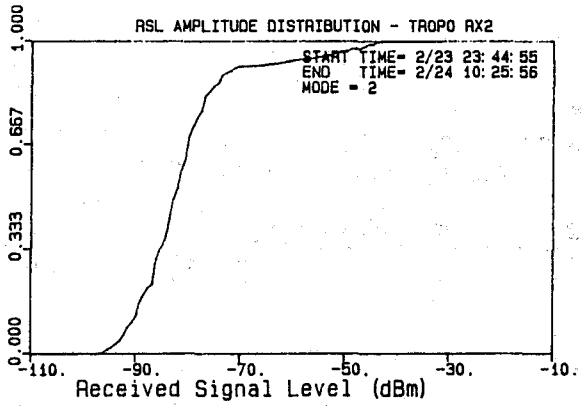
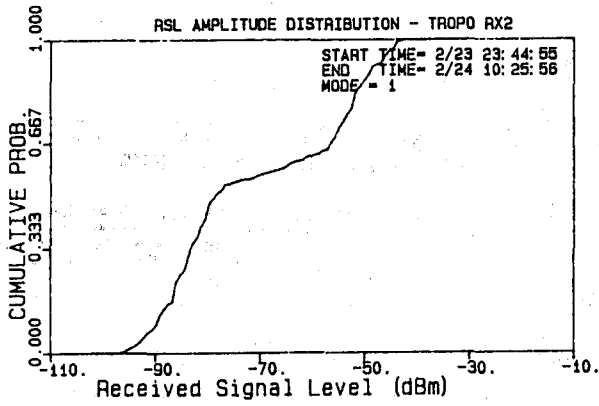
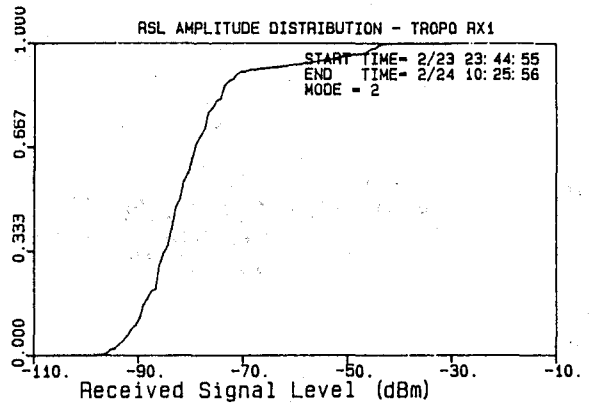
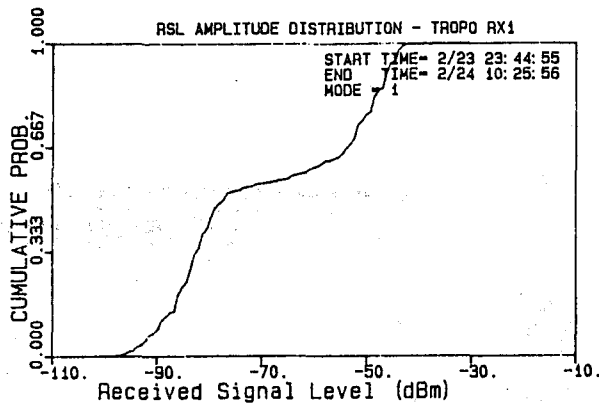


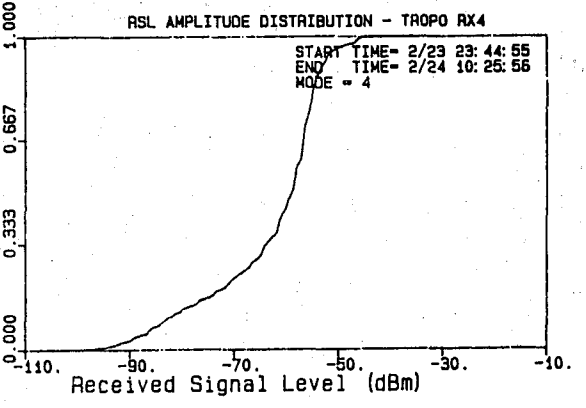
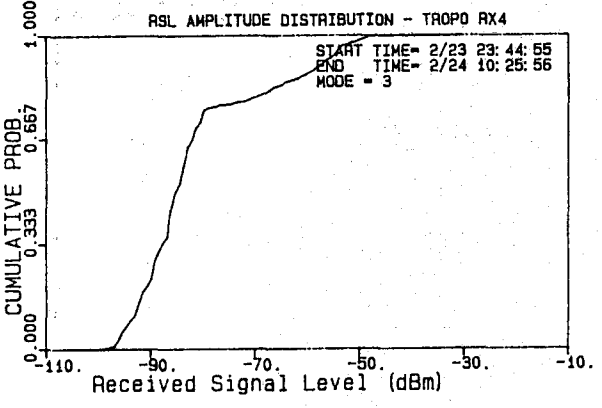
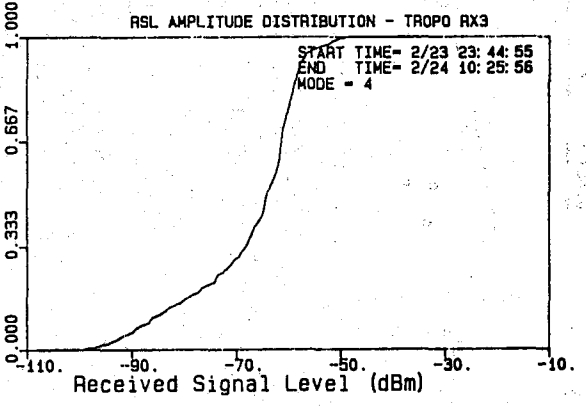
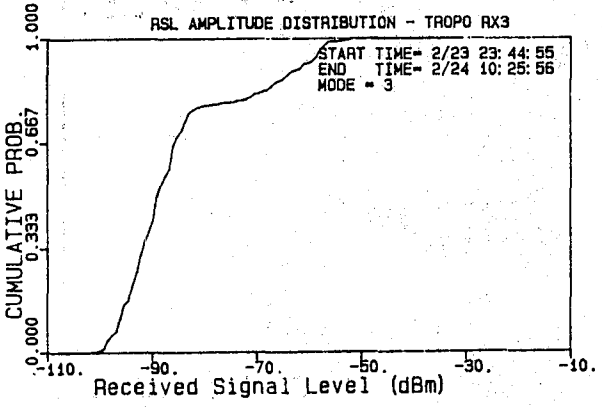
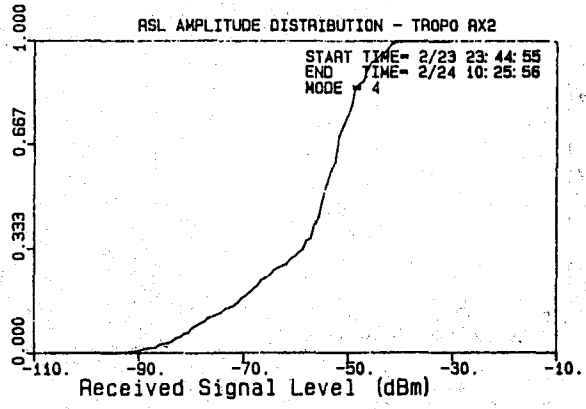
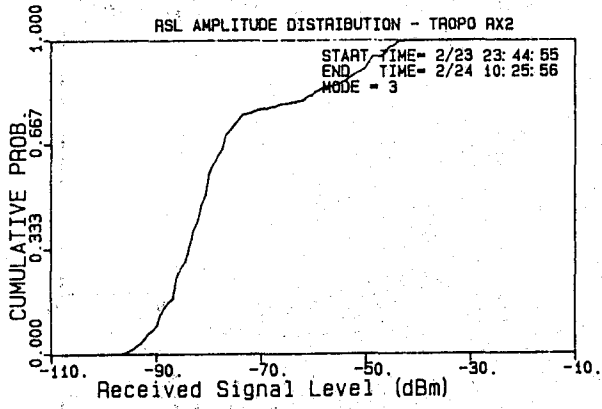
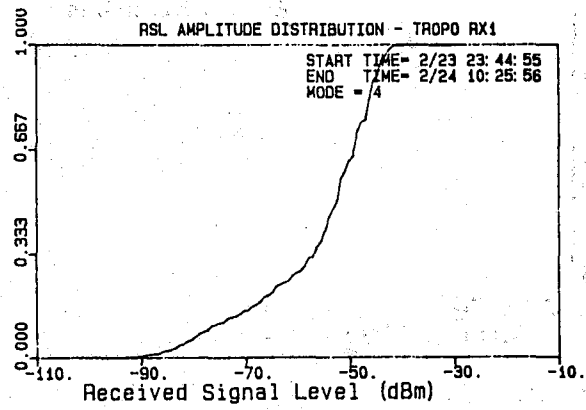
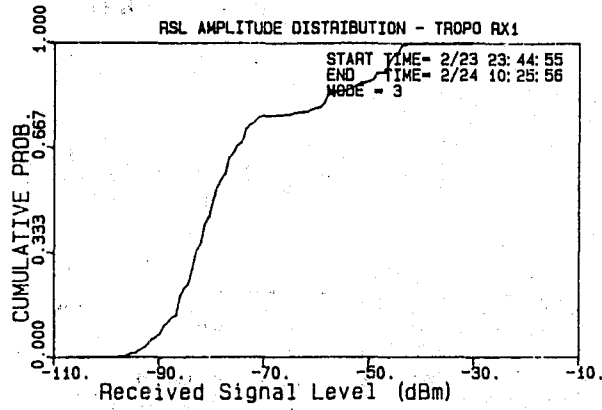


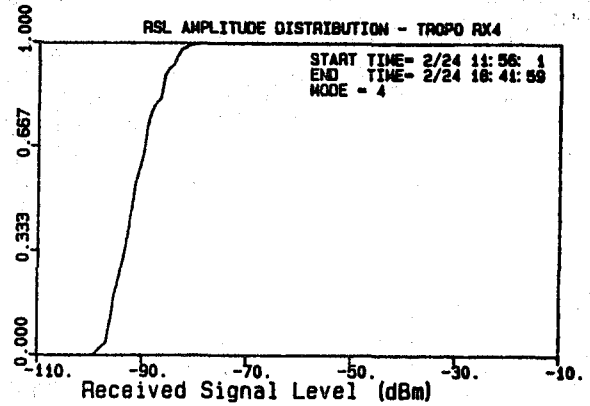
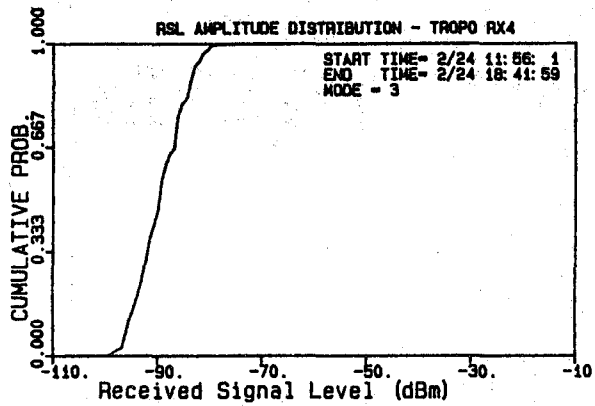
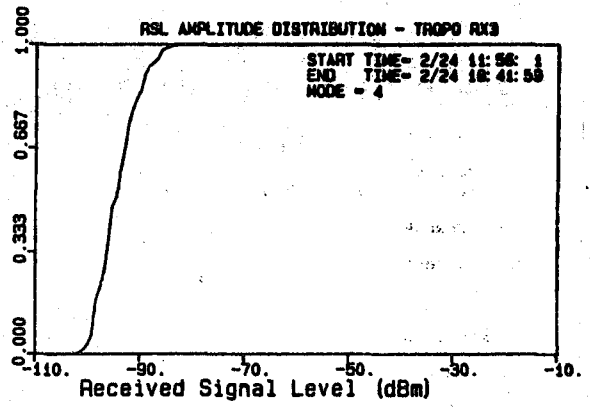
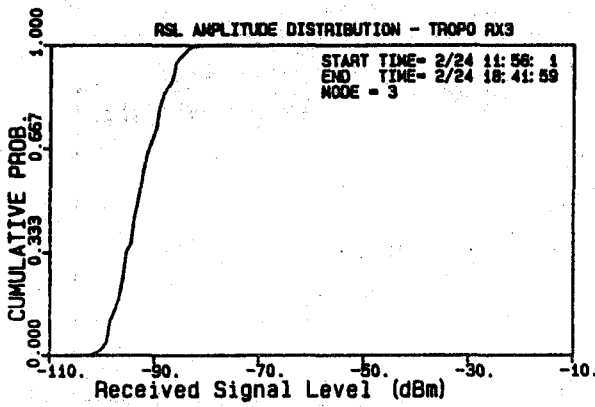
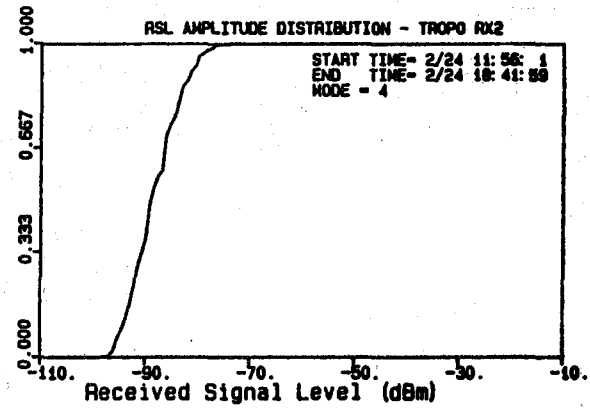
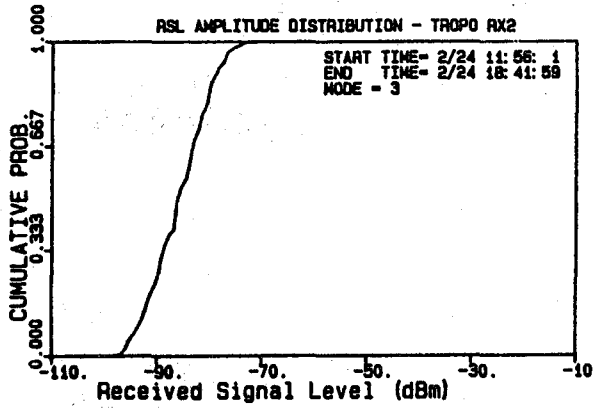
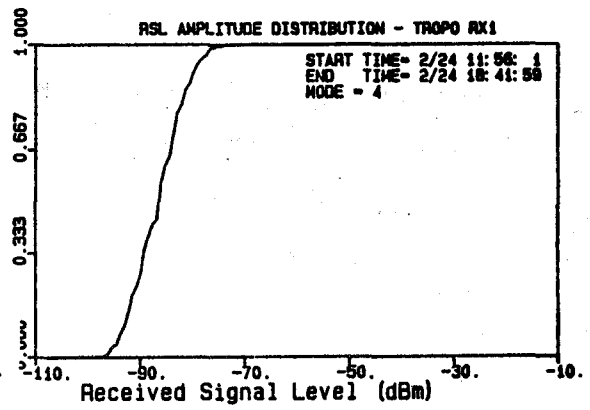
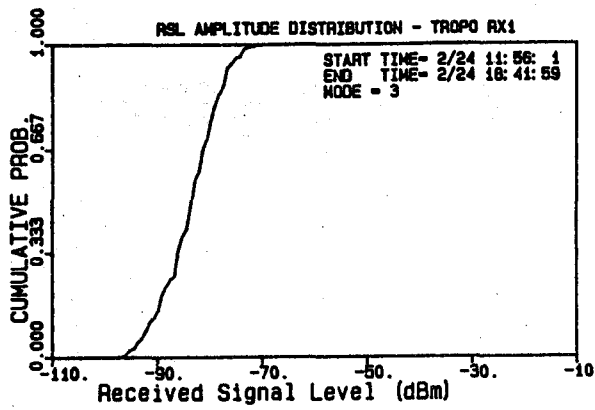


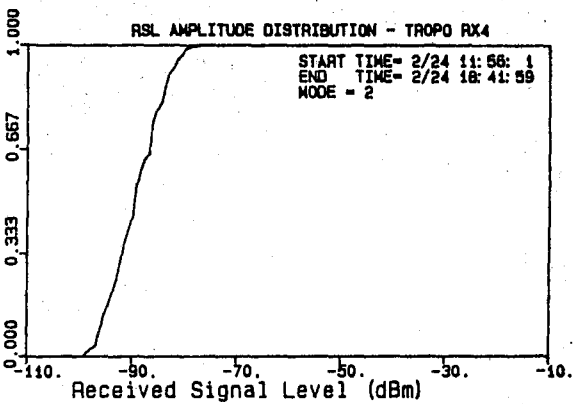
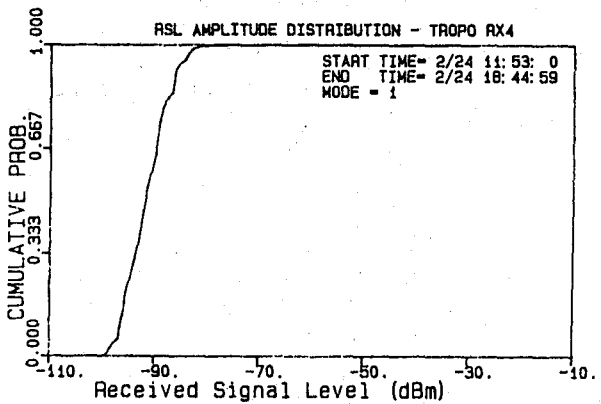
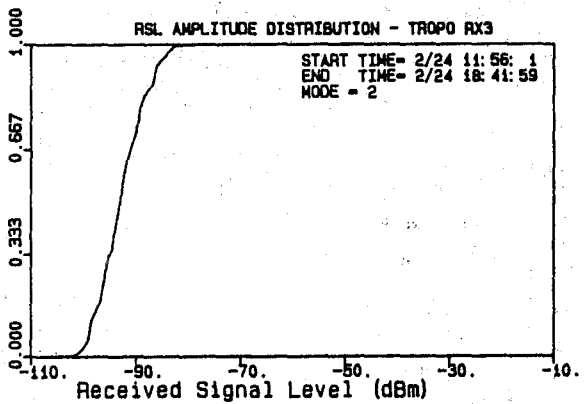
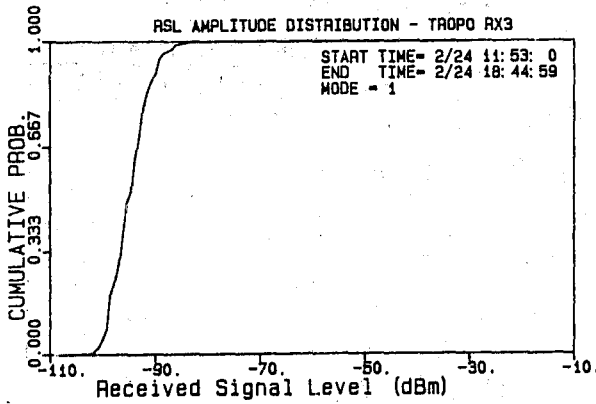
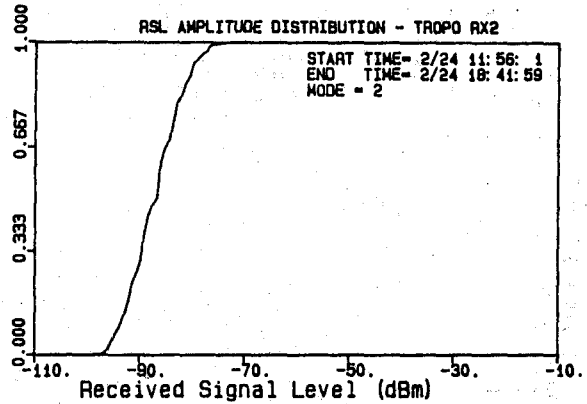
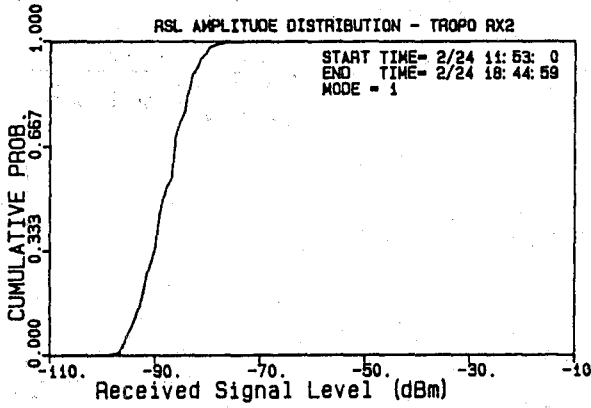
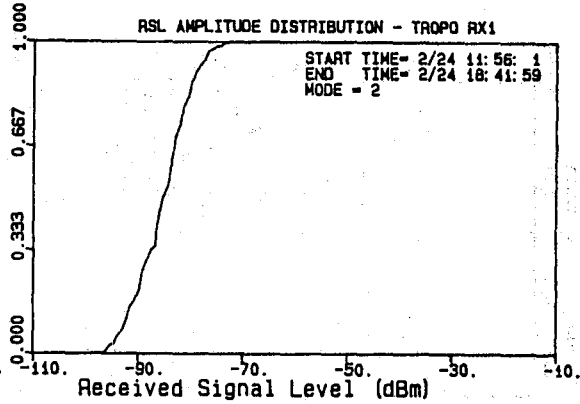
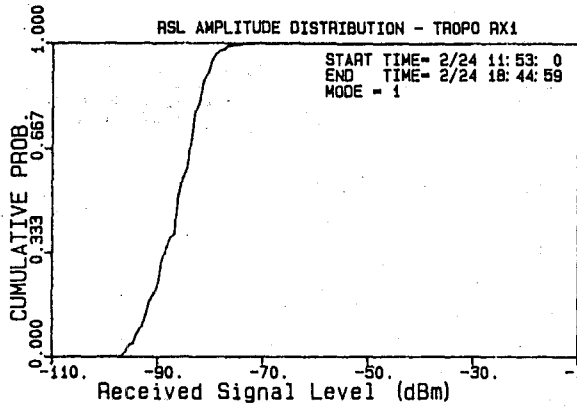


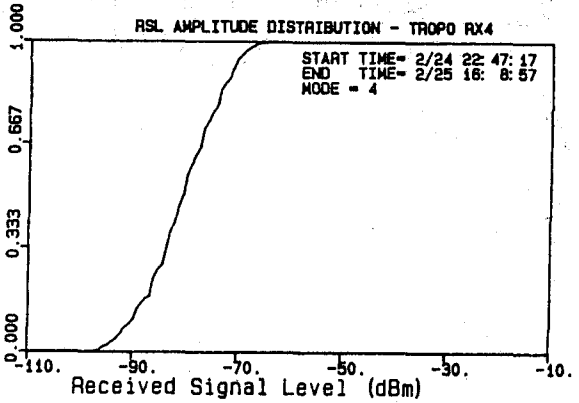
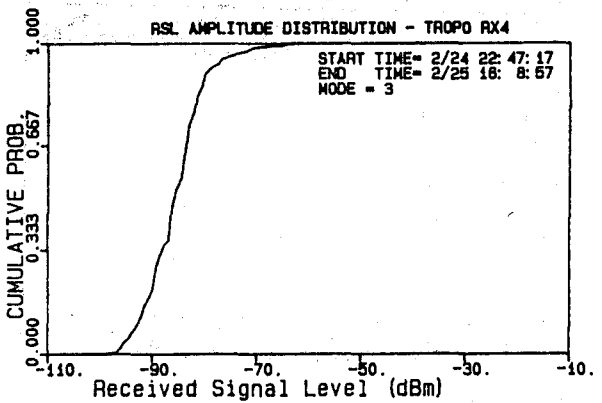
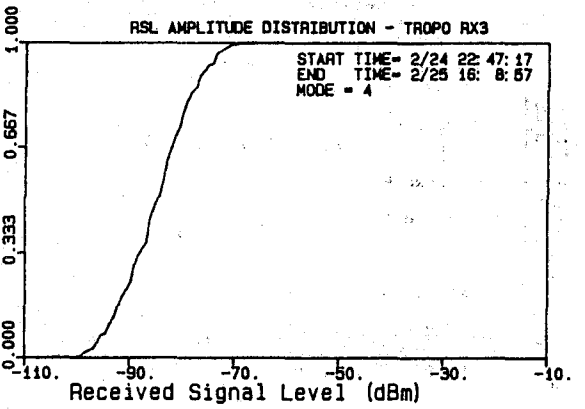
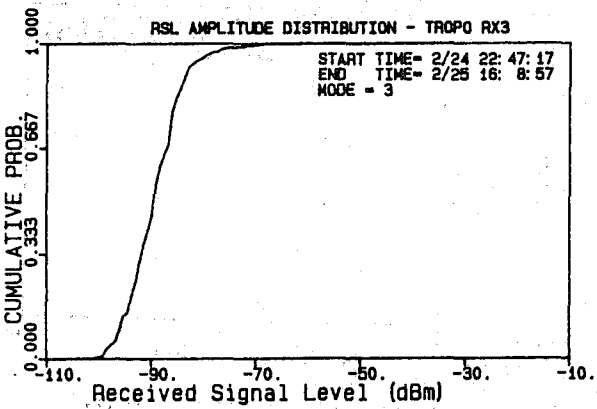
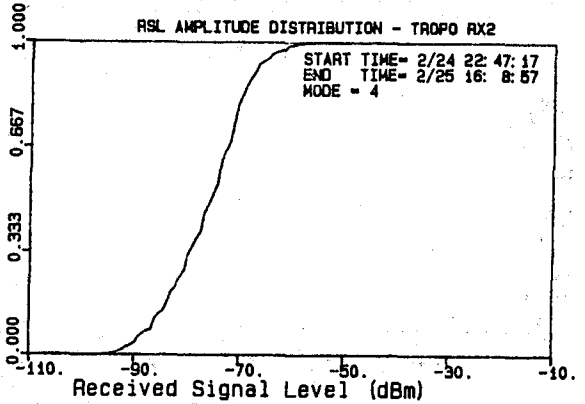
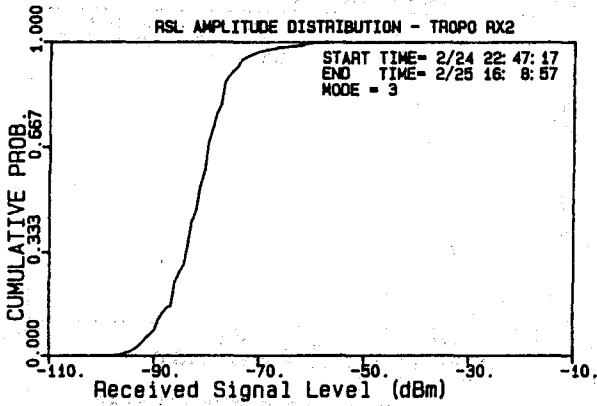
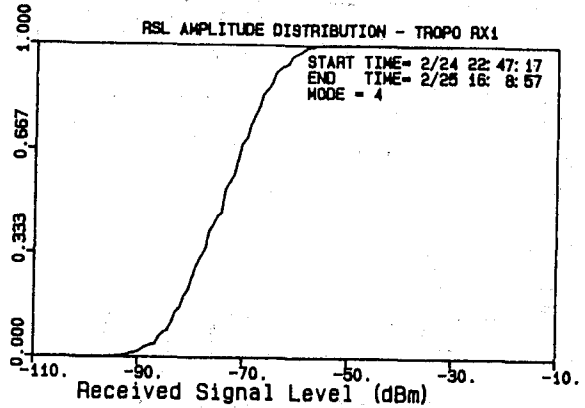
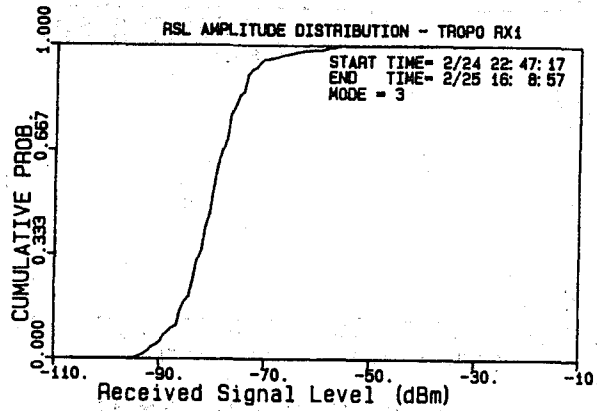


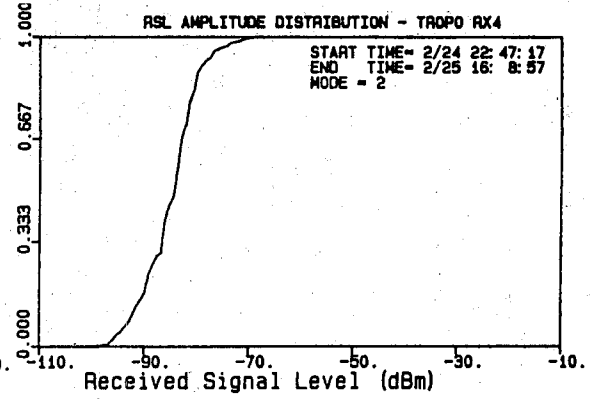
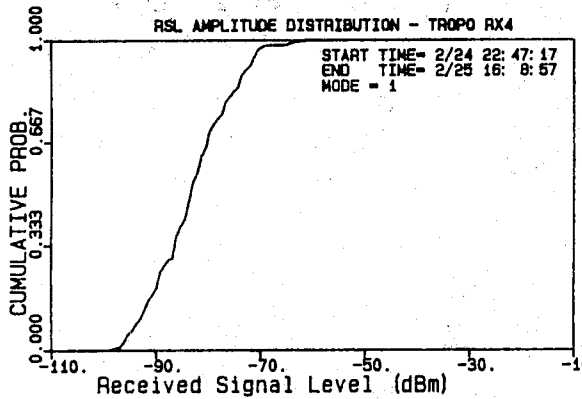
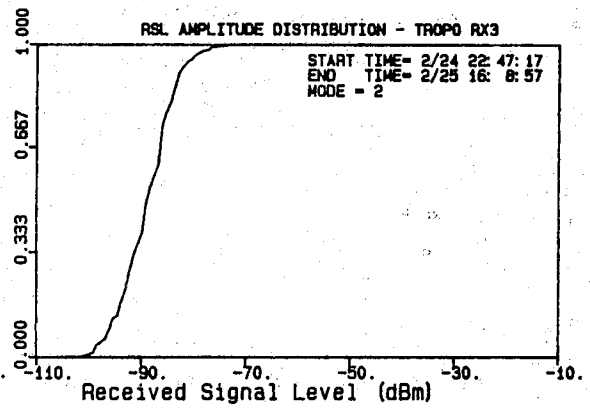
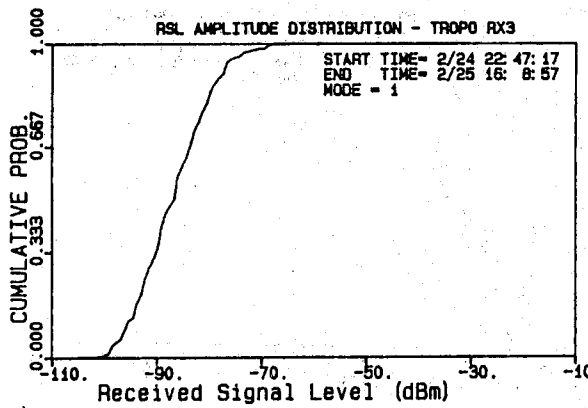
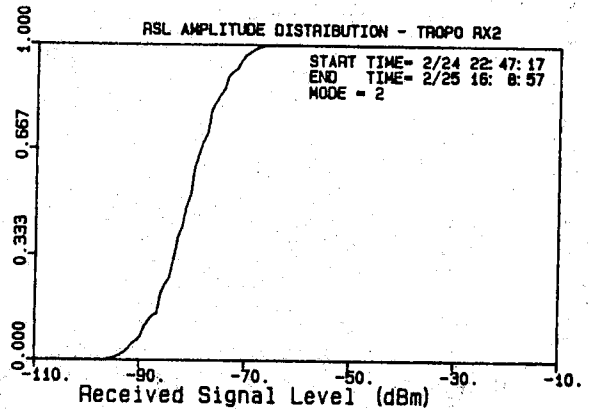
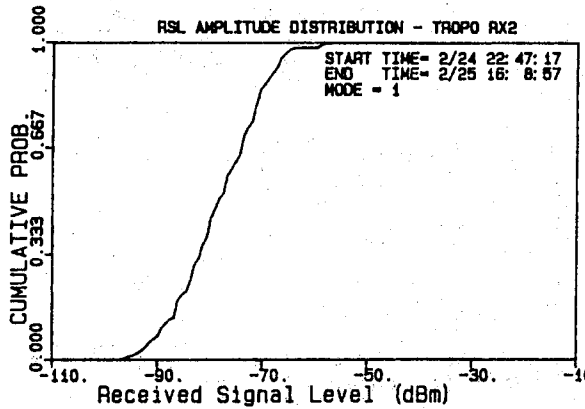
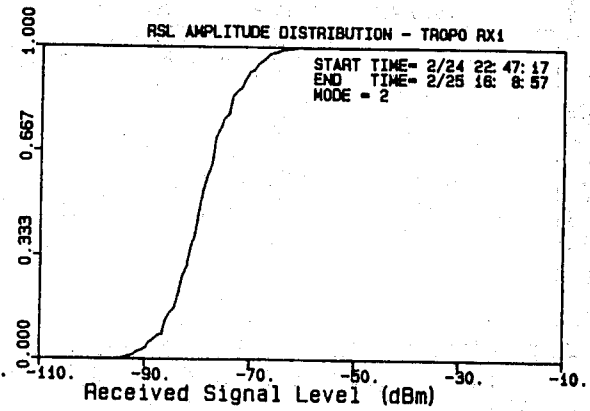
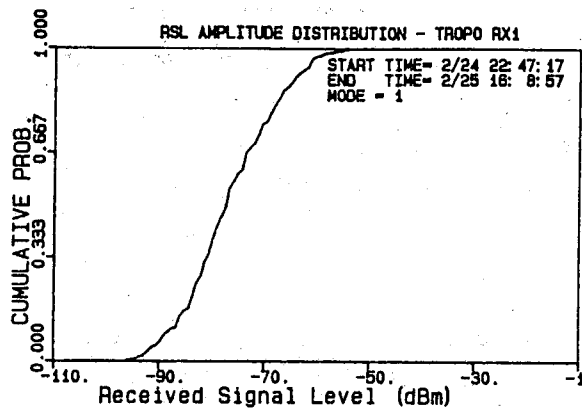


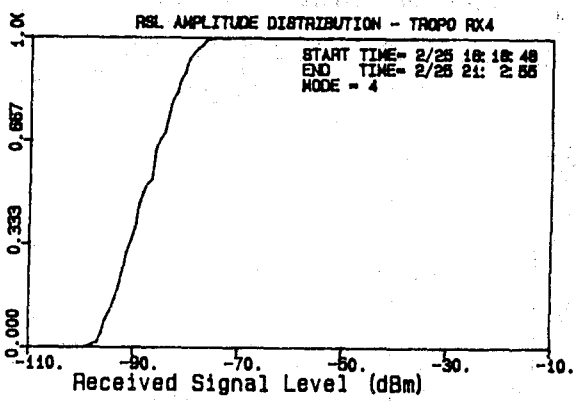
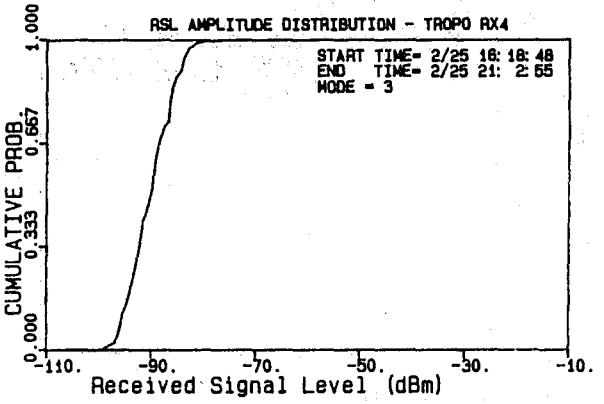
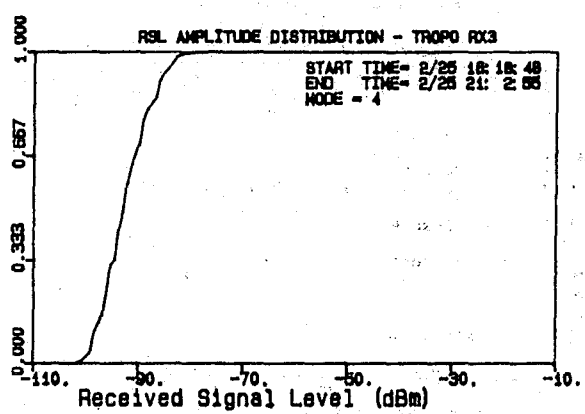
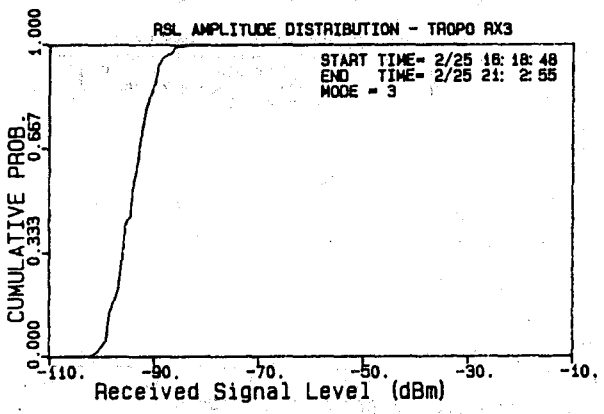
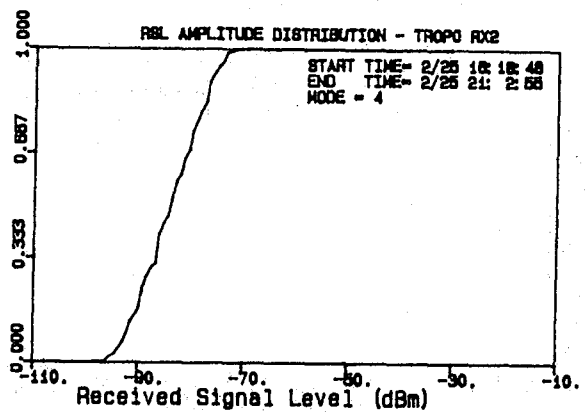
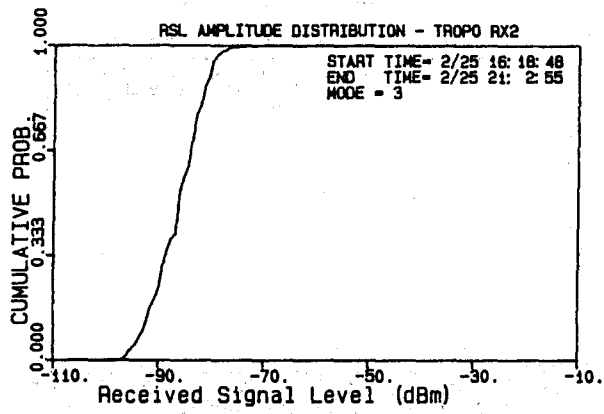
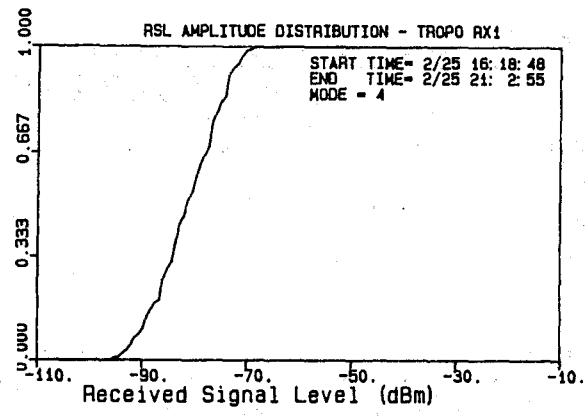
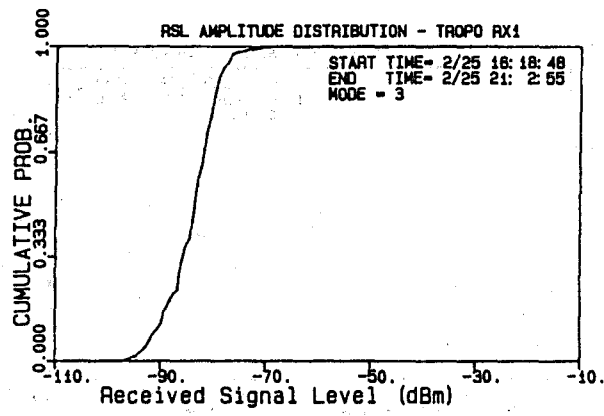


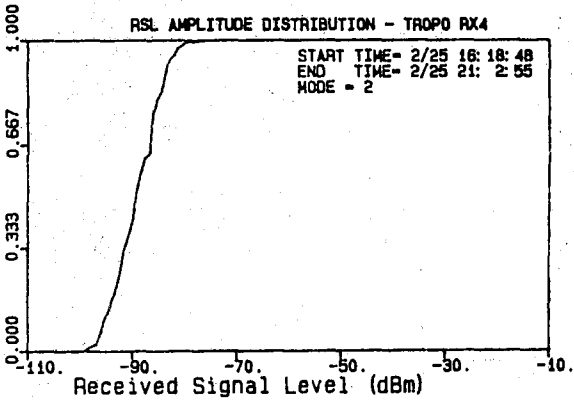
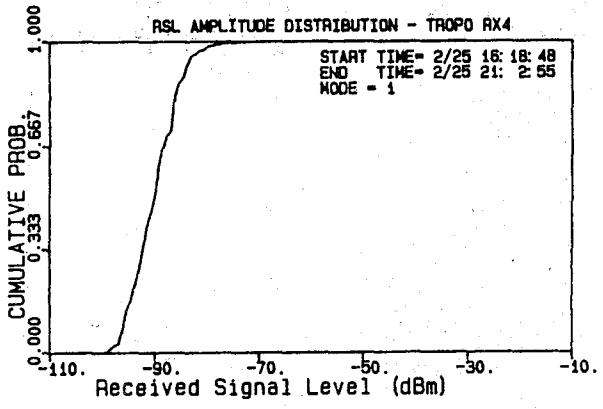
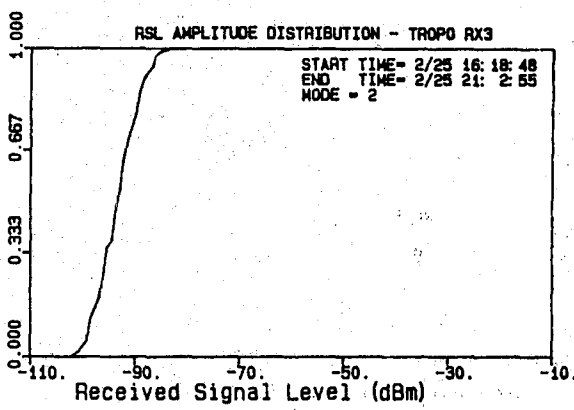
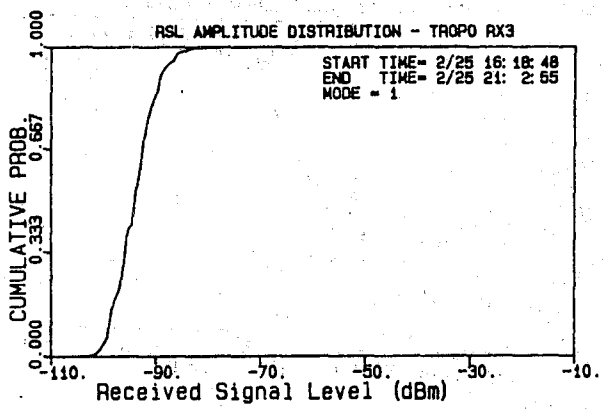
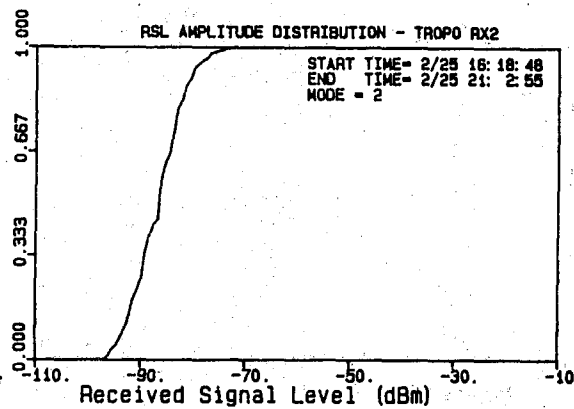
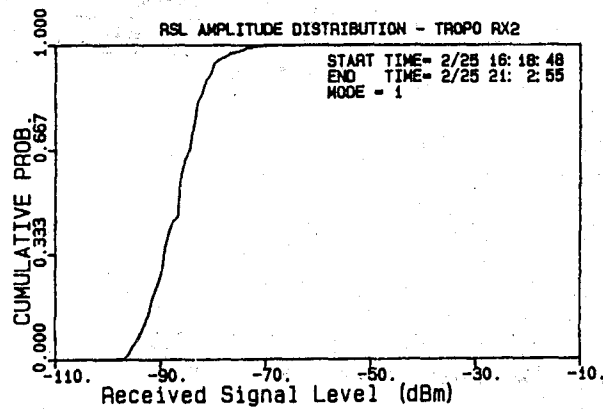
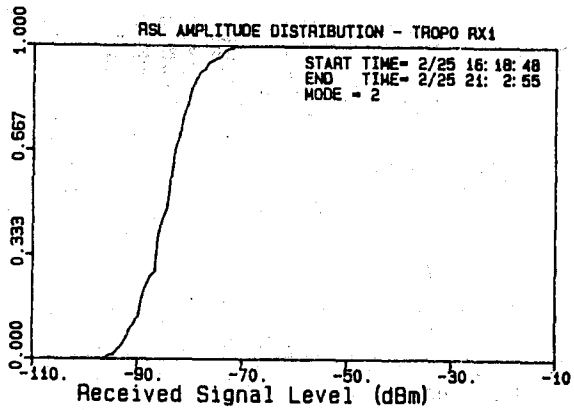
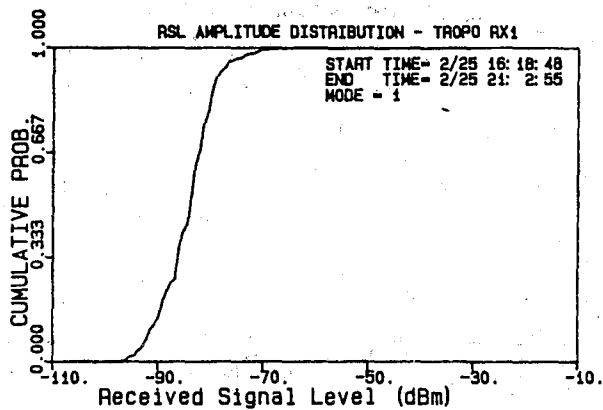


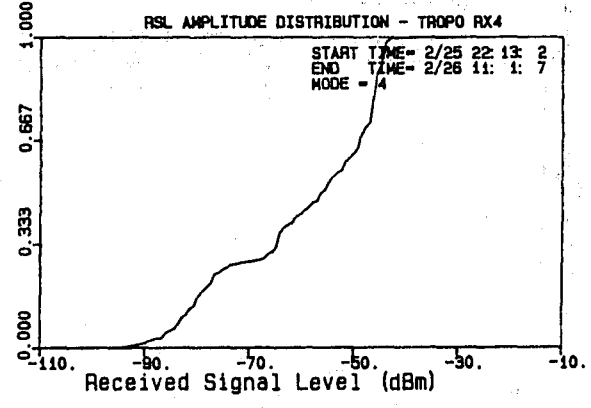
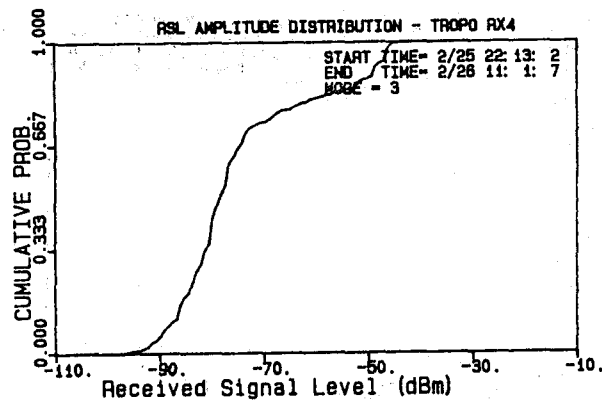
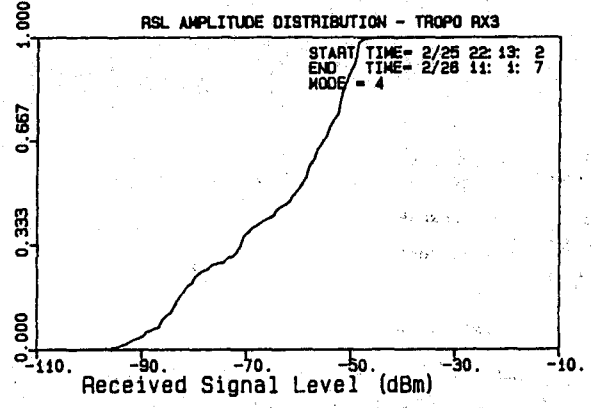
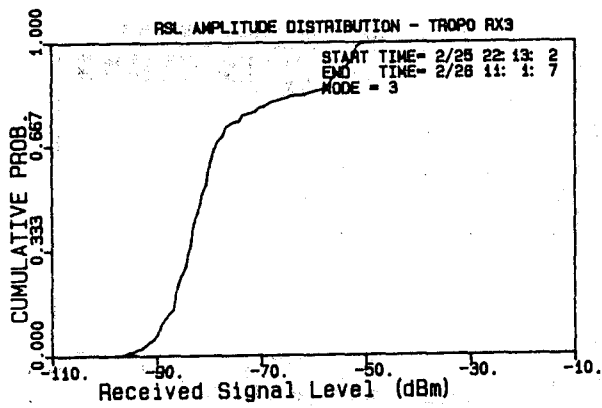
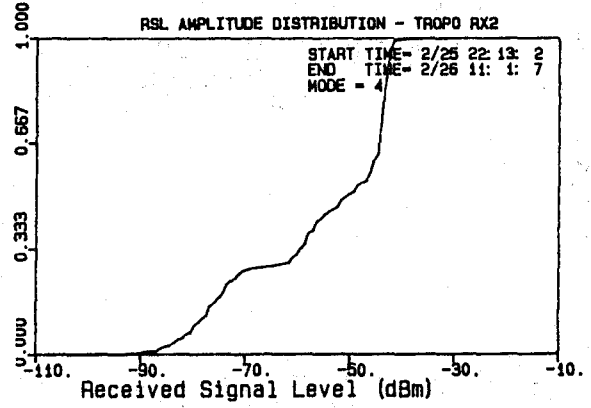
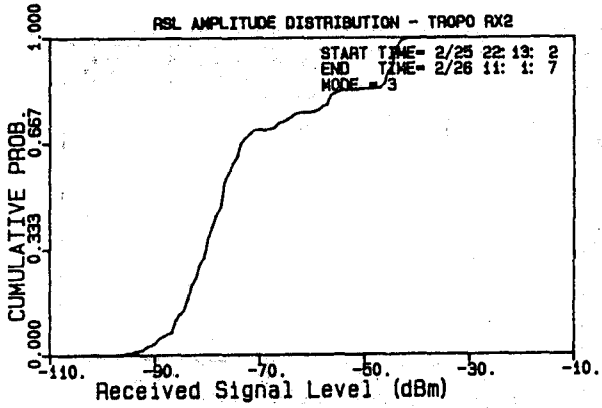
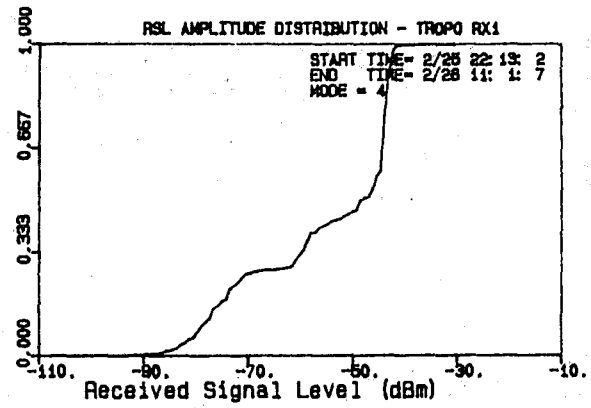
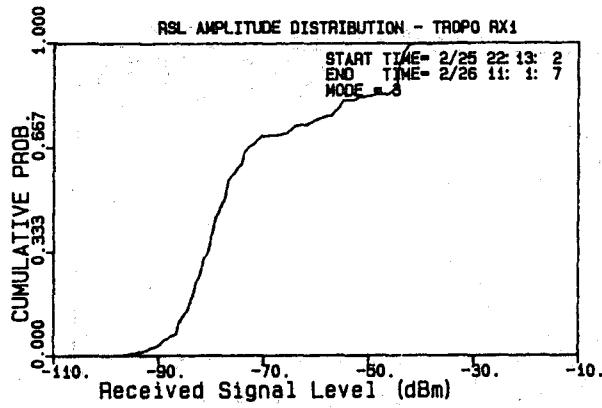


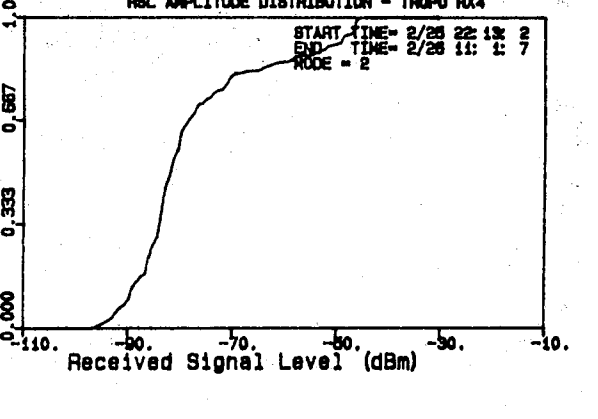
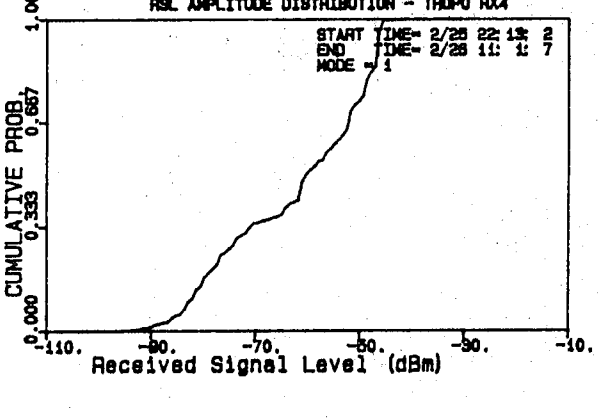
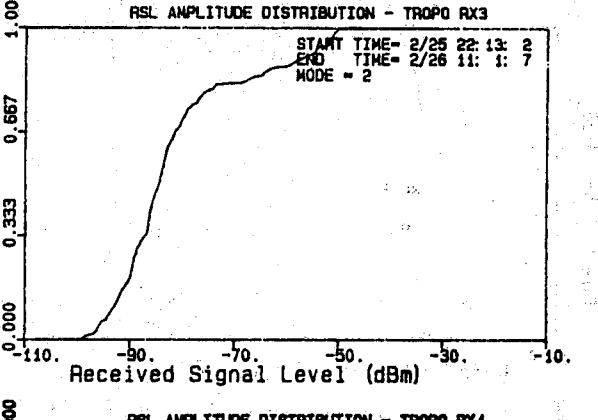
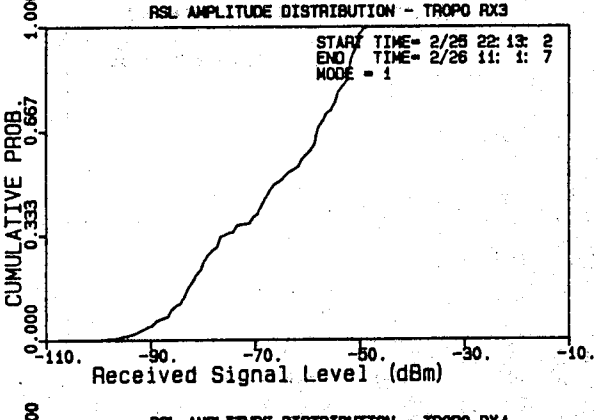
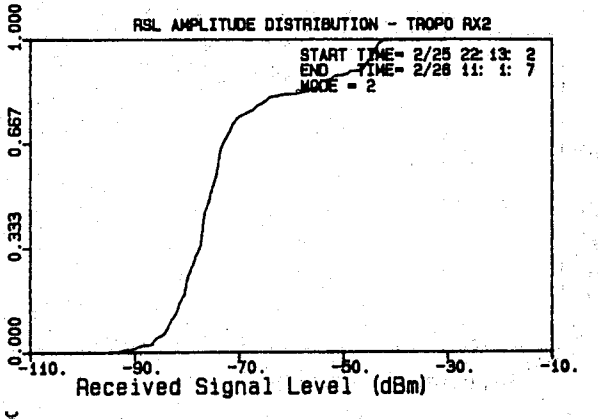
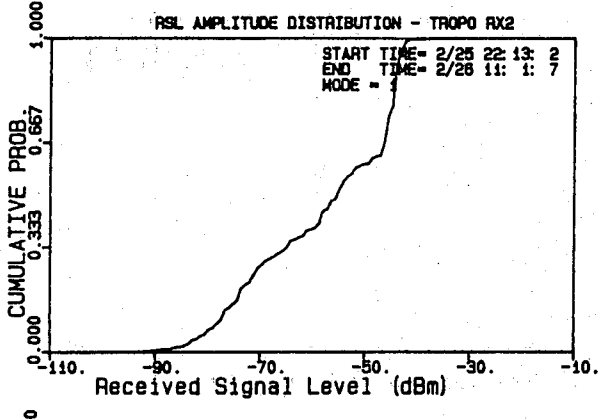
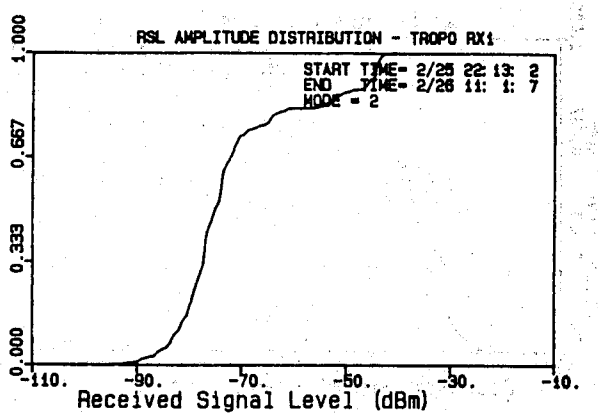
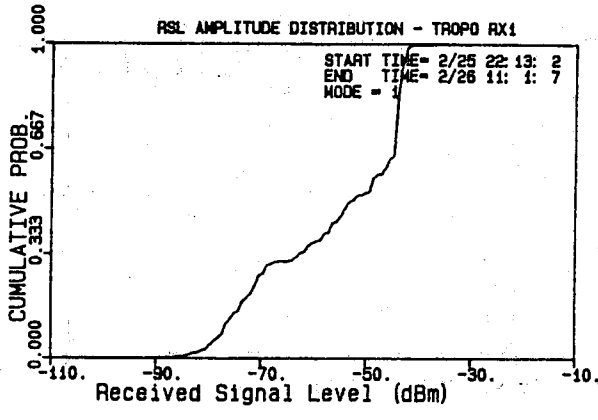


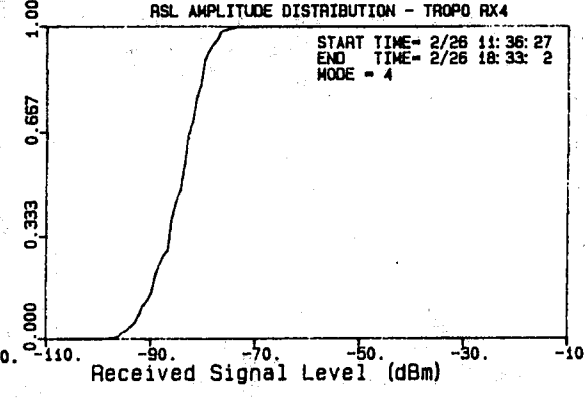
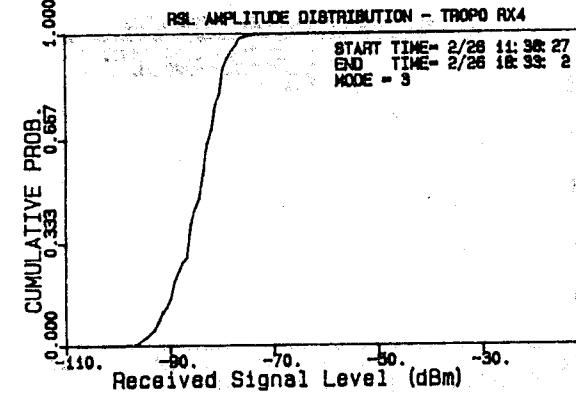
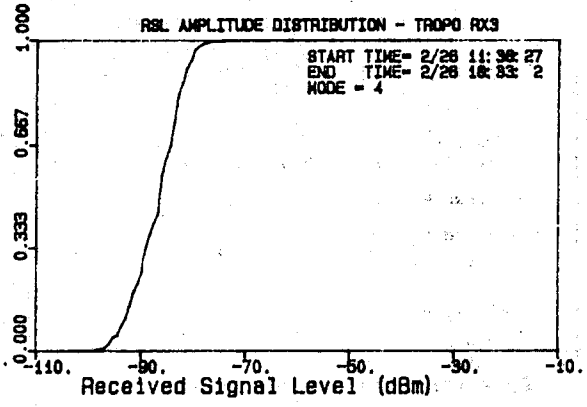
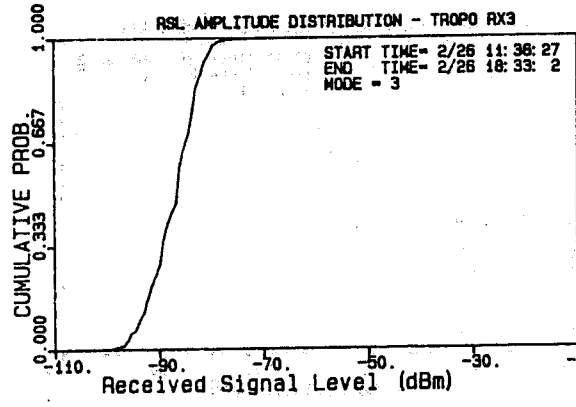
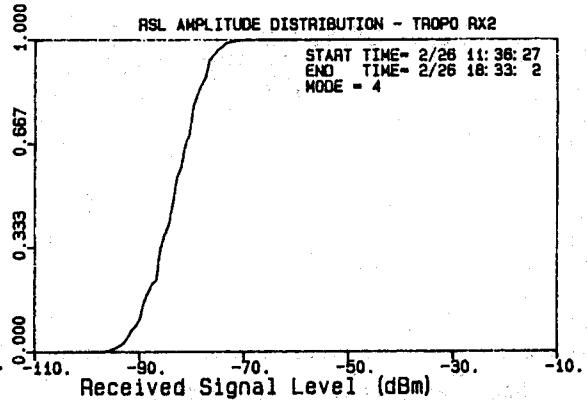
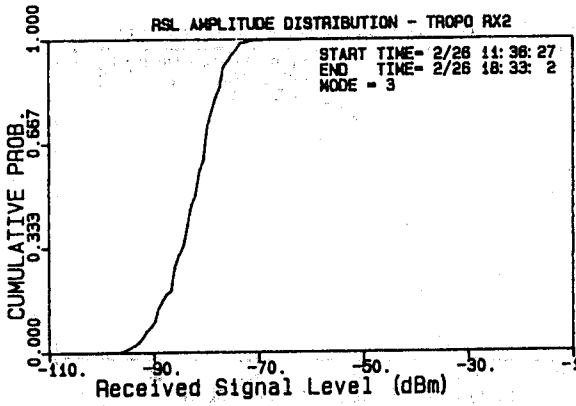
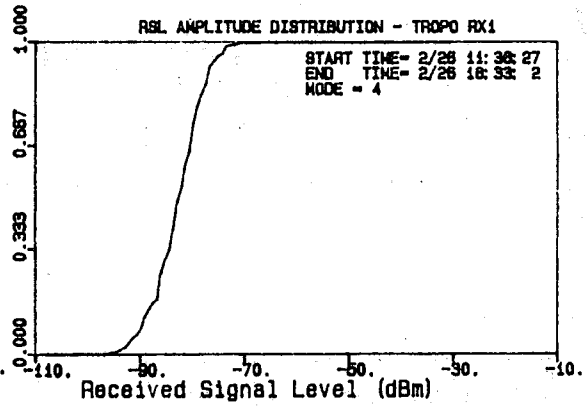
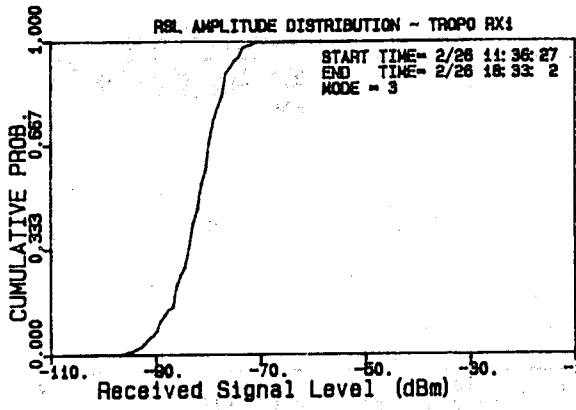


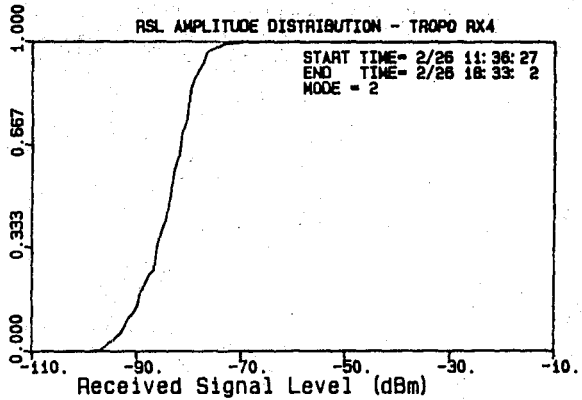
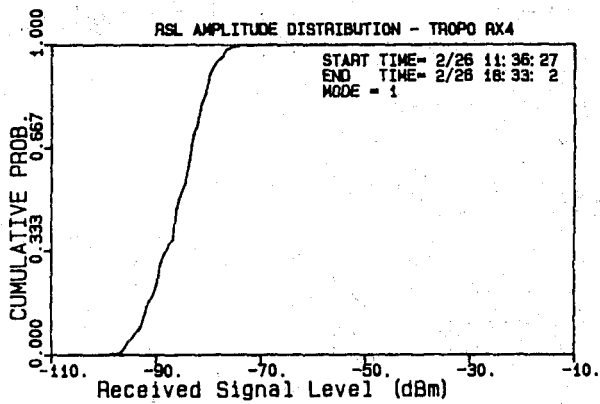
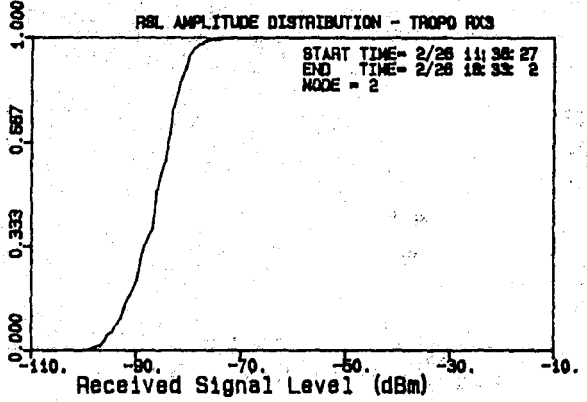
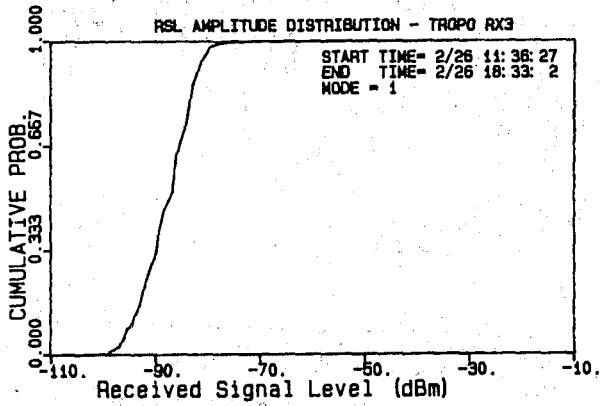
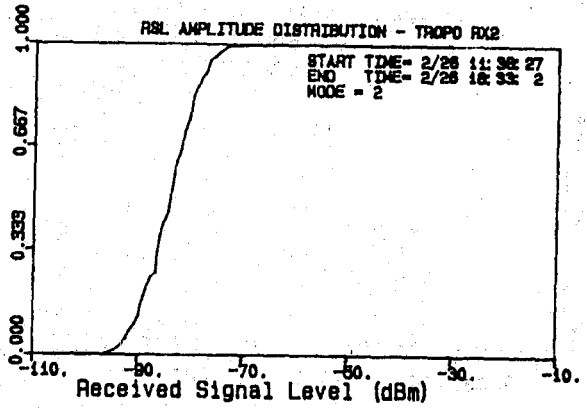
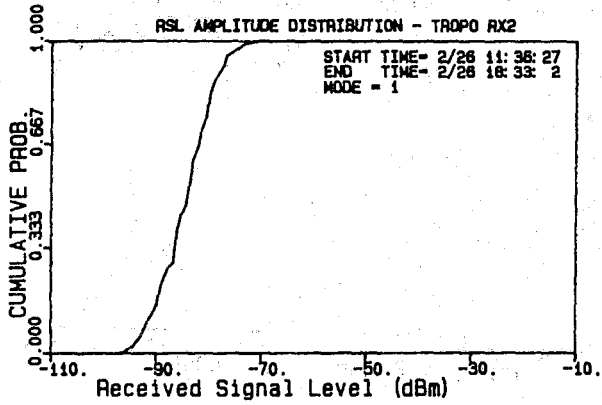
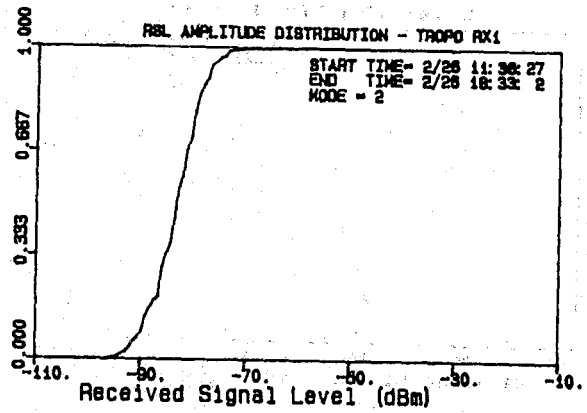
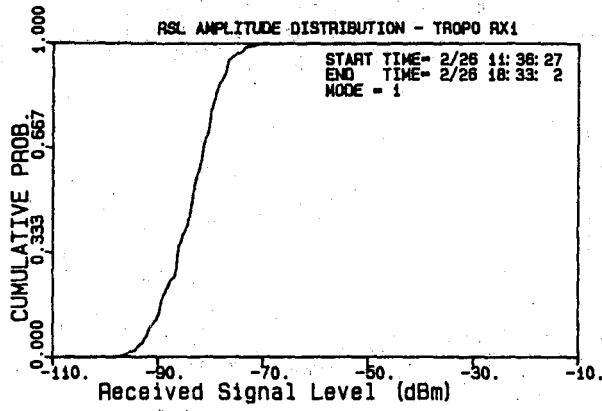


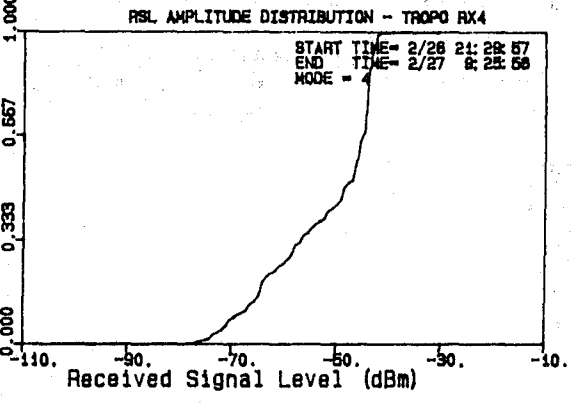
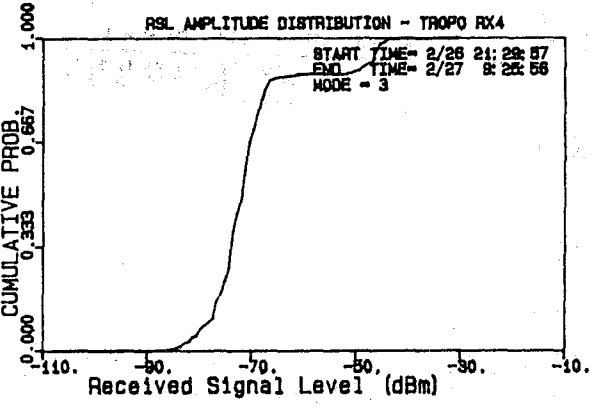
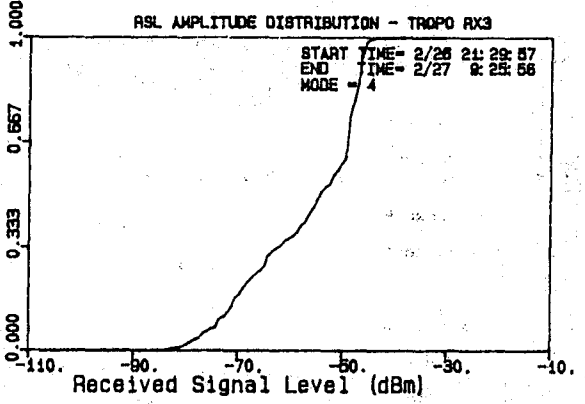
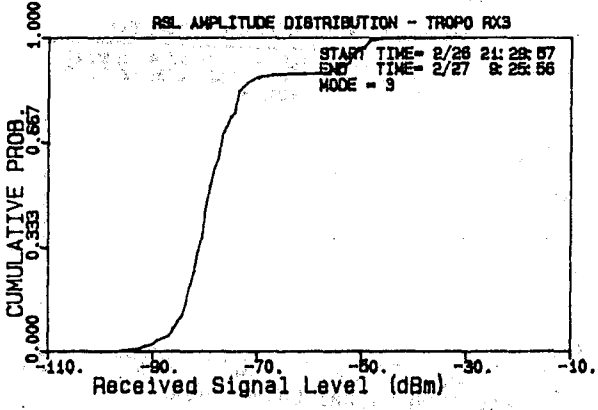
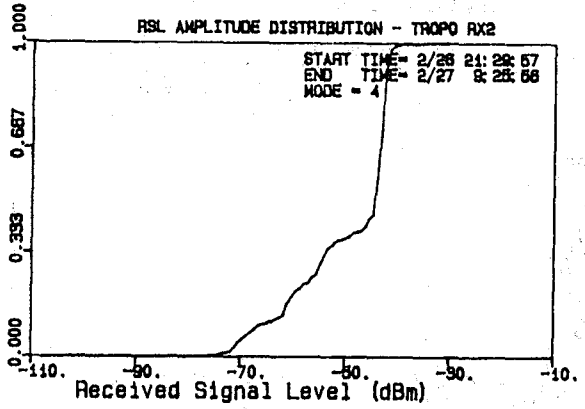
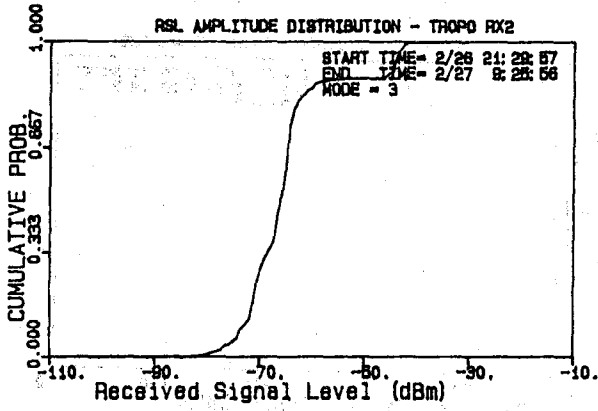
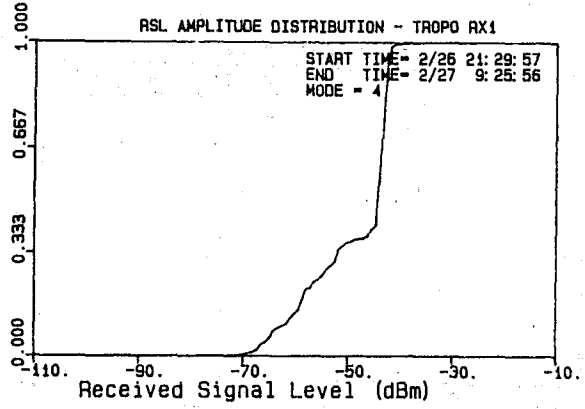
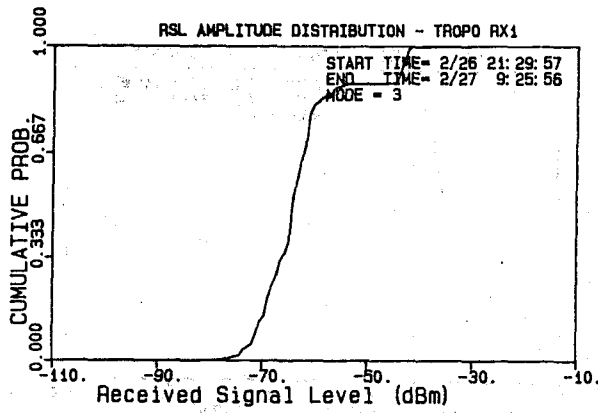


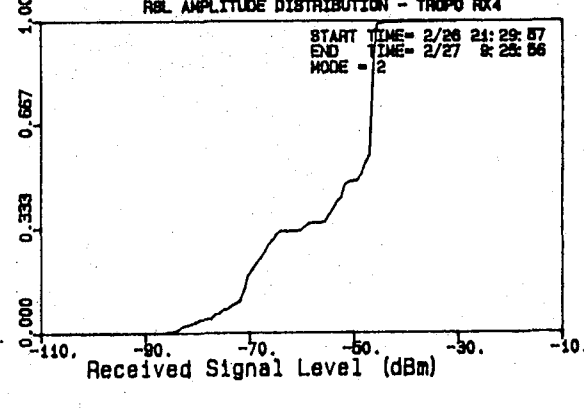
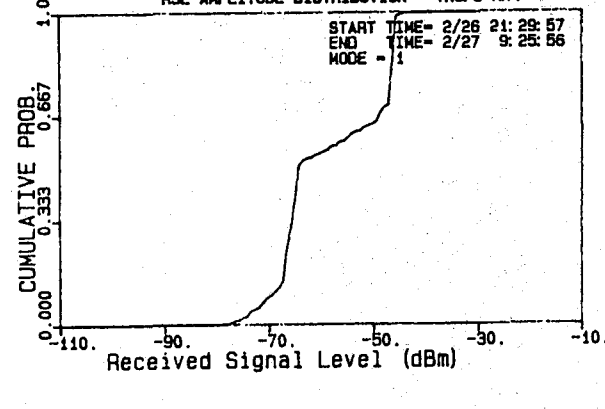
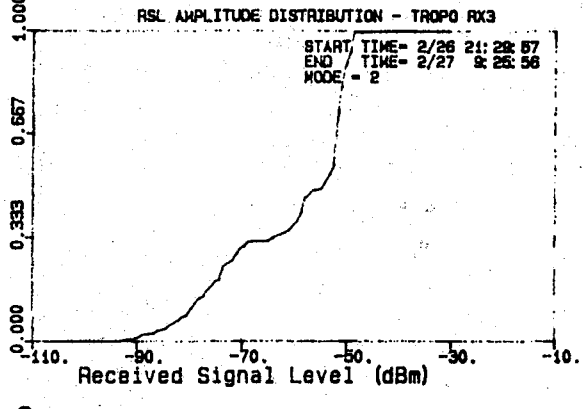
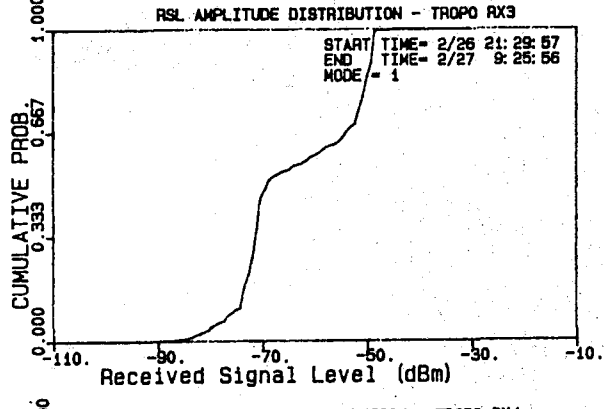
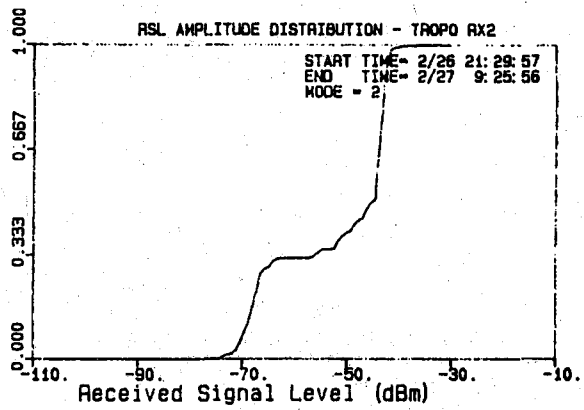
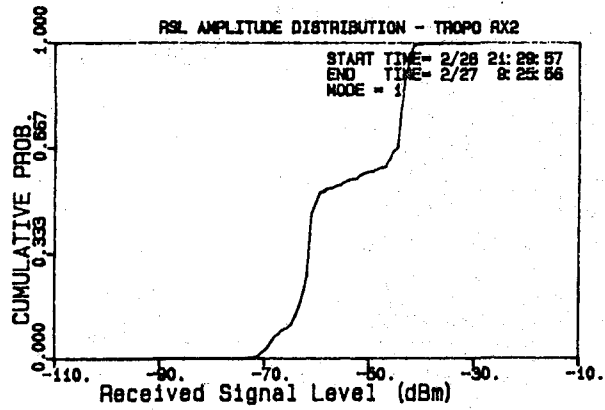
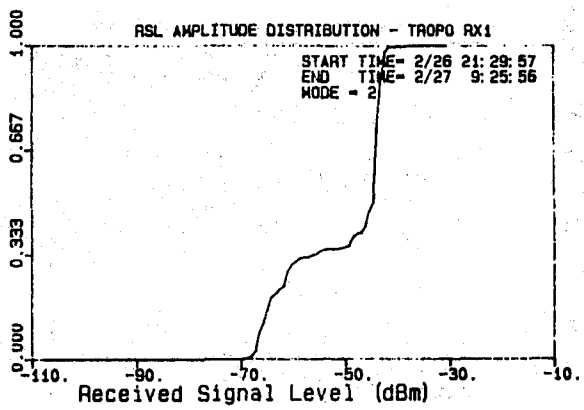
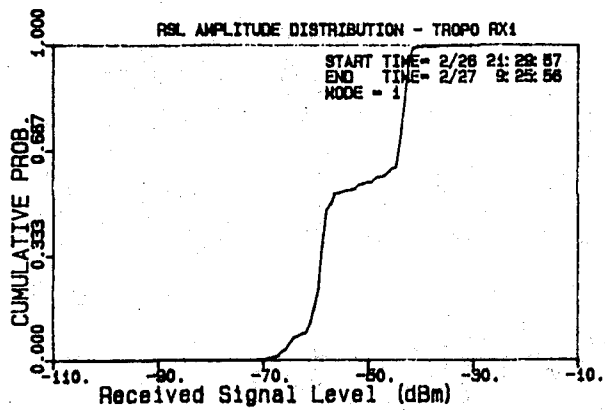


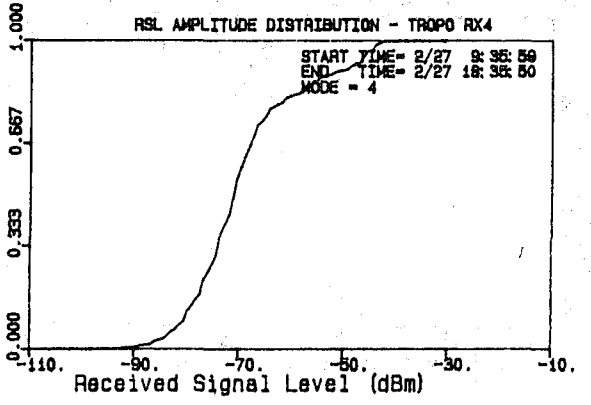
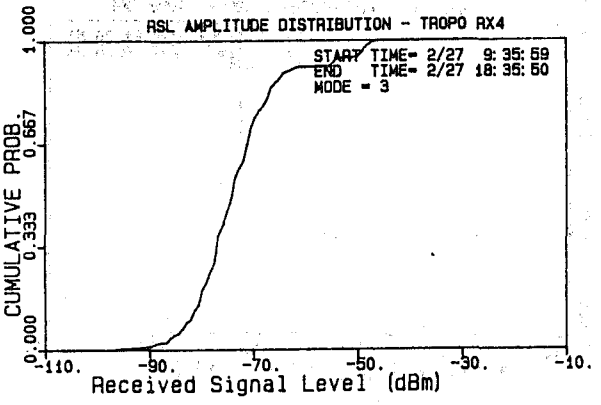
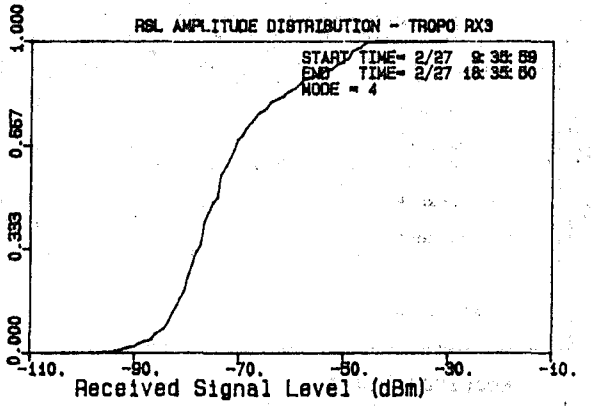
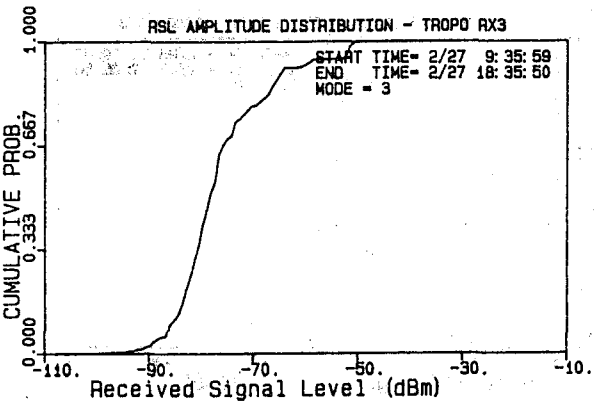
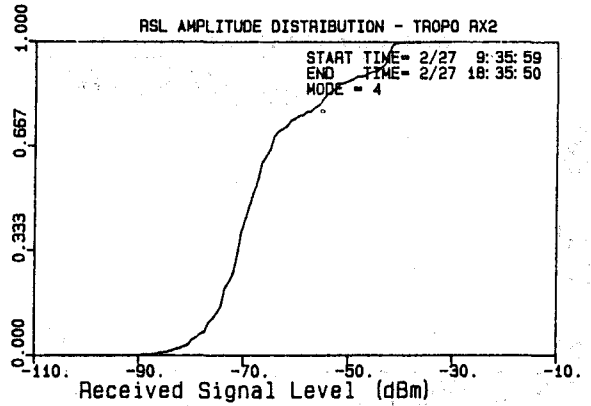
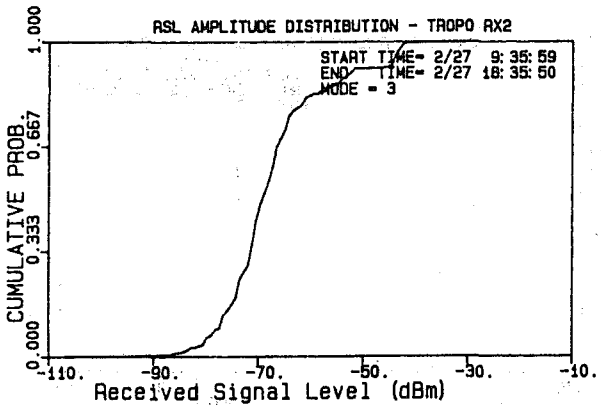
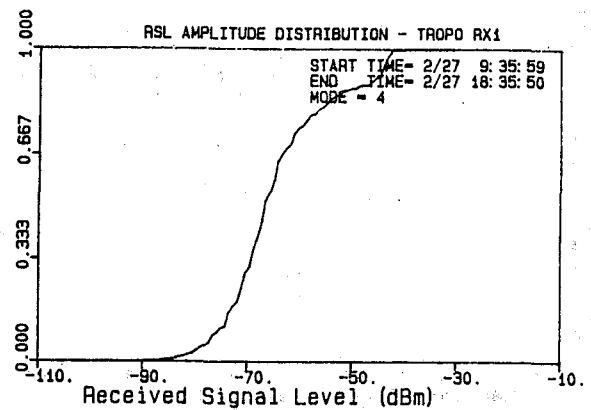
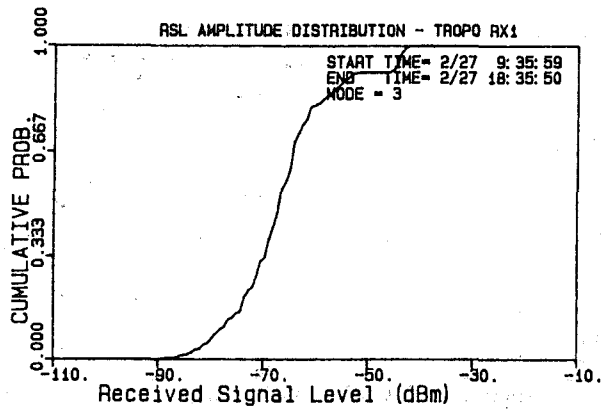


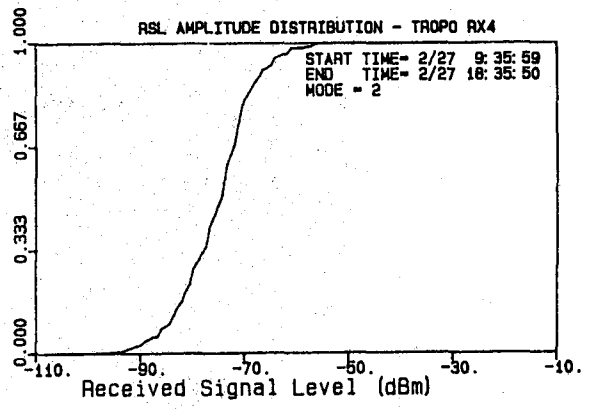
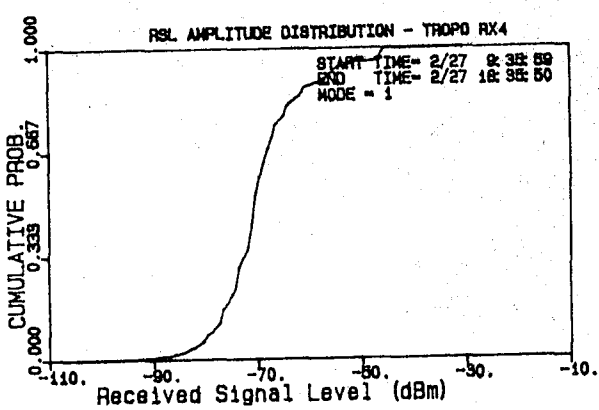
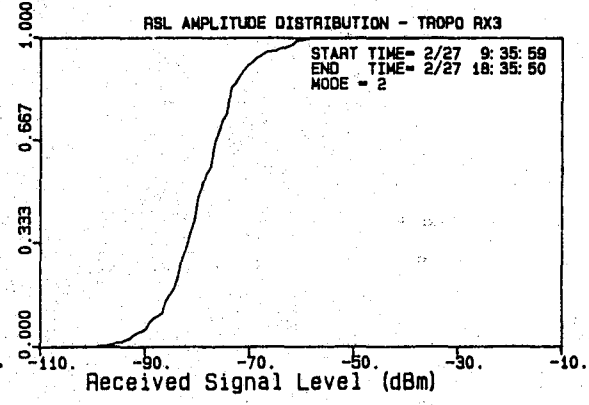
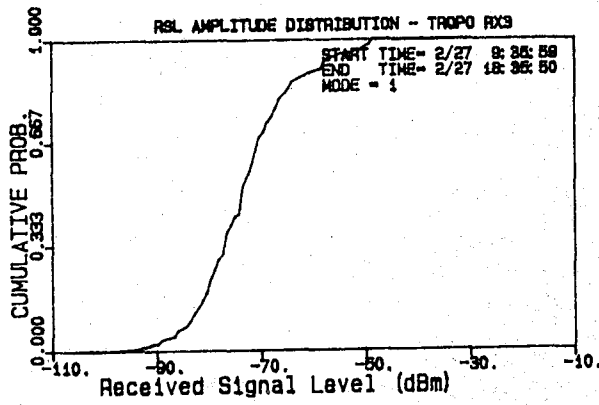
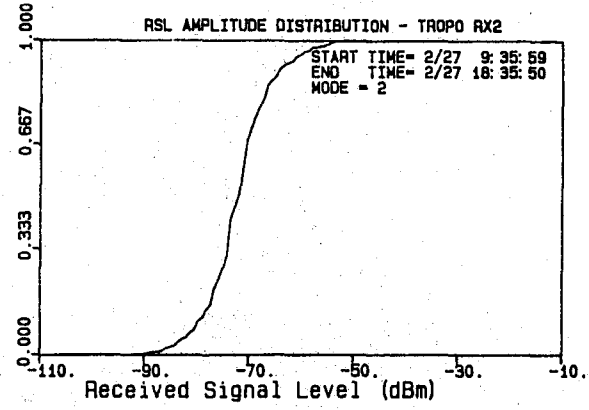
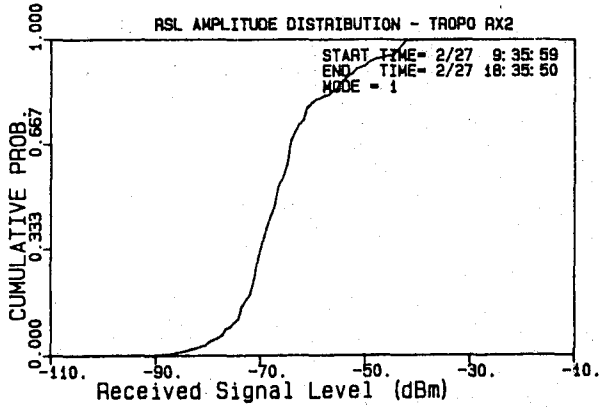
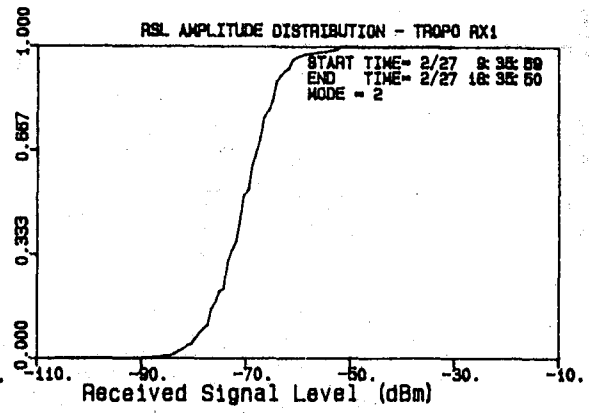
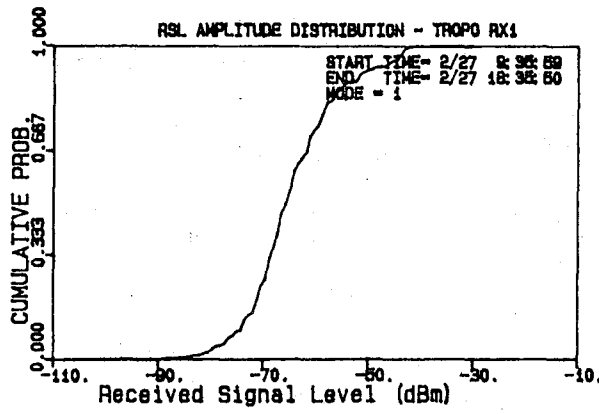


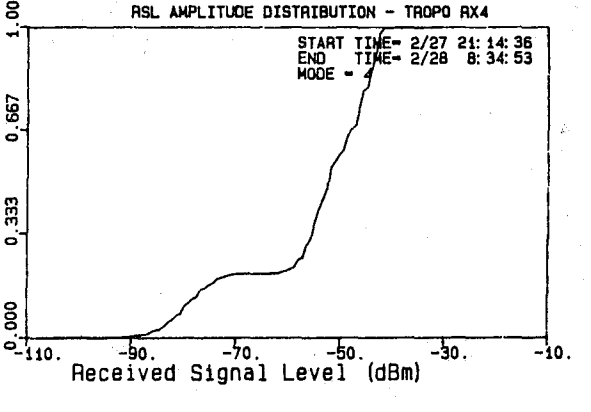
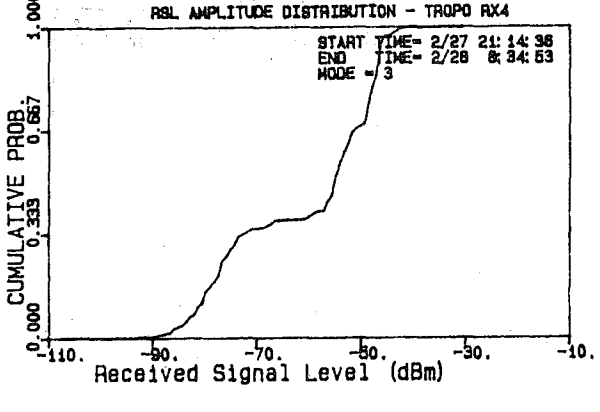
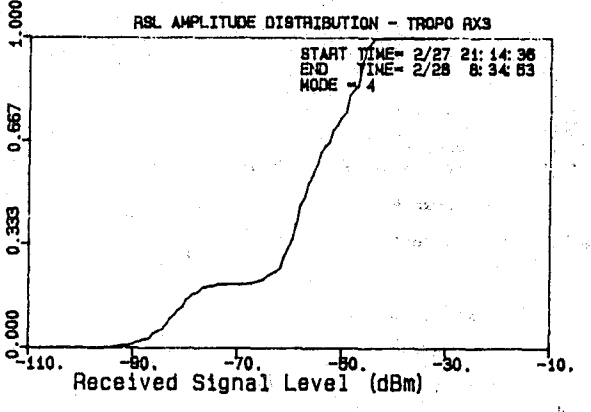
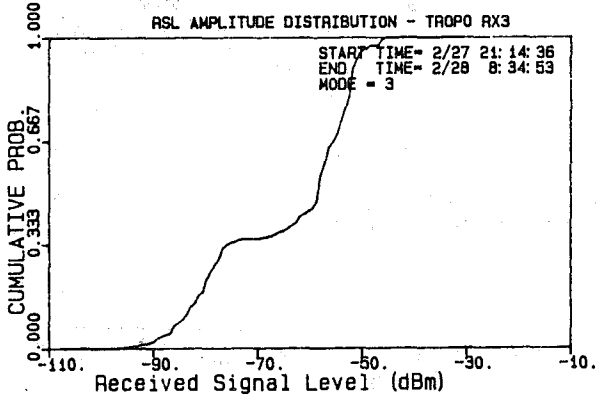
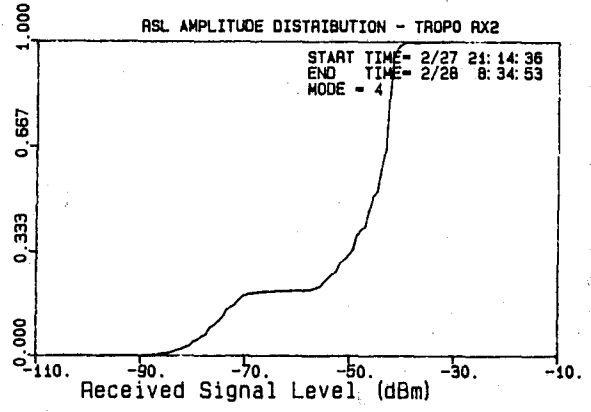
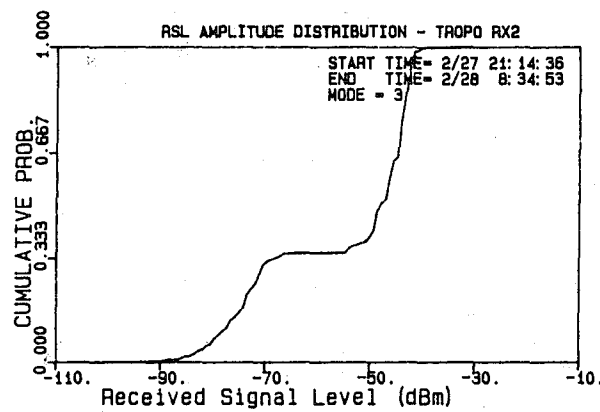
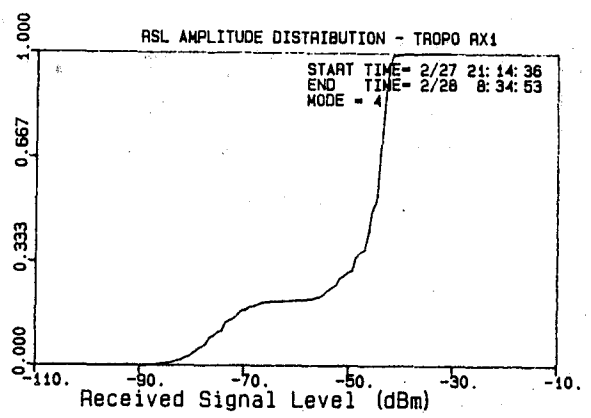
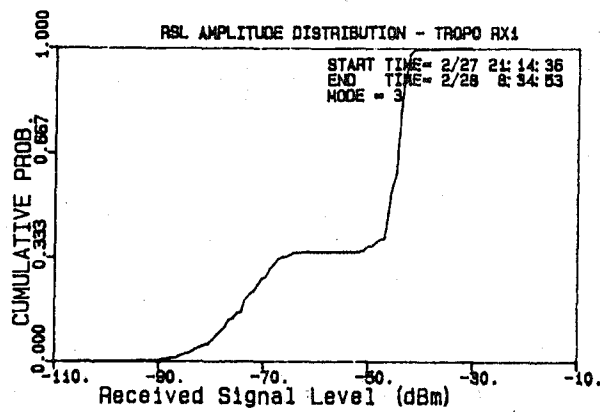


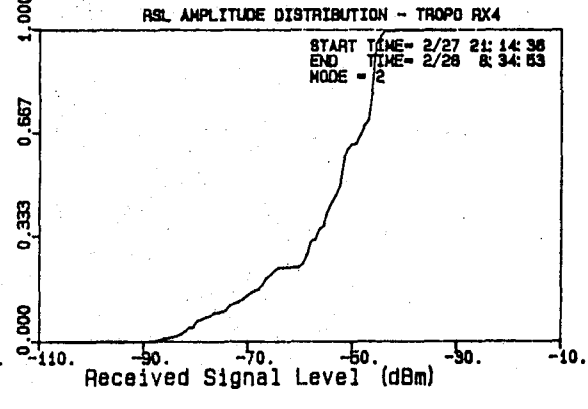
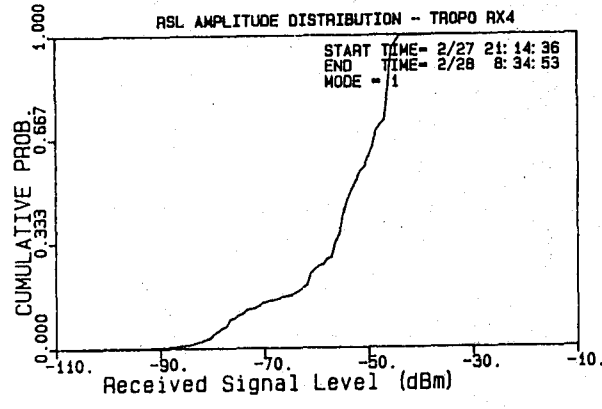
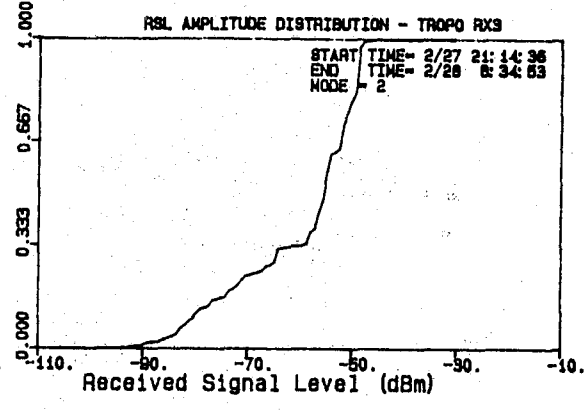
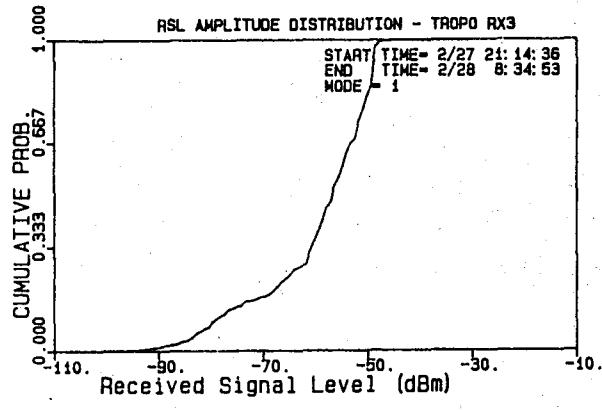
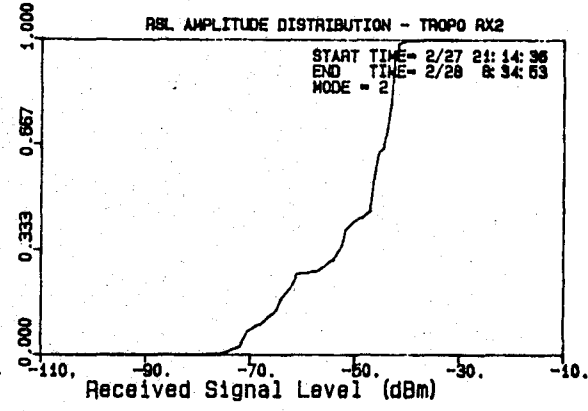
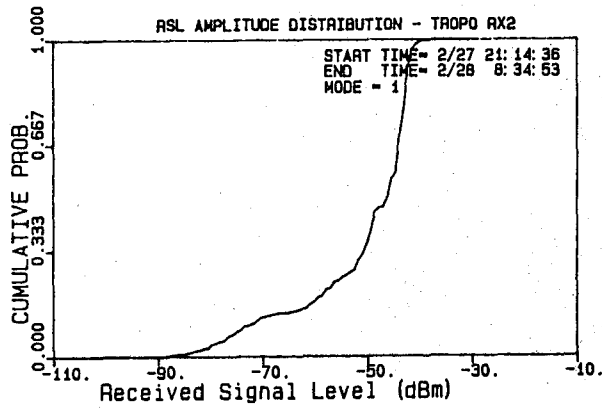
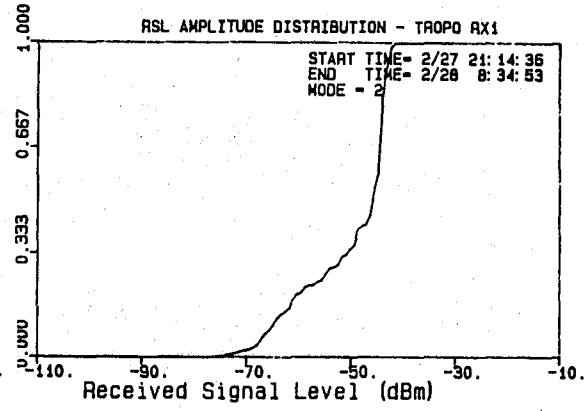
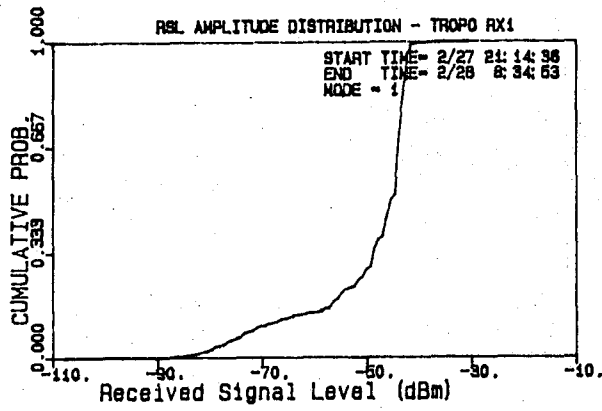










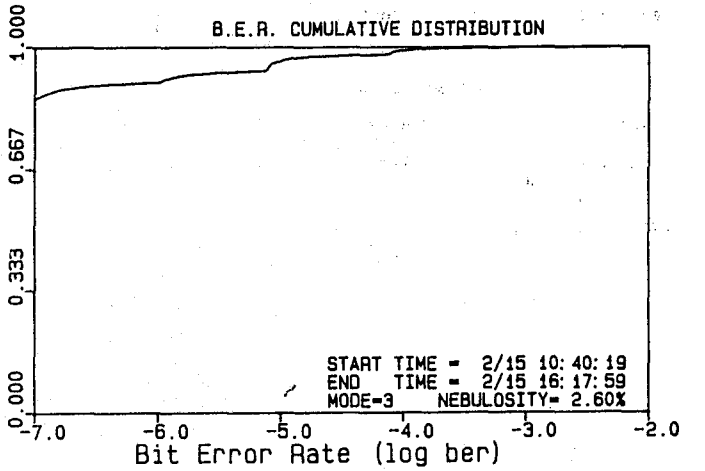
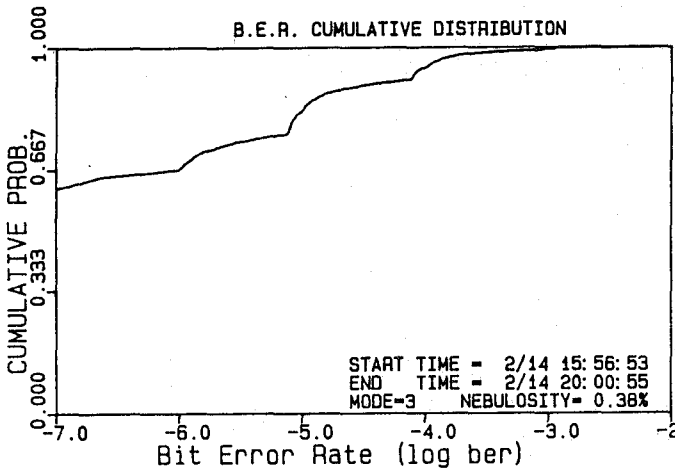
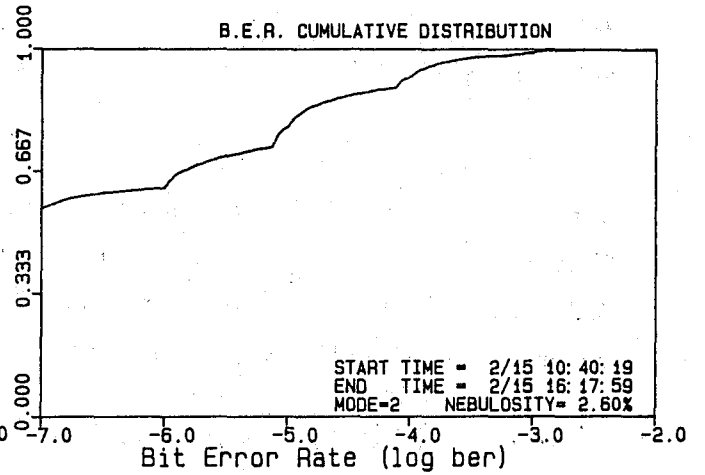
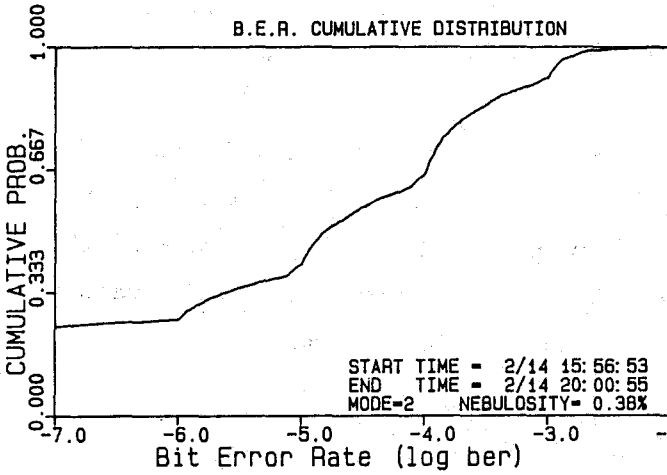
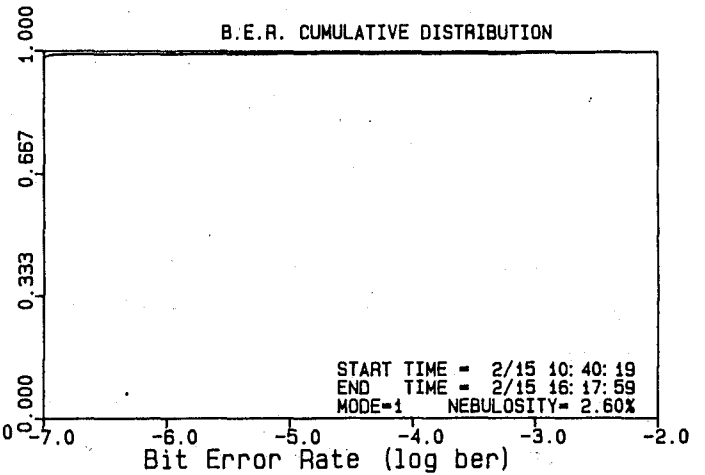
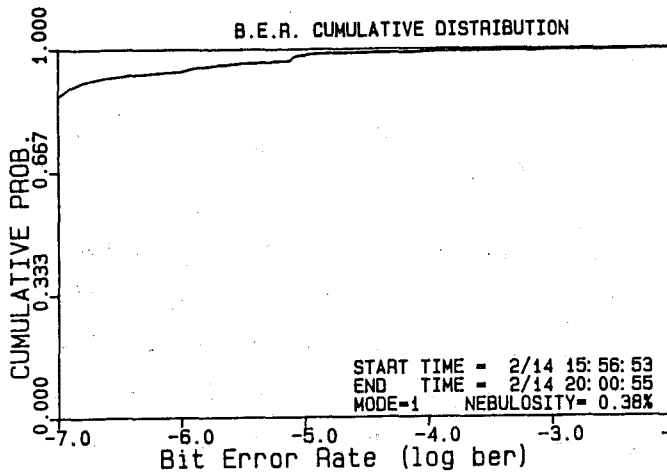


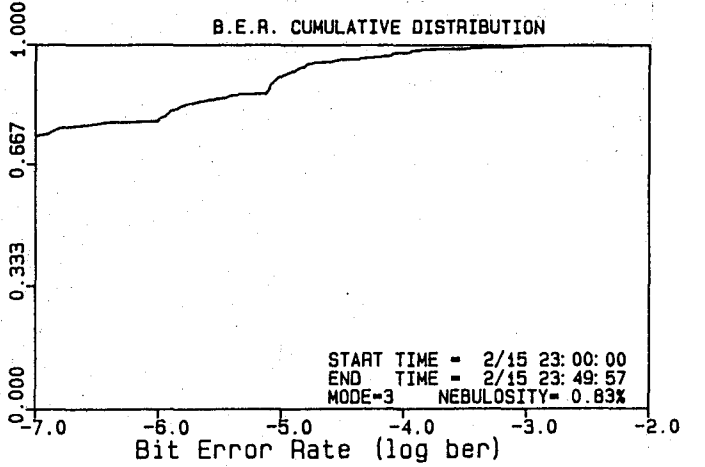
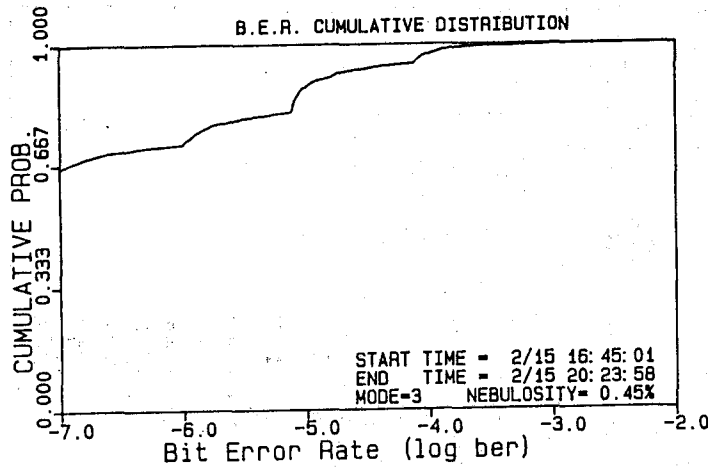
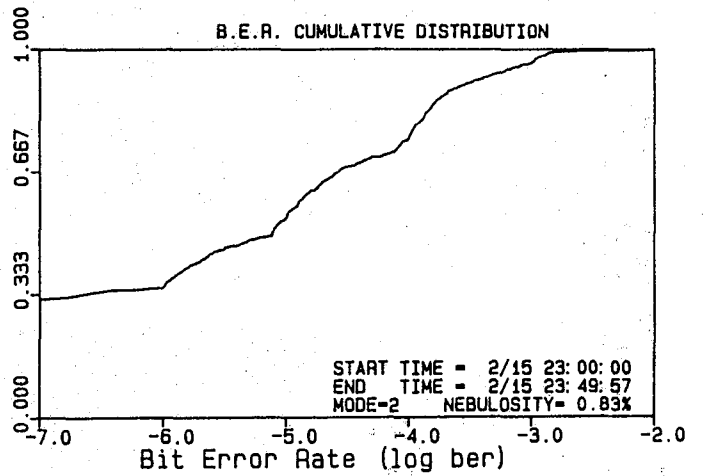
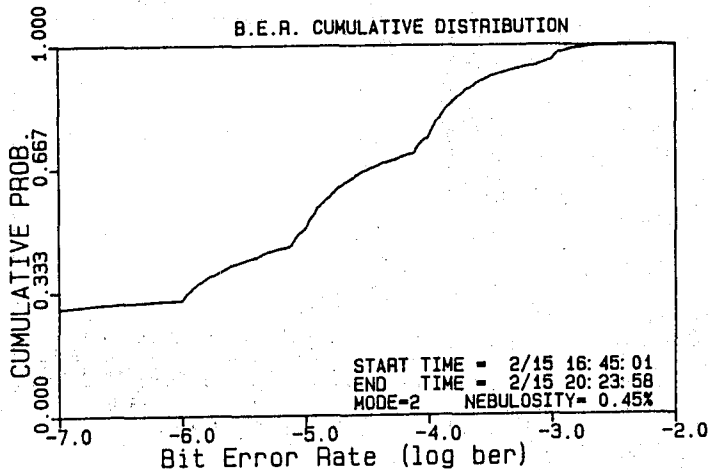
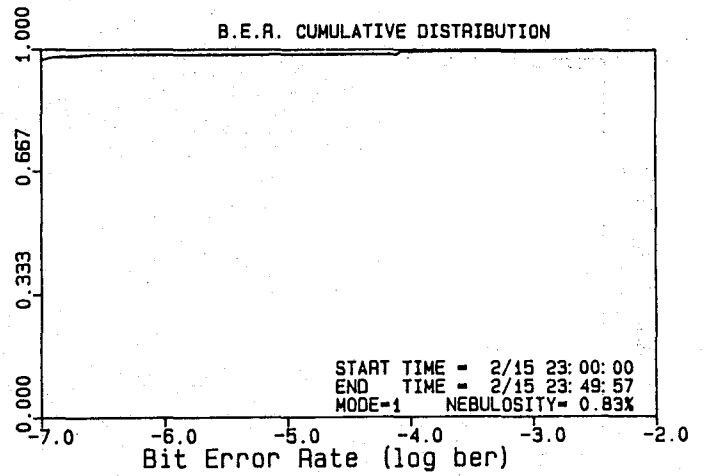
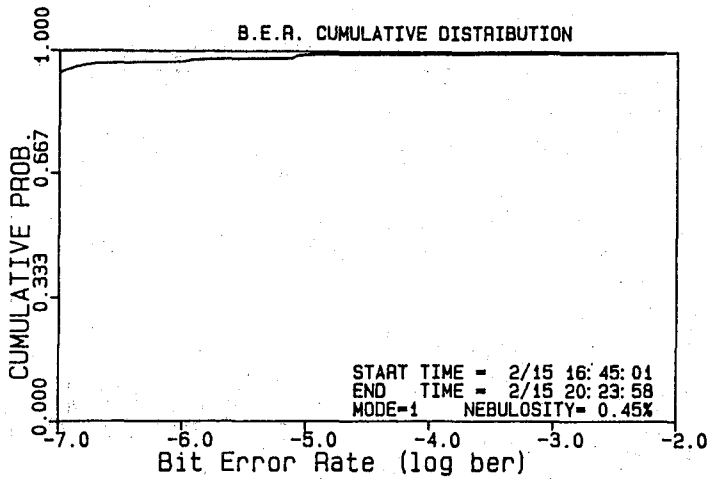
APPENDIX E

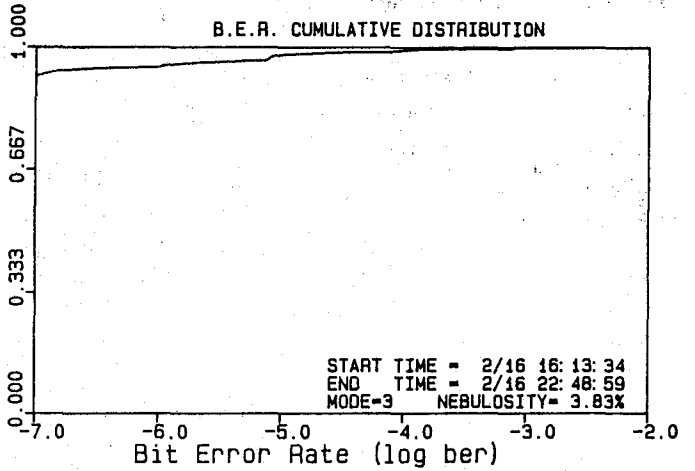
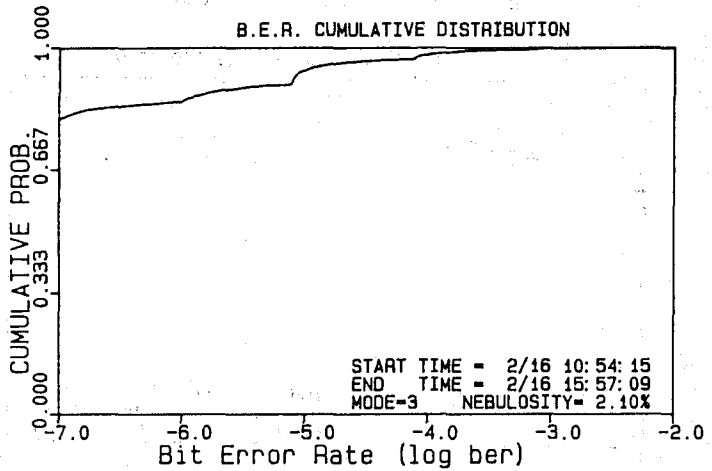
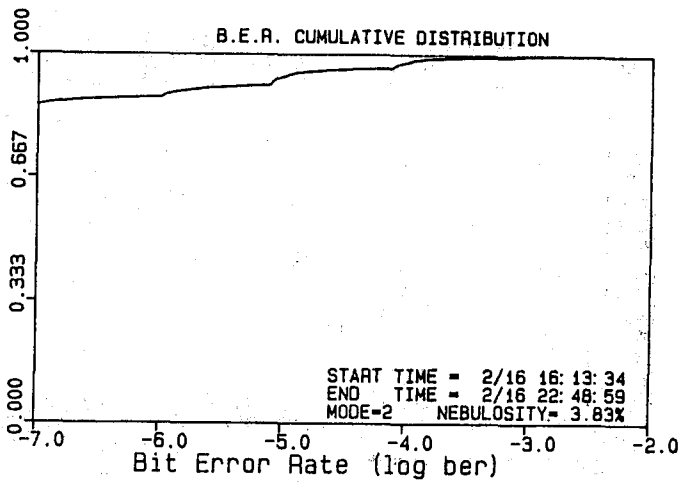
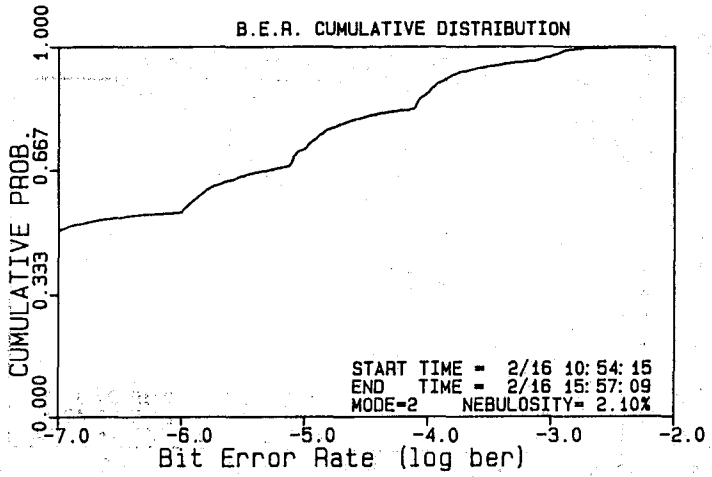
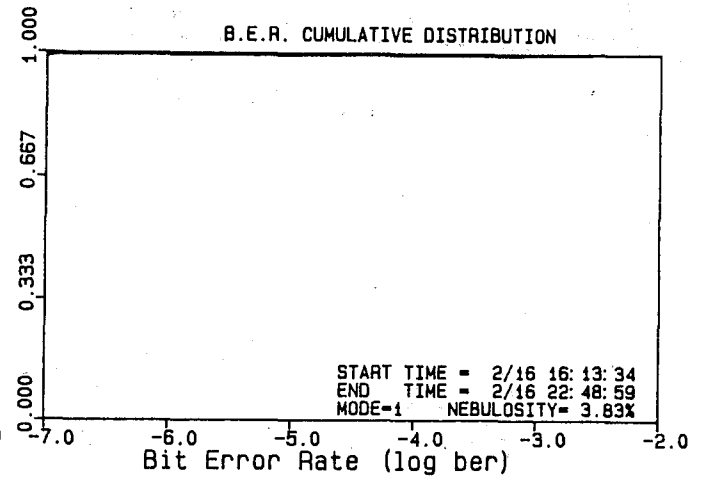
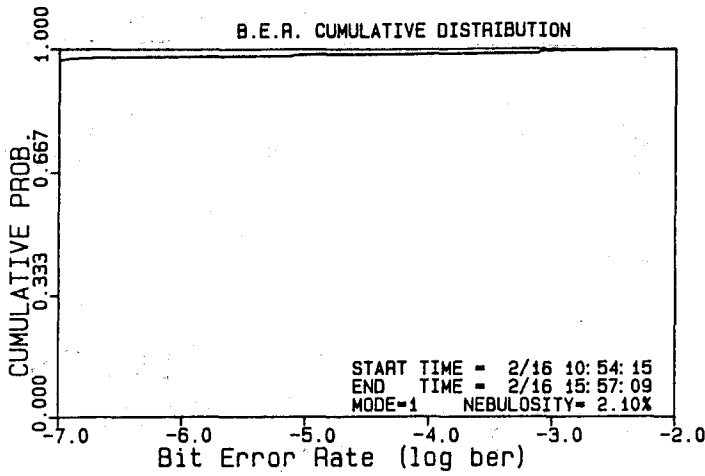
Cumulative Distributions of 1-Second BER

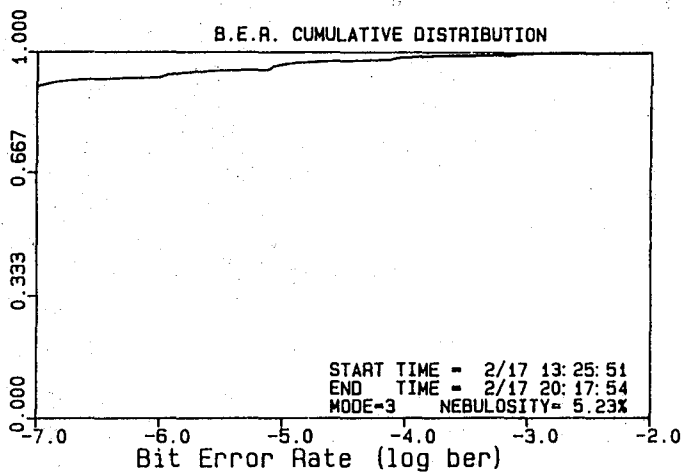
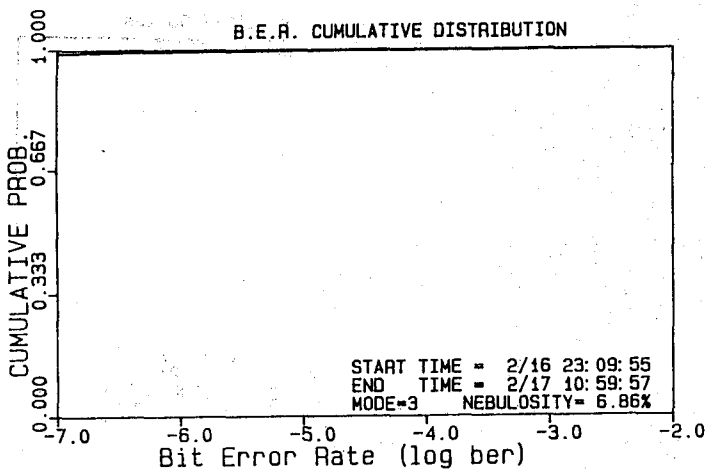
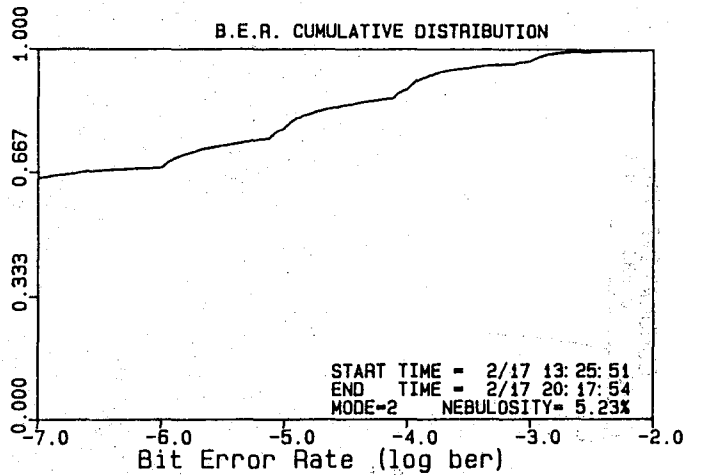
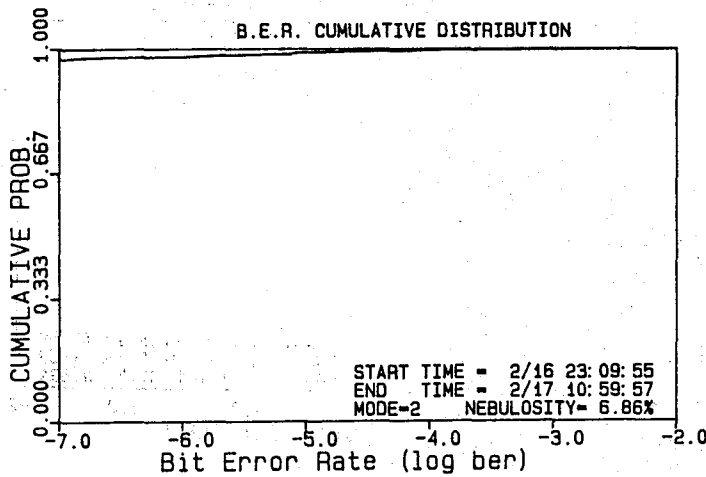
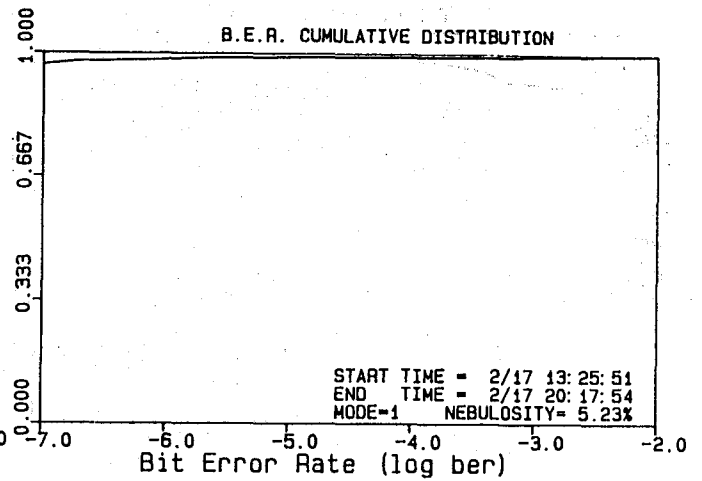
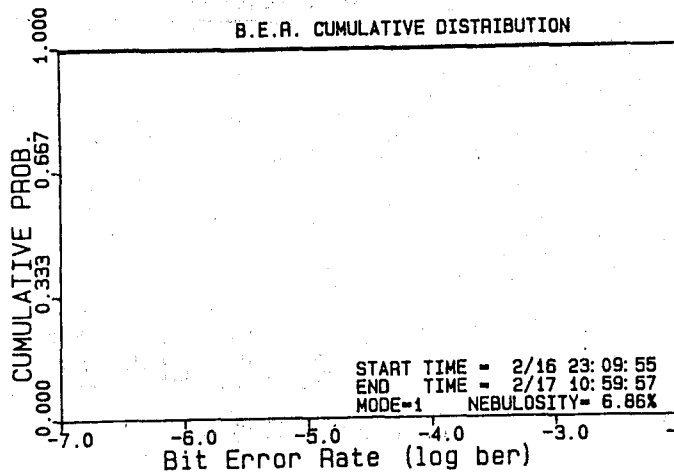
Two aspects of the BER distributions in this appendix require explanation. First, the values of BERs that are plotted have been scaled down from their actual values by a factor of 6.280. The reason is because the BERs were calculated assuming a bit rate equal to the 9.696 Mbps of the mission bit stream, whereas only one 1.544 TI bank was monitored. Thus, the actual BERs are greater than the plotted values by the factor $9.696/1.544 = 6.280$. For example, a BER plotted as 10^{-5} is actually equal to 6.28×10^{-5} , etc.

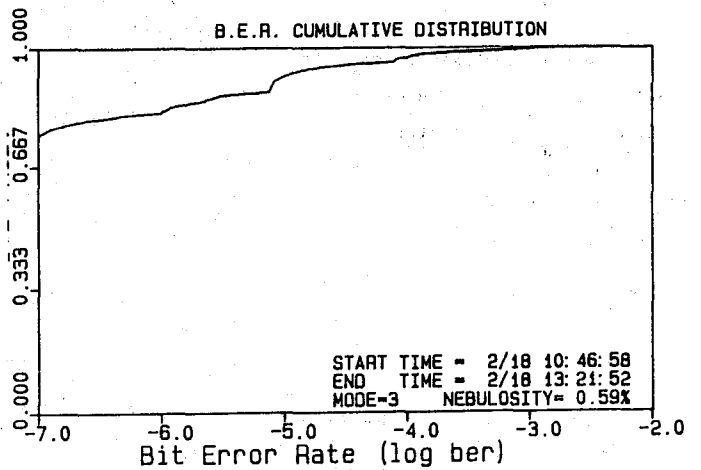
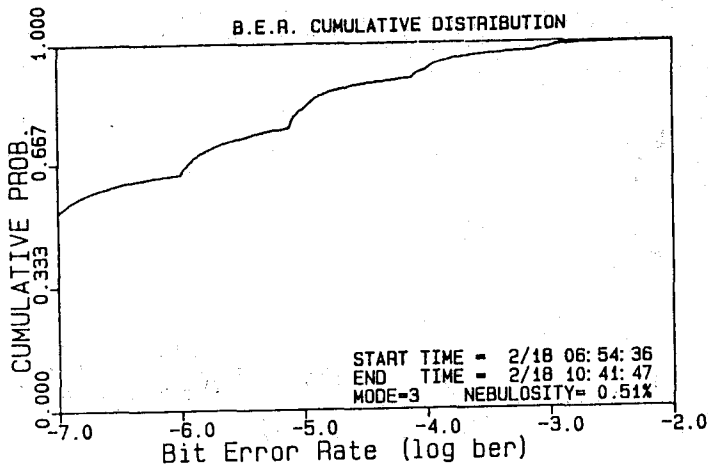
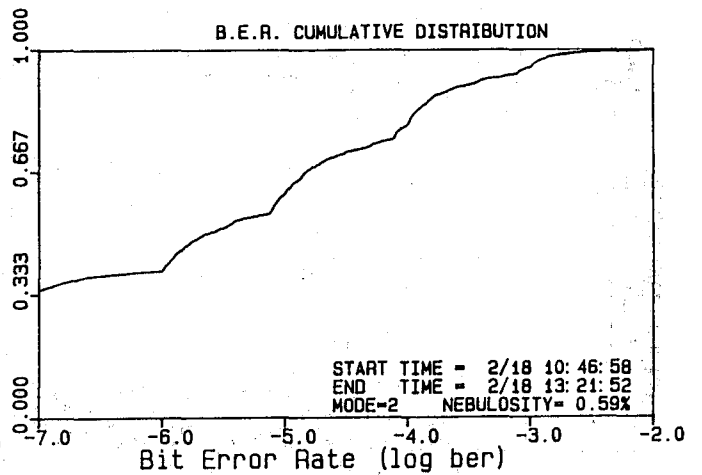
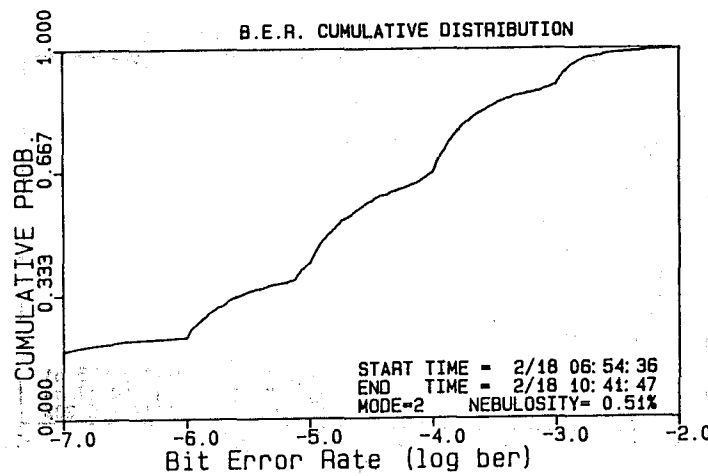
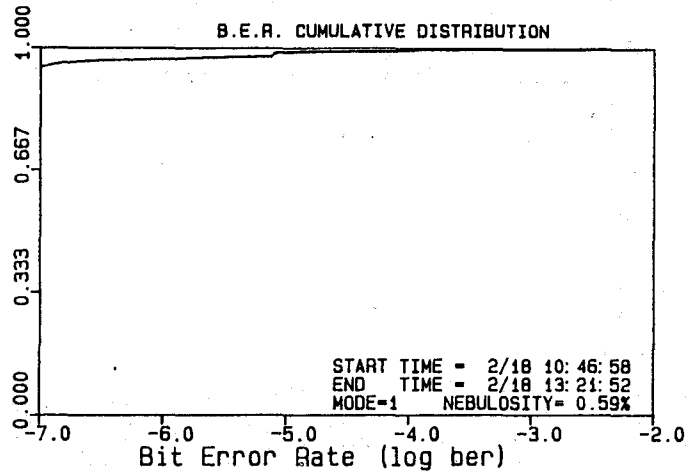
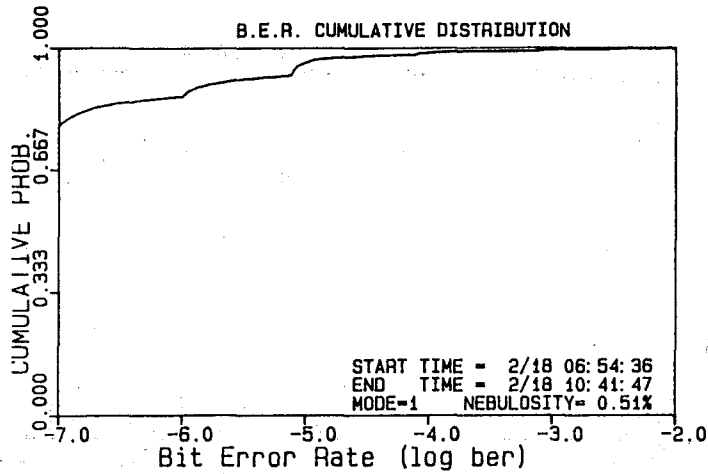
Second, the BER scale is linear (not logarithmic) within each decade. For example, a point half way between 10^{-5} and 10^{-4} is equal to 5.5×10^{-5} , etc. This peculiarity of the BER scale accounts for the scalloped appearance of the BER distributions, but in no way affects their correctness. This rather unconventional scale was chosen in order to simplify the software.

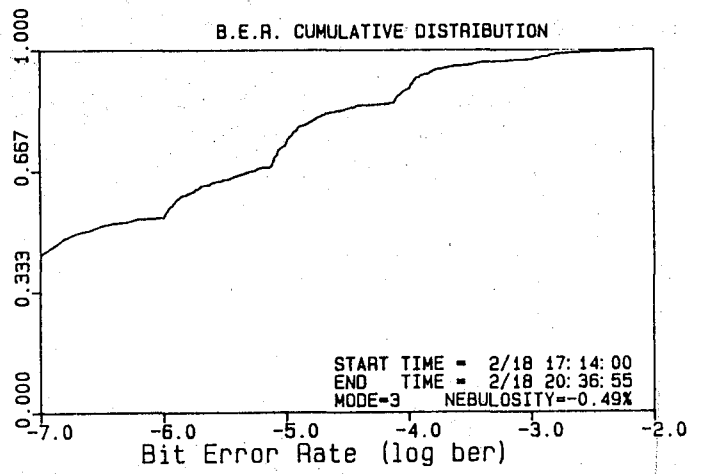
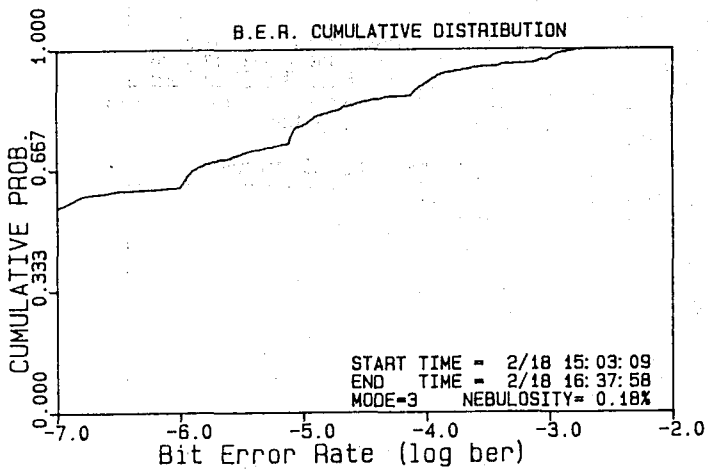
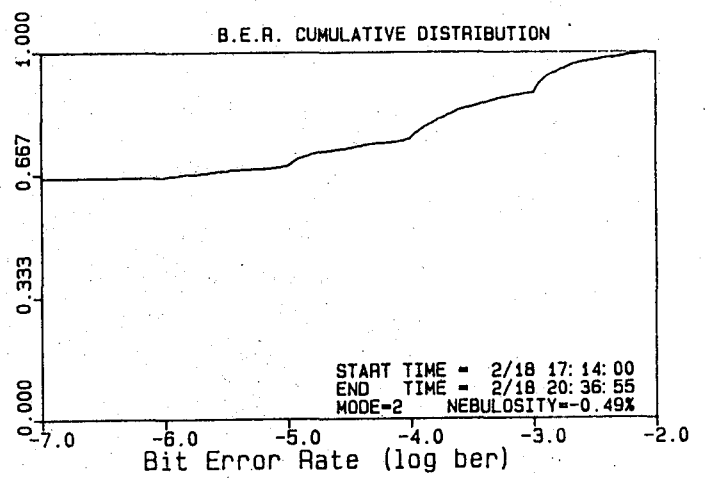
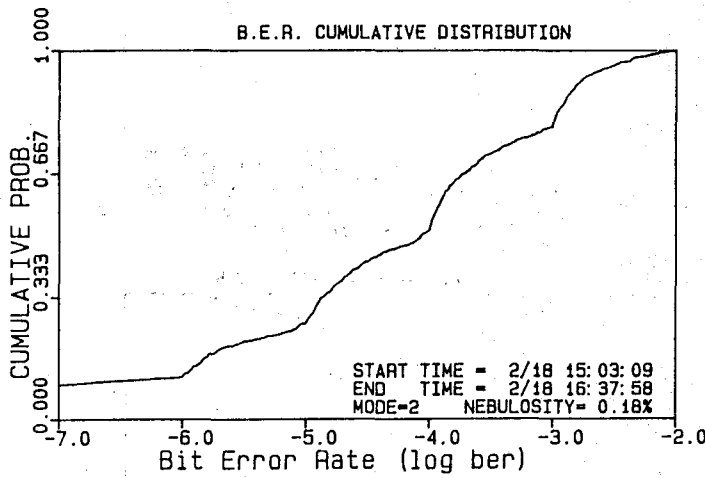
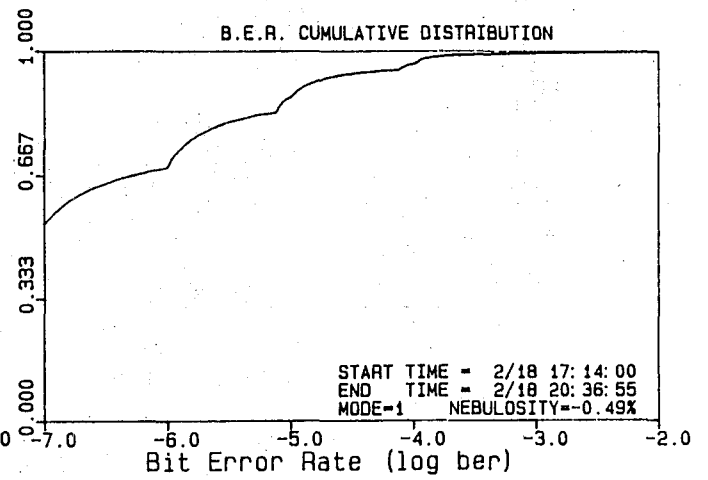
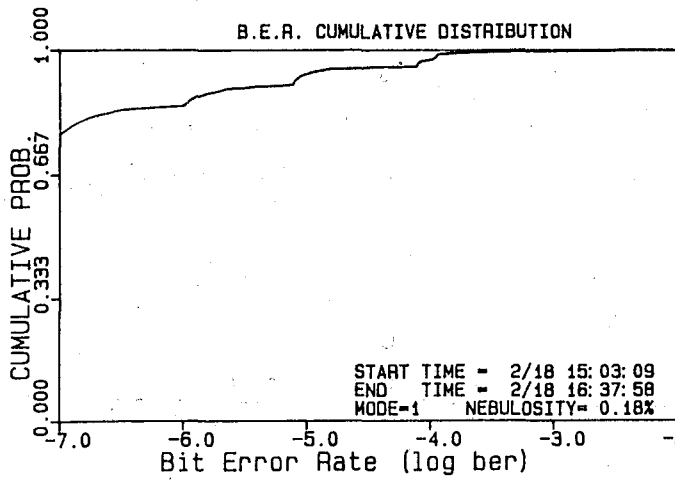


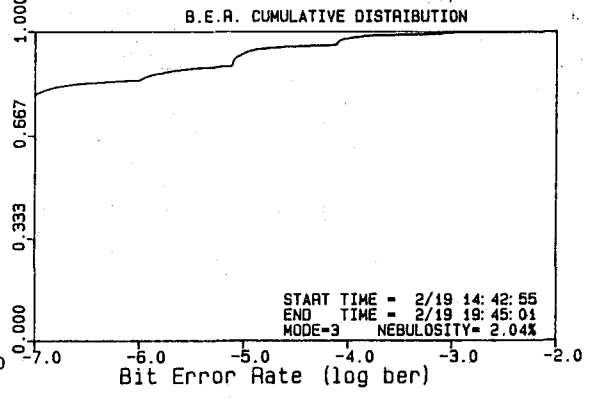
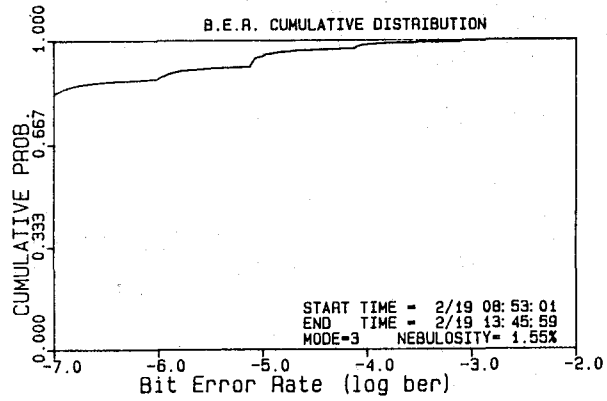
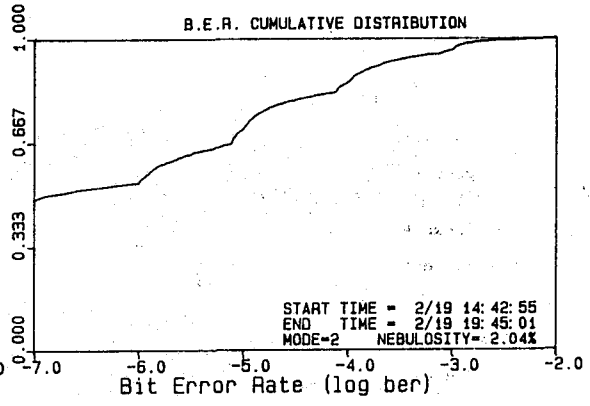
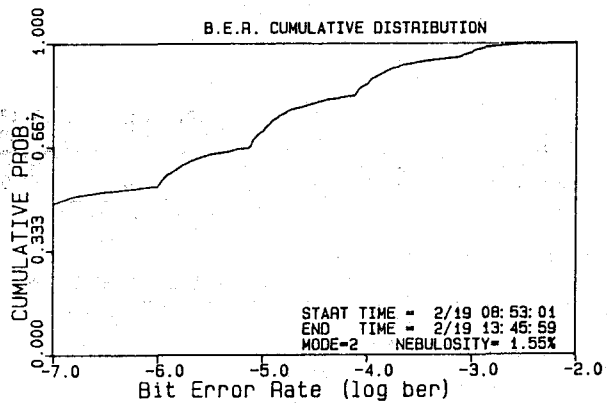
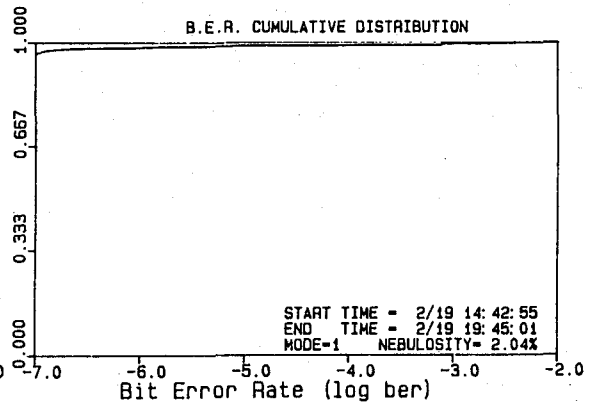
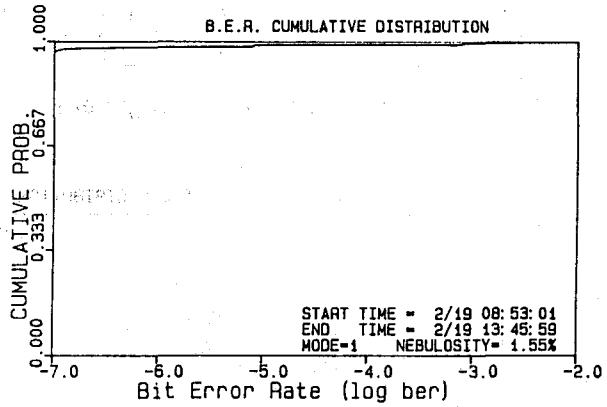
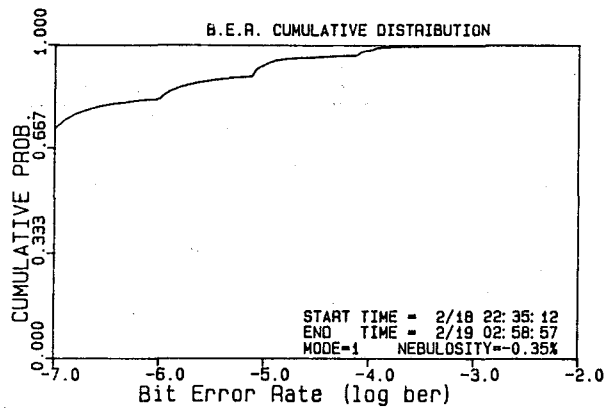


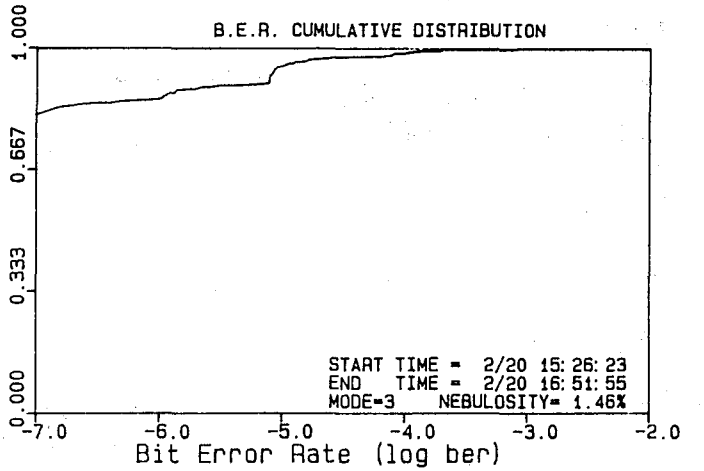
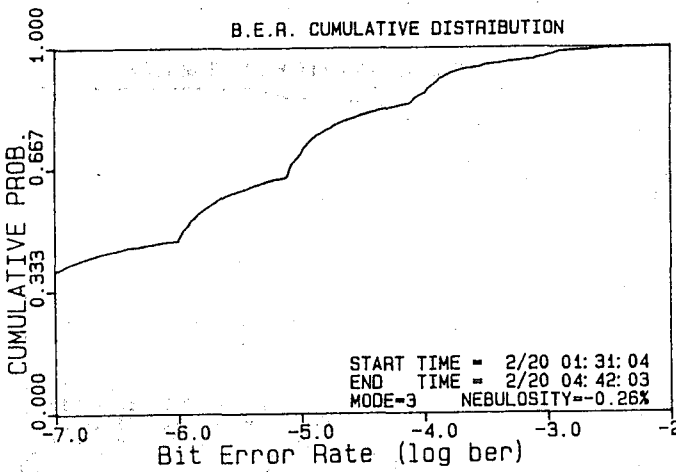
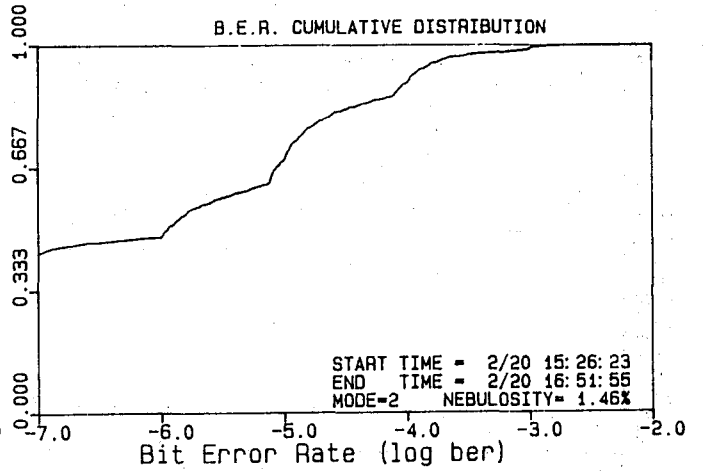
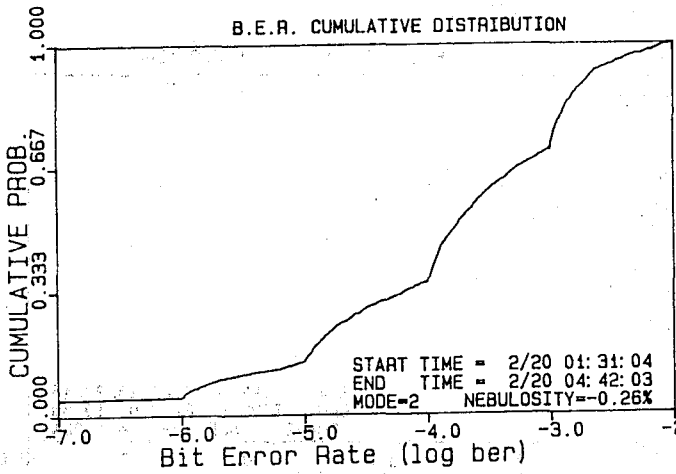
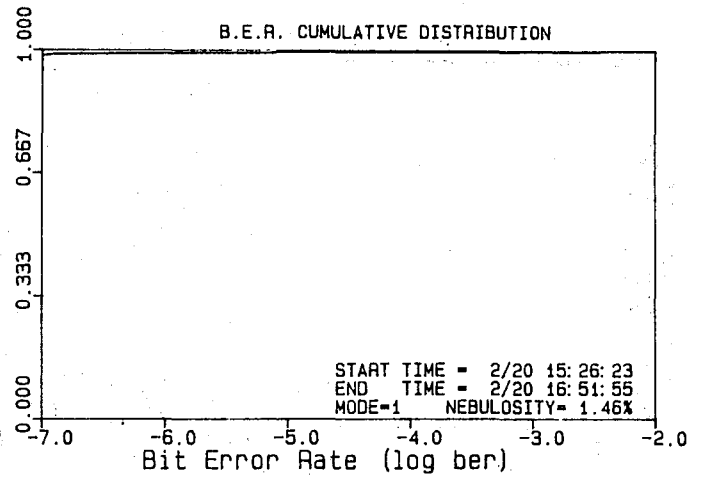
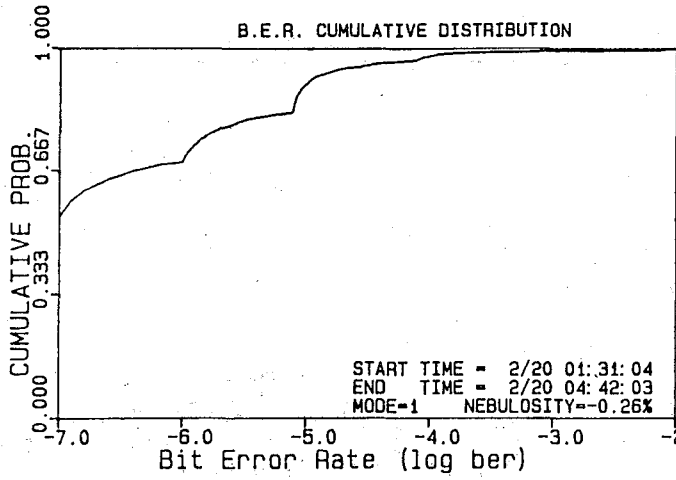


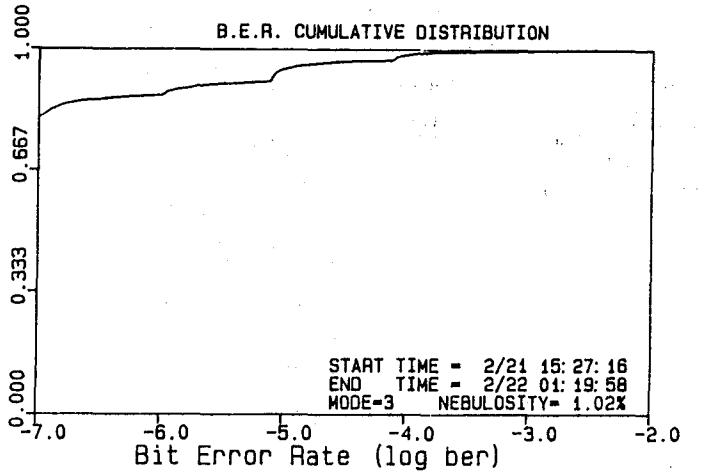
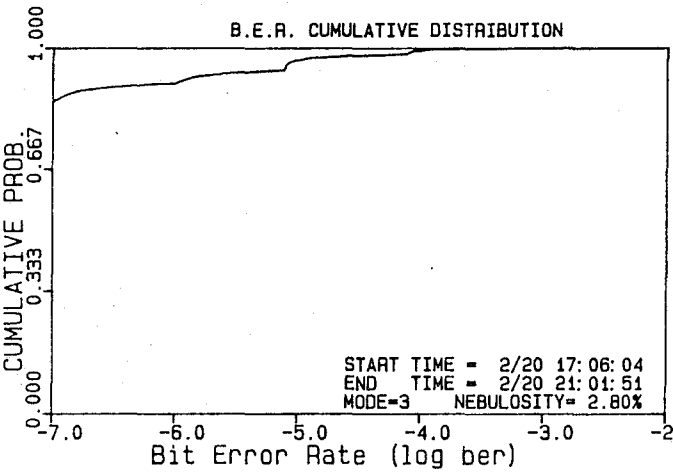
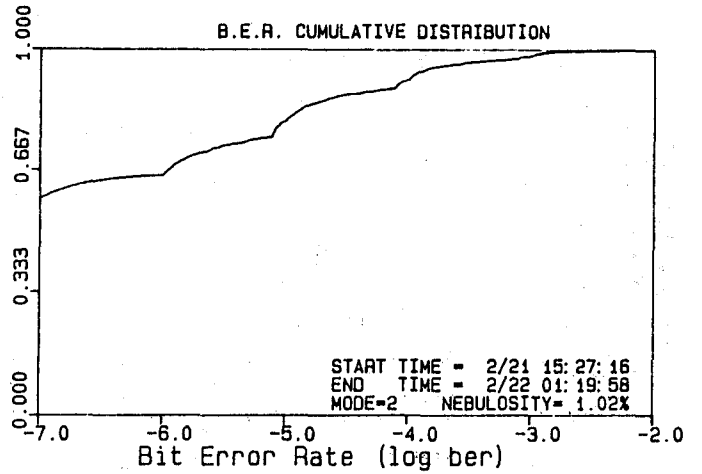
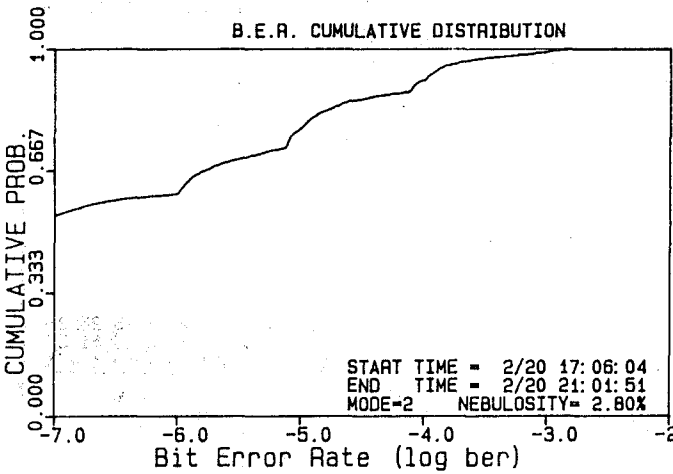
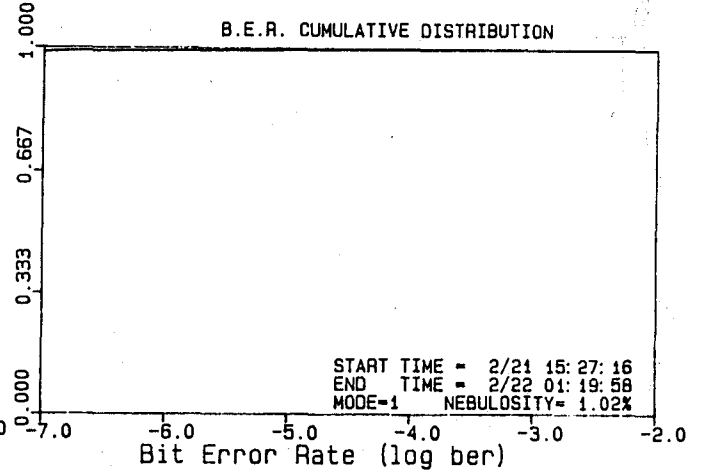
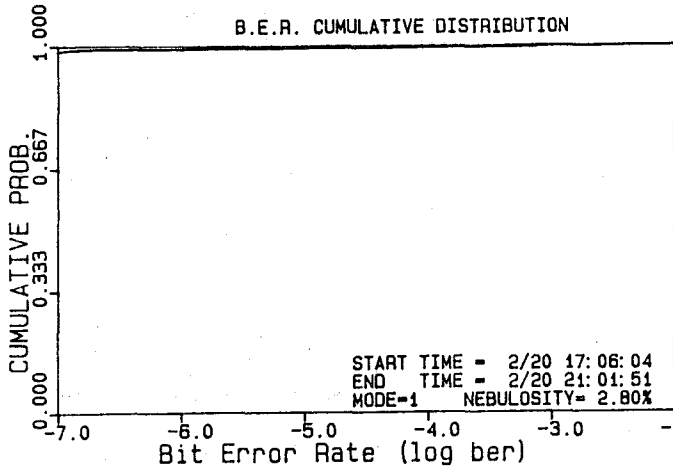


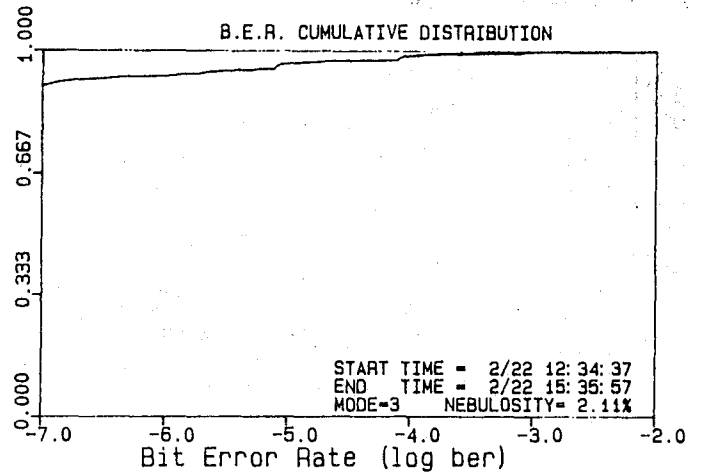
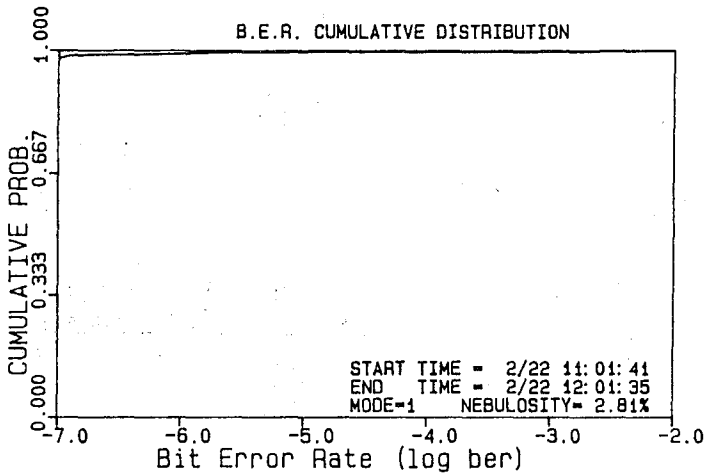
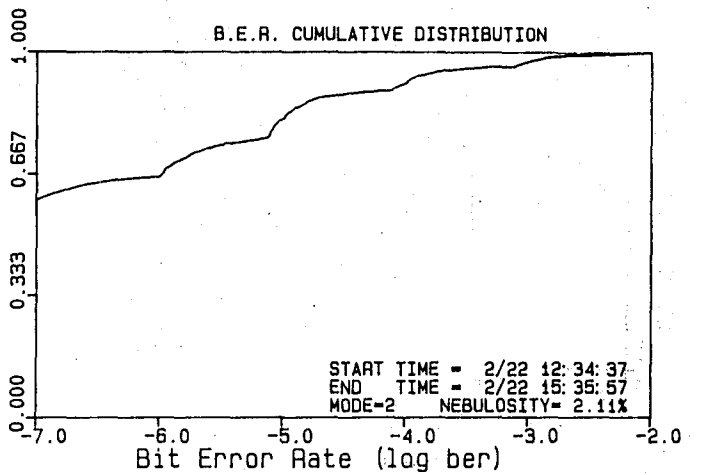
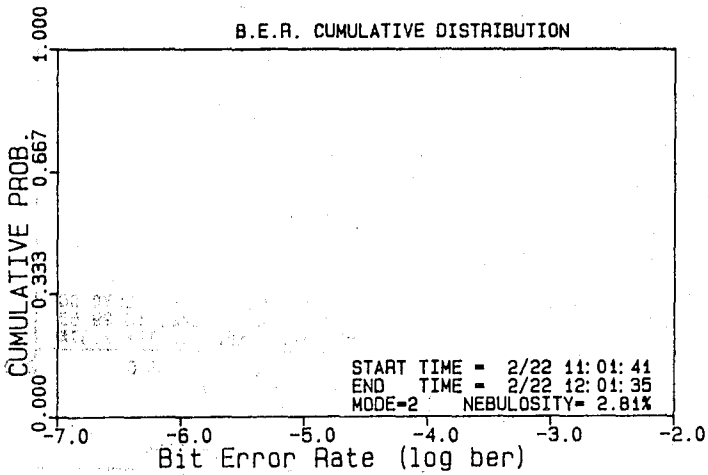
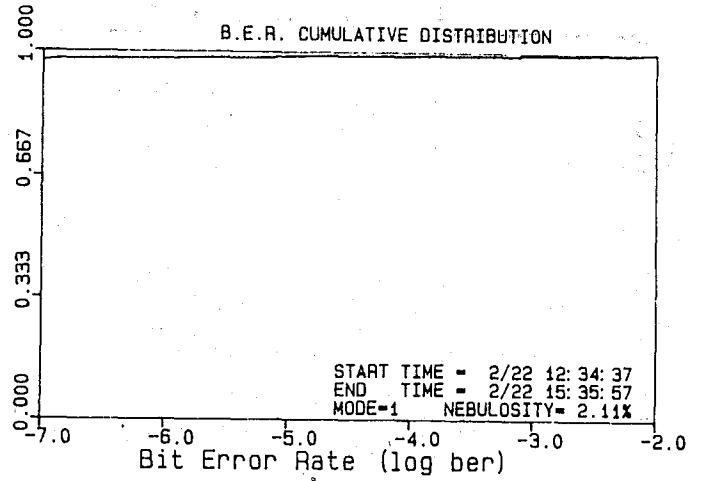
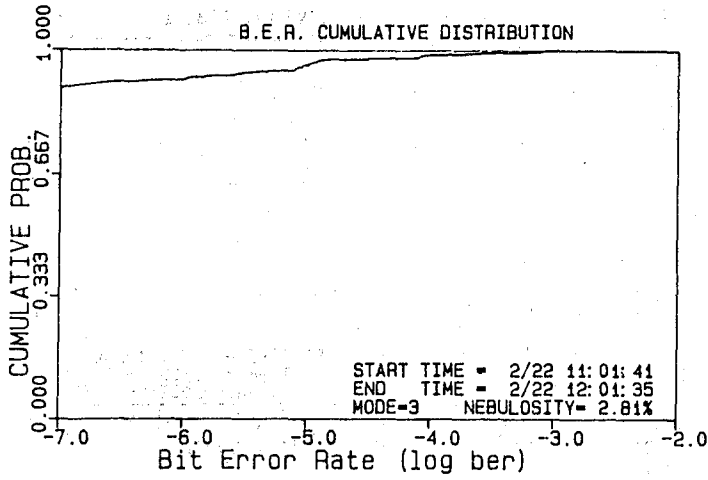


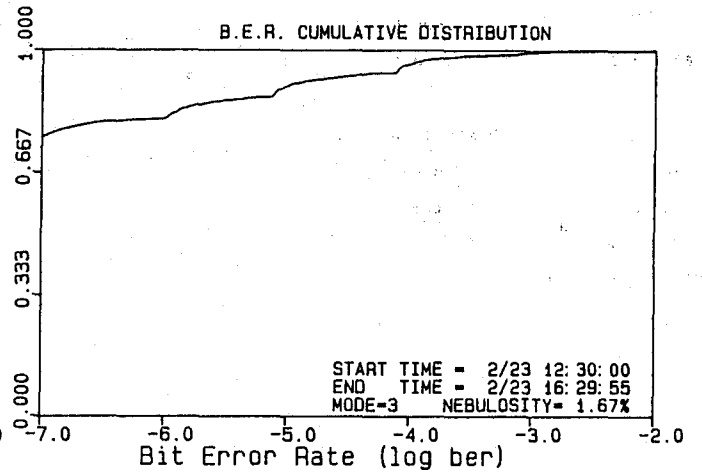
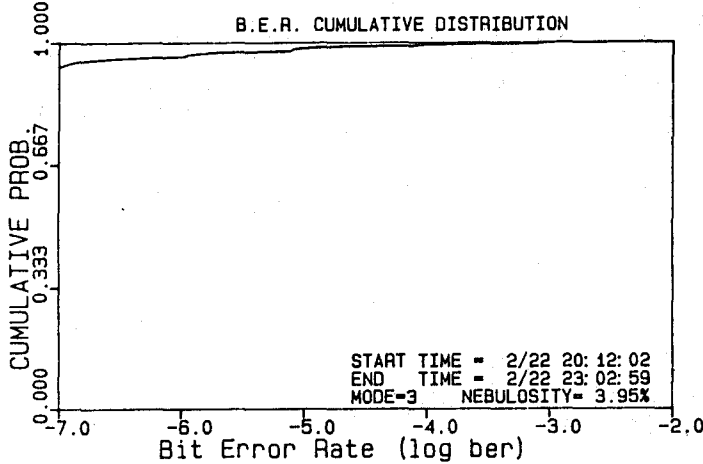
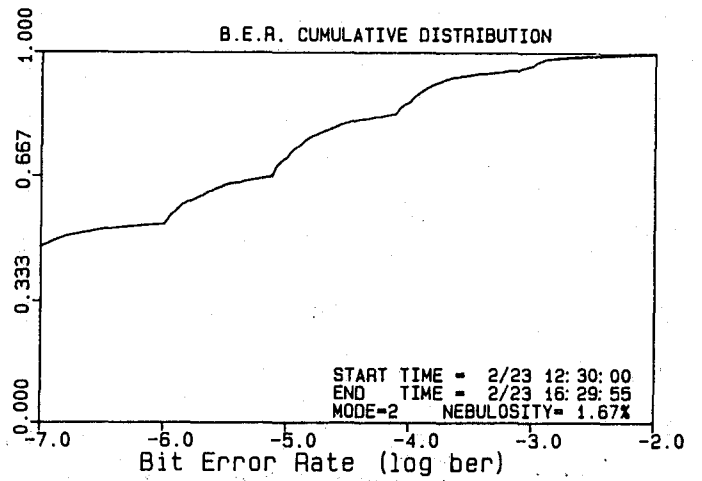
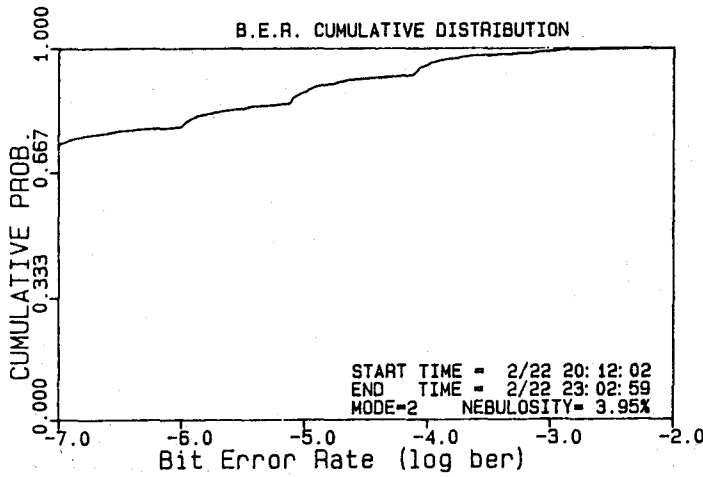
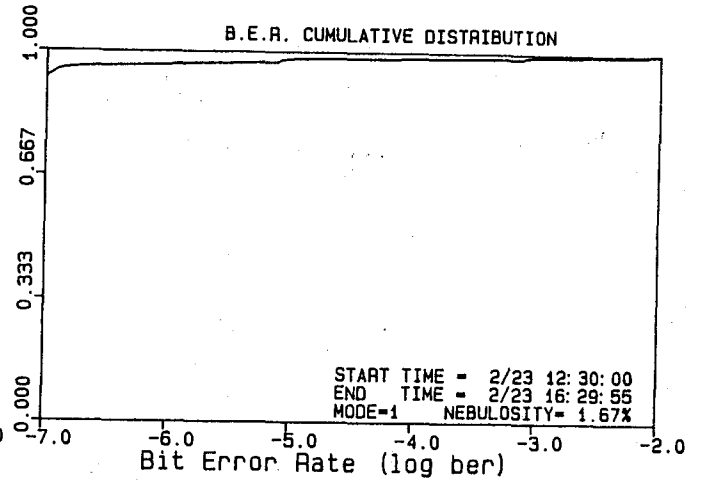
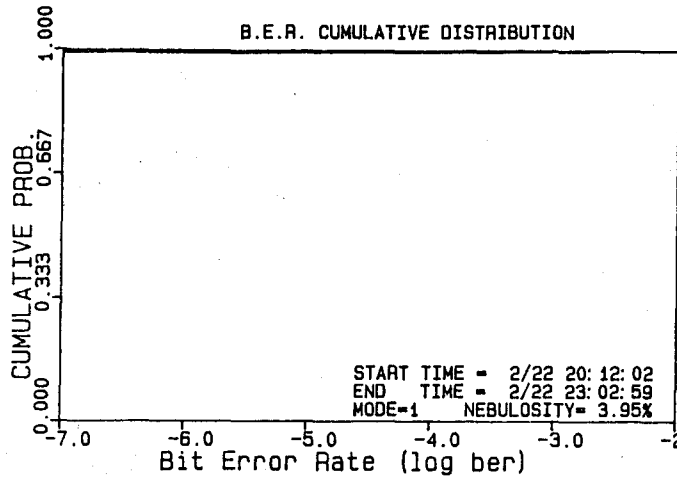


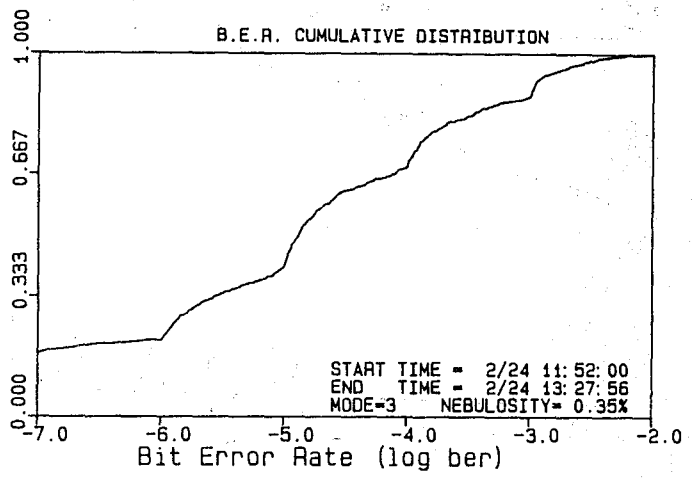
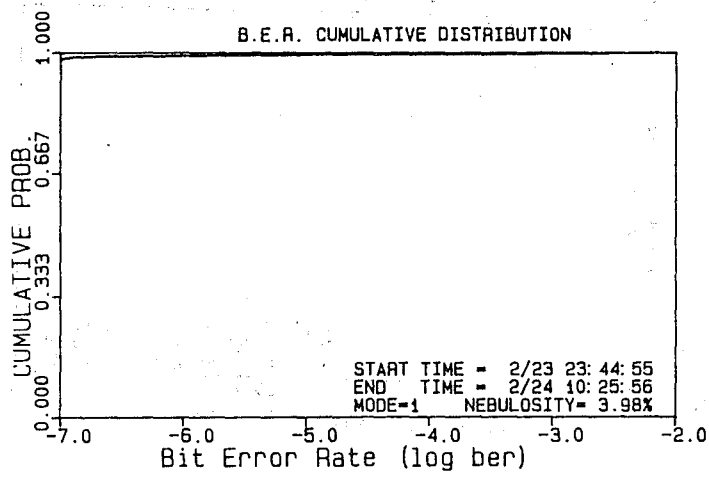
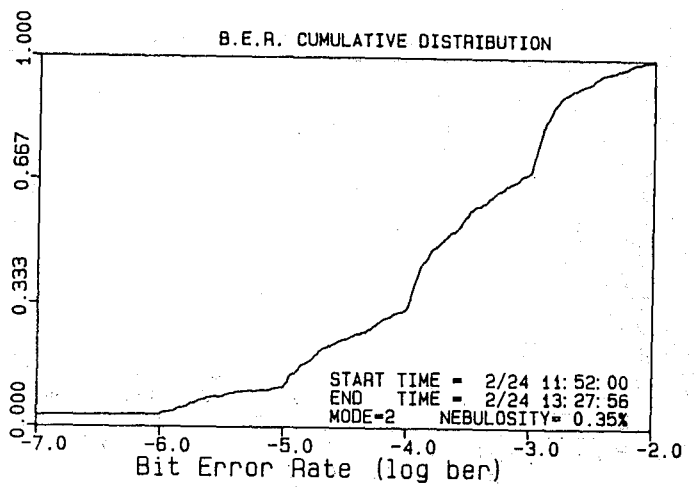
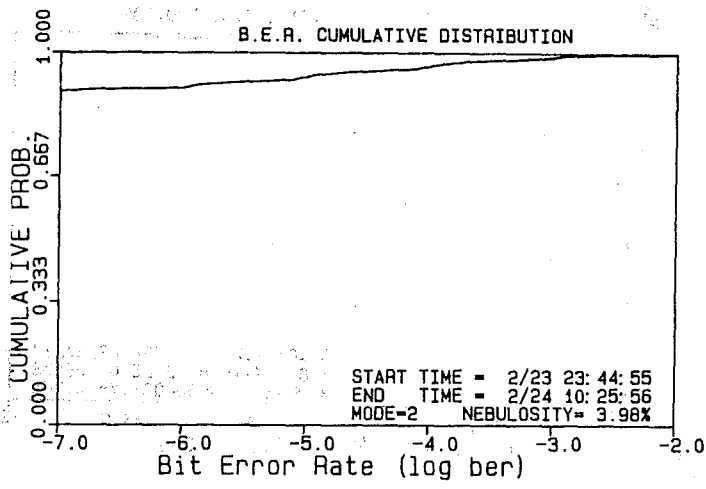
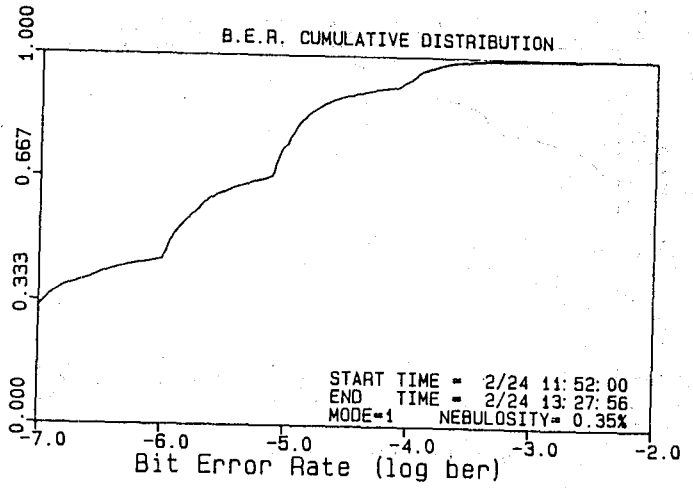
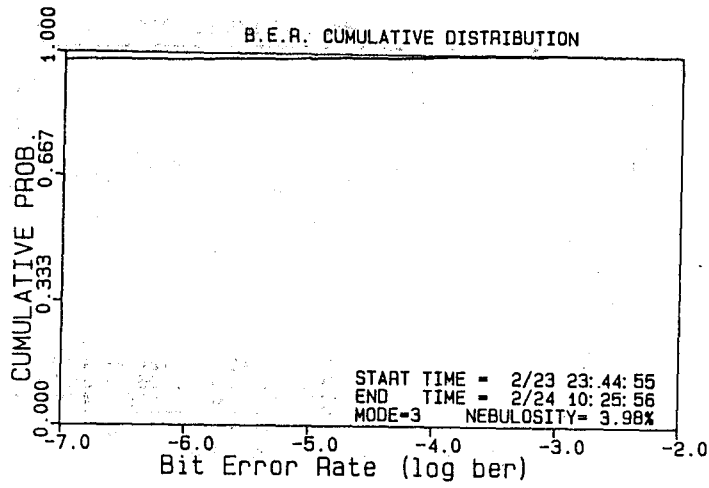


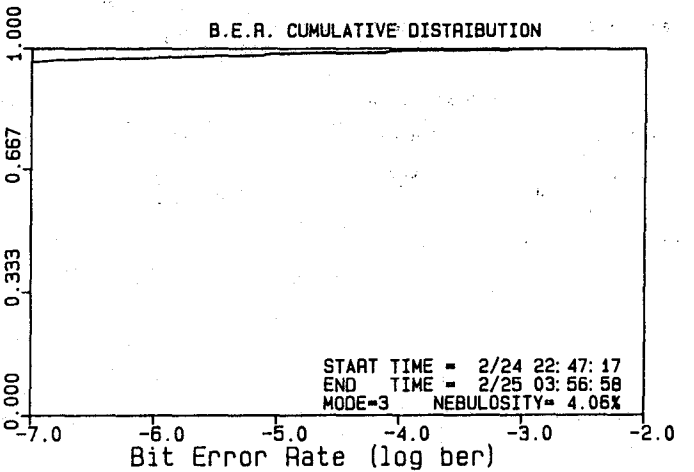
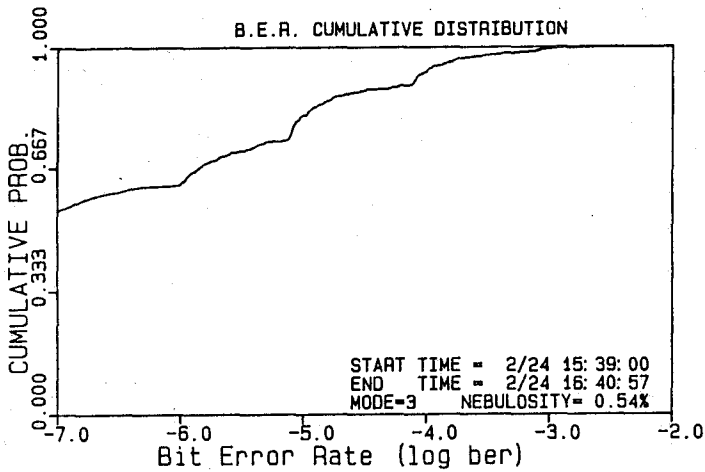
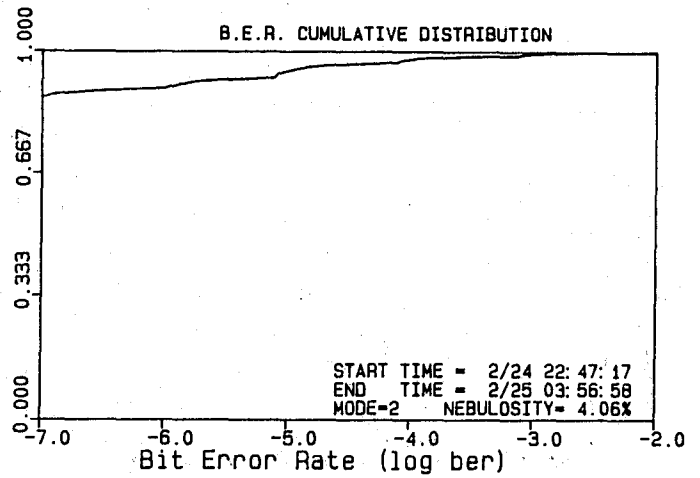
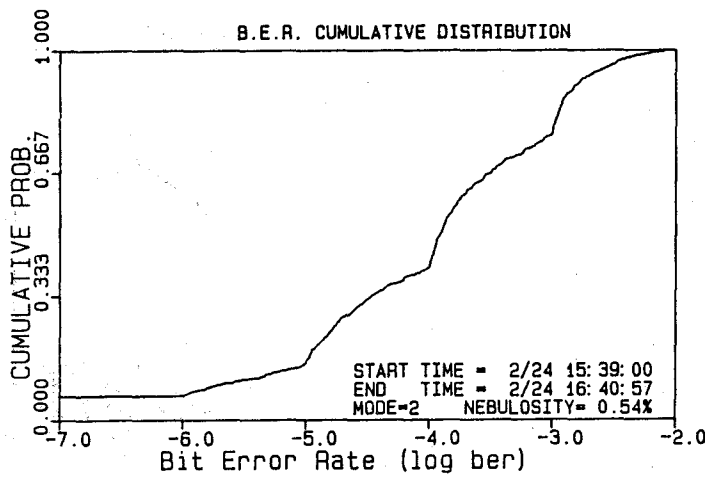
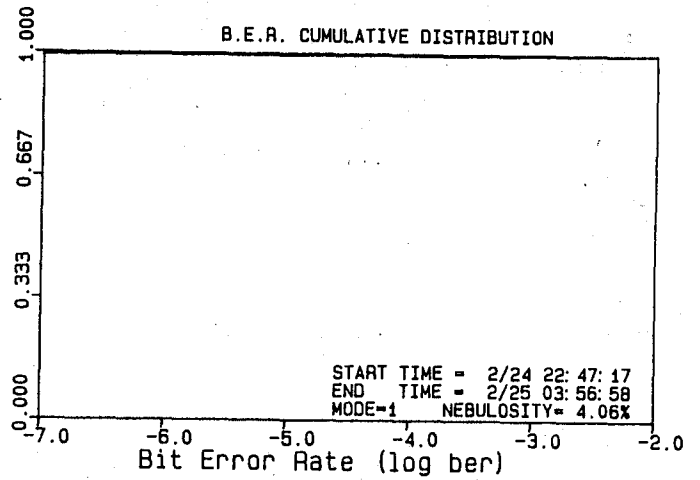
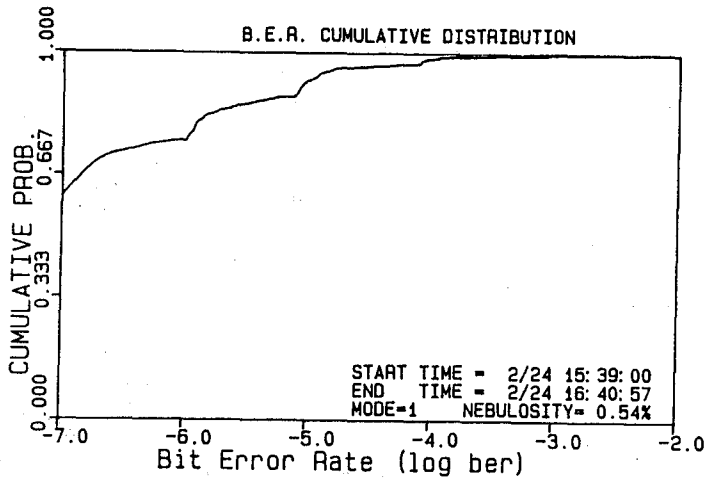


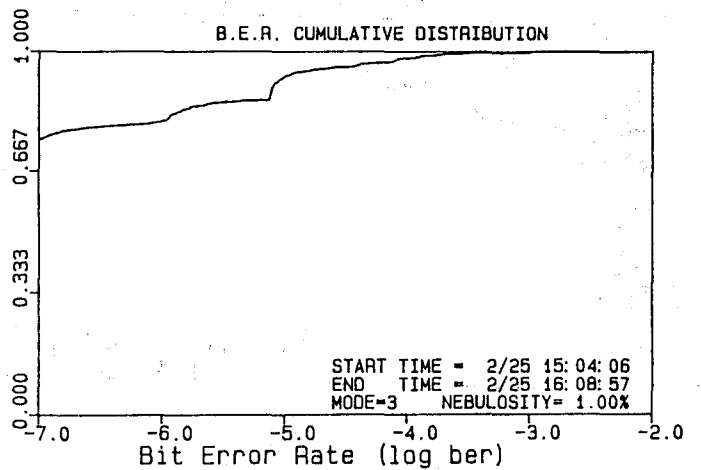
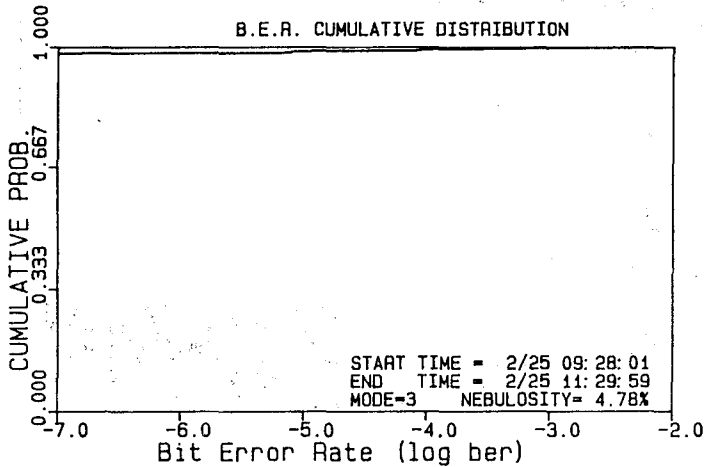
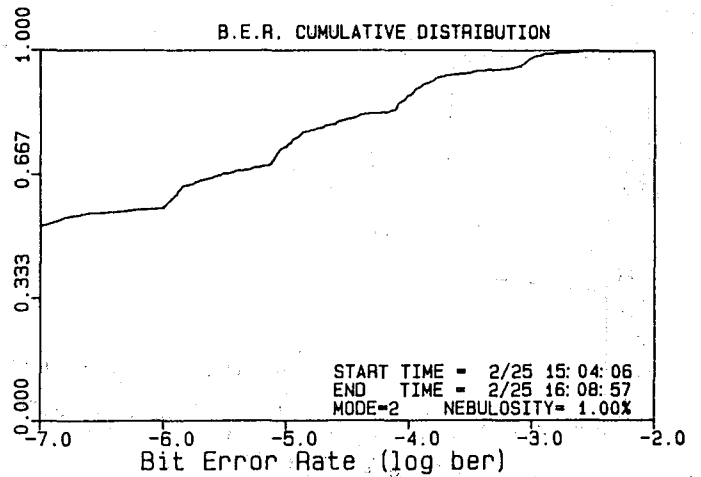
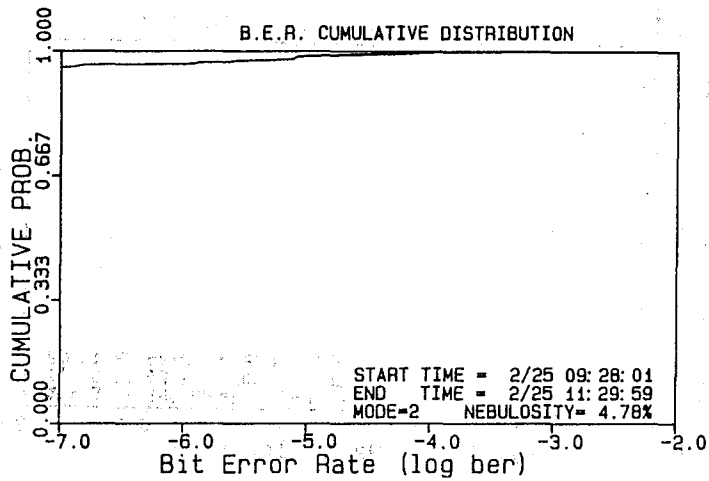
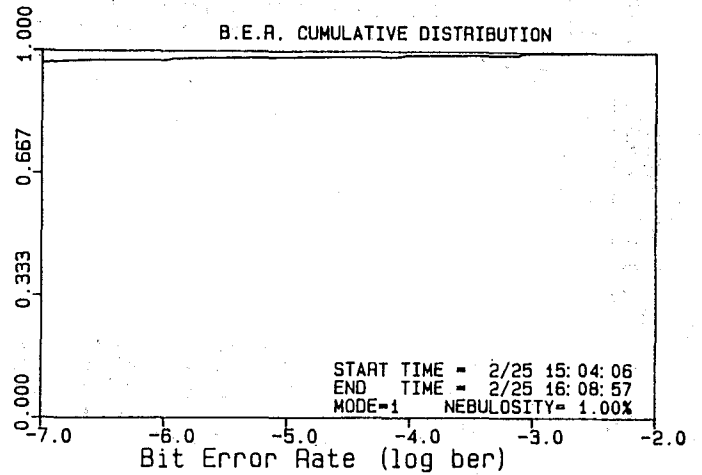
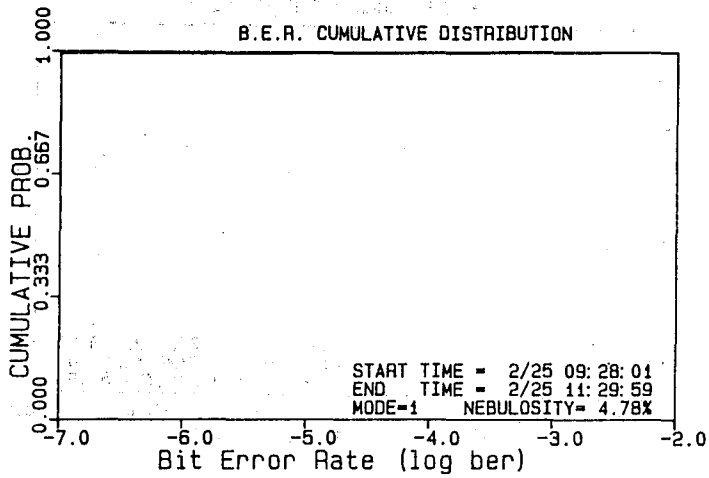


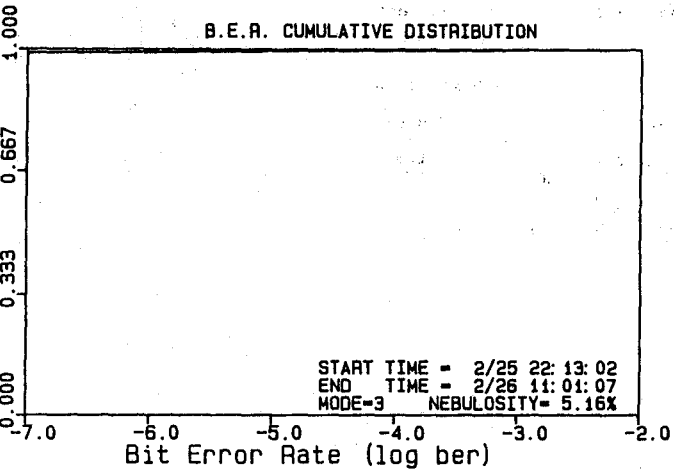
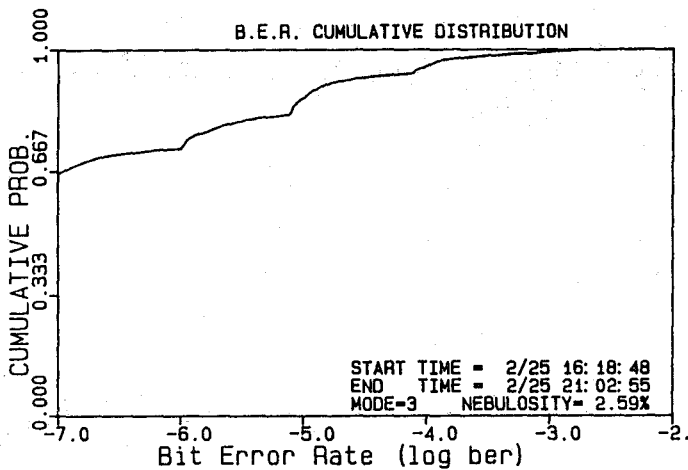
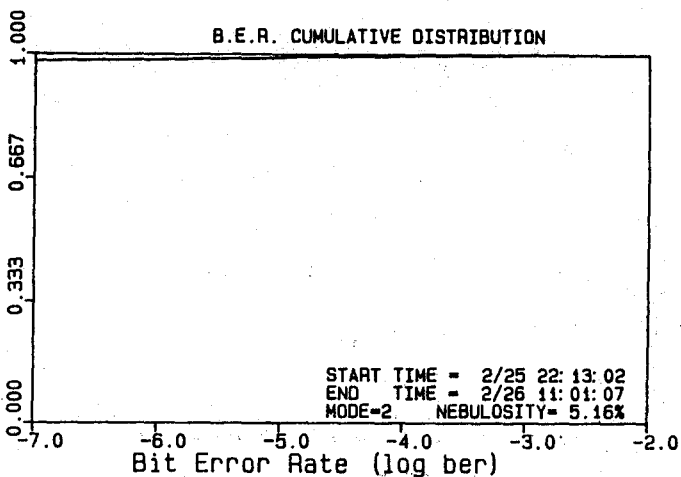
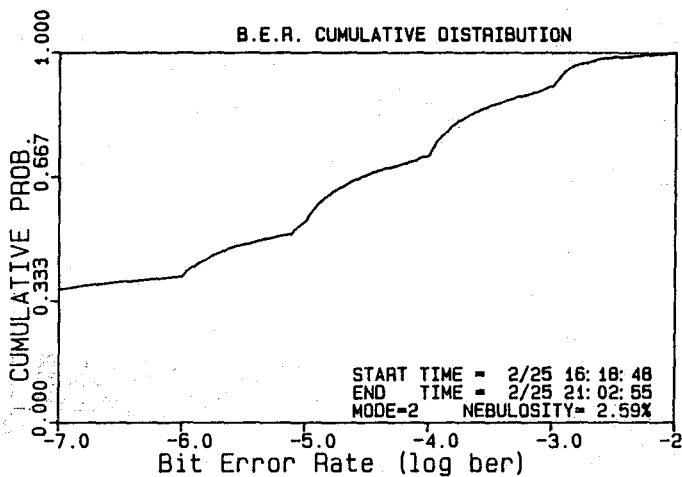
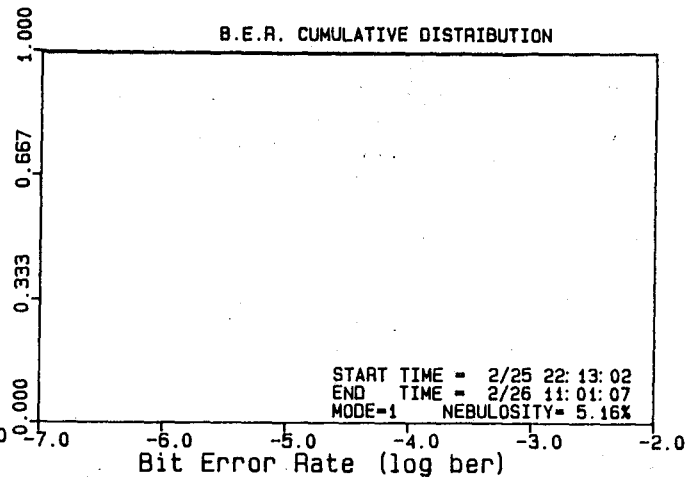
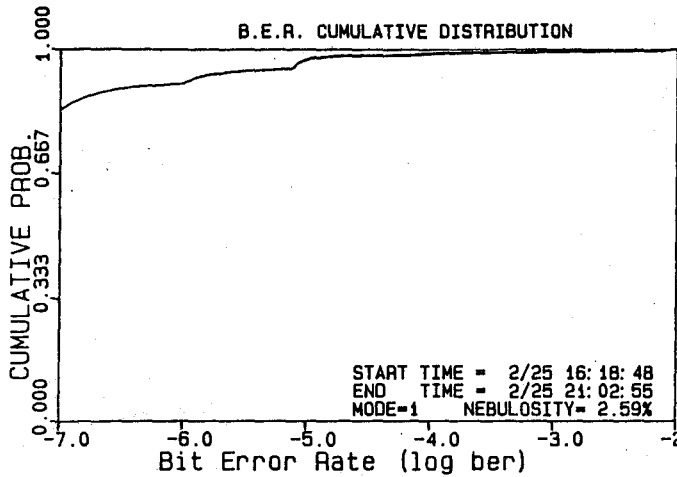


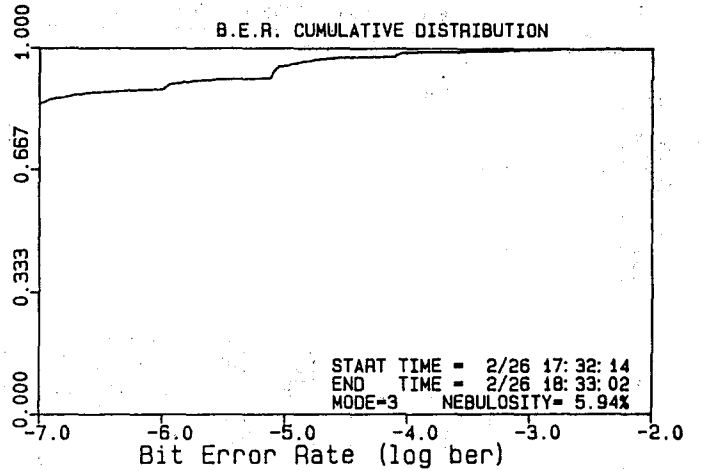
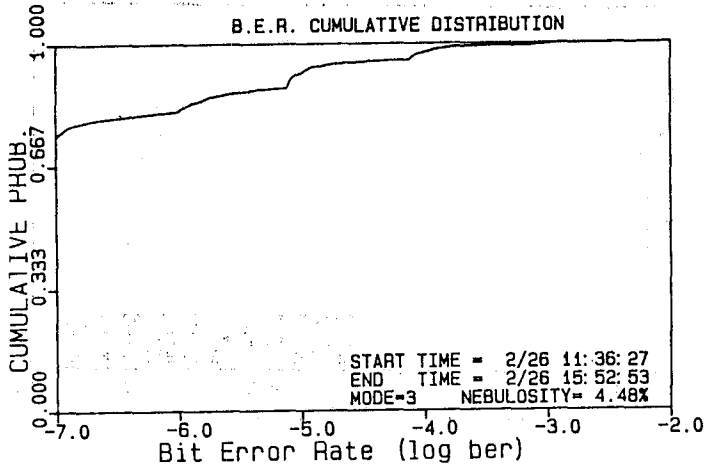
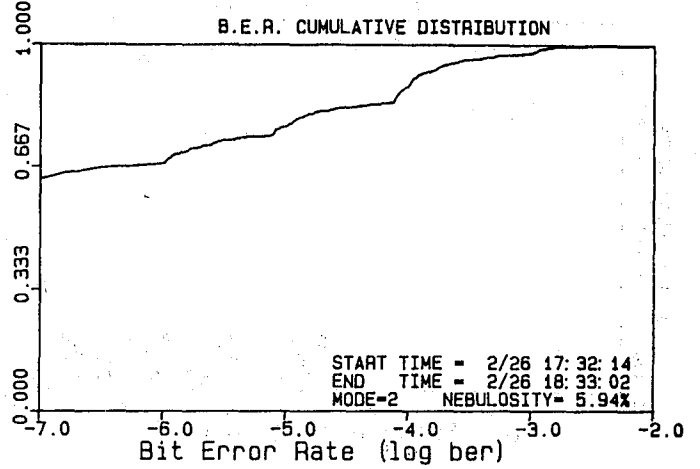
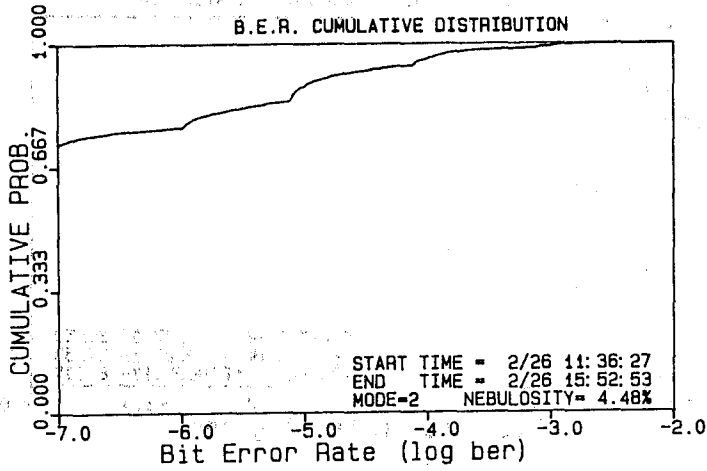
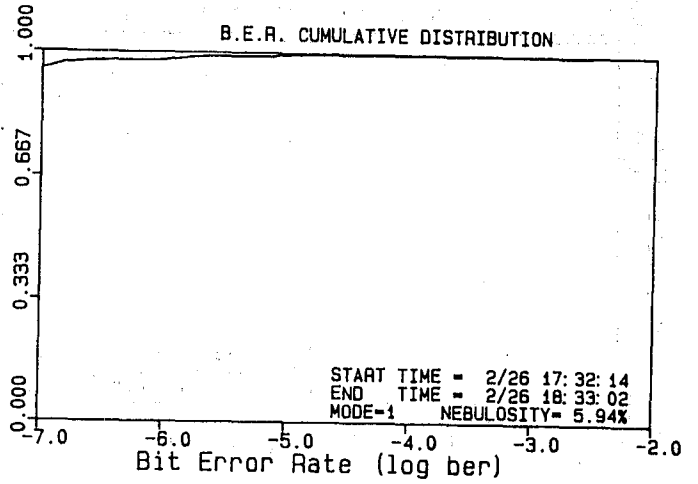
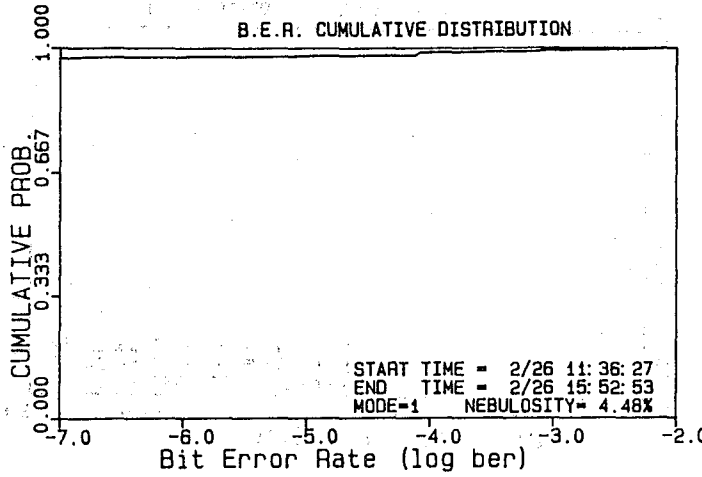


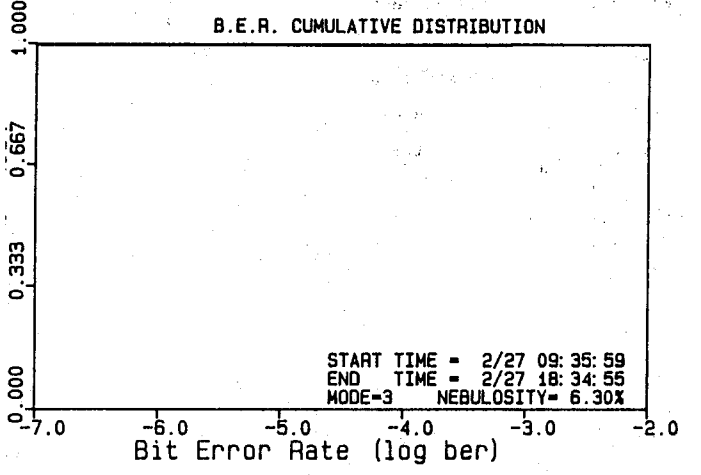
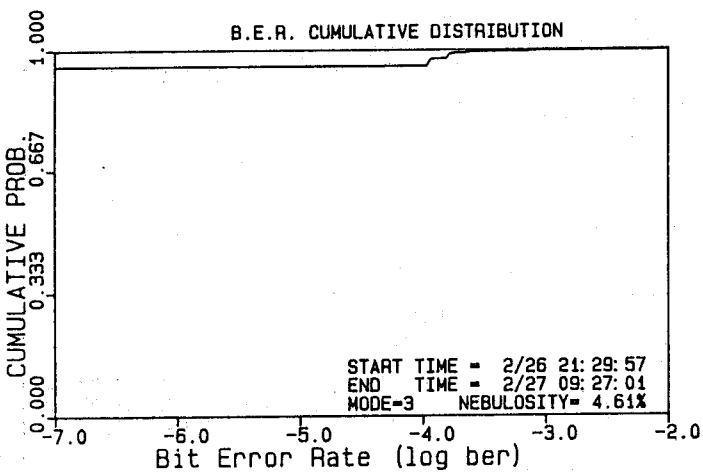
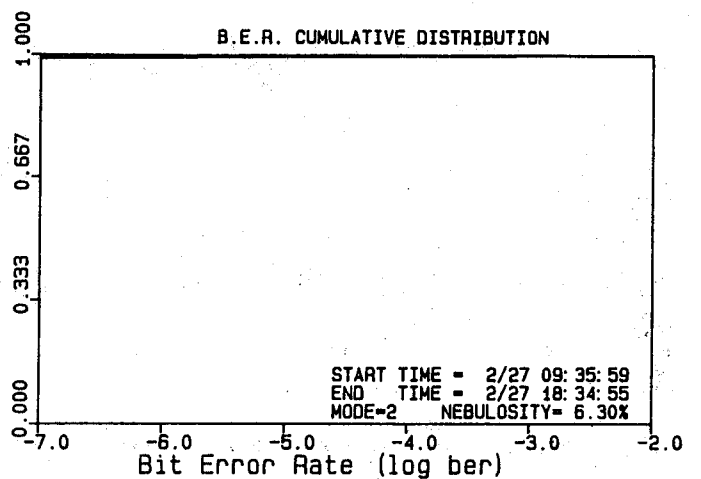
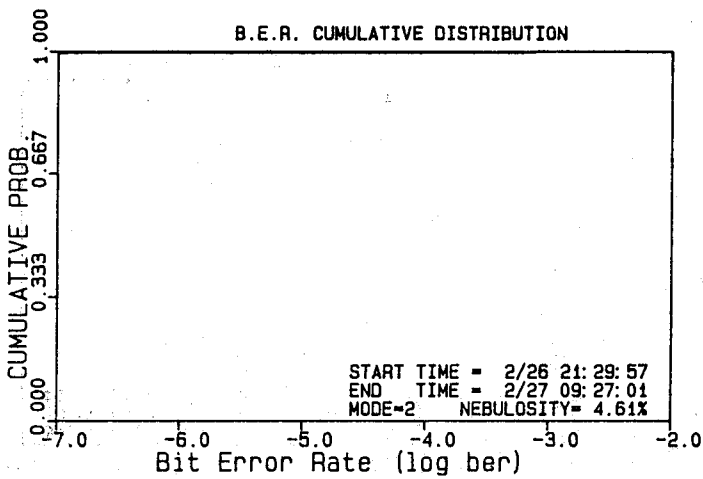
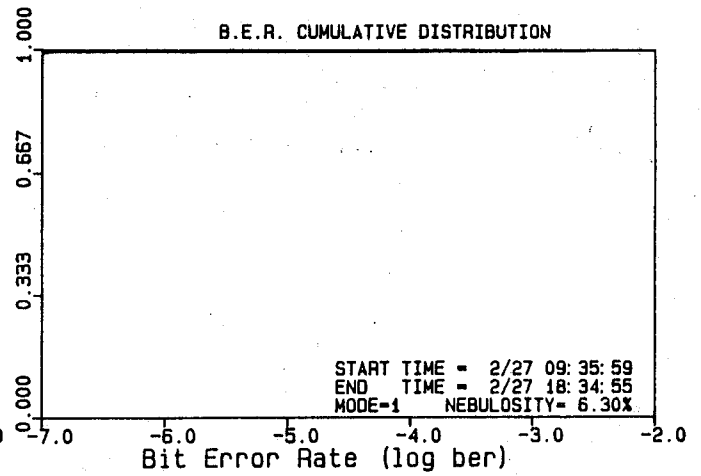
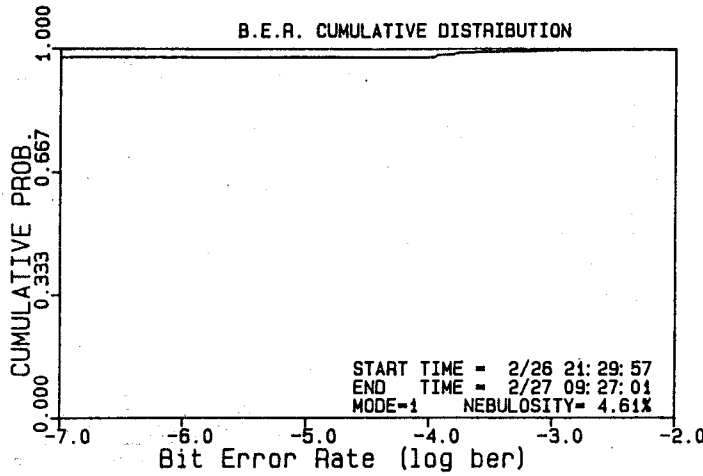


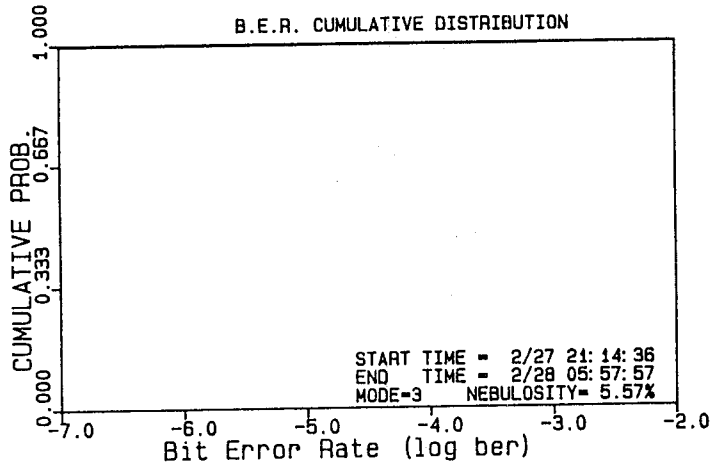
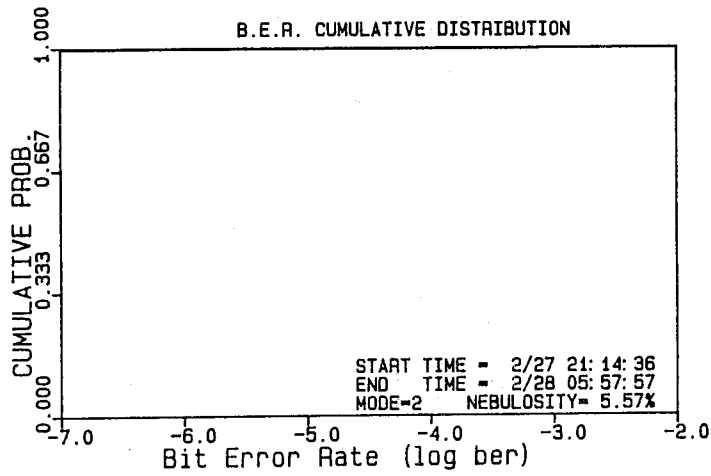
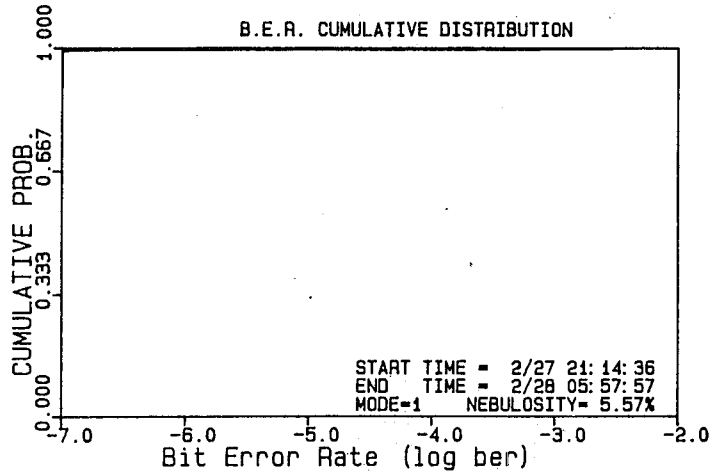














APPENDIX F

Meteorological Data

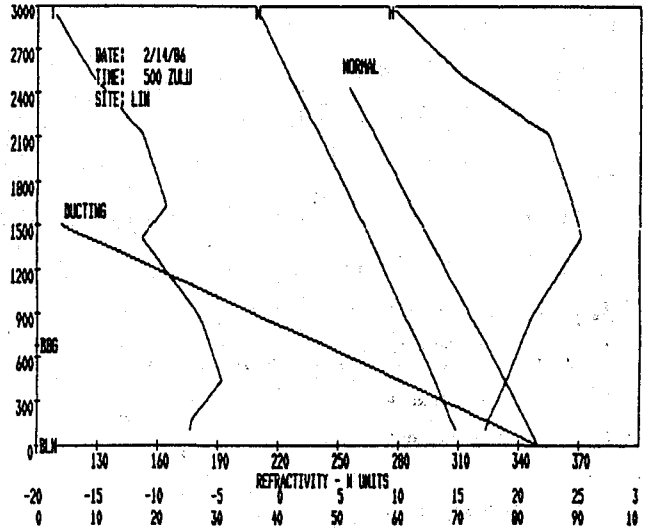
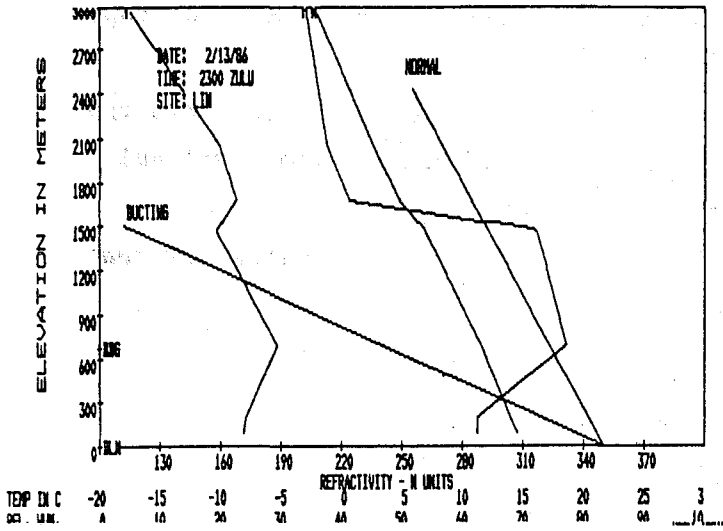
Meteorological data available from the Hannover, Lindenberg, and Berlin sites are presented in chronological order in this appendix. Whenever simultaneous data are available for all three sites, the computer plots of those data are presented for all three sites in vertical format, i.e., Hannover data are plotted at the top of the page, Lindenberg plots are directly beneath the Hannover graph, and Berlin data for the same time are presented at the bottom of the column. Then, the graphics for the next time with available data are presented immediately following, again with Hannover data at the top, Lindenberg in the middle, and Berlin at the bottom.

If data are available for only one or two sites at a given time, then the correct portion of the page is blank with the expression N.A. (not available) written in the blank portion(s) for that (those) site(s).

If the data from the sites are not simultaneous, then the graphs for that period are slightly staggered across the page.

N.A.

N.A.

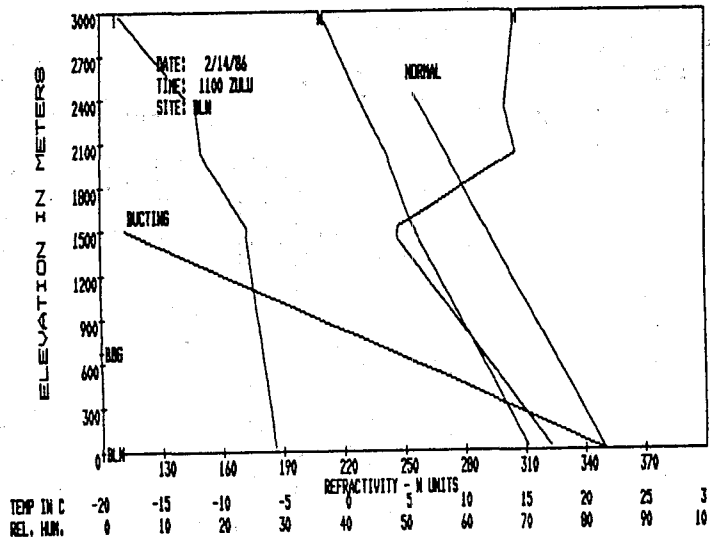
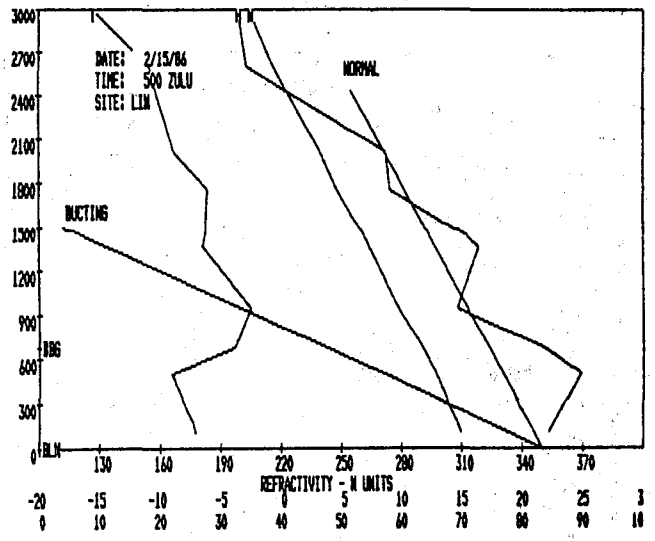
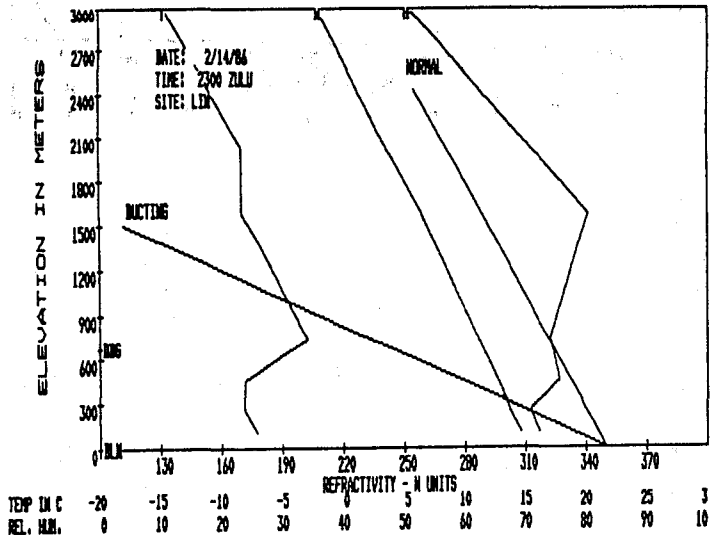


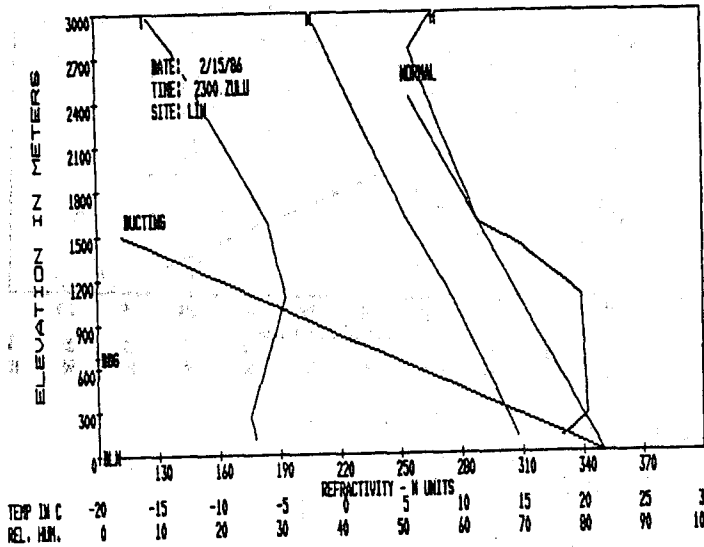
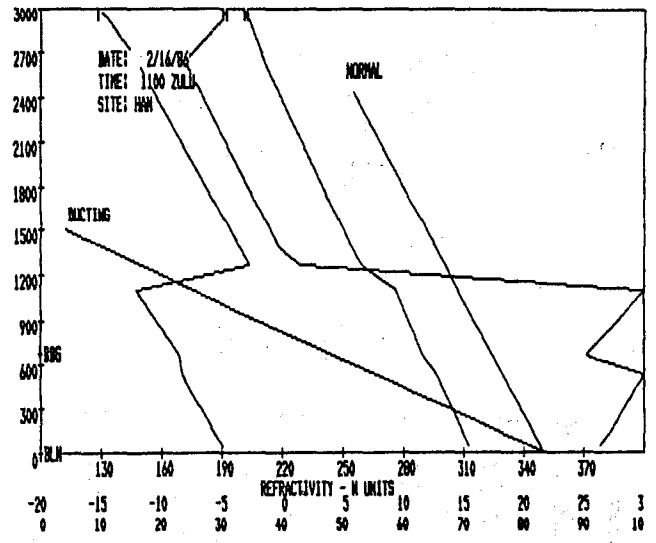
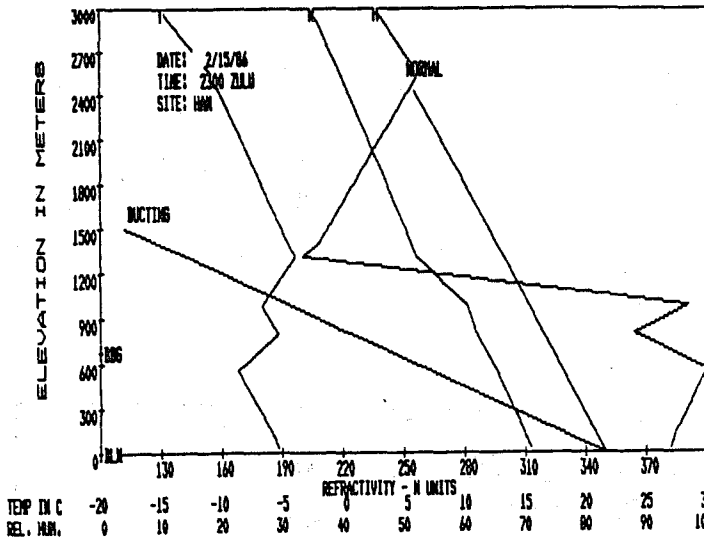
N.A.

N.A.

N.A.

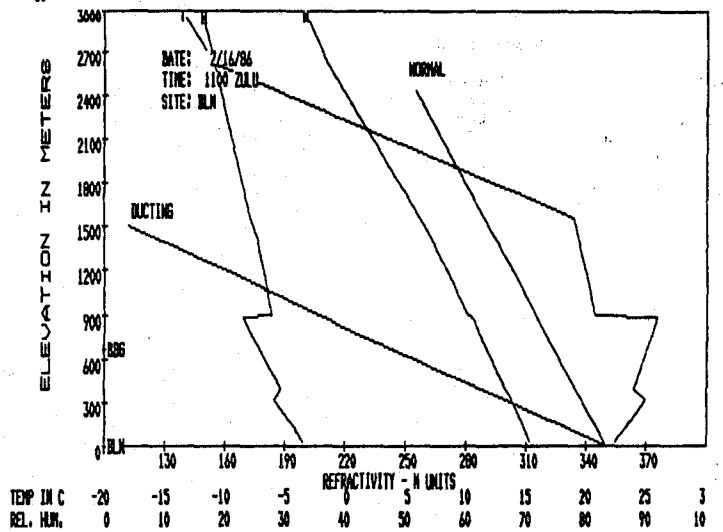
N.A.



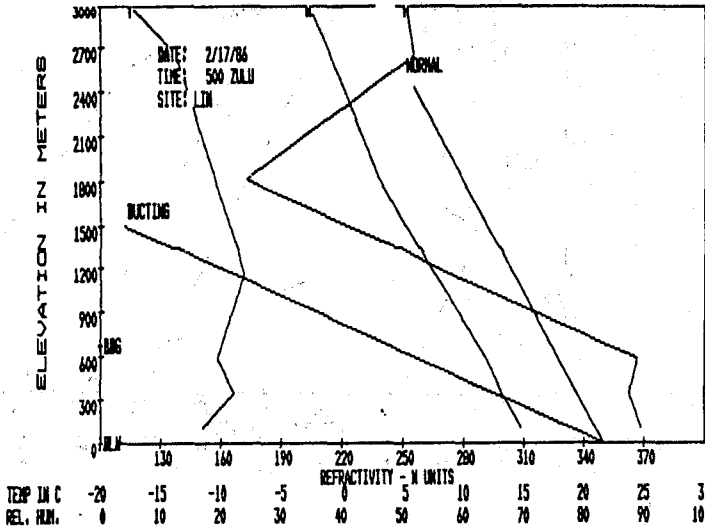
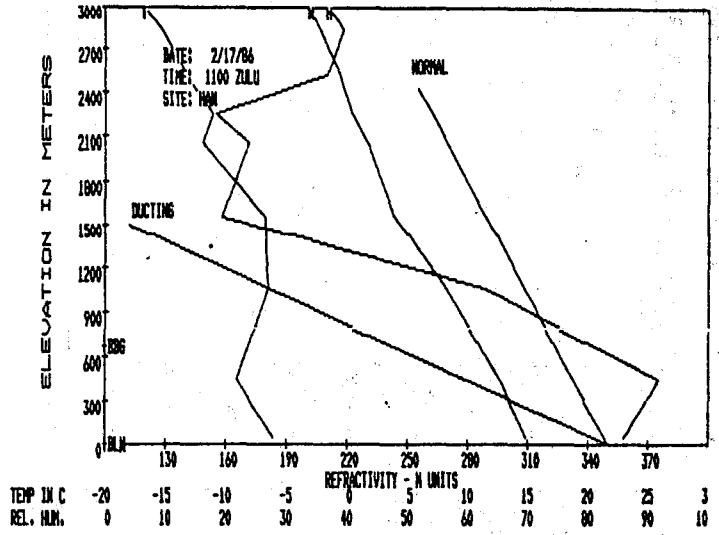


N.A.

N.A.



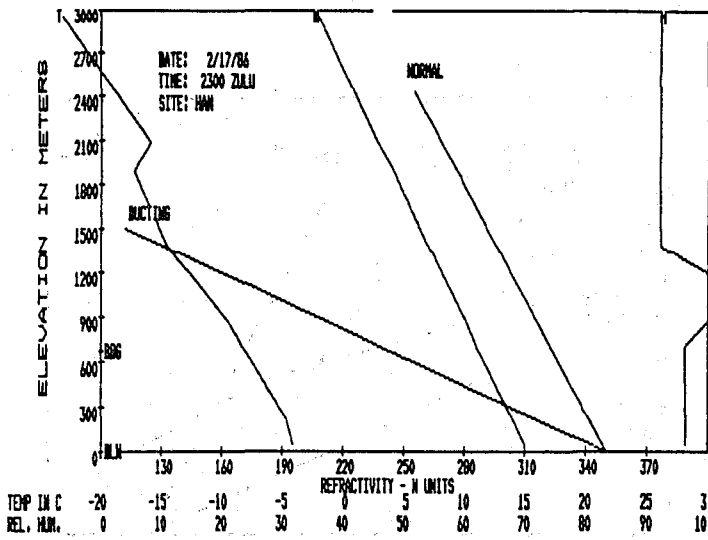
N.A.



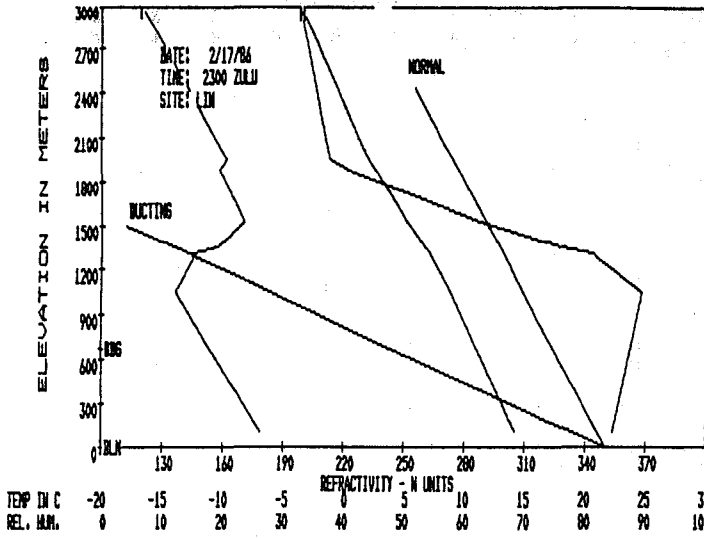
N.A.

N.A.

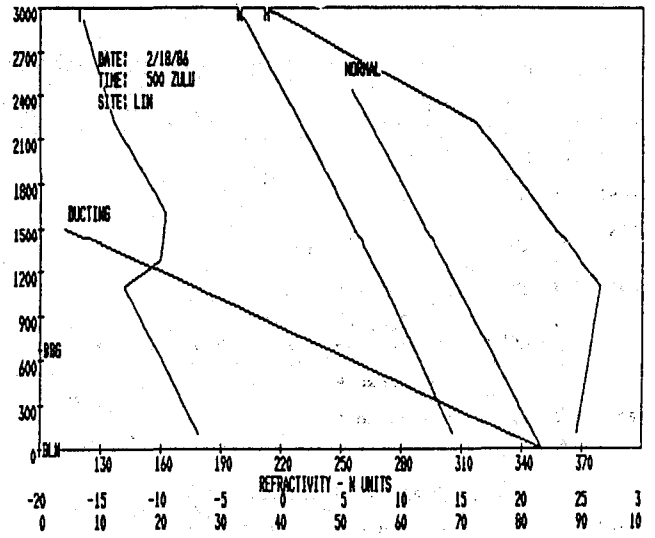
N.A.



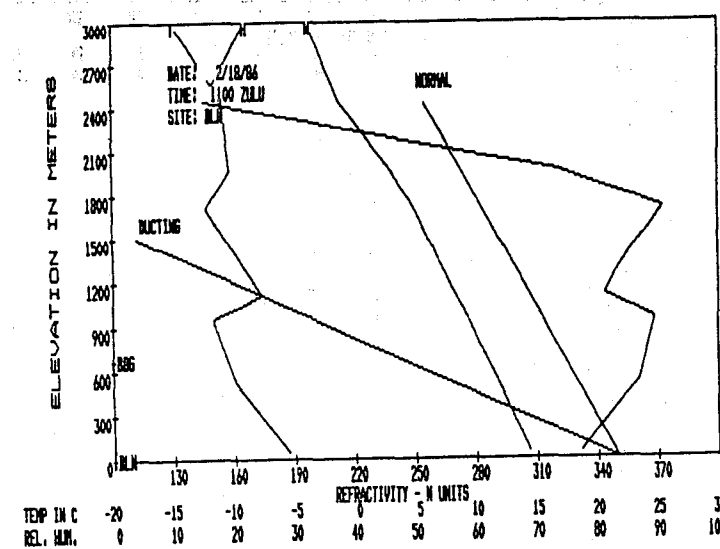
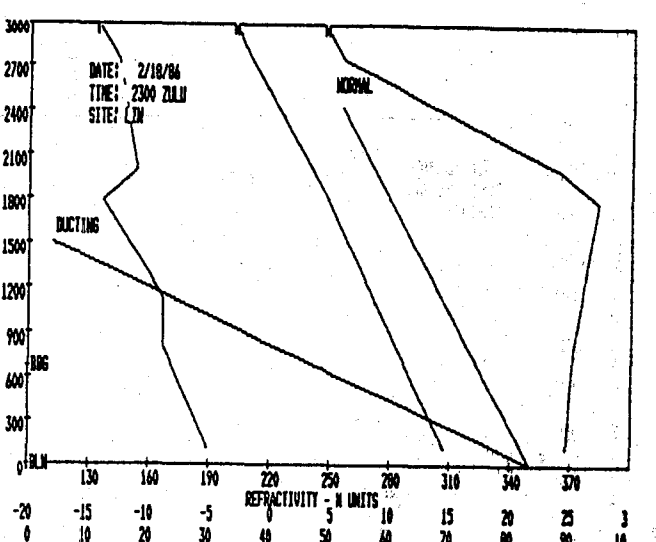
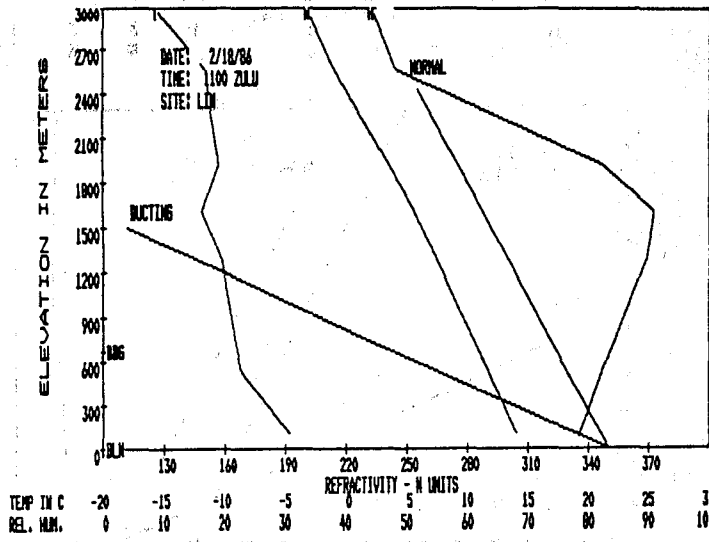
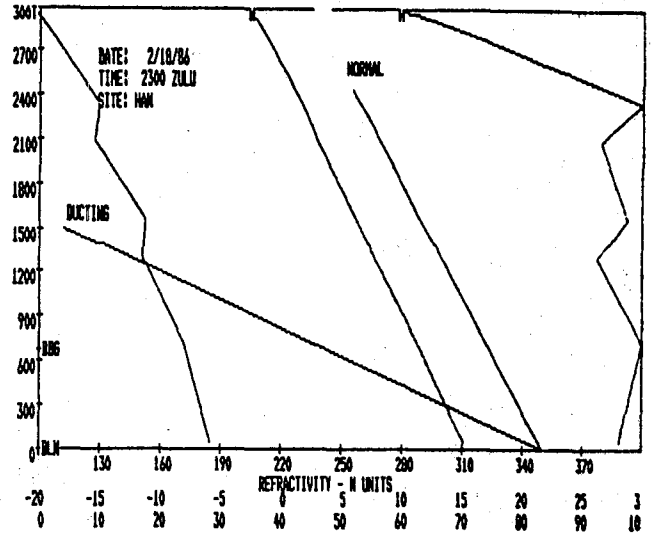
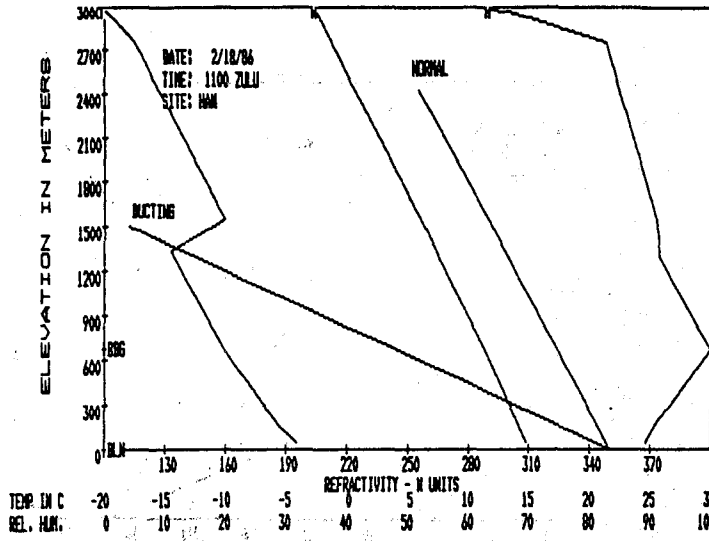
N. A.



N. A.

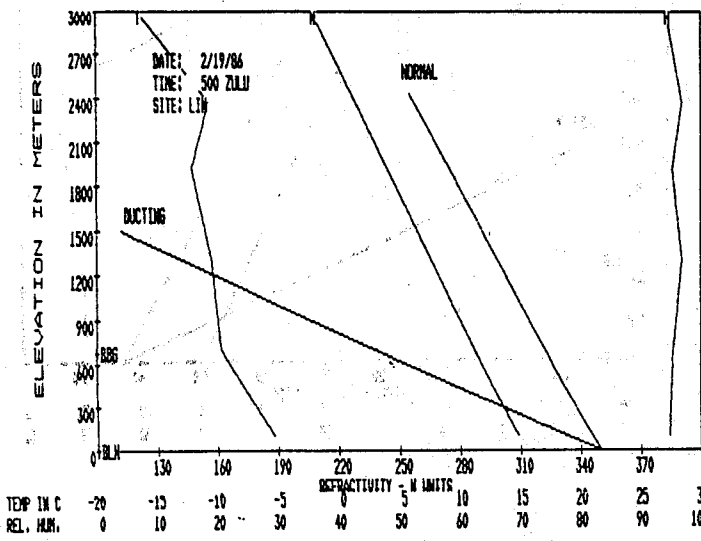
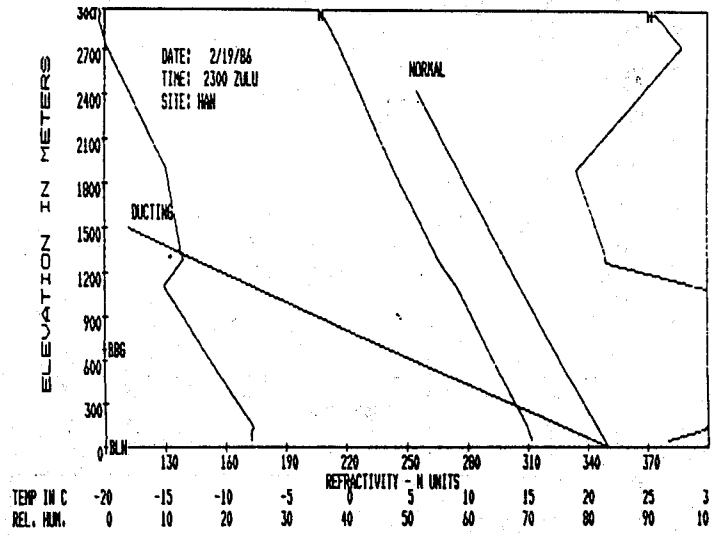


N. A.

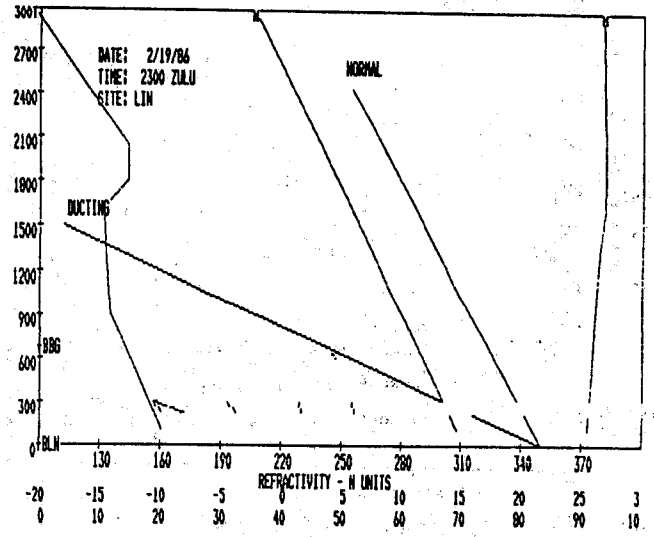


N.A.

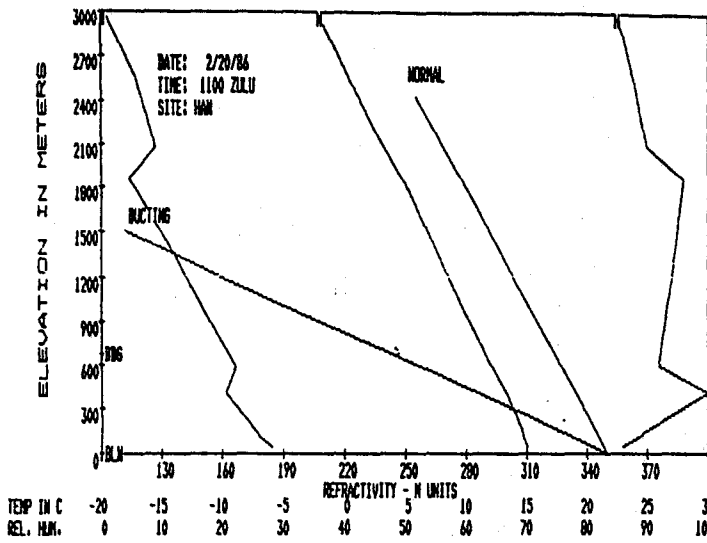
N.A.



N.A.

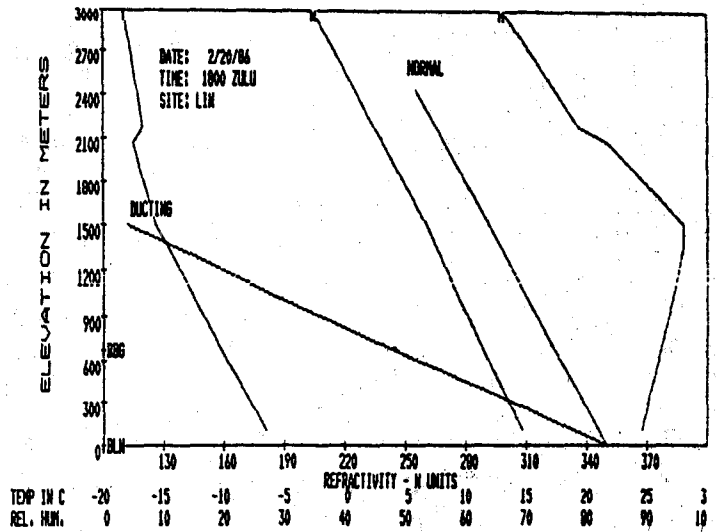


N.A.

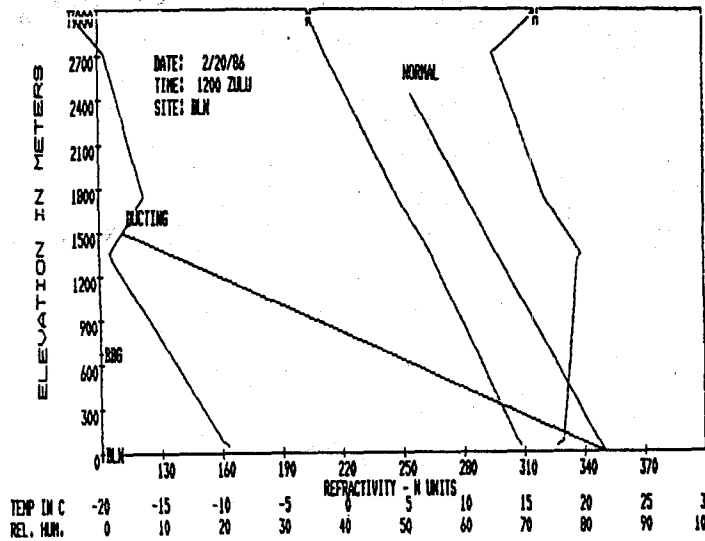


N.A.

N.A.

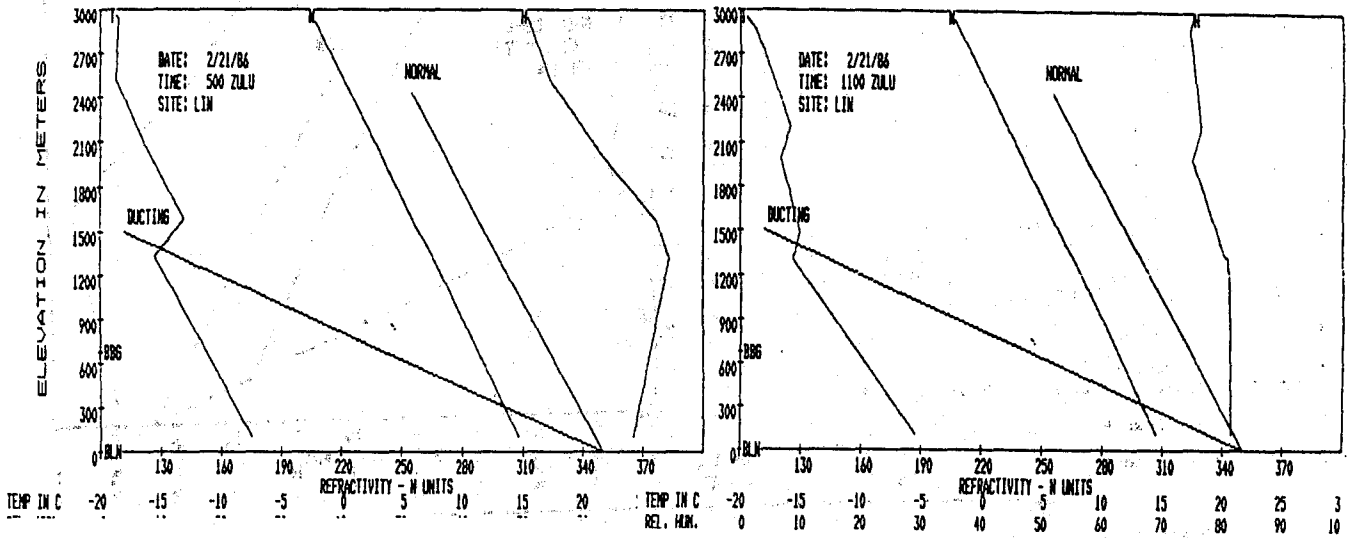


N.A.



N.A.

N.A.

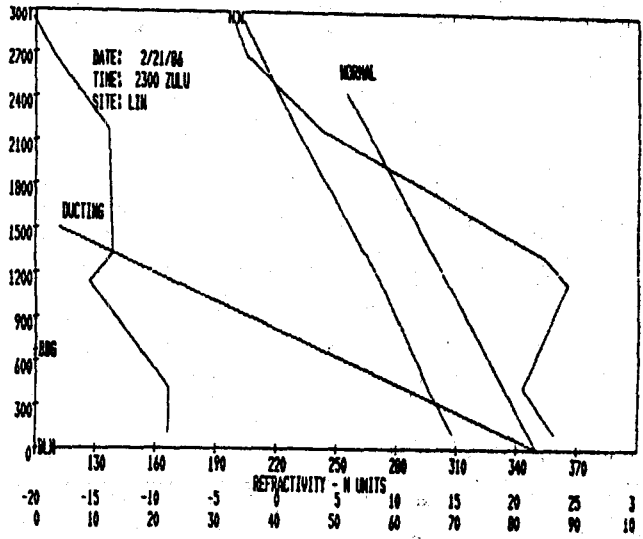
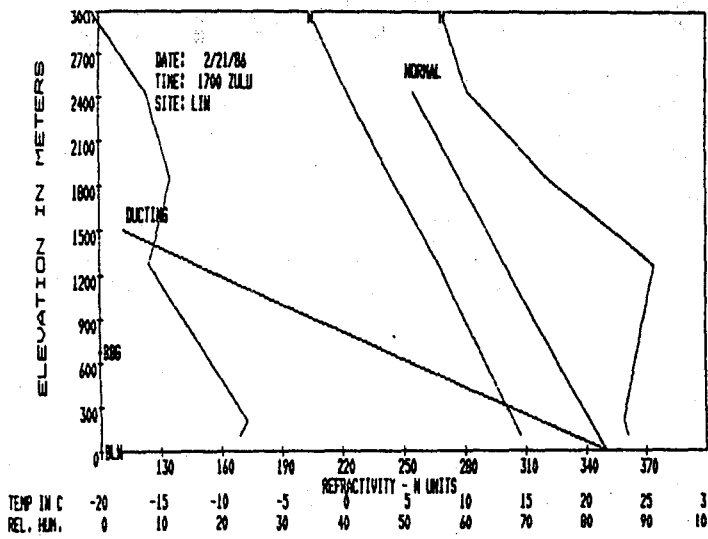


N.A.

N.A.

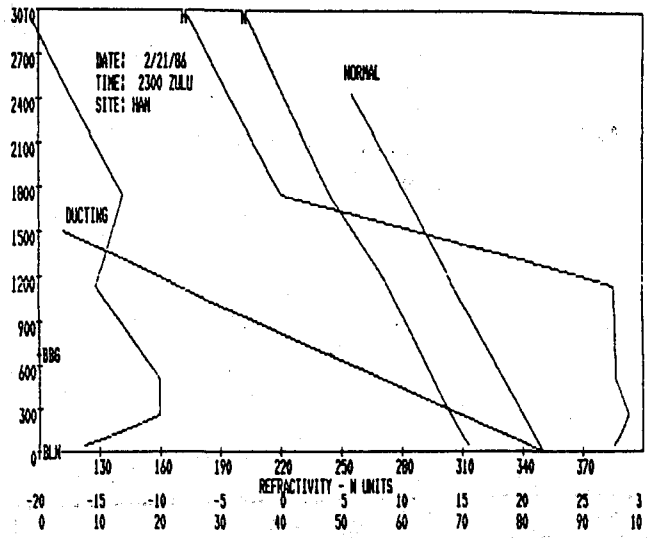
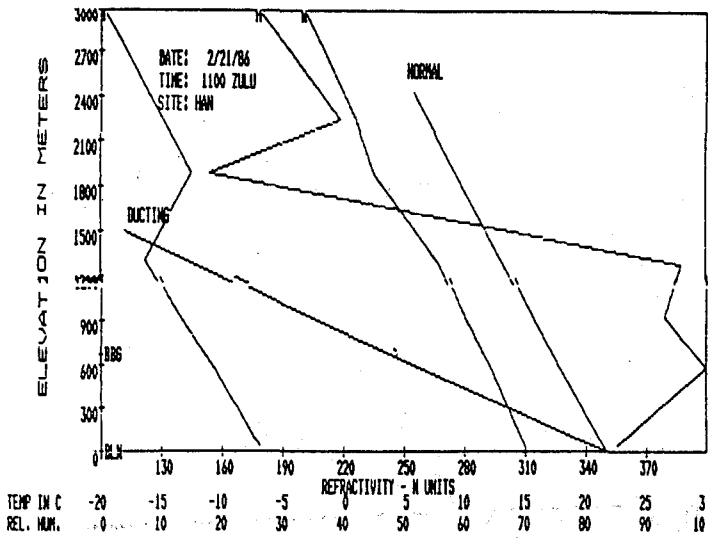
N.A.

N.A.



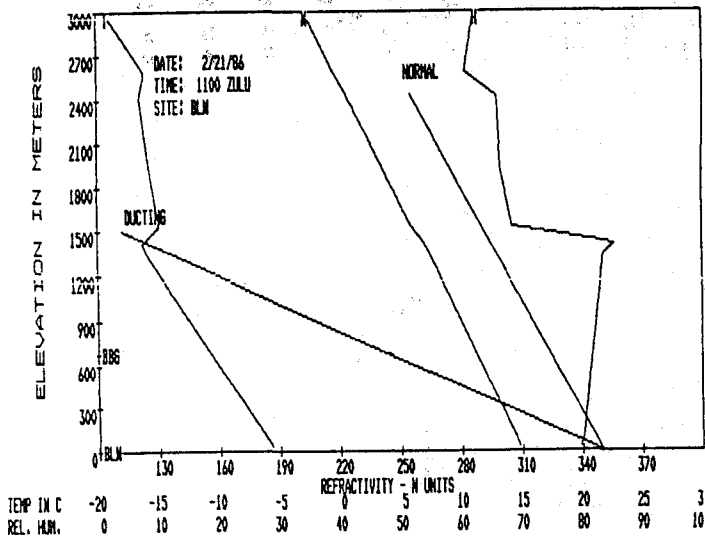
N.A.

N.A.

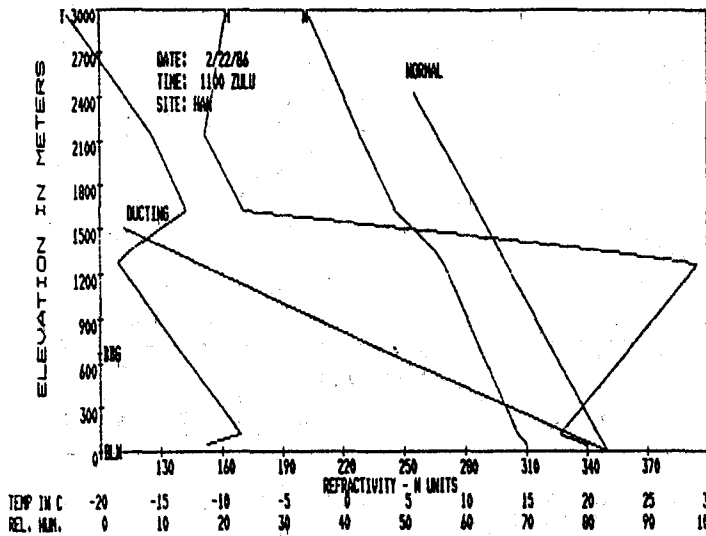


N.A.

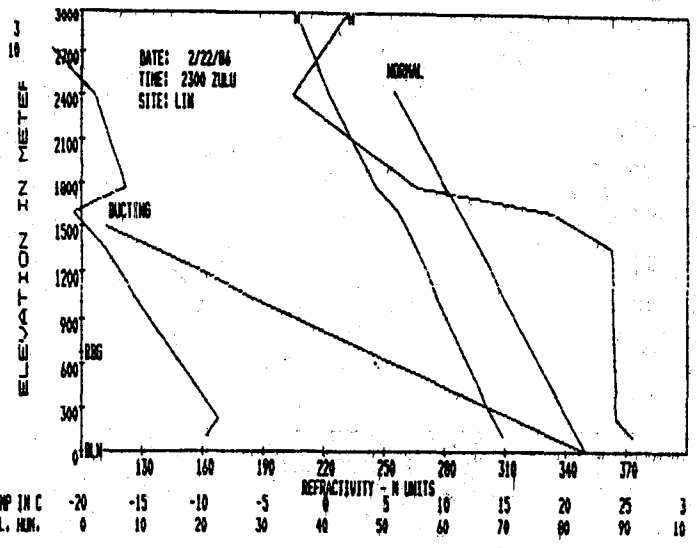
N.A.



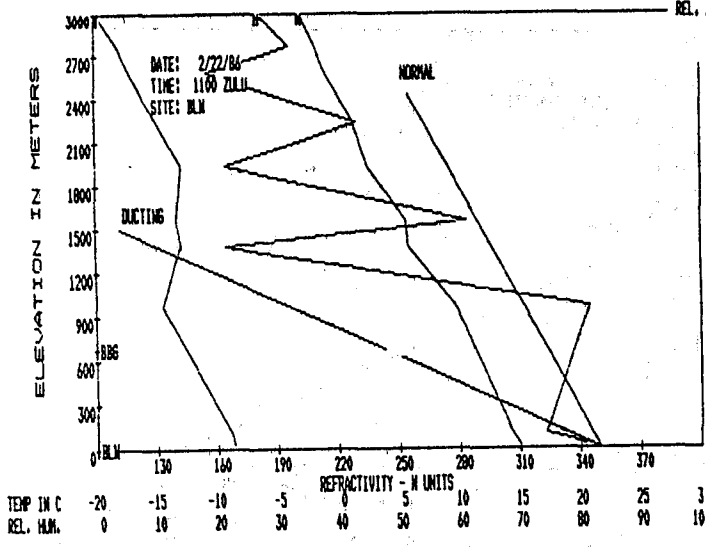
N.A.



N.A.

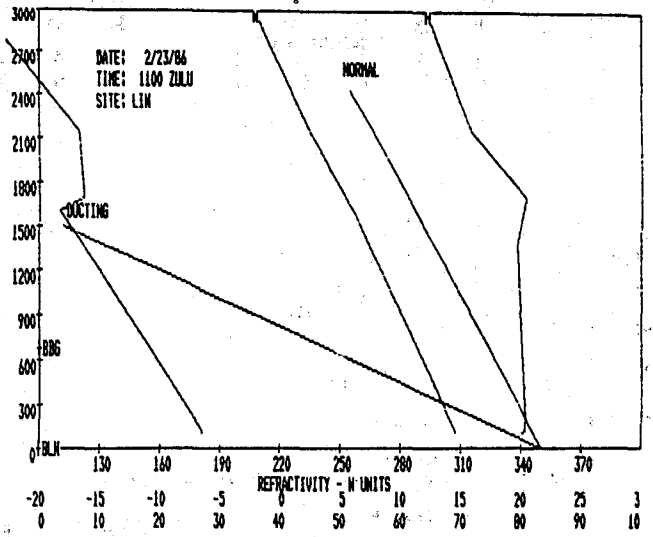
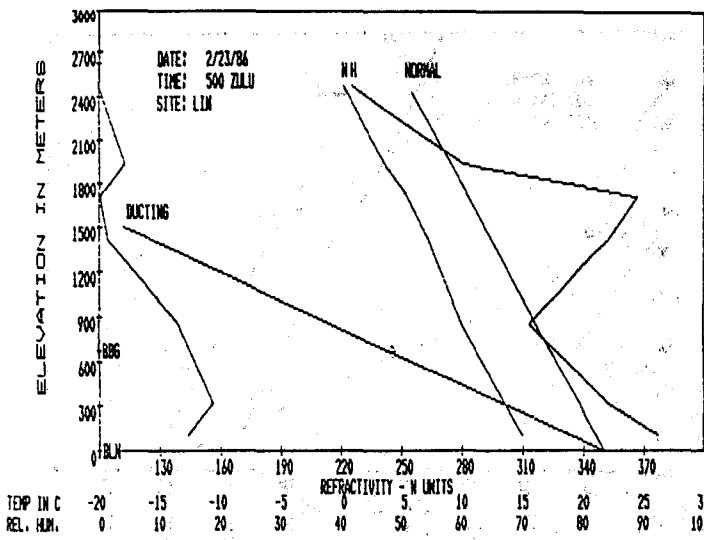
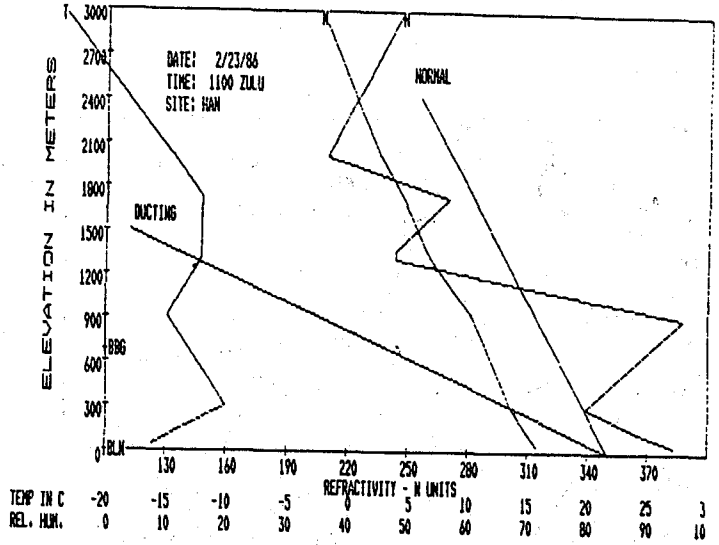


N.A.

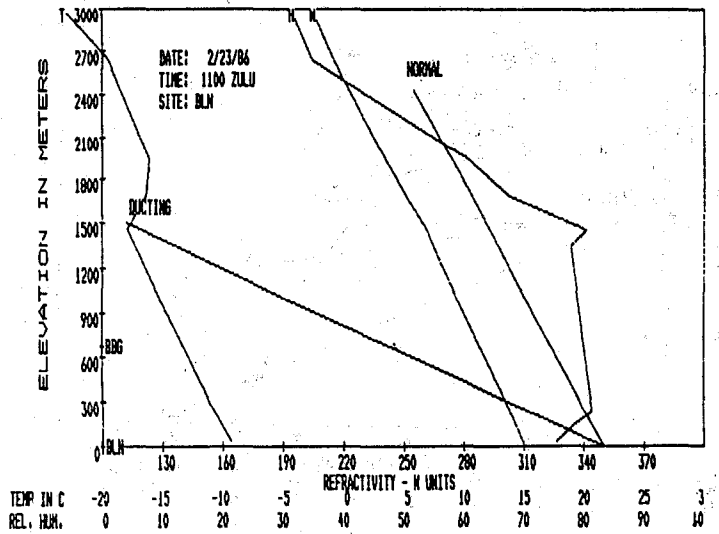


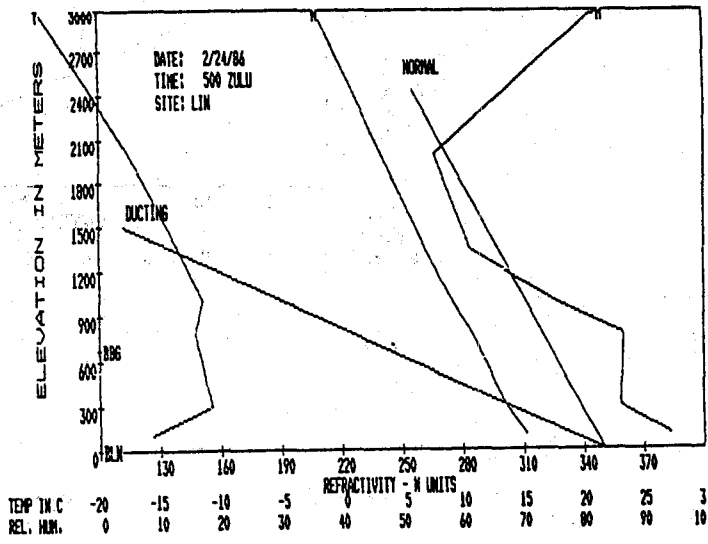
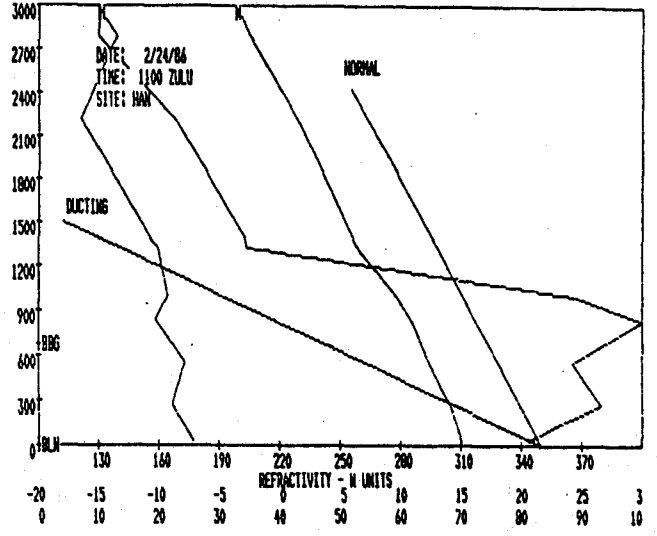
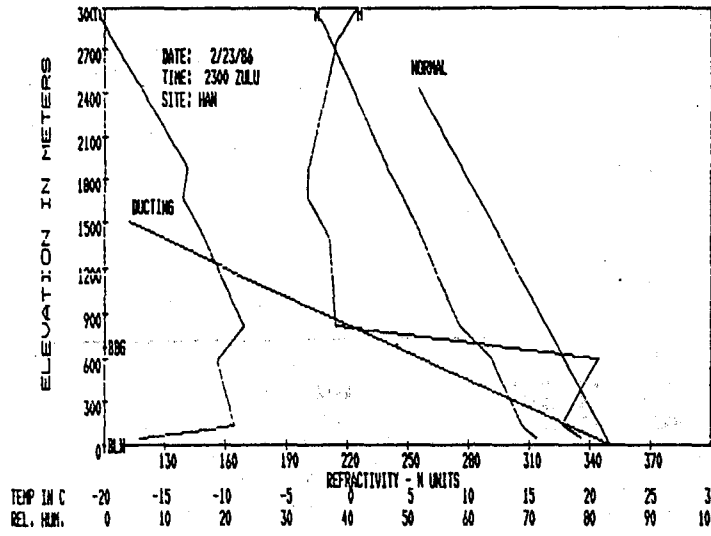
N.A.

N.A.



N.A.





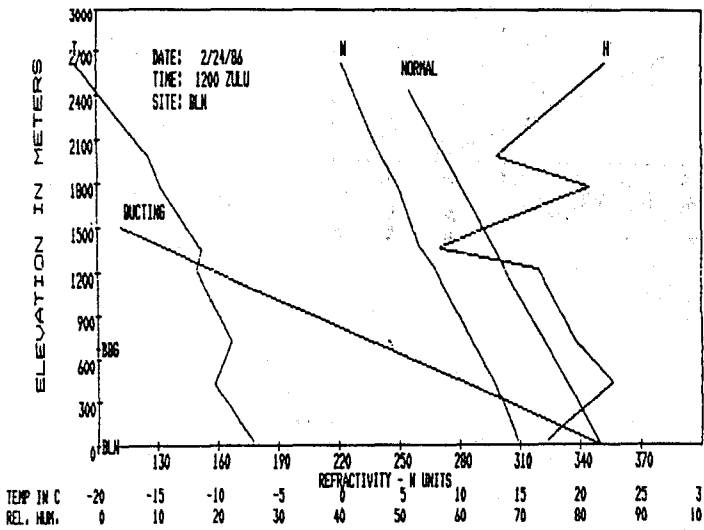
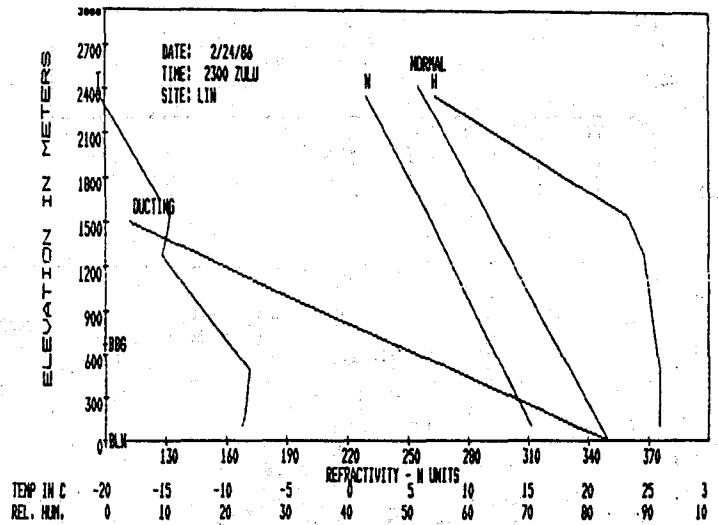
N. A.

N. A.

N.A.

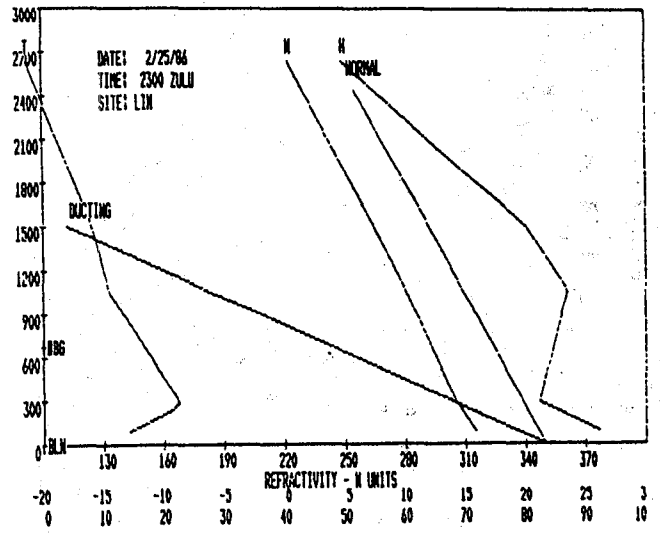
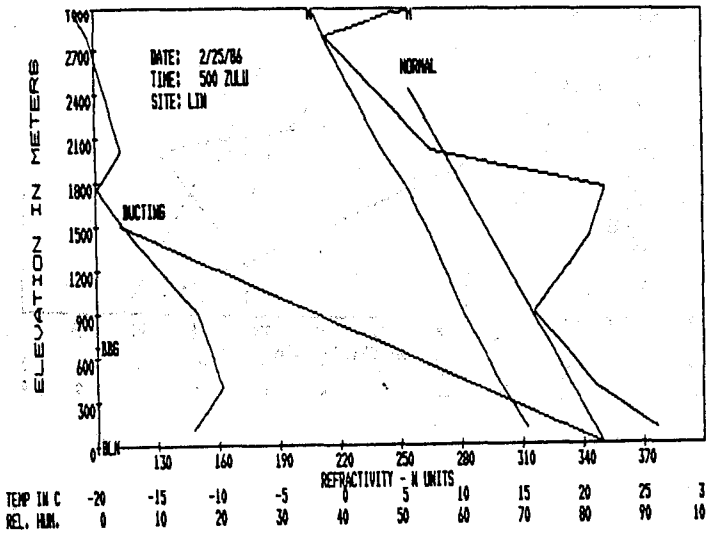
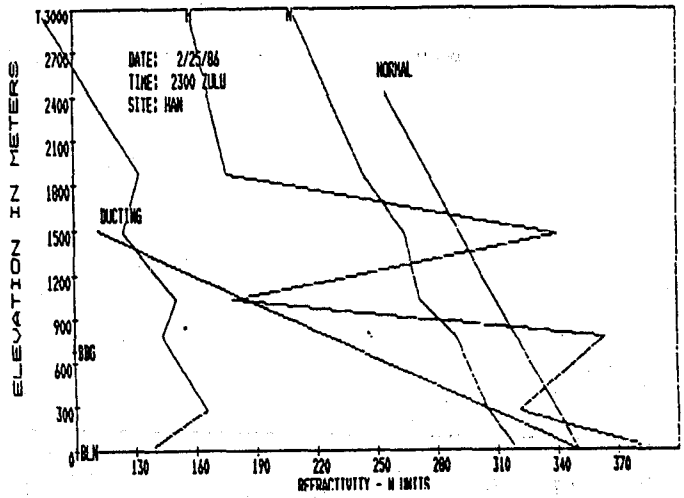
N.A.

N.A.



N.A.

N.A.

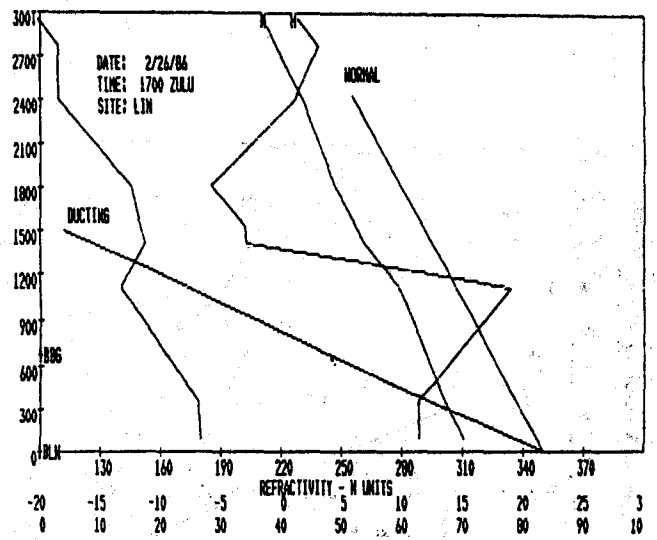
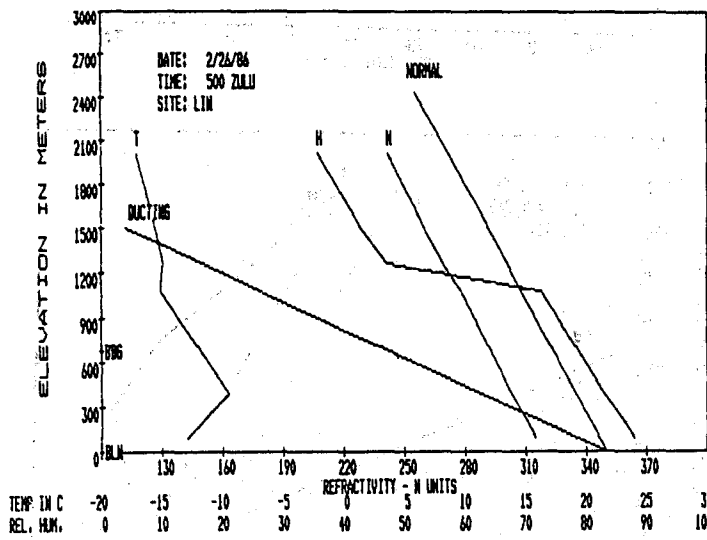


N.A.

N.A.

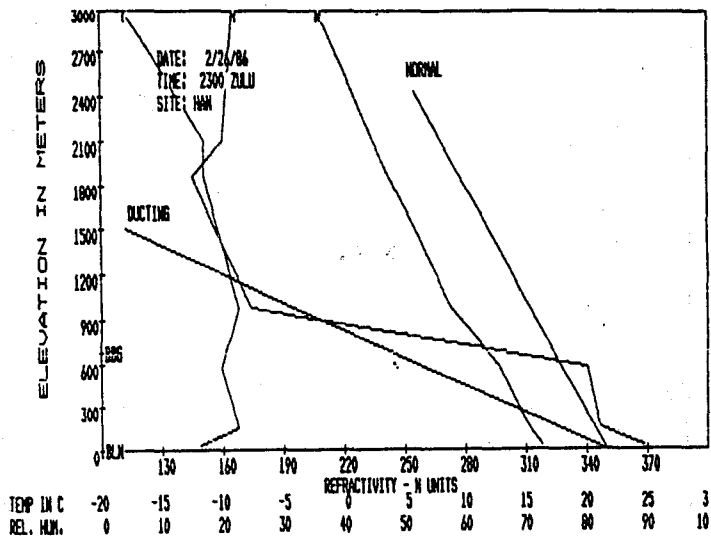
N.A.

N.A.

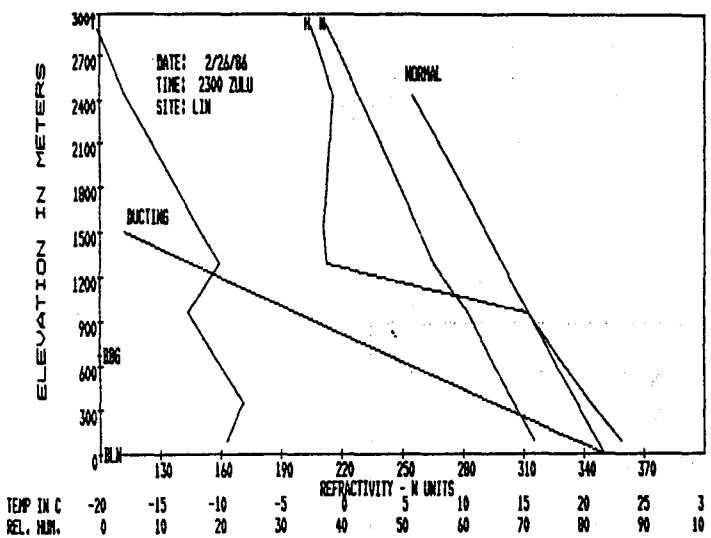


N.A.

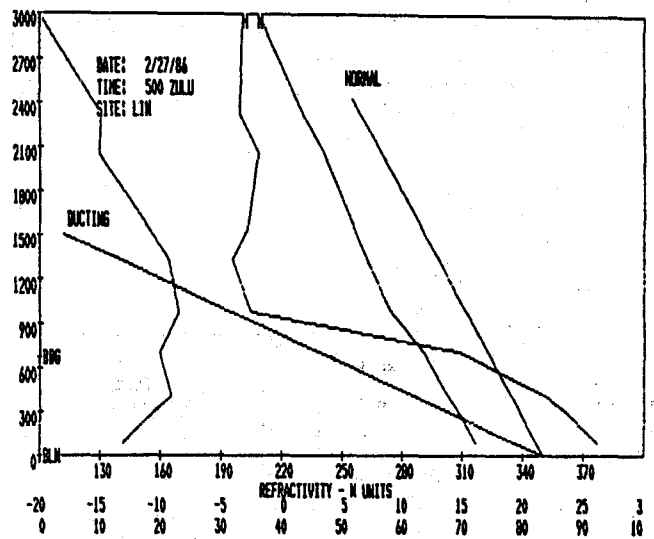
N.A.



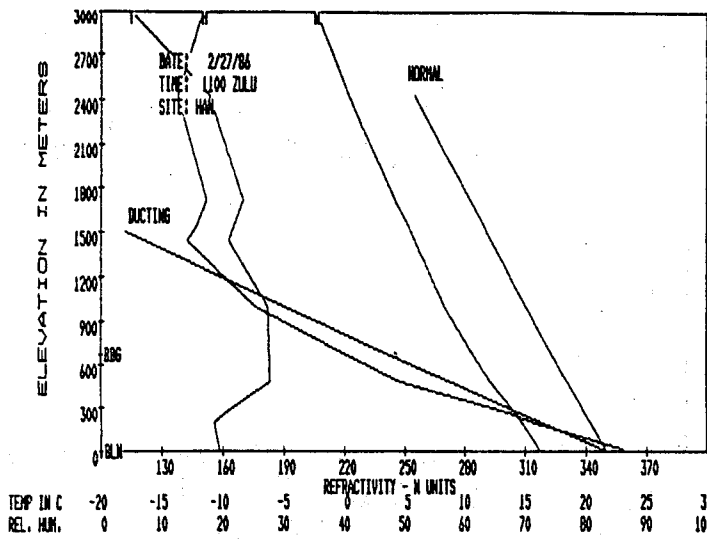
N.A.



N.A.



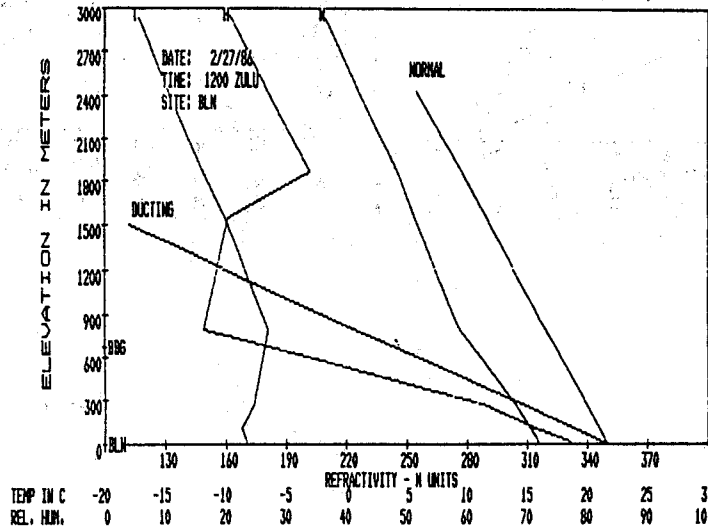
N.A.

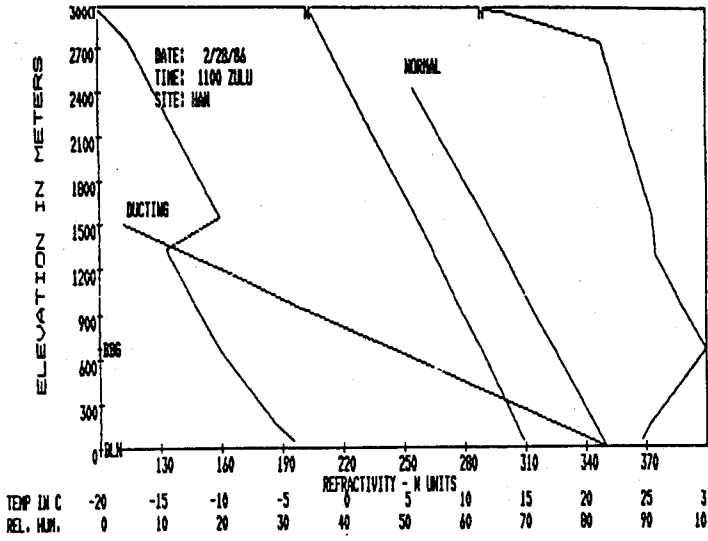


N.A.

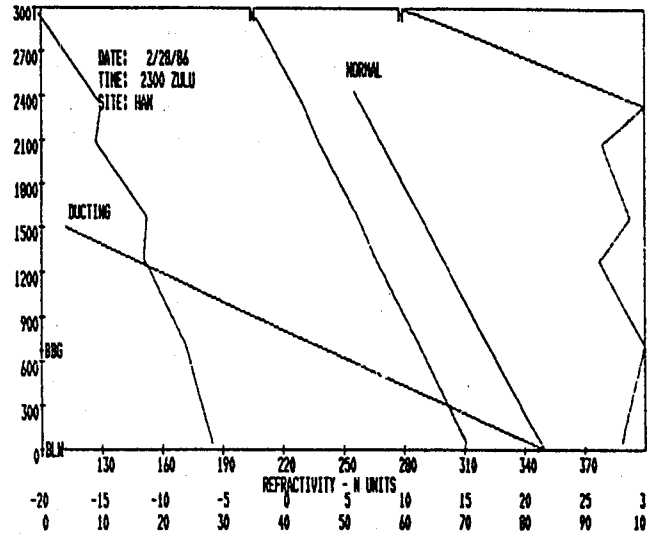
N.A.

N.A.

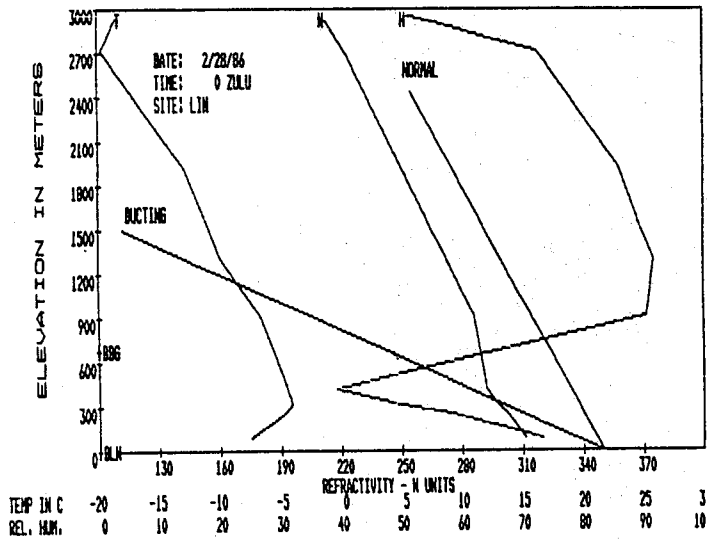




N.A.



N.A.



N.A.

BIBLIOGRAPHIC DATA SHEET

	1. PUBLICATION NO. NTIA Report 88-232	2. Gov't Accession No.	3. Recipient's Accession No.
4. TITLE AND SUBTITLE Propagation and Performance Measurements Over the Berlin-Bocksberg Digital Troposcatter Communications Link		5. Publication Date March 1988	
7. AUTHOR(S) John J. Lemmon and Timothy J. Riley		6. Performing Organization Code NTIA/ITS	
8. PERFORMING ORGANIZATION NAME AND ADDRESS National Telecommunication and Information Admin. Institute for Telecommunication Sciences 325 Broadway Boulder, CO 80303		9. Project/Task/Work Unit No.	
11. Sponsoring Organization Name and Address U.S. Army Information Systems Engineering Center USAISEC Ft. Huachuca, AZ 85613-5301		10. Contract/Grant No.	
		12. Type of Report and Period Covered	
		13.	
14. SUPPLEMENTARY NOTES			
15. ABSTRACT (A 200-word or less factual summary of most significant information. If document includes a significant bibliography or literature survey, mention it here.) <p>This report discusses propagation and performance measurements that were obtained over a digital troposcatter communication link between Bocksberg, West Germany, and West Berlin. The measurements were unusual because three general types of data were collected simultaneously over the link: propagation data, digital performance data, and meteorological data. The propagation data include received signal level (RSL) and multipath measurements made with a channel probe; the performance data consist of bit-error data obtained from a 1.544 Mbps T1 bank; and the meteorological data (in the form of radiosonde messages) have been used to generate profiles of the radio refractive index over the link.</p> <p>The basic principles and instrumentation of the channel probe and the test configurations used to obtain these data are discussed. Then the (cont.)</p>			
16. Key Words (Alphabetical order, separated by semicolons) Key words: multipath; PN channel probe; troposcatter			
17. AVAILABILITY STATEMENT <input checked="" type="checkbox"/> UNLIMITED. <input type="checkbox"/> FOR OFFICIAL DISTRIBUTION.		18. Security Class. (This report) None	20. Number of pages 160
		19. Security Class. (This page) None	21. Price:

Abstract (cont.)

results of analyses of these data are presented and discussed. These results include the measured impulse response of the channel, delay spread, RSL, bit-error ratios, and refractive index profiles. Potential relationships among these results are investigated in order to assess the impact of various troposcatter channel conditions on digital radio performance. In particular, the report discusses both the definition and methods of utilizing the all-important parameter of delay spread. These considerations range from the simple parameter of 2σ values to a more complete evaluation of the dynamic properties of delay-spread derived from the channel probe data.

Previous studies have addressed many facets of troposcatter propagation. This report attempts to bring all of these facets together, to present a more complete description of the troposcatter channel, and to enhance future digital upgrades of existing troposcatter links.